

LINEARIZER DEVELOPMENT FOR WIDEBAND SIGNAL TRANSMISSION USING SOFTWARE DEFINED RADIOS

Ph.D THESIS

by

KARAN GUMBER



**DEPARTMENT OF ELECTRONICS AND COMMUNICATION ENGINEERING
INDIAN INSTITUTE OF TECHNOLOGY ROORKEE
ROORKEE - 247667, INDIA
APRIL, 2019**



LINEARIZER DEVELOPMENT FOR WIDEBAND SIGNAL TRANSMISSION USING SOFTWARE DEFINED RADIOS

A THESIS

*Submitted in partial fulfilment of the
requirements for the award of the degree*

of

DOCTOR OF PHILOSOPHY

in

ELECTRONICS AND COMMUNICATION ENGINEERING

by

KARAN GUMBER



**DEPARTMENT OF ELECTRONICS AND COMMUNICATION ENGINEERING
INDIAN INSTITUTE OF TECHNOLOGY ROORKEE
ROORKEE – 247 667 (INDIA)
APRIL, 2019**







**©INDIAN INSTITUTE OF TECHNOLOGY ROORKEE, ROORKEE- 2019
ALL RIGHTS RESERVED**





INDIAN INSTITUTE OF TECHNOLOGY ROORKEE ROORKEE

CANDIDATE'S DECLARATION

I hereby certify that the work which is being presented in the thesis entitled **“LINEARIZER DEVELOPMENT FOR WIDEBAND SIGNAL TRANSMISSION USING SOFTWARE DEFINED RADIOS”** in partial fulfilment of the requirements for the award of the Degree of Doctor of Philosophy and submitted in the Department of Electronics and Communication Engineering of the Indian Institute of Technology Roorkee, Roorkee is an authentic record of my own work carried out during a period from December, 2014 to April, 2019 under the supervision of Dr. Meenakshi Rawat, Assistant Professor, Department of Electronics and Communication Engineering, Indian Institute of Technology Roorkee, Roorkee.

The matter presented in this thesis has not been submitted by me for the award of any other degree of this or any other Institute.

(KARAN GUMBER)

This is to certify that the above statement made by the candidate is correct to the best of my knowledge.

(Meenakshi Rawat)
Supervisor

The Ph. D. Viva-Voce Examination of Mr. KARAN GUMBER, Research Scholar, has been held on August 22, 2019.

Chairperson, SRC

Signature of External Examiner

This is to certify that the student has made all the corrections in the thesis.

Signature of Supervisor

Head of the Department

Dated:







A wise knows the truth that, “I do nothing at all”!

Bhagavat Gita

Abstract

The imperative demand of hungry data consumer is motivating research activities around the world to develop wideband systems. In response to meet this demand, the wireless communication industry steadily marches towards the next generation of network technology. The upcoming fifth generation (5G) promises data rates that are one hundred times faster than the existing networks, vastly improved connection and signal quality. However, the path towards 5G is not an easy one; as there are many significant challenges facing the design of radio frequency (RF) system and its real-world implementation; such as the use of Ultra-Wideband (UWB) signaling and inter-/multi-band transmission. These challenges led to the introduction of spectral efficient complex modulation schemes. These modern wireless waveforms result in the high peak to average power ratio of the signal that pushes the power amplifier (PA) into the compression region. In the compression region, it yields maximum efficiency, however it also causes signal distortion due to the non-linearity of PA. The non-linearity of the PA causes unwanted signal spilling into the adjacent channels as well as deterioration of the in-band performance. In a wireless communication system, the spill-over effect is particularly important, and adjacent channel leakage ratio- or ACLR as it is termed-is controlled and tightly specified.

The requirement of highly linear transmitter front end along with the high efficiency mandates the deployment of linearization technique to neutralize the trade-off between linearity and efficiency of the nonlinear transmitter. This work focus on an efficient analog and hybrid circuit implementation, which are specifically tailored for PA linearization. Being analog in nature, the predistortion linearization models do not require access to the baseband information as in Digital Predistortion (DPD). In addition, the proposed predistorters also eliminate the constraint on the system bandwidth of the conventional DPD.

The novelty and focus of this work lies in the system inversion of PA nonlinearity with a custom RF components as well as circuit design and hardware implementation of analog circuits. The analog circuits are chosen to alleviate the power dependency and complexity of the digital circuits.

This work investigates three analog models which are RF-in RF-out Analog Predistorter (APD), Ultra-Broadband RF- Predistorter (UBB RF-PD) and Ultra-Broadband Multipath RF- Predistorter (UBB MRF-PD) that aim to provide linearization to UWB signals using low cost and energy

efficient passive RF components. These models alleviate the need of Field programmable Gate Array (FPGA), Analog-to-Digital converter (ADC), Digital -to- Analog converter (DAC), Mixers, wideband transmitter and receiver chains etc. and still provide commendable linearization to UWB signals.

The performance of the proposed RF-in RF-out APD and UBB RF-PD models are demonstrated using 8 component carrier (CC) 160 MHz Long-Term Evolution (LTE) signal through experimental measurements. It is also reported with measurement results that the proposed UBB MRF-PD model works efficiently for inter-/multi-band transmission.

However, the performance of the proposed analog models can also be affected by the analog imperfections in the transmitter, which are introduced by the analog components; such as analog filters and Intermodulation generators. To circumvent the limitations, we further proposed a combinational Hybrid RF- Digital Predistortion (HRF-DPD) linearization method to take the best of both the analog and digital predistortion techniques, which in turn improve the overall predistortion performance. The linear operations are controlled digitally using FPGA, which provides flexibility in terms of digital compensation of delay, gain and phase control of the signal. Moreover, the proposed resulting combinational HRF-DPD considerably reduces the hardware complexity of digital system and provides a compromise between linearity and efficiency at higher power levels.

The HRF-DPD performance is evaluated and compared with the proposed RF-in RF-out APD using contiguous and non-contiguous 8CC 160 MHz LTE signal along with several other state-of-the-art signals such as two-tone, 10 MHz, 20 MHz LTE signals as well as carrier aggregated LTE signals. Experimental results validate the dexterity of the proposed HRF-DPD linearization. The linearizability of the proposed HRF-DPD is reported to be better than the proposed RF-in RF-out APD due to digitally compensation of gain and phase of the signal.

Acknowledgements

First and foremost, I am grateful to God; by whose grace I have had the good fortune to arrive to where I am.

Having thanked the Almighty, I turn my attention to those people without whom I would not be who I am today, nor would I be writing these words:

In the beginning, I would say thanks to my supervisor Dr. Meenakshi Rawat to guide me well throughout the research work from the title's selection to finding the results. Their immense knowledge, motivation and patience have given me more power and spirit to excel in the research writing. Her aid in the acquisition of Research grants and facilities has provided me with the best mental and physical environment throughout the doctoral program. Her endless support has made my completion of the doctoral program possible. I could not have imagined having a better advisor and mentor for my Ph.D. study. Your advice on both research as well as on my career has been priceless.

Apart from my Supervisor, I won't forget to express the gratitude to rest of my thesis committee: Prof. Dharmendra Singh, Prof. Debashis Ghosh, and Prof. Raman Balasubramanian, for their insightful comments and encouragement, but also for the hard question which incited me to widen my research from various perspectives. Their suggestions and comments with regard to my thesis have helped me to improve my work.

I am also pleased to say thank you to Dr. Karun Rawat who gave access to the laboratory and research facilities, the man who also supported me well throughout the entire research program. Their immense support actually guided me to rectify numerous things that could create major challenges in the acceptance of my paper. It wouldn't have been possible to conduct this research without their precious support.

I am extremely thankful to Prof. M.V. Kartikeyan, especially for sharing his expertise so willingly and for providing me an irreplaceable advice, both on my research and my career. I am indebted to Dr. Sukwinder Singh for many fruitful discussions.

There are some friends who did not contribute to the work itself, but supported me during the work. I am forever thankful to my friends Seetal Dhillon, Tejbir Singh Sandhu, Naveen Atwal,

Paramjeet Singh, Sahil Kamra, Karan Maluja and Anakhbir Singh Sekhon for his help and frequent support.

In my daily work I have been blessed with a friendly and cheerful group of fellow students in Software Define Radios and Wireless Communication Labs: Dr. Praveen Jaraut, Dr. Chetan Pathak, Anurag Vijay Agrawal, Rupender Singh, Sujata Ghosh, Y. Mary Asha Latha, Ekta Aggrawal, Hemant Kumar Singhal, Nishant Kumar, Girish Chandra Tripathi, Anuj Kumar Sahoo, Ashish, Shipra, and Anant. They provided a friendly and cooperative atmosphere at work and also provided useful feedback and insightful comments on my work.

I express my heartfelt gratitude to my beloved parents, Smt. Neelam and Shri Ashok Kumar, my sister Shivani and my cousins Rohan Kathpal and Akhil Sharma for their unconditional love and support throughout my life. I consider myself nothing without them. They gave me enough moral support, encouragement and motivation to accomplish the personal goals. My lifeline, my father who always supported me financially so that I only pay attention to the studies and achieving my objective without any obstacle on the way.

And most of all, I owe my deepest gratitude to my wife, Meenu, for her encouragement, patience, affection, and understanding. She is certainly one of the main contributors of all the best in my life, and I am intellectually indebted to her ideas and our conversations. I thank God for the extraordinary chance of having her as wife, friend and companion. She supported me without any complaint or regret that enabled me to complete my doctoral thesis. My thesis acknowledgement would be incomplete without thanking my baby, Aaron Gumber, whose smiling face always made me happy and inspired me. He has contributed immeasurably to family enjoyment in a special way. He always tries to do everything to make his presence felt. He is the pride and joy of my life and I love him more than anything.

Truly, the past four-and-a-half years have been a fantastic ride.

Karan Gumber



*To
My Parents
Neelam Rani and Ashok Kumar
My Wife
Meenu
and my Son
Aaron Gumber.*



Contents

Abstract	i
Acknowledgements	iii
Contents	vii
List of Figures	xiii
List of Tables	xix
List of Abbreviations	xxi
1. Introduction	1
1.1 Motivation	1
1.2 Origin of Linearizers	2
1.2.1 Feedforward Linearization	4
1.2.2 Feedback Linearization	6
1.2.3 Predistortion linearization	7
1.3 The need for Predistortion Linearization	8
1.3.1 Types of Predistortion linearization	9
1.3.1.1 Digital Predistortion	10
1.3.1.2 Analog Predistortion	11
1.3.1.3 Hybrid Predistortion	13
1.4 Objectives	14
1.5 Contribution	16
1.5.1 Low Cost RFin-RFout Predistorter Linearizer for High Power amplifiers and Ultra-wideband Signals	16
1.5.2 On Control Schemes for Modified Analog Predistortion Linearizer in 5G transmitters	17
1.5.2 Ultra-Broadband RF-Predistorter Supporting Carrier Aggregation for Future 5G System	18
1.5.4 A Modified Hybrid RF Predistorter Linearizer	18

1.6	Outline and Structure	19
2.	RF-in RF-out Analog Predistorter	21
2.1	Publications from the Work	21
2.2	Introduction	22
2.3	Conventional Analog Predistortion	23
2.3.1	Fifth-order Analog Predistorter	24
2.3.2	Multi-branch Analog Predistorter	25
2.3.3	Cascaded Analog Predistorter	27
2.3.4	Limitations of the Conventional, Cascaded and Multi-branch Analog Predistortion	28
2.4	Proposed RF-in RF-out Analog Predistorter	29
2.4.1	Working Principle of the Proposed RF-in RF-out APD	30
2.4.2	Components End Use in the Proposed APD	32
2.4.3	Analysis using two tone signal	35
2.5	IM Generator Modeling	41
2.5.1	Bandwidth of IM Generator	43
2.5.2	Impact of R and C	44
2.5.3	Power Dependency of IM Generator	46
2.6	Experimental Verification	48
2.6.1	Test-bench for data extraction	48
2.6.2	Device under Test	49
2.6.3	Signal under Test	51
2.6.3.1	Two-tone signal with 100 MHz frequency spacing	51
2.6.3.2	LTE 20 MHz signal	53
2.6.3.3	Non-Contiguous 8 CC LTE 160 MHz signal	53
2.6.3.4	Contiguous 8 CC LTE 160 MHz signal	54
2.7	Comprehensive Comparison with the State-of-the-art APD Linearization	55
2.8	Conclusion	61

3. Implementation Challenges and Control Schemes	63
3.1 Introduction	63
3.1.1 Overview of the two Control Schemes	64
3.2 Conventional APD and Type-I Control Scheme for modified APD	65
3.3 Type-I Control Scheme using Vector Multiplier	66
3.4 Type-II Control Scheme using Digital Phase Shifter and Digital Attenuator	67
3.4.1 Independent phase and gain control	68
3.4.1.1 Digital Step Attenuator	68
3.4.1.2 Digital Phase Shifter	69
3.4.2 Limitation of the Vector Multiplier	69
3.4.2.1 Appropriate phase, but inappropriate gain	71
3.4.2.2 Appropriate gain, but inappropriate phase	72
3.4.2.3 Abrupt Change in Phase	72
3.4.2.4 Phase control range	73
3.4.2.5 Laborious circuit connections	73
3.5 Quantitative and Qualitative comparison	73
3.5.1 Sensitivity of Control	74
3.5.2 Nonlinearity order compensation	75
3.5.3 System complexity and power consumption	75
3.5.4 Linearizability	75
3.6 Experimental verification	76
3.6.1 Test-bench for data extraction	76
3.6.2 Device under Test	78
3.6.3 Signal under Test	79
3.6.3.1 LTE 5CC 100 MHz contiguous signal	79
3.6.3.2 LTE 10 MHz and 5 MHz signal	81
3.6.3.3 Two tone signal with frequency spacing of 150 MHz	82
3.6.4 Adaptive spectrum Monitoring	84
3.7 Conclusion	88

4. Ultra-Broadband RF Predistorter	89
4.1 Introduction	89
4.1.1 Inter-band and Intra-band Transmission	89
4.2 Carrier Aggregation and the Predistortion	91
4.2.1 Multi-band CA and the Proposed UBB MRF-PD	92
4.3 Proposed Ultra-Broadband RF-Predistortion and Ultra-Broadband Multipath RF-Predistortion	94
4.3.1 Reforms and Benefits	95
4.3.2 Component Description	96
4.3.2.1 Wilkinson Power Divider	96
4.3.2.2 Band Pass Filter	97
4.3.2.3 Digital Phase Shifter	98
4.3.2.4 Digital Step Attenuator and Linear Gain Amplifier	99
4.3.2.5 Passive Intermodulation Generator	100
4.3.2.6 Digital Step Attenuator	101
4.3.2.7 Wilkinson Power Combiner	101
4.4 PIMG Modeling and Case Studies	102
4.4.1 Case Studies of the PIMG	105
4.4.2 Video Bandwidth of the PIMG	106
4.5 Experimental Verification	107
4.5.1 Test-bench for data extraction	107
4.5.2 Device under Test	109
4.5.3 Signal under Test	111
4.5.3.1 8CC 160 MHz Contiguous signal	111
4.5.3.2 Two tone signal with 100 MHz frequency spacing	113
4.5.3.3 Inter-/Multi-band LTE signal	114
4.6 Comprehensive Comparison with the State-of-the-art UBB-Predistortion Linearization	116
4.7 Conventional Digital Predistortion and its limitation imposed on 5G	120
4.7.1 Conventional Digital Predistortion	120

4.7.2	System NMSE versus Signal Bandwidth	120
4.7.3	Linearization Bandwidth constraint of the Conventional DPD	121
4.7.4	Restriction on Data Converters	122
4.7.4.1	Sampling speed Reduction	124
4.8	Proposed UBB RF-PD/UBB MRF-PD vs. Conventional DPD/2D-DPD	125
4.9	Conclusion	126
5.	Hybrid RF-Digital Predistortion	129
5.1	Introduction	129
5.2	Proposed Hybrid RF-Digital Predistortion	130
5.3	Two Tone Analysis	132
5.4	Experimental Verification	136
5.4.1	Intermodulation generator	136
5.4.2	Test-bench for data extraction	137
5.4.3	Signal under Test	139
5.4.3.1	LTE 50 MHz and 100 MHz signals	139
5.4.3.2	Contiguous and Non-Contiguous 8CC 160MHz LTE signal	142
5.5	Comprehensive Comparison with the State-of-the-art Hybrid Predistortion Linearization	143
5.6	Challenges in the Implementation	148
5.7	Scope of the proposed technique	150
5.8	Conclusion	150
6.	Conclusions	151
6.1	Concluding Remarks	151
6.2	Suggestions for Future Work	154
	Bibliography	157



List of Figures

1.1	Typical GSM Base station Power budget.....	2
1.2	Power Consumption breakdown of Radio Base Station.....	3
1.3	The Linearity vs. Efficiency trade-off in Power Amplifier.....	3
1.4	Feedforward Linearization.....	4
1.5	Feedback Linearization.....	5
1.6	(a) Concept of Predistortion Linearization, (b) AM-AM and AM-PM distortion representation in the time domain, and (c) IMD representation in the frequency domain....	6
1.7	The fundamental concept of Digital Predistortion.....	9
1.8	Behavioral modeling procedure of device under test.....	10
1.9	Series Diode Analog Predistortion architecture.....	11
1.10	Hybrid Predistortion architecture.....	12
1.11	Roadmap for the proposed work contribution.....	15
2.1	Conventional Analog Predistorter architecture.....	23
2.2	Fifth-order Conventional Analog Predistorter architecture.....	25
2.3	Multi-branch Analog Predistorter architecture with three branch nonlinear path, where each path consists of separate delay line and Vector multiplier.....	26
2.4	Multi-branch Analog Predistorter architecture with three branch nonlinear path, where each path consists of separate delay line and error Generator.....	26
2.5	Cascaded Analog Predistorter architecture.....	27
2.6	Proposed RF-in RF-out Analog Predistorter architecture.....	29
2.7	Measured S-parameters of WPC/WPD.....	32

2.8	Single ended control voltage mode operation of MAXIM2046 VM.....	33
2.9	Working of 20 lead header connector of MAXIM2046 VM.....	34
2.10	Measured S-parameters of 3dB RRC.....	34
2.11	Analysis of IM Generator for two tone signal.....	37
2.12	Fabricated Intermodulation generator equipped with RC Filter Bank and HSMS 2822 Schottky Anti-parallel diode.....	42
2.13	Response of the IM Generator for 8CC 160MHz non-contiguous signal.....	42
2.14	Fundamental signal cancellation and IMD generation by the IM Generator for the different frequencies.....	43
2.15	Intermodulation Distortion generation with fixed $C=1\text{pF}$ and varying R	45
2.16	Intermodulation Distortion generation with fixed $R=100\Omega$ and varying C	45
2.17	IM Generator modeling for two tone signal with 100MHz frequency spacing, centered at 1.8 GHz.....	46
2.18	IM Generator modeling for two tone signal with 160MHz frequency spacing, centered at 2 GHz.....	46
2.19	IM Generator modeling for 8CC 160MHz LTE signal, centered at 2 GHz.....	47
2.20	Test-bench for data extraction of the proposed RF-in RF-out APD.....	48
2.21	AM/AM and AM/PM characteristics of ZX60V-63+ Class AB PA	49
2.22	Linear and compression region of ZX60V-63+PA using Single tone CW signal at 2 GHz.....	50
2.23	Measured Power Spectrum Density of PA with and without the proposed RF-in RF-out APD under two tone signal with a frequency spacing of 100 MHz.....	51
2.24	Measured Power Spectrum Density of PA with and without the proposed APD under 20 MHz LTE signal.....	52

2.25	Measured Power Spectrum Density of PA with and without the proposed APD excited by non-contiguous 8CC 160 MHz LTE signal.....	53
2.26	Measured Power Spectrum Density of PA with and without the proposed APD excited by contiguous 8CC 160 MHz LTE signal.....	54
2.27	ACPR of PA output with and without proposed APD at different back-off power.....	54
2.28	Measured constellation diagram with and without the proposed APD at 2 GHz under contiguous 8CC 160MHz LTE signal.....	55
3.1	Conventional APD architecture.....	64
3.2	Proposed Type-I Control Scheme for the modified APD architecture.....	65
3.3	Proposed modified APD architecture, where Vector Multiplier is used as a Control Scheme.....	66
3.4	Proposed Type-II Control Scheme for the modified APD architecture.....	67
3.5	Test-bench for the characterization of MAX2046 Vector Multiplier.....	69
3.6	Phase plot of MAX2046 VM at different frequencies by varying V_Q supply, where V_I is kept constant.....	70
3.7	Gain plot of MAX2046 VM for the entire frequency band (1740 MHz -2060 MHz) under variable I and Q biasing supply (V_I and V_Q).....	70
3.8	(a) Required phase in presence of non-linearity, and (b) Required gain with precise control over phase.....	71
3.9	Test-bench of the proposed Type-II CS for data extraction.....	76
3.10	Measured AM/AM and AM/PM characteristics of ZX60 14012L-S+ PA.....	78
3.11	Linear and compression region of ZX60 14012L-S+ PA using Single tone CW signal, centered at 2 GHz.....	78
3.12	Measured Power Spectrum Density of HMC8500 GaN PA with and without the proposed APD excited by 8CC 160 MHz UBB LTE signal.....	79

3.13	ACPR improvement of 10W HMC8500 GaN PA with the proposed CS at different output back-off powers.....	80
3.14	Measured Power Spectrum Density of ZX60 14012L-S+ PA with and without the proposed Type-I and Type-II Control Scheme excited by 100 MHz LTE signal.....	80
3.15	Measured Power Spectrum Density of PA with and without the conventional and proposed APD excited by 10 MHz LTE signal.....	81
3.16	Measured Power Spectrum Density of PA with and without the CAPD and the proposed Type-I Control Scheme excited by the 5 MHz LTE signal, centered at 2 GHz.....	82
3.17	Measured Power Spectrum Density of PA excited by 150 MHz two tone signal, centered at 2 GHz (a) with and without the proposed Type-I Control Scheme, (b): with and without the proposed Type-II Control Scheme.....	83
3.18	Automatic Calibrated adaptive Analog Predistorter architecture.....	84
3.19	Block diagram of data acquisition for adaptive Analog Predistorter architecture.....	85
3.20	The transfer function of AFS390E SAW filter.....	86
3.21	Amplitude v/s DC Output Voltage of Power Detector centered at 2 GHz.....	87
4.1	(a) Contiguous and (b)Non-contiguous intra-band CA communication scenario and, (c) the inter-band CA communication scenario.....	90
4.2	(a) Intra-band, and (b) Inter-band downlink transmission.....	91
4.3	Proposed Ultra-Broadband RF-Predistorter for intra-band communication.....	94
4.4	Proposed Ultra-Broadband Multipath RF-Predistorter for inter-/multi-band communication.....	94
4.5	Analysis of PIMG excited by 10 MHz (a) two tone signal, centered at 1 GHz, (b) LTE signal, centered at 2 GHz.....	100
4.6	Fabricated PIMG mounted with RC filter banks and HSMS-2822 anti-parallel diode pair.....	102

4.7	Measured Power Spectrum Density of the Passive intermodulation generator excited by 160 MHz (a) 8CC LTE signal, (b) two tone signal.....	103
4.8	Modeling of PIMG using 10 MHz two tone signal at different input power, fixed frequency 2 GHz.....	104
4.9	Modeling of PIMG using 10 MHz two tone signal at different frequency, fixed input power 0 dBm.....	105
4.10	Power flow analysis of PIMG under various operating condition.....	106
4.11	Test-bench for data extraction of (a) UBB RF-PD, (b) UBB MRF-PD.....	108
4.12	Measured linear and compression region of 10W HMC8500 Broadband GaN PA using (a) Single tone CW (b) 8CC 160 MHz UBB LTE signal.....	110
4.13	AM/AM and AM/PM characteristics of ZFL-11 AD+.....	110
4.14	Measured linear and compression region of ZFL-11 AD+ Class AB PA using Single tone CW signal.....	111
4.15	Measured Power Spectrum Density of 10W HMC8500 PA with and without the proposed UBB RF-PD excited by 8CC 160MHz LTE signal, centered at 1.8 GHz.....	112
4.16	Measured Power Spectrum Density of ZFL-11 AD+ PA with and without the proposed UBB RF-PD excited by 8CC 160MHz LTE signal, centered at 2 GHz.....	112
4.17	Measured Power Spectrum Density of ZFL-11 AD+ PA with and without the proposed UBB RF-PD excited by 100 MHz two tone signal at 1.85 GHz.....	113
4.18	Intermodulation characteristics of ZFL-11 AD+ PA with and without the proposed UBB RF-PD at different output power.....	114
4.19	Measured Power Spectrum Density of HMC8500 PA with and without the proposed UBB MRF-PD at the (a) lower band consists of 1.4 MHz LTE signal, centered at 1111 MHz, (b) upper band consists of 160 MHz LTE signal, centered at 2010 MHz.....	115
4.20	Measured Power Spectrum Density of ZX60V-63+ PA with and without the proposed UBB MRF-PD excited by 2CC 1GHz LTE inter-band signal.....	115

4.21	Conventional DPD architecture.....	120
4.22	(a) DPD System performance deterioration observed in experimental setup in terms of NMSE for increasing LTE signal bandwidth, (b) Measurement setup for Data extraction.....	121
4.23	Impact of ADC saturation for Broadband signal.....	123
5.1	The proposed Hybrid RF-Digital Predistortion Architecture.....	130
5.2	Hardware realization of the proposed Hybrid RF-Digital Predistortion Architecture.....	131
5.3	Two tone test of IM Generator	134
5.4	Flowchart for automatic phase delay compensation.....	135
5.5	Simulated S parameters of RRC.....	136
5.6	Test bench for data extraction of HRF-DPD.....	137
5.7	AM/AM and AM/PM characteristics of 15W Class AB PA.....	137
5.8	Cancellation of fundamental signal and generation of in-band IMD for (a) LTE 50 MHz, (b) LTE 100 MHz signal.....	139
5.9	Cancellation of in-band IMD for (a) LTE 50 MHz, (b) LTE 100 MHz signal.....	139
5.10	Output of phase adjusted IM generator (RRC) showing the out-of band IM3 and IM5 generation of the two carrier LTE 100 MHz signal.....	140
5.11	Measured Power Spectrum Density HRF-DPD showing cancellation of out-of-band IM3 and IM5 of LTE 100 MHz signal.....	141
5.12	Measured Power Spectrum Density of PA with and without the proposed RF-in RF-out APD and HRF-DPD excited by contiguous 8CC 160 MHz LTE signal.....	142
5.13	Measured Power Spectrum Density of PA with and without the proposed RF-in RF-out APD and HRF-DPD excited by non-contiguous 8CC 160 MHz LTE signal.....	143

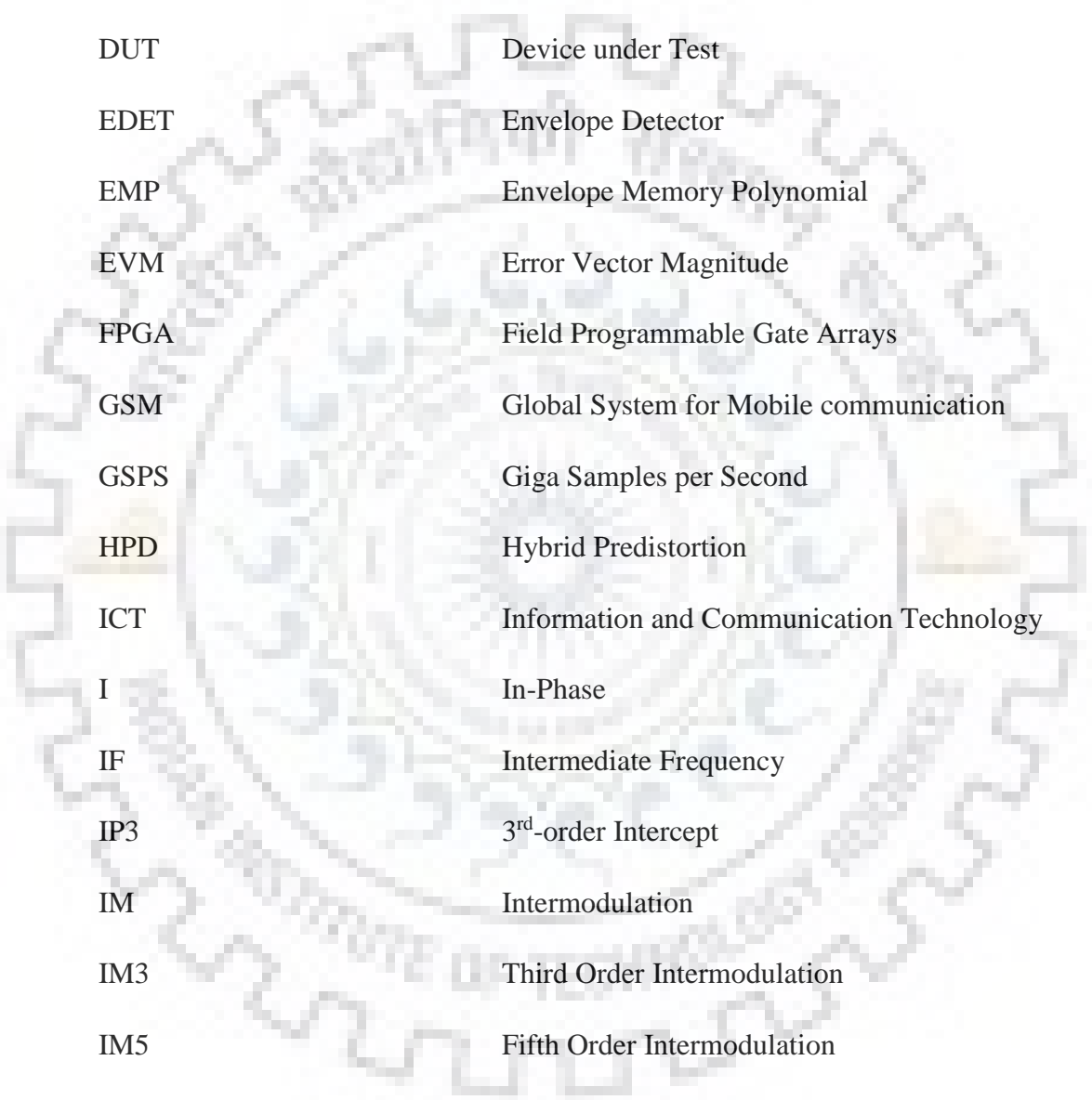
List of Tables

1.1	Comparison of Different Linearization Techniques.....	7
1.2	Comparison of Different Predistortion Linearization Techniques.....	13
2.1	Performance comparison of PA with/without the Proposed APD.....	52
2.2	Performance comparison of the State-of-the-Art APD Linearizer.....	56
2.3	Salient Features of Various APD Predistorter Linearizer.....	57
3.1	Various Combinations of Voltages at 2 GHz for fixed 2.5 dB Gain.....	72
3.2	Power Requirement at 2 GHz to generate different IM products.....	74
3.3	IMD Correction before and after Type-I and Type-II Control Schemes.....	83
4.1	Inter-band Component Carrier and IM Products.....	90
4.2	Various Operating Conditions of the PIMG.....	105
4.3	IMD Correction before and after UBB RF-PD Linearization.....	113
4.4	Performance comparison of the State-of-the-Art HPD Linearizer.....	116
4.5	Salient Features of Various HPD Predistorter Linearizer.....	118
5.1	Near Band ACLR Performance with and without the HRF-DPD Linearizer.....	140
5.2	Away From the Band ACLR Performance with and without the proposed HRF-DPD Linearizer for LTE 100 MHz Signal.....	141
5.3	Component Requirement in Various Predistorter Linearizer.....	144
5.4	Bandwidth and Other Specifications of Various Predistorter Linearizer.....	145
5.5	Various Hybrid Predistortion Linearizer.....	146
6.1	Pros and Cons of the Proposed Predistorter Linearizer.....	153



List of Abbreviations

Abbreviation	Definition
4G	Fourth Generation
5G	Fifth Generation
ACPR	Adjacent Channel Power Ratio
ADC	Analog-to-Digital Converter
ADS	Advance Design System
AM-AM	Amplitude Modulation to Amplitude Modulation
AM-PM	Amplitude Modulation to Phase Modulation
APD	Analog Predistortion
BPF	Band Pass Filter
BS	Base Station
C	Capacitor
CA	Carrier Aggregation
CAPD	Conventional Analog Predistortion
CAPEX	Capital Expenditure
CC	Component Carrier
CMOS	Complementary Metal-Oxide-Semiconductor
CS	Control Schemes
CW	Continuous Wave
DAC	Digital-to-Analog Converter
dB	Decibel



DPD	Digital Predistortion
DPS	Digital Phase Shifter
DSA	Digital Step Attenuator
DSP	Digital Signal Processing
DUT	Device under Test
EDET	Envelope Detector
EMP	Envelope Memory Polynomial
EVM	Error Vector Magnitude
FPGA	Field Programmable Gate Arrays
GSM	Global System for Mobile communication
GSPS	Giga Samples per Second
HPD	Hybrid Predistortion
ICT	Information and Communication Technology
I	In-Phase
IF	Intermediate Frequency
IP3	3 rd -order Intercept
IM	Intermodulation
IM3	Third Order Intermodulation
IM5	Fifth Order Intermodulation
IM7	Seventh Order Intermodulation
IMD	Intermodulation Distortion
LA	Linear Amplifier
LGA	Linear Gain Amplifier

LO	Local Oscillator
LTE	Long-Term Evolution
LUT	Look Up Tables
MSPS	Mega Samples per Second
NMSE	Normalized Mean Square Error
OBO	Output Back-Off
OBOP	Output Back-Off Power
OIP	Output Intercept Point
OIP3	3 rd -order OIP
OIP5	5 th -order OIP
OPEX	Operational Expenditure
P1dB	1-dB Compression Point
P3dB	3-dB compression point
PA	Power Amplifier
PAE	Power Added Efficiency
PAPR	Peak to Average Power Ratio
PIMG	Passive Intermodulation Generator
PLL	Phase Locked Loop
PS	Phase Shifter
PSD	Power Spectral Density
PVT	Process Voltage and Temperature
Q	Quadrature-Phase
QAM	Quadrature Amplitude Modulation

R	Resistor
RAM	Random Access Memory
RMS	Root Mean Square
RRC	Rat Race Coupler
RF	Radio Frequency
SAW	Surface Acoustic Wave
SNR	Signal to Noise Ratio
TWT	Travelling Wave Tube
UBB	Ultra-Broadband
UBB RF-PD	Ultra-Broadband RF-Predistorter
UBB MRF-PD	Ultra-Broadband Multipath RF-Predistorter
UWB	Ultra-Wideband
VBW	Video Bandwidth
VGA	Variable Gain Amplifier
VM	Vector Multiplier
VNA	Vector Network Analyzer
WPC	Wilkinson Power Combiner
WPD	Wilkinson Power Divider

Chapter 1

Introduction

1.1 Motivation

The human ambition is to make every upcoming generation superior, goaded by the obviously insatiable demand for high speed and massive connectivity, which led to define a ubiquitous network, one that would together provide low latency and massive connections at very high speed. The global upsurge of pervasive mobile communication requiring high speed and greater spectral efficiency has resulted in the development of future fifth generation (5G) communication. Discussion about the 5G standard have converged into full fledge conversation that has captured the attention of researchers around the world. As the users are fascinated to new broadband services such as video streaming, virtual reality, mobile based multimedia, etc., the thirst for wireless communication keeps fueling. The total mobile traffic is rising at a compound rate of 45% per annum [1].

A unique event in the history was witnessed in 2014; in which total number of mobile devices surpassed world population [1], [2]. It is anticipated that we will witness the world monthly data traffic around 107 Exabyte/month in 2023, which is about 9 times to the volume of traffic in 2017 [3]. As the number of mobile users is increasing day by day, it requires the deployment of the higher capacity cellular network. Cellular mobile phones fueled the mobile data consumption. The upcoming 5G communication aims at better channel capacity, increased data rate and better spectral efficiency than the current fourth generation (4G) communication standard. It is anticipated that to cater to the needs of this next-generation (5G) wireless standard, mobile systems and base stations (BS) will require new and faster application processors, basebands and radio frequency (RF) devices [4].

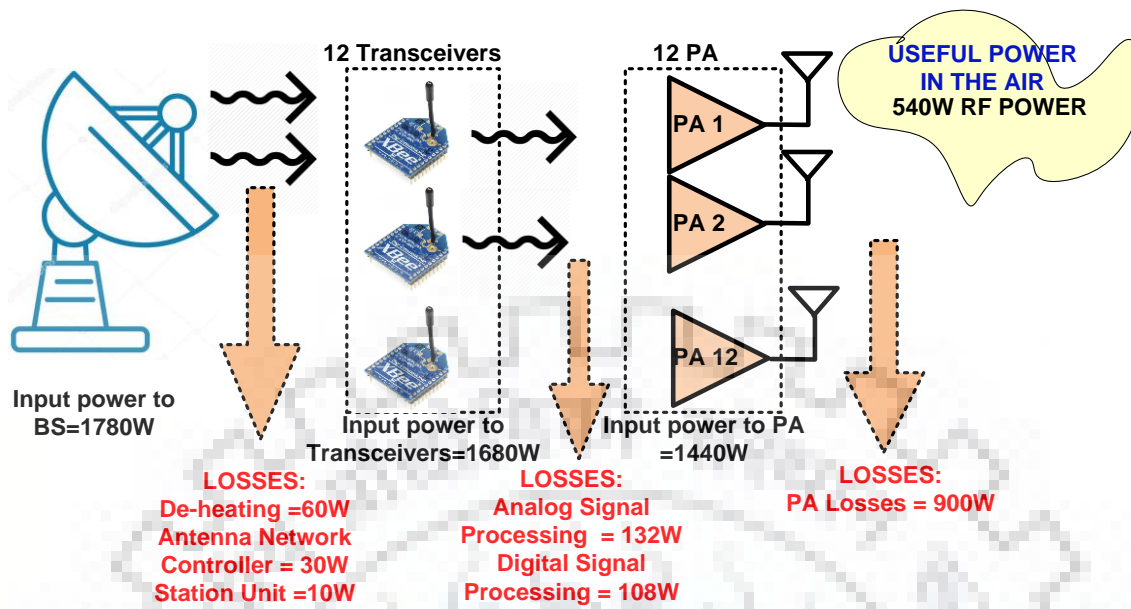


Figure 1.1: Typical GSM Base station Power budget.

The relentless quest for higher data rates is stressing on signal bandwidth. Wider signal bandwidth is envisioned to provide order-of-magnitude improvement in data rate, which further enhances the system capacity [5]-[7].

1.2 Origin of Linearizers

Before accounting for the huge expansion in the scale promised by 5G at present, the information and communications technology (ICT) sector was responsible for 2% of estimated global carbon emissions from human activity in 2007 [8], [9]. In 2020, this figure is set to grow at 6%. The one-third of that amount is influenced by the wireless communication industry, in which a large share is contributed by the power amplifier (PA) and its associated circuitry.

The PA is a crucial element of any communication system to communicate the signals to significant distances, and its performance defines the overall BS specification [10]-[18]. A typical Global System for Mobile communication (GSM) BS power consumption is shown in Figure 1.1. The total power consumption of a BS is 1780W out of which only 30% of useful power is emitted in the air. The power which is received at the input of the PA is typically 1440W, out of which 540W is the useful power which is emitted into the air.

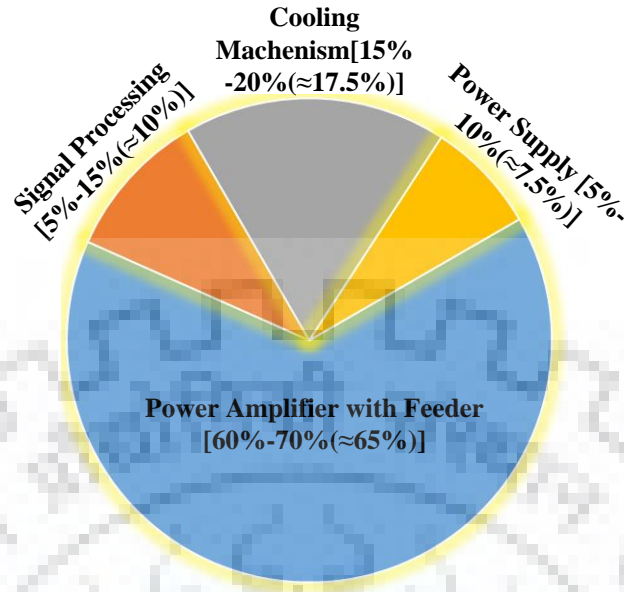


Figure 1.2: Power Consumption breakdown of Radio Base Station.

Thereby, the efficiency of PA with a typical GSM BS is only 37%. The largest share of power in a BS is consumed by a PA which is shown in Figure 1.2. As an outcome, the study of how to improve the energy efficiency of the PA has become an area of substantial attention to numerous researchers.

The PA in the RF transmitters must have two aspects: high efficiency in conjunction with good linearity, where high efficiency extends the battery lifespan in handset applications,

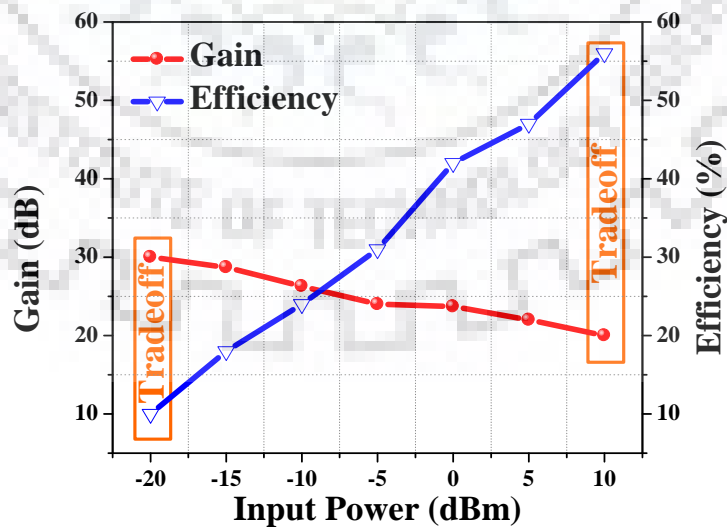


Figure 1.3: The Linearity vs. Efficiency trade-off in Power Amplifier.

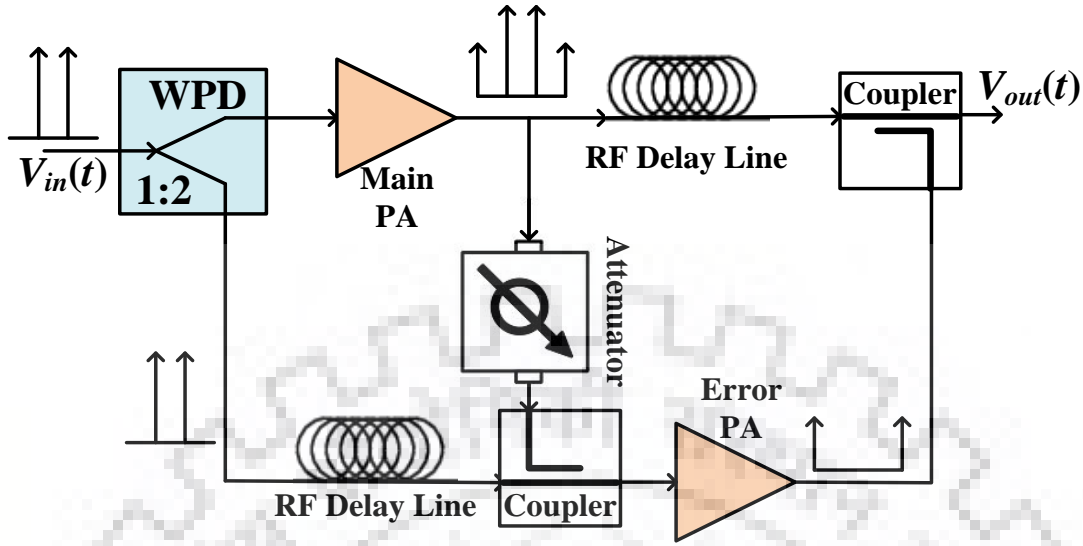


Figure 1.4: Feedforward Linearization.

and good linearity ensures the quality of the signal transmitted from an RF transmitter. The basic trade-off between the linearity and efficiency is illustrated in Figure 1.3. When the PA operates in the linear region it yields low energy efficiency. Conversely, in order to get high efficiency, PA operates in the saturation region that results in the generation of strong nonlinear distortion of the signal. The most common approach for improving the Intermodulation (IM) products of an amplifier is to choose a load line that will optimize the amplifier input-to-output transfer function. The linearity of a device changes as a function of operating point and load line. Moreover, effective energy management of PA is required for reducing the carbon footprint in the BS.

The desire to circumvent the trade-off between the linearity and efficiency has led to the development of various linearization techniques. Researchers have proposed various techniques for the linearization of RF PA such as feedback, feed-forward and pre-distortion.

1.2.1 Feedforward Linearization

These techniques target to reduce the intermodulation distortion (IMD) of the PA with the main focus on third-order IMD. The feedforward linearization technique is shown in Figure 1.4. The signal is divided into two paths using Wilkinson Power Divider (WPD). One part

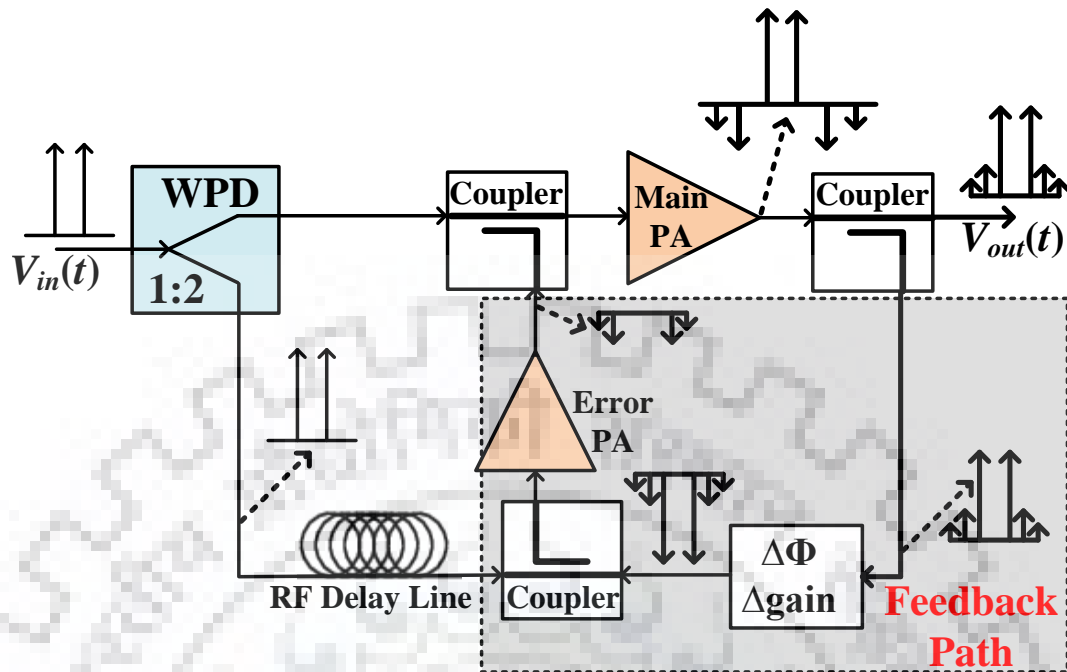


Figure 1.5: Feedback Linearization.

of the signal drives PA and generates amplified signals as well as IMD components. In the first loop, an error signal is generated which is a subtraction of amplified distorted signal and part of original signal received via second path. The attenuation and phase are provided such that the original signal is cancelled and only IMD components remain. This ‘error signal’ containing IMD terms is amplified via ‘error amplifier’ such that it cancels the distortion component of the primary amplifier [19]-[21] as shown in Figure 1.4. The final result is ideally a distortion free signal. The error amplifier operates at much lower power levels as compared with main amplifier therefore the error does not contribute to the distortion of the output spectrum.

There are several advantages to this technique. The distortion can be completely canceled (theoretically). Also, this method has no closed feedback loop, and is thus unconditionally stable. Eventually, this benefit comes at the cost of a requirement for a high degree of matching in both phase and magnitude of all the system components. Unfortunately, this method is also difficult to implement in a typical high-power transmitter. As the final amplifier device is typically the most expensive component in the transmitter, use of an additional device to improve performance is not usually cost-effective. Moreover, the second amplifier needs to have a close gain tracking versus the primary amplifier. As this is

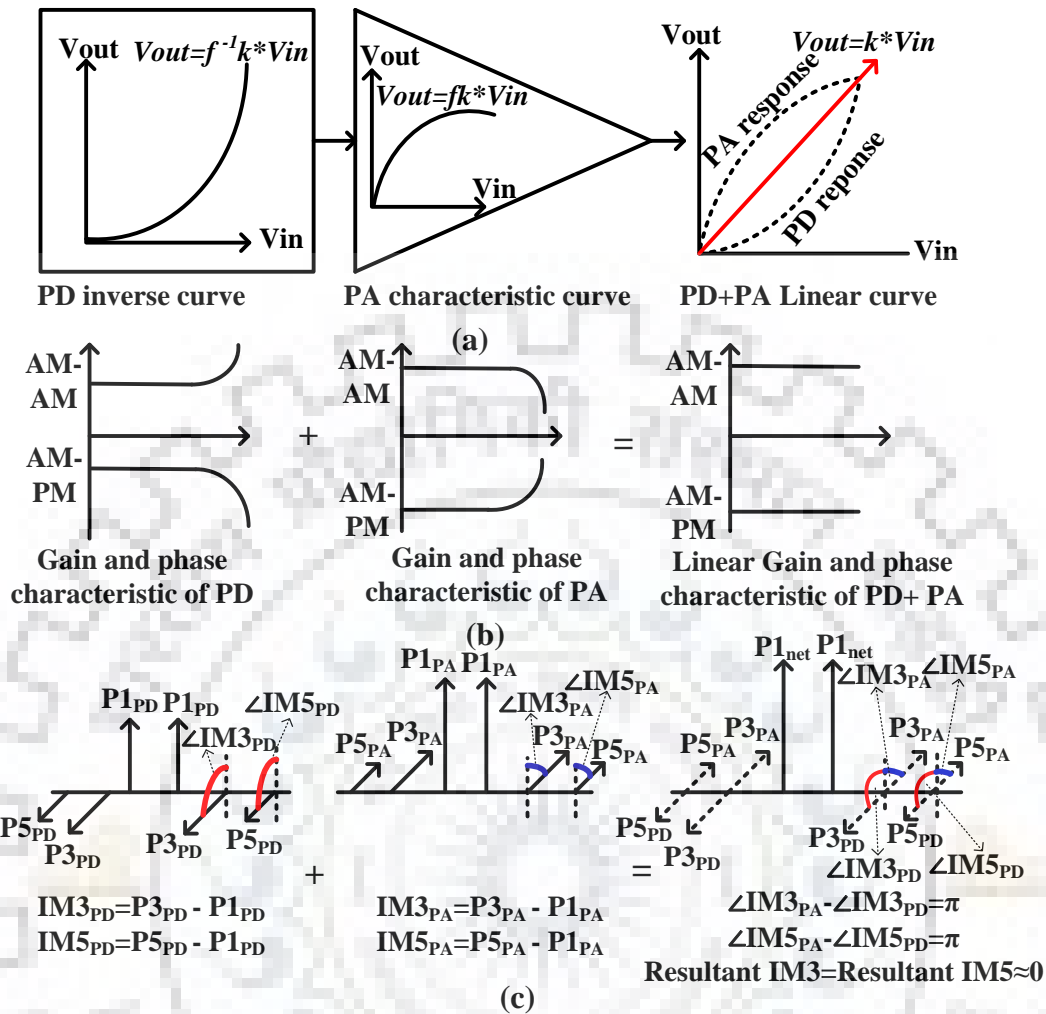


Figure 1.6: (a) Concept of Predistortion Linearization, (b) AM-AM and AM-PM distortion representation in the time domain, and (c) IMD representation in the frequency domain.

difficult to assure in a small signal amplifier, it is even more complicated in a large signal application, where effects such as temperature, gain change versus signal level, etc. need to be accounted for.

1.2.2 Feedback Linearization

Feedback is a closed-loop technique that samples the output waveform, and subtracts this sample from the waveform input to the amplifier which is shown in Figure 1.5. With this negative feedback technique, distortion present at the output of the amplifier is used to

TABLE 1.1
COMPARISON OF DIFFERENT LINEARIZATION TECHNIQUES

Parameters	Feedback	Feedforward	Predistortion
Cancellation Performance	Low	High	High
Bandwidth	Narrow	Wide	Wide
Complexity and Size	Medium	Large	Small
Power Added Efficiency (PAE)	Medium	Low	High
Suitable for Multicarrier	Low	High	High

modify the input waveform. In amplifiers, the output is typically compressed. A sample of the output signal, fed back in the correct amplitude and phase, will accentuate the peak of the input waveform which allows the amplifier to return this modified input waveform to the desired shape at the output [22].

There are, however, drawbacks to use of feedback in high power transmitter applications. It is desirable to have a high-gain final amplifier stage; feedback reduces the gain of the amplifier stage. The signal bandwidth requirement of the newer modulation system stretching into the hundreds of MHz creates difficulty in deploying feedback linearization techniques due to the need for qualifying stability criterion. Hence, the solution to handle wider signal bandwidth is the predistortion linearization.

1.2.3 Predistortion Linearization

Predistortion is conceptually the simplest approach of linearization for an RF PA. The concept of predistortion linearization is shown in Figure 1.6. To compensate for the nonlinearity of PA, predistortion has inverse amplitude modulation to amplitude modulation (AM-AM) and amplitude modulation to phase modulation (AM-PM) characteristic to that of the PA [23]-[26]. It creates the inverse of the PA transfer function at

the input to the amplifier. This solution may be implemented with low-power components. Predistortion method takes the advantage of low complexity and stable operations. The comparison of different linearization techniques is carried out in Table 1.1. Among predistortion linearization [27]-[29], feedback linearization [22] and feed-forward linearization techniques [19]-[21], predistortion linearization techniques are more attractive solution due to its simplicity, wideband operation and cost effectiveness. To deal with the high peak to average power ratio (PAPR) signal, predistortion linearization is a classical approach that also maintains a tradeoff between efficiency and linearity. In fact, predistortion is also used to reduce the spectral regrowth of transmitted signal and to combat IMD that leaks into adjacent channels. The predistortion makes it possible for PA to achieve greater efficiency with less output back-off (OBO) power.

1.3 The need for Predistortion Linearization

According to Shannon-Hartley theorem, the need for higher channel capacity can be fulfilled by spectral efficient modulation schemes and wider channel bandwidth [30]. The peak data rate increases linearly with the channel bandwidth. Moreover the use of spectrally efficient modulation schemes such as 64-Quadrature Amplitude Modulation (QAM), 128-QAM results in high PAPR of the signal that pushes the PA into the compression region. It causes a detrimental effect due to the nonlinearity of PA, which results in the reduction of signal to noise ratio (SNR) in the communication channel.

High PAPR requires highly linear magnitude and phase response of the PA which can be achieved by significant back-off output power [31], [32]. Due to the OBO, 90% of DC power is lost in the form of heat, which in turn reduces the efficiency of PA [33]-[36]. The PA have the highest efficiency in its saturation power levels, however PA exhibits nonlinear characteristics in its saturation region leading to IMD in the output signal. The efficiency of the PA relates directly to the operating cost. To avoid this trade-off between efficiency and linearity, predistortion linearization techniques have been widely investigated.

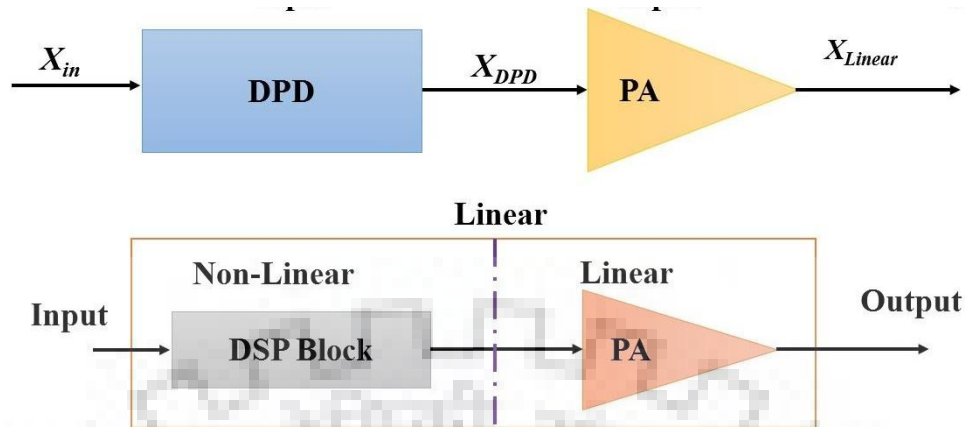


Figure 1.7: The fundamental concept of Digital Predistortion.

1.3.1 Types of Predistortion Linearization

Predistortion is a generic term given to methods and techniques that linearize a PA by making required modification to the magnitude and phase of the input signal. Predicting the overall efficiency of a predistortion system is not a straightforward process. It depends upon a number of factors such as:

- Characteristics of the input signal to be amplified i.e. bandwidth, center frequency, PAPR etc.
- Class of PA that need to be linearized.
- The amount of back-off power required to achieve the desired goal with predistortion system.
- Power consumption of Predistorter.

In all the cases, the efficiency of predistortion system is greater than the efficiency of back-off PA producing the same level of IMD. Predistortion is therefore a valuable efficiency enhancement practice where linearity is an issue in system specification.

The predistortion techniques can be further classified into three types:

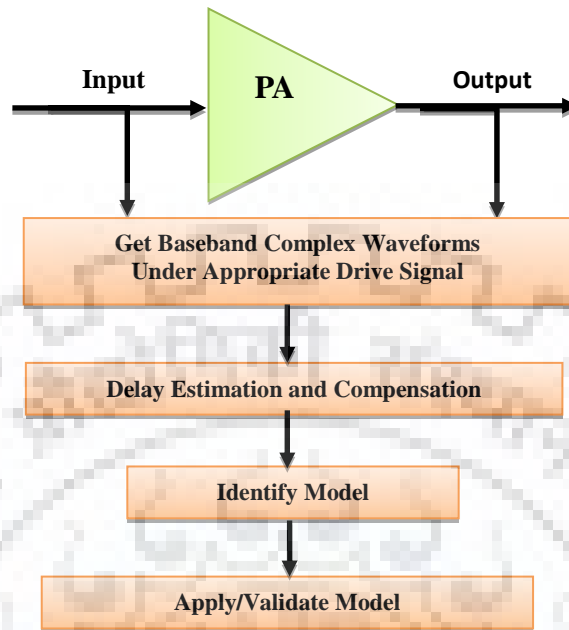


Figure 1.8: Behavioral modeling procedure of device under test.

- 1: Digital Predistortion (DPD) [37]-[49].
- 2: Analog Predistortion (APD) [50]-[54].
- 3: Hybrid Predistortion (HPD) [55]-[57].

1.3.1.1 Digital Predistortion

The attractiveness of the DPD method increases with the time, due to improvement in the device technology. The rapid advancement in the high speed Digital Signal Processing (DSP) technology has associated a new culture to the PA industry under the generic heading of “Digital Predistortion” [37]-[39]. Even the vintage APD and HPD are enjoying a new lease of life due to the introduction of digital techniques in the monitoring and control parameters.

In order to reduce the distortion and improve signal quality, a baseband signal should be passed through DPD linearizer implemented in DSP that, in an ideal case, is the PA’s inverse transfer function shown in Figure 1.7 [40]-[48].

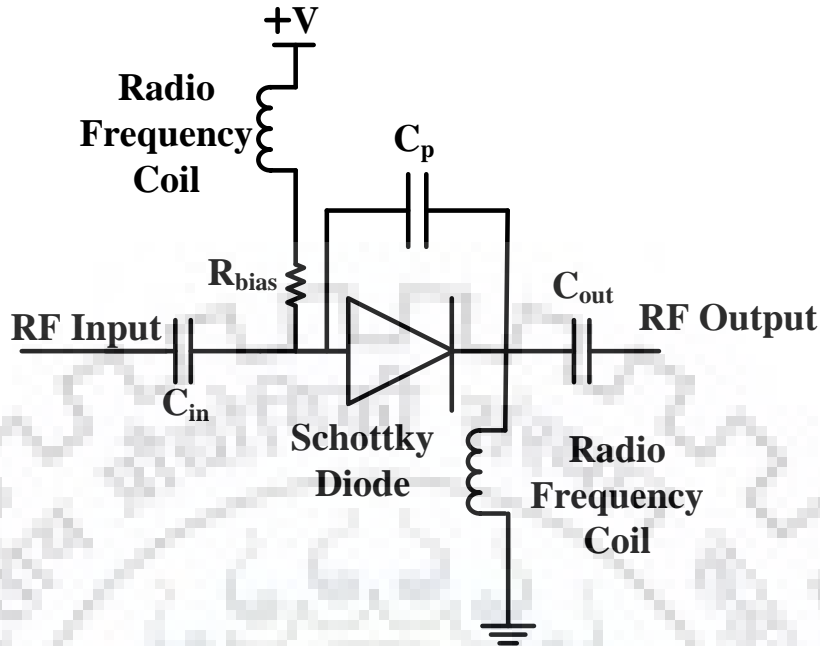


Figure 1.9: Series Diode Analog Predistortion architecture.

The overall transmitter response is linear. The predistortion is performed in the digitized version of the Intermediate Frequency (IF) signal. The efficiency of DPD is limited by the large power consumption of analog-to-digital converter (ADC), digital-to-analog converter (DAC), field programmable gate arrays (FPGA), and transmitter and receiver chains.

In DPD, Behavioral modeling of device under test (DUT) is very important in order to accurately quantify PA nonlinearities and memory effects. The predistortion function is equivalent to behavioural modelling of the PA inverse transfer function which is obtained by the substitution of the PA input and output signals with appropriate small-signal gain normalization [49]. The procedure to achieve the behavioural modelling of the PA is given in Figure 1.8.

1.3.1.2 Analog Predistortion

APD linearization has a long history, which has been extensively used for the nonlinearity compensation of Travelling Wave Tube (TWT) [50]. It is still in use for the linearization of high PA used in the high frequency band. The detailed theory behind APD is treated

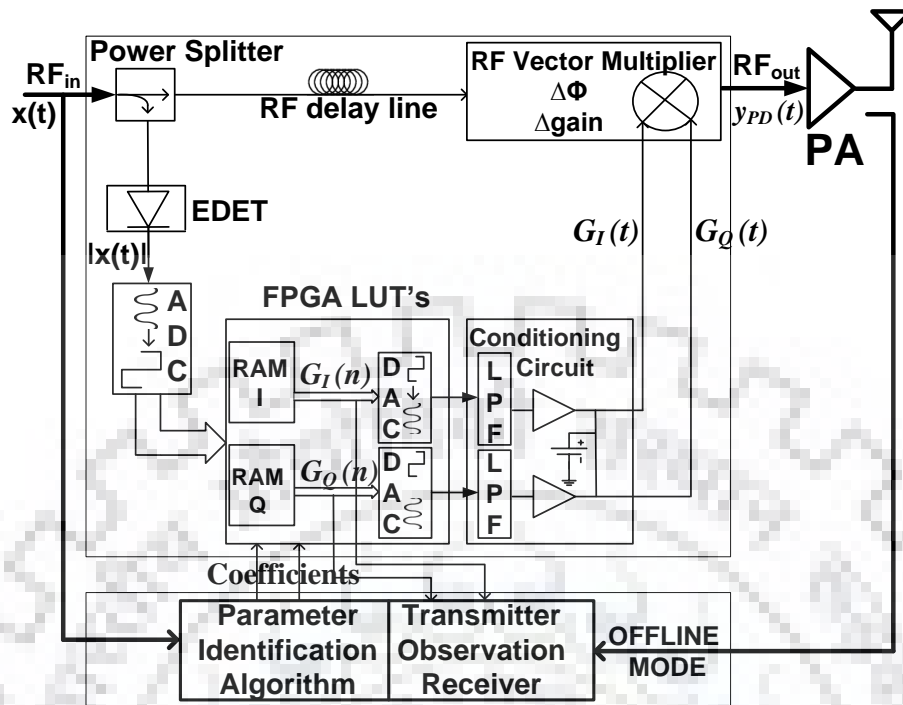


Figure 1.10: Hybrid Predistortion architecture.

in Chapter 2. However, the simplest form of APD is a series diode, which is illustrated in Figure 1.9, with applications in RF and IF domains. The other forms of APD linearizer such as Conventional Analog Predistortion (CAPD), Multi-branch APD, and Cascaded APD etc. are elaborated in the next chapter.

To achieve a negative phase and positive magnitude variation, it uses a simple Schottky diode with a parallel capacitor [51]. The adjustment in the values of parallel capacitance and bias resistance shown in Figure 1.9 allows the APD characteristics to be matched to the PA under consideration. It will neither result in a large efficiency nor in spectacular linearity, but is nevertheless very simple and cost effective [52].

Despite a long history, APD techniques have never reached mainstream use. The APD linearization cannot outperform DPD techniques due to their limited accuracy and dynamic range of analog components. If such analog tactics can provide satisfactory performances, then they may become more desirable solutions for the BS due to their lower power consumption and lower complexity [51]-[54]. The shortcoming of the CAPD is one of the

TABLE 1.2

COMPARISON OF DIFFERENT PREDISTORTION LINEARIZATION TECHNIQUES

Parameters	Analog Predistortion	Digital Predistortion	Hybrid Predistortion
Correction Level	For correcting moderate order nonlinearity	For correcting higher order nonlinearity	For correcting higher order nonlinearity
Complexity	Low	Moderate	High
Hardware requirement	Ultra	Low	Ultra
Input Signal	RF modulated signal	Digital Baseband signal	Input signal is RF under the control of Digital circuits

focus in this work. It presents an analog linearization system that supports the PA to operate at high efficiency and provide better linearity simultaneously.

1.3.1.3 Hybrid Predistortion

HPD is an intermediate solution between analog pre-distortion and baseband DPD, where, the non-linear predistortion function is implemented in the digital domain and corrections are applied in the analog domain [55]. Figure 1.10 shows the architecture of an HPD, which provides higher accuracy than APD and better bandwidth than DPD [56]. The operational bandwidth is not limited by DSP computational speeds, hence provides wideband operation because the signal manipulation is done directly on RF signal under the control of digital circuits. It refers to a technique that synthesizes the predistortion function i.e. envelope memory polynomial (EMP) in the digital domain and uses its output to control the phase and magnitude of an RF modulated signal.

Correction loop includes ADC, DAC, vector multiplier (VM) and envelope detector (EDET), which is used for correcting the signal as per need. It is a mixed signal approach, which involves implementing DPD in the form of look up table (LUT). As shown in Figure 1.10, the predistortion function is implemented in FPGA, however, the correction is applied

using in-phase (I) and quadrature-phase (Q) controls of RF VM which eventually controls the gain and phase of the RF modulated signal. The RF delay line ensures the correction applied to the correct samples after processing delay in FPGA. Since, the EDET in HPD extracts the envelope of the input modulated signal, the predistortion function should depend on the magnitude of the input signal only. Therefore, the nonlinear predistortion function in [56], [57] uses the EMP formulation, which is adaptation of popular memory polynomial (MP) model. EMP model allows simpler and effective hardware implementation as this polynomial function depends only on the envelope of preceding input signals. However, as the order of nonlinearity increases in EMP, it requires a large dynamic range to build up on hardware blocks, which causes limitations in the implementation.

A brief comparison of these three techniques are carried out in Table 1.2

1.4 Objectives

The focus of this work is to expand the scope of Hybrid and APD research, and deployment of predistortion techniques beyond the current 4G systems. The challenges that one faces in the mitigation and characterization of nonlinear effects in RF transmitters is the imperfection of analog components to carry out the proper execution of mitigation techniques. The digital techniques are capable of providing accurate characterization, however, they are limited by bandwidth restrictions of digital circuits. Hence, the reduction in IM product while investigating the practical limitations of analog and digital techniques and proposing the solutions to circumvent such limitations is the research focus. The research objectives are listed below:

Objective 1: Study of viable components and development of suitable system level solutions: The predistortion solutions require the design and procurement of various active and passive components. Such components should be designed or chosen according to some predefined criterion. As the success of the solution depends heavily on such components, characterization of each component is required. In case of inherent limitation of any component, system level description may need to be modified.

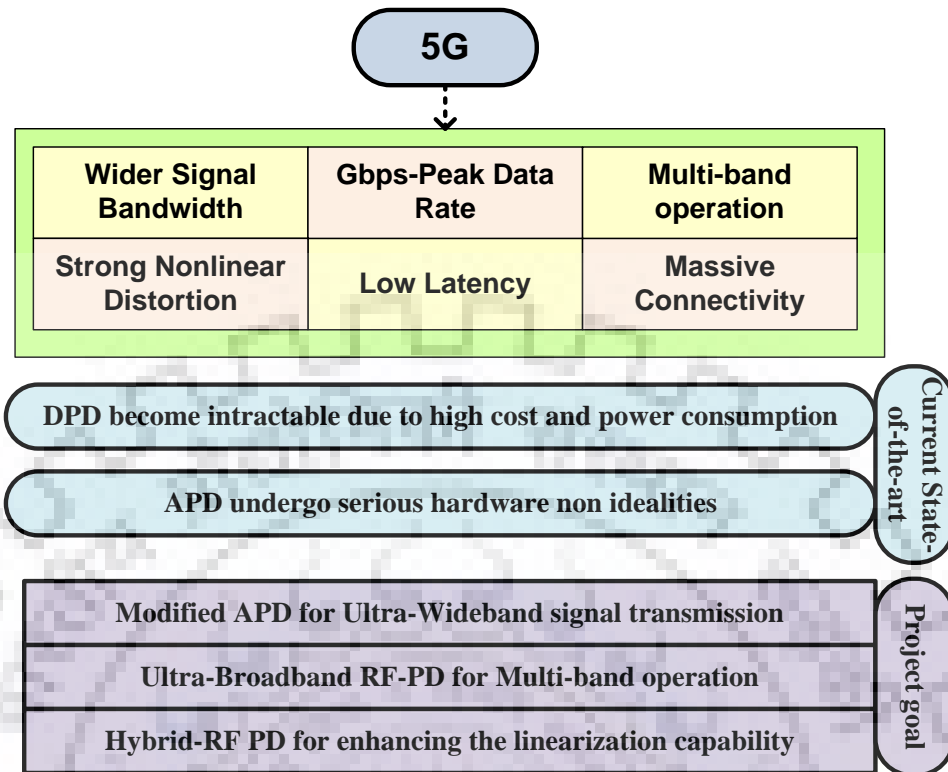


Figure 1.11: Roadmap for the proposed work contribution.

Objective 2: Development of HRF-DPD architecture, which is a combination of analog and digital counterpart. As previously discussed, APD provides low-cost, broadband, smaller size linearization solution at the cost of limited linearization performance, whereas DPD provides a better linearization solution at the cost of higher cost and limited bandwidth. One of the main theme of this research is to investigate a method to take the best of both the methods to provide a compromise between bandwidth, cost and size criterion.

Objective 3: Extension of third order IMD cancellation scheme of APD to higher order IMD cancellation for broadband signals (4G/5G). The state-of-the-art techniques focus on reducing the third order intermodulation (IM3). This is considered sufficient condition as 3rd order distortion components are proven to be highest among all IMD terms. However, with a focus on transmission efficiency, highly nonlinear PAs are being designed, therefore there is a need to investigate techniques to account for higher order IMD terms.

Objective 4: Scope for enhanced spectral efficiency (4G/5G) schemes such as carrier aggregation/multiband transmission for within proposed linearizer. Apart from enhancing transmitter power efficiency, enhancing spectrum efficiency is also focus of current and upcoming communication generations. Performance analysis of proposed predistortion systems for spectrum efficient advanced techniques such as multiband operation or carrier aggregation (CA) should be carried out.

Objective 5: Identification and efforts towards removing practical implementation road-blocks of proposed linearizers. The state-of-the-art Digital DPD models in current linearizer imposes restriction on data converters such as ADC, DAC, FPGA, and transmitter and receiver chains for carrier CA Ultra-Wideband (UWB) signal transmission. Similarly, state-of-the-art CAPD undergoes serious hardware non idealities that compromise the quality of signal. One of the focus is to study the limitations of practical implementation and propose suitable solutions.

1.5 Contribution

A visual illustration of the roadmap of the proposed work is given in Figure 1.11. The proposed work will detect the limitations of the previous state-of-the-art linearization techniques and will propose and validate a new analog and hybrid linearization schemes to address those constraints. The implementation of the RF-in RF-out APD, Ultra-Broadband RF-Predistorter (UBB RF-PD), and Hybrid RF-Digital Predistortion (HRF-DPD) has been carried out with the aim to get better performances in terms of Adjacent Channel Power Ratio (ACPR), Error Vector Magnitude (EVM), IM3 and fifth order intermodulation (IM5) product.

1.5.1 Low Cost RF_{in} - RF_{out} Predistorter Linearizer for High Power amplifiers and Ultra-wideband Signals

To facilitate higher data rates in future 5G communication, the demands for the wideband signals are continuously increasing which creates challenge in employing DPD for the linearization of RF PA in Ultra-broadband (UBB) systems. System bandwidth constraint of

conventional DPD does not provide sufficient linearization of wideband signals. Hence, a low cost RF_{in} - RF_{out} APD architecture has been designed to target higher order IM products of high PA in the 5G BS, which requires higher bandwidth operation. Compared with the existing APD, proposed RF_{in} - RF_{out} APD exhibit better ACPR performance and provide cost effective linearization solutions using passive components. It poses several advantages over digital and hybrid envelope predistortion methods that includes compact size, simple circuitry and ability to process UWB efficiently. The requirement of data converters, FPGA and reconstruction filters are relaxed in the proposed APD architecture. On the other hand, it suffers from the limitation on the amount of IMD reduction achievable compared with the digital system. The performance of the proposed APD is appraised in terms of EVM, IM and ACPR. The proposed APD is verified using two tone signal with frequency spacing of 100 MHz, contiguous and non-contiguous 8 component carrier (CC) 160 MHz signal. Measurement results demonstrate the system dexterity and targets the higher order intermodes.

1.5.2 On Control Schemes for Modified Analog Predistortion Linearizer in 5G transmitters

The performance of the conventional APD is dependent on appropriate control of gain and phase of predistortion signal. State-of-the-art work in Analog/ Hybrid linearization solutions mostly utilizes VM for such a control. This work points out the limitations of such a scheme and proposes two control schemes capable of extracting better benefits of the APD scheme. These two control schemes are more feasible than the conventional APD, as Type-I control scheme uses the same hardware which was used in conventional APD to linearize wideband signal which is not possible with conventional APD. In Type-II control scheme, independent control over the gain and phase of predistortion signal provides better linearizability as compared with conventional APD. An experimental validation is carried out by linearizing ZX60V-2534MA-S+ PA from Mini-circuits, excited by 5CC 100 MHz and 8CC 160 MHz signal.

1.5.3 Ultra-Broadband RF-Predistorter Supporting Carrier Aggregation for Future 5G System

In this work, two RF-in-RF-out predistorter architectures are proposed for the linearization of UWB signals that can effectively suppress the PA intermodes from 200 MHz to 2.5 GHz. First scheme is UBB RF-PD which is suitable for intra-band CA communication, while second scheme is Ultra-Broadband Multipath RF-Predistorter (UBB MRF-PD) that works well for inter-/multi-band communication. These schemes provide an attractive solution for PA in 5G BS driven by CA signals. It also provides a linearizer solution for repeaters in long distance communication, where baseband data is not readily available. Similar to APD, it also eliminates the use of data converters, FPGA, but still provides the well-intentioned linearization using the energy efficient passive intermodulation generator. Three application scenarios have been investigated (a) intra-band: contiguous 160 MHz 8CC, Long-Term Evolution (LTE) signal, (b) intra-band: two-tone signal with frequency spacing of 100 MHz, and (c) inter-/multi-band: 2 CC LTE signal with frequency spacing of 900 MHz, where lower and upper CC is occupying 1.4 MHz and 160 MHz instantaneous bandwidth respectively. For verification, the proposed UBB RF-PD and UBB MRF-PD is implemented with a 10-W HMC8500 GaN PA and ZFL-11 AD+ PA.

1.5.4 A Modified Hybrid RF Predistorter Linearizer for Ultra Wideband 5G Systems

A wideband HRF-DPD linearization technique is reported to compensate for the nonlinearity of UWB PA for 5G systems driven by CA and wideband modulated signals. The proposed methodology is suitable for 5G PA design since its power overhead and system bandwidth does not increase with an increase in the signal bandwidth. Taking advantage of recent available DSP solutions, the proposed method reduces hardware requirements of the conventional APD by alleviating the need of VM, branch line coupler and delay lines. Such linear operations are controlled digitally, which provides flexibility in terms of digitally compensation of delay, gain and phase control of the signal. For

establishing a proof of concept, HRF-DPD is implemented with a 15-W Class-AB PA and tested using a 100 MHz and 50 MHz long term LTE-CA signal at 2 GHz.

In addition to improving the in-band and out-of-band performance, it also eliminates the system bandwidth constraint, which is a major drawback of conventional DPD. The proposed method also supports the filter-less linearization of UWB PA for reconfigurable frequencies. In a nutshell, the proposed solution significantly improves the system accuracy and provides a lower overhead power consumption and lower cost solution that is practically viable for future 5G applications. This contribution has been reported in the IEEE Journal on Emerging and Selected Topics in Circuits and Systems [59], which is elaborated in Chapter 5.

1.6 Outline and Structure

The remainder of the proposed work is based on the five objectives discussed above. It consists of six chapters. Each chapter initiates with a brief overview of the concerned problem and motivation behind the study. Subsequently, the simulation framework, measurement test-bench, analysis, and measurement results are presented and discussed. A brief discussion of each chapter is presented below:

Chapter 2 presents a novel RF-in RF-out APD proposed architecture for UWB signal transmission and description of each component used in the design. It also provides a comprehensive comparison of the proposed APD scheme with the state-of-the-art linearization. The superiority of the proposed APD is established by elaborating eliminate the constraint on system bandwidth of conventional DPD.

Chapter 3 deals with the control schemes that provides appropriate phase and gain control of the IMD generated by the predistortion architecture, to cancel the IMD of PA. These two control schemes are compared in terms of control sensitivity, complexity and linearization capability. This chapter highlights some inherent limitations of the conventional and proposed RF-in RF-out APD and therefore proposes another control scheme with slight enhancements to overcome the constraints of VM.

Chapter 4 presents a new technique for multiband communication which is known as UBB MRF-PD. The proposed RF-predistortion schemes are easier to integrate with multiband PA due to its ability to operate in UWB environment ranging from 200 MHz to 2.5 GHz.

Chapter 5 provides a novel HRF-DPD linearizer which makes best of ‘analog’ and digital’ signal processing techniques. The proposed method is used to linearize the UWB PA distortions by cancelling its in-band and out-of band distortion. It also provides a comprehensive comparison of the proposed HRF-DPD architectures with previous state-of-the-art HPD architectures.

Chapter 6 concludes the reported work. Conclusions are drawn based on the analysis and preceding results, and finally sketches potential avenues for future work and further research.



Chapter 2

RF-in RF-out Analog Predistorter for Wideband Signal Transmission

2.1 Publications from the Work

Journal Publications:

1. K. Gumber and M. Rawat, "Low cost RFin-RFout predistorter linearizer for high power amplifiers and ultra-wideband signals," *IEEE Trans. Instrum. Meas.*, vol. 67, no. 9, pp. 2069-2081, Mar. 2018.
2. K. Gumber and M. Rawat, "A modified hybrid RF predistorter linearizer for ultra-wideband 5G systems," *IEEE J. Emerg. Sel. Topics Circuits Syst.*, vol. 7, no. 4, pp. 547-557, Dec. 2017.

Conference Presentations:

3. K. Gumber and M. Rawat, "Modified RF_{in}-RF_{out} broadband predistorter for 5G communication system," *IEEE International Symposium on Circuits and Systems (ISCAS)*, Florence, Italy, May 2018.
4. K. Gumber, P. Jaraut, M. Rawat, and K. Rawat, "Digitally assisted analog predistortion technique for power amplifier," *IEEE 88th Microwave Measurement Conference (ARFTG)*, Austin, TX, USA, Dec. 2016.
5. K. Gumber and M. Rawat, "Digital predistorter design using linear splines and its fixed point implementation," *Asia-Pacific Microwave Conference (APMC)*, New Delhi, India, Dec. 2016.
6. The abstract has been selected for presentation at the *National Conference for Communication (NCC) 2019* Graduate Student Day workshop will be held at IISc

Bangalore, titled “Low cost RF predistortion for carrier aggregated ultra-wideband signals”.

Publication in Pipeline:

7. K. Gumber and M. Rawat, “Broadband RF Predistorter Supporting Carrier Aggregation for Future 5G system” *IEEE Trans. Instrum. Meas.* (Submitted).
8. K. Gumber and M. Rawat, “Modified Analog Predistortion Linearizer Control Schemes for Wideband Signal Transmission in 5G,” *IET Microw. Antennas Propag.* (Submitted).

2.2 Introduction

Any contemporary design of the predistortion linearizer is required to provide a performance advantage over the existing linearization system. To achieve the aggressive target of 5G-communication systems such as wider signal bandwidth, massive connectivity, low latency etc. the design targets for the predistortion systems are as follows [60]:

Linearization Performance: Required adjacent levels specified by 3 GPP that provide sufficient linearity and dynamic range by cancelling in-band and out-of-band distortion components. A predistortion System that allows the PA to achieve higher efficiency while operating at higher average output power is a must requirement for PA in any front end of a radio transmitter.

Ability to process wideband signals: With the 5G, the definition of ‘wideband’ signal includes much higher bandwidth. LTE-CA will push the signal bandwidth up to 100 MHz for the time division duplex system. The system bandwidth should be wide enough to accommodate wideband signal of 100 MHz specified by the 5G system.

System complexity and cost: To handle the new requirements of 5G, the BS usage and equipment cost upgrades should be such that it is profitable. All the components, which contribute to the system, must be less complex and cost effective. In the CAPD architecture, passive analog components are used to generate the predistortion signal. It

alleviates the need for ADC, DAC and FPGA that reduce the complexity, operational expenditure (OPEX) and capital expenditure (CAPEX).

System efficiency: The predistortion architecture should be able to minimize the power consumption that enhances the overall efficiency of a system. It can be implemented with analog components having low dissipated power. The efficiency of the system can also be raised by increasing the level of P1dB compression point.

These design aspects affect the overall performance of the system. A fundamental advantage of the CAPD architecture is its ability to linearize wideband signal, simple structure and low cost implementation. The requirement of FPGA, data converters (DAC and ADC), reconstruction filters, wideband transmitter and receiver paths are relaxed in the APD architecture. It is, therefore, a potential candidate for use in multicarrier repeater systems, satellite communication [61]-[63] etc.

2.3 Conventional Analog Predistorter

The simplest practical form of the CAPD is shown in Figure 2.1. The CAPD, as shown in Figure 2.1, consists of two paths: upper path which is also known as linear path and lower path which is called nonlinear IM generation path [64], [65].

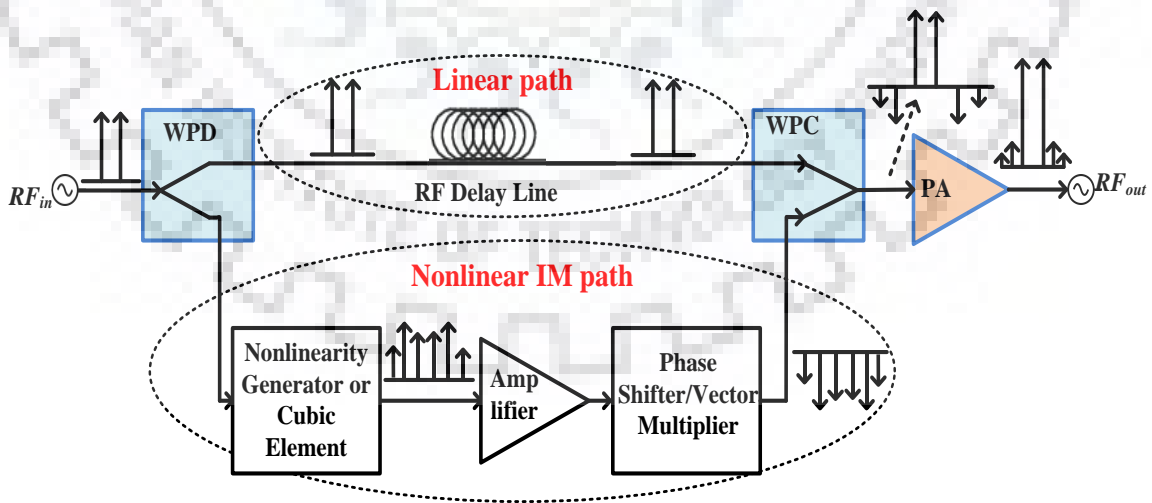


Figure 2.1: Conventional Analog Predistorter architecture.

The linear path of CAPD is composed of a delay line that carries the fundamental signal, while, the nonlinear IM path is composed of a Phase Shifter (PS)/VM, nonlinearity/cubic element and variable gain amplifier (VGA). The input signal is divided into two paths using WPD. The nonlinearity generator cancels the fundamental signal and generate the required IM products, which is given in the input of PS/VM via VGA. In the CAPD, PS/VM was used after cubic element to optimize the phase of the expanded signal containing all the necessary IMD components. CAPD is an attractive solution as the predistortion signal is not generated in the digital domain and need not go through DAC [6]. CAPD has two main functions

- (1) Generating intermodulation distortion signals that are similar to the distortion signal generated by the PA under test.
- (2) Appropriate phase and gain control of these IMD signals to cancel the IMD generated by the PA.

To compensate for the distortion generated by the nonlinearity of PA, the new IMD product is introduced by a combination of VGA and cubic element. The PS will provide the necessary phase shift to the nonlinear signal coming from cubic element. The phase of the nonlinear signal is adjusted by PS in such a way that it counteracts the nonlinear distortion of PA. This signal combines with the signal coming from the linear path using Wilkinson Power Combiner (WPC) and given at the input of the PA. The CAPD has been popular for use in linearizing TWT amplifiers because linearization criterion for Satellite communication application is rather relaxed and it is sufficient to focus on IM3 characteristics only. The performance of CAPD is limited to the higher order IM products, hence it is not an appropriate choice for solid-state high PA. In order to enhance the linearization performance of CAPD and to target higher order IMDs, it has been implemented in various configurations: fifth-order, multi-branch APD, cascaded APD, etc.

2.3.1 Fifth-order Analog Predistorter

The fifth order APD shown in Figure 2.2 removes the limitation of CAPD, at the cost of the additional nonlinear path. Individual paths are deployed in fifth-order APD for the

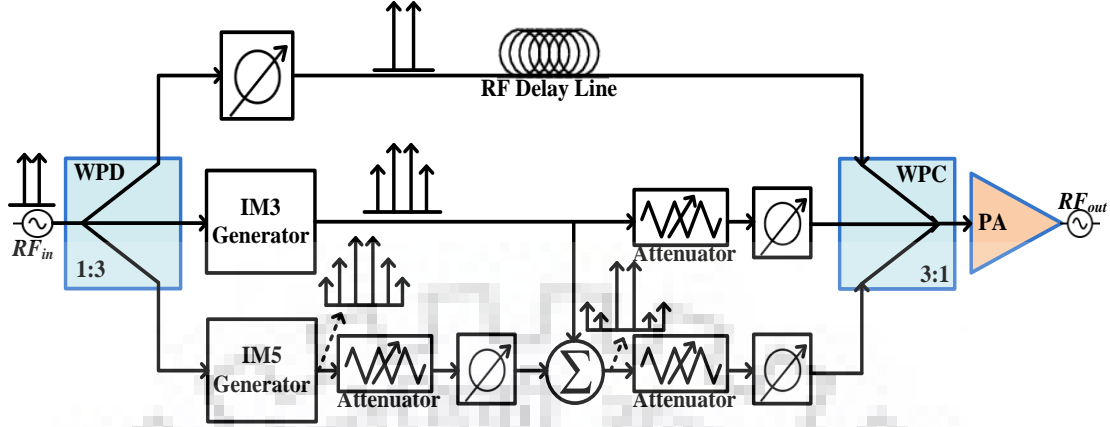


Figure 2.2: Fifth-order Conventional Analog Predistorter architecture.

generation of IM3 and IM5 in order to simultaneously compensate for the IM3 and IM5 of PA [66]. The basic operation is similar to CAPD, but it exhibits one more nonlinear path. The additional nonlinear path can provide the IM5 with the help of IM5 generator. The output of IM5 generator is given at the input of attenuator and PS for monitoring the gain and phase of IM5 components. Similarly, the output of IM3 generator are monitored using an individual PS and attenuator in a separate branch. The output of IM3 and IM5 generator are combined with the fundamental signal and given at the input of PA. However, addition of nonlinear path results in complex and bulky circuit.

2.3.2 Multi-branch Analog Predistorter

By adding the nonlinear paths in to the CAPD, multi-branch APD have been developed with different delay difference in each nonlinear path. These delay differences compensate the memory effects of the PA. Two versions of multi-branch APD are proposed in [67], [68], which are shown in Figure 2.3 and Figure 2.4.

Multi-branch APD 1: The first version of multi-branch APD is shown in Figure 2.3, where each nonlinear path employs a separate VM [67]. In the nonlinear path, the output of error generator is further divided into three paths using 1:3 WPD, where each path employs the individual VM and delay lines with various delay differences. The nonlinearity in each path remains same, but it can be advanced or delayed depending upon the requirement. The VM provides the gain and phase monitoring to the predistorted signal in each nonlinear path.

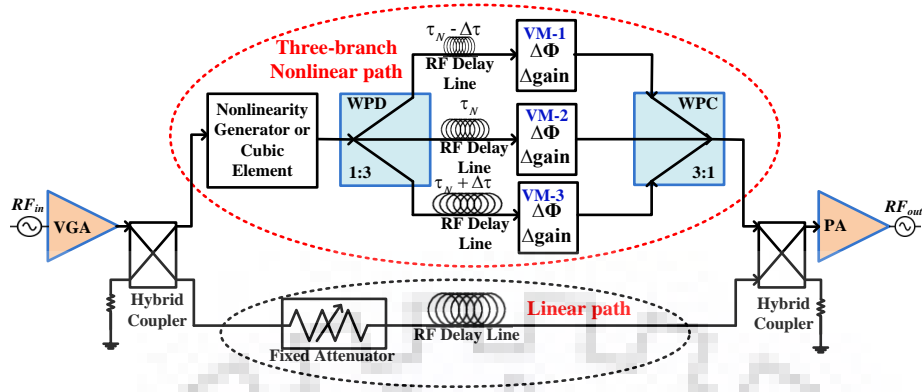


Figure 2.3: Multi-branch Analog Predistorter architecture with three branch nonlinear path, where each path consists of separate delay line and Vector multiplier.

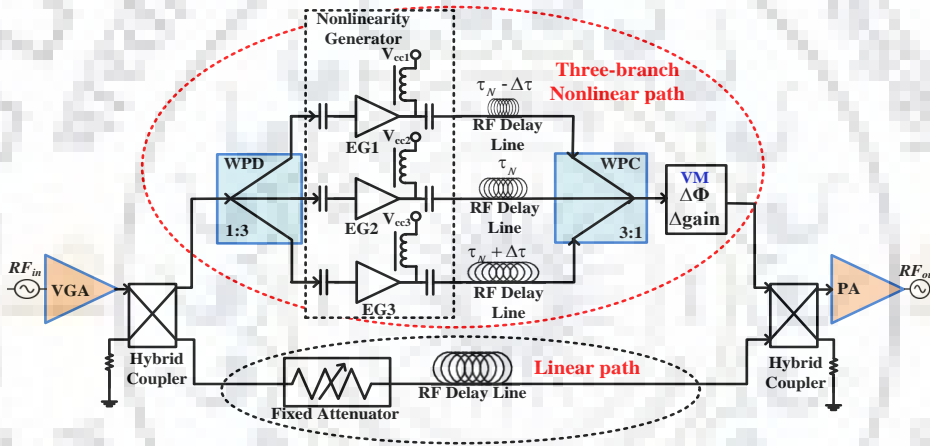


Figure 2.4: Multi-branch Analog Predistorter architecture with three branch nonlinear path, where each path consists of separate delay line and error Generator

Depending upon the delay difference, the gain and phase requirement in each path can be different. The output of VM is further combined using 3:1 WPC, to generate a predistortion signal. The predistortion signal, contains the high order, instantaneous and past sample of the input signal that helps to compensate the memory effects of PA. The predistortion signal is further combined with the fundamental signal and given in the input of the PA.

The linearizability of the PA can be improved by controlling the delay difference and number of nonlinear paths according to the memory effect and input signal bandwidth of the modulated signal.

Multi-branch APD 2: The second version of multi-branch APD is shown in Figure 2.4 that exhibits a separate error generator in each path [68]. In each nonlinear path, gain amplifier is used as a nonlinear element, where nonlinearity of an amplifier is generated with the help of low supply voltage. Similar to version 1, each path employs a separate delay lines with a different delay difference that helps to improve the linearizability of system by compensating the memory effects of PA. The nonlinear path composed of three transistors based error generator connected in parallel with a different delay line and a VM. The nonlinearity of the transistor base gain amplifier is generated with the help of low supply voltage which are summed up with a different delay difference. The combined signal is given to the input of VM for phase and gain monitoring and then transformed into the predistortion signal. It is simple and cost effective than version 1 due to control parameter as it requires only one VM. Instead of using an individual VM in each branch it deploys a single VM in the nonlinear path that monitors the gain and phase of the predistortion signal.

2.3.3 Cascaded Analog Predistorter

It is the cascaded combination of the two CAPD, which is used to cancel the IM3 and IM5 of PA [69]. Figure 2.5 shows the schematic of cascaded APD that provides the high order predistortion function. The input signal after the linear path and the predistortion signal after the nonlinear IMD path are $V_{lin}(t)$ and $V_{n-lin}(t)$ respectively. The $V_{out}(t)$ is the sum signal after each CAPD and $F_N(\bullet)$ is the corresponding nonlinear function of each nonlinearity generator/cubic element.

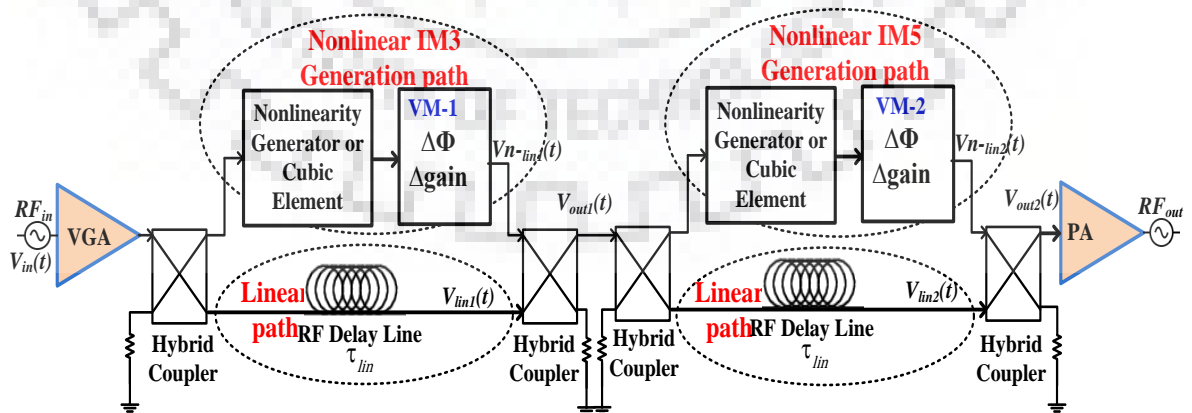


Figure 2.5: Cascaded Analog Predistorter architecture.

Therefore, the signal at the output of cascaded APD can be expressed as:

$$V_{out2}(t) = V_{lin2}(t) + V_{n-lin2}(t) \quad (2.1)$$

$$V_{out2}(t) = V_{out1}(t - \tau_{lin}) + F_{N2}(V_{out1}(t)) \quad (2.2)$$

$$V_{out2}(t) = V_{in}(t - 2\tau_{lin}) + F_{N1}(V_{in}(t - \tau_{lin})) + F_{N2}[(V_{in}(t - \tau_{lin})) + V_{N1}(V_{in}(t))] \quad (2.3)$$

The first term is the fundamental input signal after associated delay time and the second term corresponds to IM3 generation. The last term corresponds to IM5 generation, which is produced by the IM3 and fundamental part. To simplify the realization of fifth order APD, two 3rd-order CAPD can be placed in cascade to generate fifth order nonlinearity [69]. Higher number of 3rd-order CAPDs can be cascaded, if the requirement is to realize functions with nonlinearity order higher than five.

2.3.4 Limitations of the Conventional, Cascaded and Multi branch Analog Predistortion

The above configurations of APD can effectively compensate IM5 of PA, if the input signal is narrowband. For example, consider a case where the bandwidth of the input signal is 10 MHz, the error generator expands the signal bandwidth to 50 MHz, which should be accommodated by the PS/VM in the nonlinear IMD path of APD.

Consider a case, when the input signal is wideband whose bandwidth approaches 100 MHz. To compensate IM5 in APD, the cubic/nonlinear element expands it to 500 MHz. This expanded bandwidth signal is given in the input of PS/VM. As PS/VM is a narrow band component, it is unable to accurately capture and adjust the phase of the 500 MHz UWB signal. Therefore, the APD is unable to provide linearization in wideband stimulus.

One problem, which is more usually seen in the CAPD, is that it is not able to provide simultaneous suppression of IM3 and IM5 of the PA, which is necessary to improve the linearity of a modulated signal [64]-[69].

If the diodes in the anti-parallel configuration are not perfectly matched, it will generate the

residual second order IMD that can interact with the PA nonlinearity and generate unwanted IMD components.

Increasing the number of nonlinear branches in the multi-branch and fifth order APD adds the cost and complexity to the system. Moreover, the delay lines which are used in these APD are bulky too.

These drawbacks of the CAPD, multi-branch and fifth order APD is addressed in the proposed RF-in RF-out APD, in which narrow band VM is used in conjunction with an IM generator to linearize the wideband signal.

2.4 Proposed RF-in RF-out Analog Predistorter

The proposed RF-in RF-out APD is shown in Figure 2.6 which is a modification of the CAPD given in [64]-[71]. The modification is the mutual exchange in the position of the VM and the IM generator passive circuit which is a 3dB 180° rat race coupler (RRC) mounted with a resistor (R), capacitor (C) and anti-parallel diode pair in the nonlinear IMD generator path. This change is adopted to capture the wideband signal depending on the bandwidth of VM and passive IM generator. The principal advantage of the proposed RF_{in}-RF_{out} APD is as follows:

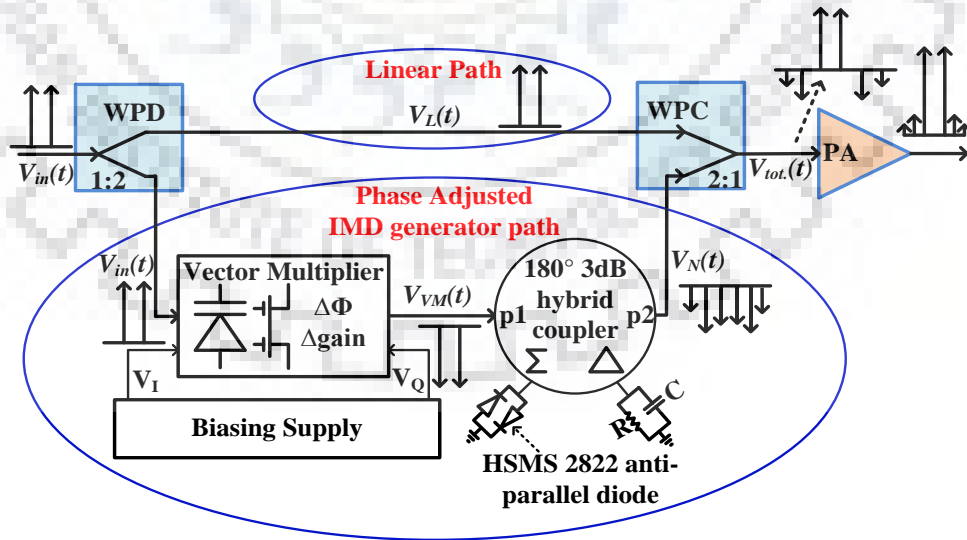


Figure 2.6: Proposed RF-in RF-out Analog Predistorter architecture.

Unconditionally stable: It is an open loop predistortion technique, hence does not pose any stability issues like feedback linearization.

Ease of Implementation: It is perceived to require fewer components, which can be relatively low cost. Due to the elimination of bulky delay lines means that it can easily plug with microwave circuits without difficulty.

Wideband Linearization capability: The modification in the proposed RF_{in}-RF_{out} APD favor the linearization of wideband signal.

The key benefit of the proposed RF-in RF-out APD is that it does not require the knowledge of baseband signal, ability to process UWB signal and can be plugged before any PA for any RF signal.

2.4.1 Working Principle of the Proposed RF-in RF-out APD

The proposed RF-in RF-out APD consists of upper and lower path: upper path carries the original fundamental signal and lower path is the phase variable IMD generator path which carries nonlinear information. The objective is to discard the fundamental signal in the lower IMD generator path, thereby providing independent control of the IMD components relative to the original fundamental signal. The input signal is divided into two paths, i.e. upper and lower path using a WPD. The upper path is the linear path which carries the original fundamental signal via SMA coaxial cable. The lower path is a combination of VM (MAX2046) and IM generator passive circuit, this combination optimize the magnitude and phase of the original fundamental signal. In the lower path, VM provides suitable modification in the amplitude and phase of the original fundamental signal to obtain the exact inverse predistortion signal that counteracts the 3rd IMD nonlinear distortion of PA. The phase adjusted output of VM is given as input to IM generator. IM generator is a passive circuit composed of four ports that is fabricated to generate odd order intermodes and to cancel the fundamental signal. The output of IM generator is combined with the original fundamental signal using WPC and given on the input of the PA.

In the proposed RF-in RF-out APD, the VM need to be operable for the bandwidth of the

input signal, while in the CAPD this requirement is $5\times$ signal bandwidth. In the proposed RF-in RF-out APD, there is a need to optimize the phase and amplitude of the original fundamental signal in the phase optimized IMD generator path. Correspondingly, the phase of IMD is adjusted as compared to that of the fundamental signal. But in the CAPD, there is a need to adjust the phase and amplitude of the distorted signal with much wider bandwidth that contains the high order IM products. The bandwidth of the proposed APD can be detected from the maximum operable bandwidth of the IM generator circuit and VM..

It is to be noted that it is different from a feed-forward architecture [72], [73] where the correction signal is applied at the PA output, therefore the correction signal is required to have enough power to be able to cancel the IMD components at the PA output. In the proposed architecture, a correction is applied at PA input. The key benefit of the RF-in RF-out APD is that it does not need to provide power to IMD terms (as in Feedforward technique) and it does not require the knowledge of baseband signal (as in DPD). If the predistortion circuit is designed appropriately, the IMD generated by predistortion circuit can suppress the IMD components that are generated by the PA [74]. It provides nonlinearity cancellation in the analog domain, therefore it can provide moderate linearity improvement as compared to HPD and DPD. The signal at the input of PA, according to Fig. 2.6, is the combination of linear and nonlinear IMD generator path that is given by:

$$V_{tot.}(t) = V_L(t) + V_N(t) \quad (2.4)$$

$$V_{tot.}(t) = V_{in}(t - \tau_L) + F(V_{in}(t - \tau_N)) \quad (2.5)$$

where V_{in} is the fundamental signal at the input of APD, τ_N and τ_L are the corresponding delay in nonlinear IMD generator and linear path respectively. The delay in the IMD generator path (τ_N) is due to VM and 3dB coupler hence (2.5) can be written as:

$$V_{PD}(t) = V_{in}(t - \tau_L) + F(V_{in}(t - \tau_{VM} - \tau_{RRC})) \quad (2.6)$$

where $F(\cdot)$ is a nonlinear function, depicting nonlinear distortion generator in the IMD path. The first term is fundamental part and the second term corresponds to IM generation. The

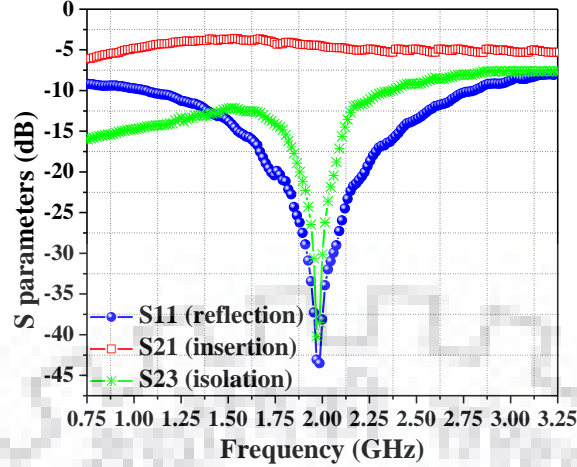


Figure 2.7: Measured S-parameters of WPC/WPD.

group delay of the system has a relation to the phase of the system. The crude delay of the nonlinear path is compensated using VM. The fine-tuning of delay in the nonlinear branch can be compensated by varying the phase angle of the predistortion signal using VM. By varying the V_I and V_Q of VM in the nonlinear path, we can control the phase of predistortion signal. By doing so, the signal from two branches can be combined easily with appropriate phase.

2.4.2 Components End Use in the Proposed APD

The description of all the components used in the RF-in RF-out APD is as follows:

Wilkinson power divider/combiner: The WPD splits the input RF signal into two branches, one is the linear path and the other is the nonlinear IMD generator path. In the linear path, the input fundamental signal directly goes to the input of WPC via SMA coaxial cable, and the same signal approaches through VM and IM generator in the nonlinear path. The signal from these two paths are combined using WPC. The measured S- parameters of WPD/WPC are shown in Figure 2.7.

Vector Multiplier: It is used to vary the magnitude and phase of the RF signal [75], [76]. In CAPD architecture, VM is used after IM generator to shift the phase and amplitude of signals containing all necessary IMD components. To adjust the phase of higher order IMD, the VM needs to capture the signal whose bandwidth is around 5 times to that of the

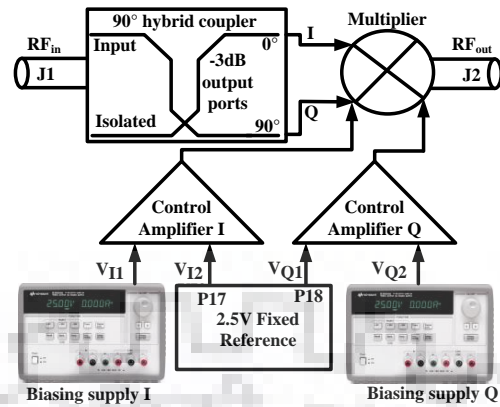


Figure 2.8: Single ended control voltage mode operation of MAXIM2046 VM.

input signal bandwidth. This was not a limitation earlier because the maximum bandwidth of the signal is not more than 20 MHz. For 20 MHz input signal, the IM generator produces the signal of bandwidth 100 MHz and the VM needs to capture this signal to target higher order IMD₅. But the 5G communication standard demands the wider signal bandwidth that can go beyond 100 MHz under sub 6 GHz band. Hence, the IM generator produces the signal of bandwidth 500 MHz or more. The VM is not able to capture that much high bandwidth signal because the maximum capturing bandwidth of MAX2046 VM is only 320 MHz. So, the viable solution is to use VM before IM generator such that VM changes the amplitude and phase of the fundamental signal before IM generator. By doing this, the VM needs to process only 100 MHz signal instead of 500 MHz signal.

Working principle of MAX2046 VM: The internal circuitry of the VM is shown in Figure 2.8. It consists of 20-pin lead header connector which is used to vary the gain and phase of the input RF signal. Initially, R6 is open as shown in Figure 2.9. By installing a 0Ω resistor in place of R6, we are able to achieve 2.5V reference output voltage at pin 17 and pin 18 (P17 & P18). This on-chip voltage is required for single ended control voltage mode operation.

From P17 and P18, this fixed voltage is provided to V_{I2} and V_{Q2} which is pin 2 and pin 6 (P2 & P6) respectively.

Another way to get fixed 2.5V on-chip reference supply at P2 & P6 is done by installing a 0Ω resistor in place of R2 and R4. It makes 2.5V permanent at V_{I2} and V_{Q2} . Individual

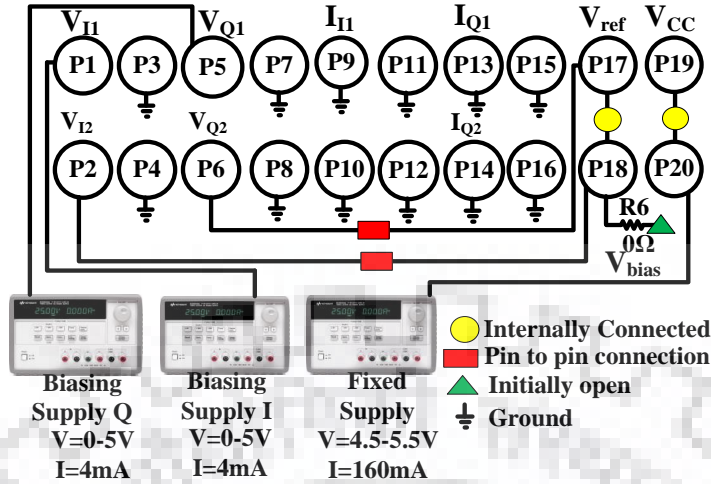


Figure 2.9: Working of 20 lead header connector of MAXIM2046 VM.

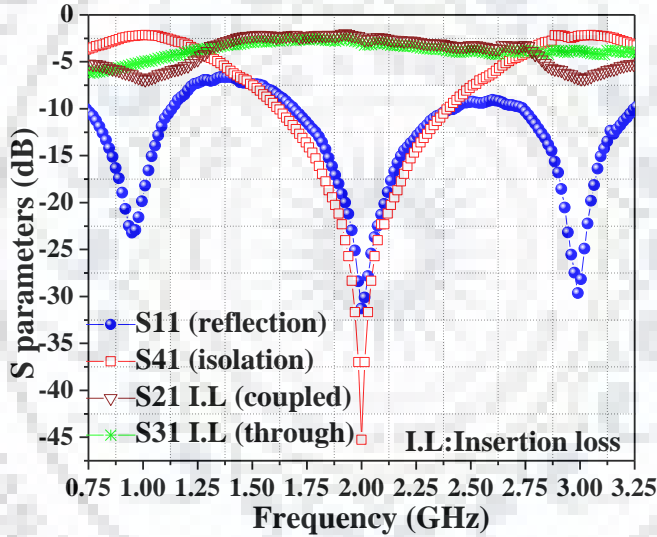


Figure 2.10: Measured S-parameters of 3dB RRC.

variable biasing supply I and Q are connected to V_{I1} and V_{Q1} which is pin 1 and pin 5 (P1 & P5) on 20 pin connector as shown in Figure 2.9. It can be varied from 0 to 5V to adjust the magnitude and phase of the fundamental signal. The magnitude and phase of the input fundamental signal is dependent on the difference between the biasing voltages, i.e. $|V_{Q2}-V_{Q1}|$ and $|V_{I2}-V_{I1}|$. One more supply is also required which is connected to pin 19 or pin 20 that is capable of delivering 4.5V-5.5V and 160mA. P19 and P20 are internally connected. For single ended voltage mode operation ground all the current control I and Q

pins, i.e. $I11$, $IQ1$, $I12$ and $IQ2$. If the operation is the single ended current mode, in this case open all the voltage control I and Q pins, i.e. $V11$, $VQ1$, $V12$ and $VQ2$ [77].

180° 3-dB hybrid coupler or rat race coupler/IM Generator: It is a four-port passive circuit that has been designed and fabricated for the suppression of fundamental signal and a generation of IMD components in the nonlinear IMD path. The measured S- parameters of the 3dB-180° hybrid coupler are shown in Figure 2.10. The detailed description of the IM generator is featured in Section 2.4.

The output of VM is given as input to port 1 of IM generator. From port 4 of IM generator, the output is provided at the input of WPC that combines predistortion signal with the fundamental signal. The bandwidth of the proposed RF-in RF-out APD architecture can be observed from the maximum capturing bandwidth of VM and IM generator.

2.4.3 Analysis using two tone signal

The signal given in the input of the proposed RF-in RF-out APD consist of two tones situated at frequency f_1 and f_2 is given as:

$$V_{in}(t) = \text{Re} \left\{ A(t) \left[\left(e^{j\omega_1 t} + e^{j\omega_2 t} \right) e^{j\phi_m[A(t)]} \right] \right\} \quad (2.7)$$

$$V_{in}(t) = A(t) \left[\cos(\omega_1 t + \phi_{in}[A(t)]) + \cos(\omega_2 t + \phi_{in}[A(t)]) \right] \quad (2.8)$$

where $A(t)$ and $\phi_{in}(t)$ is the amplitude and phase of the input signal. This signal is split into two paths using WPD, where one signal directly given in the input of WPC using linear path. Similarly, in the nonlinear IMD path it is given in the input of VM.

The phase and magnitude of the input signal are adjusted by the VM in such a way that the IMD produced by the IM generator circuit counteracts the nonlinear distortion of PA. By adjusting the control voltage of the VM (V_I and V_Q), different combination of phase and magnitude characteristics can be obtained. Depending on the phase and magnitude of fundamental signal adjusted by VM, the nonlinearity of IM generator can be tailored to match the nonlinearity of PA over a wide frequency range. After variation in the phase and

magnitude of the original input signal, the output of VM is given as:

$$V_{VM}(t) = (A(t) \pm \Delta A(t)) \begin{bmatrix} \cos(\omega_1 t + \phi_{PD}[A(t) \pm \Delta A(t)]) + \\ \cos(\omega_2 t + \phi_{PD}[A(t) \pm \Delta A(t)]) \end{bmatrix} \quad (2.9)$$

where $A(t) \pm \Delta A(t)$ represent the change in magnitude of predistortion signal, ϕ_{PD} is the phase of the predistorted signal in the nonlinear IMD path. As shown in Figure 1.6, the phase difference between the IMD produced by the PA and predistortion signal is given by $\phi_{PA} - \phi_{PD} = \Pi$. Hence, the above equation can be written as:

$$V_{VM}(t) = (A(t) \pm \Delta A(t)) \begin{bmatrix} \left(\cos(\omega_1 t + [\phi_{PA}(A(t) \pm \Delta A(t)) - \Pi]) \right) + \\ \left(\cos(\omega_2 t + [\phi_{PA}(A(t) \pm \Delta A(t)) - \Pi]) \right) \end{bmatrix} \quad (2.10)$$

Applying a simple trigonometric function on (2.10) yields:

$$V_{VM}(t) = (A(t) \pm \Delta A(t)) \left\{ \begin{array}{l} \left[\begin{array}{l} (\cos \omega_1 t) (\cos(\phi_{PA}(A(t) \pm \Delta A(t)) - \Pi)) - \\ (\sin \omega_1 t) (\sin(\phi_{PA}(A(t) \pm \Delta A(t)) - \Pi)) \end{array} \right] + \\ \left[\begin{array}{l} (\cos \omega_2 t) (\cos(\phi_{PA}(A(t) \pm \Delta A(t)) - \Pi)) - \\ (\sin \omega_2 t) (\sin(\phi_{PA}(A(t) \pm \Delta A(t)) - \Pi)) \end{array} \right] \end{array} \right\} \quad (2.11)$$

$$V_{VM}(t) = (A(t) \pm \Delta A(t)) \left\{ \begin{array}{l} \left[\begin{array}{l} (\cos \omega_1 t) \left[\begin{array}{l} (\cos \phi_{PA}(A(t) \pm \Delta A(t)) (\cos \Pi)) - \\ (\sin \phi_{PA}(A(t) \pm \Delta A(t)) (\sin \Pi)) \end{array} \right] - \\ (\sin \omega_1 t) \left[\begin{array}{l} (\sin \phi_{PA}(A(t) \pm \Delta A(t)) (\cos \Pi)) - \\ (\cos \phi_{PA}(A(t) \pm \Delta A(t)) (\sin \Pi)) \end{array} \right] \end{array} \right] + \\ \left[\begin{array}{l} (\cos \omega_2 t) \left[\begin{array}{l} (\cos \phi_{PA}(A(t) \pm \Delta A(t)) (\cos \Pi)) - \\ (\sin \phi_{PA}(A(t) \pm \Delta A(t)) (\sin \Pi)) \end{array} \right] - \\ (\sin \omega_2 t) \left[\begin{array}{l} (\sin \phi_{PA}(A(t) \pm \Delta A(t)) (\cos \Pi)) - \\ (\cos \phi_{PA}(A(t) \pm \Delta A(t)) (\sin \Pi)) \end{array} \right] \end{array} \right] \end{array} \right\} \quad (2.12)$$

$$V_{VM}(t) = (A(t) \pm \Delta A(t)) \left\{ \begin{array}{l} \left[\begin{array}{l} -(\cos \omega_1 t)(\cos \phi_{PA}(A(t) \pm \Delta A(t))) \\ +(\sin \omega_1 t)(\sin \phi_{PA}(A(t) \pm \Delta A(t))) \end{array} \right] + \\ \left[\begin{array}{l} -(\cos \omega_2 t)(\cos \phi_{PA}(A(t) \pm \Delta A(t))) \\ +(\sin \omega_2 t)(\sin \phi_{PA}(A(t) \pm \Delta A(t))) \end{array} \right] \end{array} \right\} \quad (2.13)$$

$$V_{VM}(t) = -(A(t) \pm \Delta A(t)) \left[\begin{array}{l} \cos(\omega_1 t + \phi_{PA}[A(t) \pm \Delta A(t)]) + \\ \cos(\omega_2 t + \phi_{PA}[A(t) \pm \Delta A(t)]) \end{array} \right] \quad (2.14)$$

-ve sign in the above equation represents phase inversion. The signal at the output of the PA is 180° out-of-phase with respect to the signal in (2.14). The output of VM ($V_{VM}(t)$) is given in the input of IM generator that generates odd order IM products and cancel the fundamental signal. The output of IM generator is shown in Figure 2.11 which is expanded as:

$$V_N(t) = a_1 V_{VM}(t) + a_3 V_{VM}^3(t) + a_5 V_{VM}^5(t) \quad (2.15)$$

Assuming that the PA is highly nonlinear, it will generate the nonlinearity up to IM5. One important thing that must be taken care while using APD, is that the IMD generated by the PA must match with the nonlinearity generated by the IM generator.

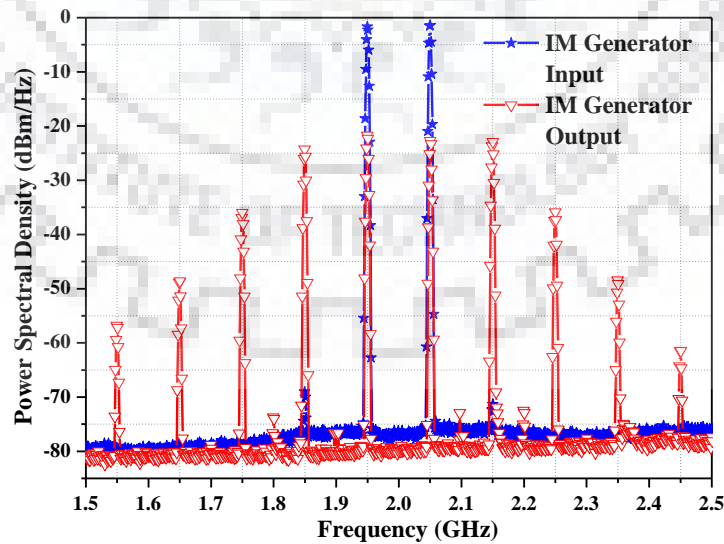


Figure 2.11: Analysis of IM Generator for two tone signal.

APD is unable to provide the required linearization, if the nonlinearity generated by PA is higher than the nonlinearity generated by RRC. Conversely, if the nonlinearity generated by RRC is higher than the nonlinearity generated by PA. In this case, APD system adds its own distortion and limits the linearizer capability.

Ideally, the phase difference between the IMD produced by the PA and PD signal is given by $\phi_{PA} - \phi_{PD} = \Pi$ to counteract the nonlinear distortion of PA. For simplicity, let $(\omega_1 t + \phi_{PA}[A(t) \pm \Delta A(t)]) = \omega_1$ and $(\omega_2 t + \phi_{PA}[A(t) \pm \Delta A(t)]) = \omega_2$.

$$V_N(t) = \underbrace{-a_1 \overline{M}(t)(\cos \omega_1 + \cos \omega_2)}_A \underbrace{-a_3 \overline{M}^3(t)(\cos \omega_1 + \cos \omega_2)^3}_B \underbrace{-a_5 \overline{M}^5(t)(\cos \omega_1 + \cos \omega_2)^5}_C \quad (2.16)$$

The IM generator has the capability to cancel the fundamental signal that lies at frequency ω_1 and ω_2 . Equation shown as 'A' in (2.16) is the fundamental signal, hence it can be discarded. Rest B and C are solved by parts.

$$B = -a_3 \overline{M}^3(t) \left[\begin{array}{l} \cos^3 \omega_1 t + \cos^3 \omega_2 t + 3 \cos^2 \omega_1 t \cdot \cos \omega_2 t \\ + 3 \cos^2 \omega_2 t \cdot \cos \omega_1 t \end{array} \right] \quad (2.17)$$

$$B = -a_3 \overline{M}^3(t) \left(\begin{array}{l} \frac{1}{4} (3 \cos \omega_1 t + \cos 3 \omega_1 t) + \frac{1}{4} (3 \cos \omega_2 t + \cos 3 \omega_2 t) \\ + \frac{3}{2} (1 + \cos 2 \omega_1 t) \cos \omega_2 t + \frac{3}{2} (1 + \cos 2 \omega_2 t) \cos \omega_1 t \end{array} \right) \quad (2.18)$$

The first term in (2.18) is the fundamental signal, hence it can be discarded. The second term is the 3rd order harmonics that lie at frequency $3\omega_1$ and $3\omega_2$, hence it can also be easily filtered out using band pass filter (BPF) [78], [79]. Therefore, (2.18) can be re-written as:

$$B = -\frac{3}{2} a_3 \overline{M}^3(t) \left[\begin{array}{l} \cos \omega_1 t + \cos \omega_2 t + \\ \cos \omega_2 t \cos 2 \omega_1 t + \cos \omega_1 t \cos 2 \omega_2 t \end{array} \right] \quad (2.19)$$

Again discarding the fundamental signal in (2.19), and solving it yields:

$$B = -\frac{3}{4}a_3\overline{M}^3(t) \left[\begin{array}{l} \cos(2\omega_1 + \omega_2) + \cos(2\omega_1 - \omega_2) + \\ \cos(2\omega_2 + \omega_1) + \cos(2\omega_2 - \omega_1) \end{array} \right] \quad (2.20)$$

The IM3 components that lies at frequency $2\omega_1 + \omega_2$, $2\omega_2 + \omega_1$ can be easily filtered out using BPF, hence it can be discarded in (2.20):

$$B = -\frac{3}{4}a_3\overline{M}^3(t) [\cos(2\omega_1 - \omega_2) + \cos(2\omega_2 - \omega_1)] \quad (2.21)$$

(2.21) consist of IM3 that lies $2\omega_1 - \omega_2$, $2\omega_2 - \omega_1$, which is very close to fundamental signal. Further, solving 'C' in (2.13) leads to:

$$C = -a_5\overline{M}^5(t) \left(\begin{array}{l} \underbrace{(\cos^5 \omega_1 + \cos^5 \omega_2)}_I + 5 \underbrace{(\cos^4 \omega_1 \cos \omega_2 + \cos \omega_1 \cos^4 \omega_2)}_{II} \\ + 10 \underbrace{(\cos^3 \omega_1 \cos^2 \omega_2 + \cos^2 \omega_1 \cos^3 \omega_2)}_{III} \end{array} \right) \quad (2.22)$$

To find the solution of (2.22), I, II and III are solved in parts:

$$I = \frac{1}{16} \left[\begin{array}{l} 10(\cos \omega_1 + \cos \omega_2) + 5(\cos 3\omega_1 + \cos 3\omega_2) \\ + (\cos 5\omega_1 + \cos 5\omega_2) \end{array} \right] \quad (2.23)$$

The first term in (2.23) is the fundamental signal, hence it can be discarded. Similarly, second and third term corresponds to 3rd and 5th order harmonics that lie at frequency $3\omega_1$ and $3\omega_2$, and $5\omega_1$ and $5\omega_2$, respectively. These harmonics lie far away from the main fundamental signal, and hence it can easily be filtered out using BPF.

$$II = \frac{5}{8} \left[\begin{array}{l} 3(\cos \omega_1 + \cos \omega_2) + 4(\cos 2\omega_1 \cos \omega_2 + \cos \omega_1 \cos 2\omega_2) \\ + (\cos 4\omega_1 \cos \omega_2 + \cos \omega_1 \cos 4\omega_2) \end{array} \right] \quad (2.24)$$

The first term in (2.24) is the fundamental signal, hence it can be discarded and solving the rest of the (2.24) yield:

$$II = \frac{5}{8} \left\{ \begin{array}{l} 2 \left(\cos(2\omega_1 + \omega_2) + \cos(2\omega_1 - \omega_2) \right) + \\ + \cos(2\omega_2 + \omega_1) + \cos(2\omega_2 - \omega_1) \end{array} \right\} + \left\{ \begin{array}{l} 1 \left(\cos(4\omega_1 + \omega_2) + \cos(4\omega_1 - \omega_2) \right) + \\ \frac{1}{2} \left(\cos(4\omega_2 + \omega_1) + \cos(4\omega_2 - \omega_1) \right) \end{array} \right\} \quad (2.25)$$

(2.25) consists of IM3 and IM5 components. After discarding IM3 components that lies at frequency $2\omega_1 + \omega_2$, $2\omega_2 + \omega_1$ and IM5 components that lies at frequency $4\omega_1 + \omega_2$, $4\omega_1 - \omega_2$, $4\omega_2 + \omega_1$ and $4\omega_2 - \omega_1$, (2.25) can be rewritten as:

$$II = \frac{5}{4} \left[\cos(2\omega_1 - \omega_2) + \cos(2\omega_2 - \omega_1) \right] \quad (2.26)$$

$$III = 10 \left[\begin{array}{l} \frac{1}{4} (3 \cos \omega_1 + \cos 3\omega_1) \cdot \frac{1}{2} (1 + \cos 2\omega_2) \\ + \frac{1}{4} (3 \cos \omega_2 + \cos 3\omega_2) \cdot \frac{1}{2} (1 + \cos \omega_1) \end{array} \right] \quad (2.27)$$

$$III = \frac{5}{4} \left\{ \begin{array}{l} (\cos 3\omega_1 + \cos 3\omega_2) \\ \frac{1}{2} \left(\cos(3\omega_1 - 2\omega_2) + \cos(3\omega_1 + 2\omega_2) \right) \\ \cos(3\omega_2 - 2\omega_1) + \cos(3\omega_2 + 2\omega_1) \end{array} \right\} + \left\{ \begin{array}{l} \frac{3}{2} \left(\cos(2\omega_1 + \omega_2) + \cos(2\omega_1 - \omega_2) \right) \\ \cos(2\omega_2 + \omega_1) + \cos(2\omega_2 - \omega_1) \end{array} \right\} \quad (2.28)$$

The first term in (2.28) is the fundamental signal, and the second term corresponds to third order harmonics that lies at frequency $3\omega_1$ and $3\omega_2$, hence both are discarded. Correspondingly, third and fourth term corresponds to IM5 and IM3. The IM5 components that lies at frequency $3\omega_1 + 2\omega_2$, $3\omega_2 + 2\omega_1$ and the IM3 components that lies at frequency $2\omega_1 + \omega_2$, $2\omega_2 + \omega_1$ can be easily filtered out using BPF. After discarding all these terms (2.28) can be rewritten as:

$$III = \frac{5}{8} \left\{ \begin{array}{l} \cos(3\omega_1 - 2\omega_2) + \cos(3\omega_2 - 2\omega_1) + \\ 3 \left(\cos(2\omega_1 - \omega_2) + \cos(2\omega_2 - \omega_1) \right) \end{array} \right\} \quad (2.29)$$

Combining I, II and III in (2.22) and it can be rewritten as:

$$C = -a_5 \overline{M}^5(t) \left[\begin{array}{l} \frac{25}{8} [\cos(2\omega_1 - \omega_2) + \cos(2\omega_2 - \omega_1)] + \\ \frac{5}{8} [\cos(3\omega_1 - 2\omega_2) + \cos(3\omega_2 - 2\omega_1)] \end{array} \right] \quad (2.30)$$

Using (2.21) and (2.30) in (2.16), it becomes:

$$\begin{aligned} V_N(t) = & -\frac{3}{4} a_3 \overline{M}^3(t) [\cos(2\omega_1 - \omega_2) + \cos(2\omega_2 - \omega_1)] \\ & - \frac{25}{8} a_5 \overline{M}^5(t) [\cos(2\omega_1 - \omega_2) + \cos(2\omega_2 - \omega_1)] \\ & - \frac{5}{8} a_5 \overline{M}^5(t) [\cos(3\omega_1 - 2\omega_2) + \cos(3\omega_2 - 2\omega_1)] \end{aligned} \quad (2.31)$$

(2.31) consists of IM3 components that lie at frequency $2\omega_1 - \omega_2$, $2\omega_2 - \omega_1$ and IM5 components that lie at frequency $3\omega_1 - 2\omega_2$, $3\omega_2 - 2\omega_1$. These IM components generated by IM generator with the opposite phase with respect to the IM components generated by PA.

The WPC combines the signal from linear and nonlinear branches with 180° phase difference so that the fundamental signal from linear path and IM components from nonlinear path have opposite phases. The signal output from linearizer drives the PA which is given as:

$$V_{tot}(t) = V_{in}(t) + V_N(t) \quad (2.32)$$

2.5 IM Generator Modeling

IMD generation components are mostly analog nonlinear components such as diodes. As odd order nonlinearity order has more impact, an anti-parallel diode pair is commonly used component. In addition to IMD generation, it is also required to suppress the main signal. When this signal containing only IMD terms is added to the input signal at 180° , it facilitates cancellation of IMDs generated at PA output. The fabricated IM generator, shown in Figure 2.12, is mounted with anti-parallel Schottky HSMS 2822 diode and RC filter bank. The capability of IM generator is judged by its ability to cancel the fundamental signal and to generate higher order IM components. A pair of the anti-parallel diode is

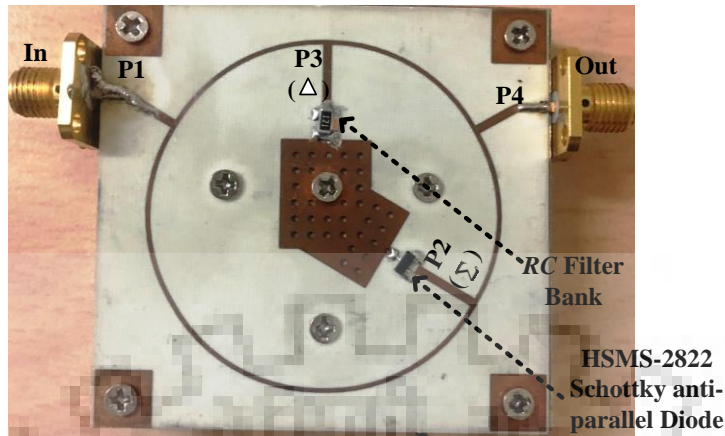


Figure 2.12: Fabricated Intermodulation generator equipped with RC Filter Bank and HSMS 2822 Schottky Anti-parallel diode.

connected on port 2 that is sigma port (P2) of the RRC as shown in Figure 2.12. Similarly, Delta port (P3) of RRC is mounted with a pair of RC filter bank, which cancel the fundamental signal. The fundamental signal cancellation from 5 dB to 30 dB has been observed with the designed IM generator. The fabricated IM generator provides cancellation up to 24 dB which is shown in Figure 2.13. It illustrates the Power Spectral Density (PSD) of IM generator when applied with non-contiguous 10000001 where 1 indicates carrier-on and 0 indicates carrier-off with total instantaneous bandwidth of 160 MHz. Apart from cancellation, it also generates in-band as well as out-of-band IMD

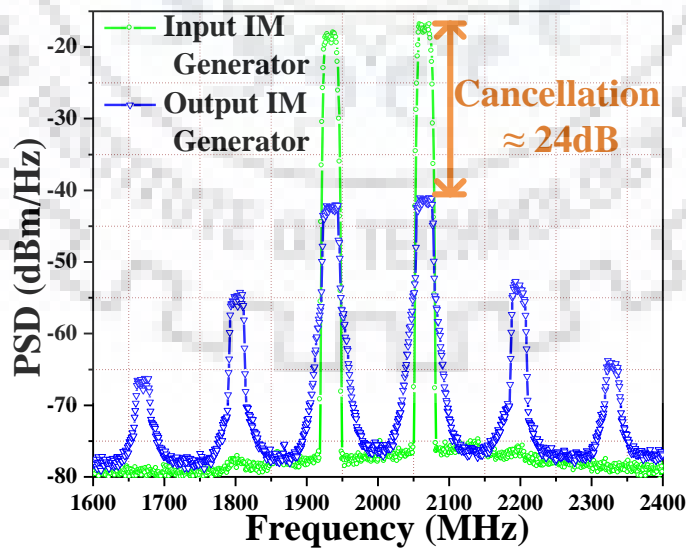


Figure 2.13: Response of the IM Generator for 8CC 160MHz non-contiguous signal.

components that will help to neutralize PA in-band and out-of-band IMD components.

The simulation of the advance design system (ADS), 2009 showed that 100Ω resistor and the 1pF capacitor are an appropriate value that can be mounted on the sigma port of RRC. In order to meet specific optimization goals, ADS can automatically modify the circuit component values to achieve best circuit performance. Once the desired results are obtained using optimization goals, one can update its schematic. The momentum simulation in ADS, 2009 revealed that above value of R and C provide a good balance between fundamental signal and predistortion signal. The IMD generation and signal cancellation required from IM generator could be tailored by varying the power of an input fundamental signal.

2.5.1 Bandwidth of IM Generator

The more accurate working bandwidth of linearizer can be observed from Figure 2.14, which shows the measured IMDs and fundamental signal cancellation by IM generator at different frequencies. It can be observed that the bandwidth of this linearization circuit is mostly defined by the bandwidth of the IM generator circuit. RRC provides up to 20-22 dB cancellation in the fundamental two-tone signal in the frequency range of 1.75 GHz to 2.25

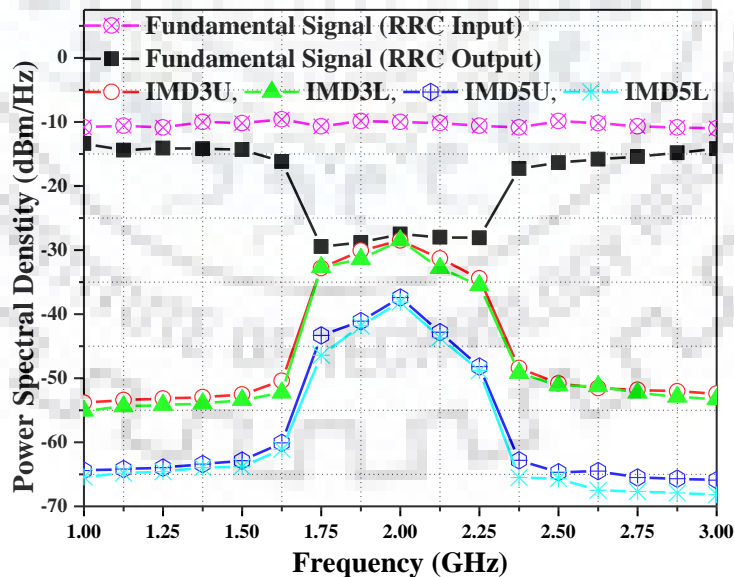


Figure 2.14: Fundamental signal cancellation and IMD generation by the IM Generator for the different frequencies.

GHz. In this band of frequencies, as required, it also produces strong IM3 and IM5 components. It provides wideband linearization performance of bandwidth up to 500 MHz, which is also depicted in Figure 2.14.

Video Bandwidth of IM generator: The video bandwidth (VBW) of an IM generator is usually expressed as the range of the frequency range over which the IM generator shows a constant and symmetrical IM product. It is usually measured with a two-tone signal where the spacing between the two tones is increased and the power levels of the lower and upper IM are monitored as a function of the tone spacing. The total output power is kept constant during the frequency spacing sweep of two tone to remove any effect due to gain variation over the frequency band. The VBW of IM generator is identified with following experiments:

Exp. 1: IM generator is excited using two tone signal with frequency spacing of 10 MHz ($\Delta f = 10$ MHz), where input power is kept constant. The input power should be high enough, such that the third order IM products (IM3H and IM3L) are generated by the IM generator. To find the VBW of IM generator, the tone spacing is increased and symmetry between IM3H and IM3L is observed. The generator (MXG N5182B) which has been used for experimental results supports the two tone spacing up to 160 MHz. It has been observed that IM3H and IM3L are symmetrical for 160 MHz two tone signal,

Exp. 2: IM generator is again excited using two tone signal with frequency spacing of 10 MHz ($\Delta f = 10$ MHz). The input power is increased, such that the PA will generate fifth order IM products (IM5H and IM5L). Similarly, for 160 MHz two tone signal, IM5H and IM5L are symmetrical.

Above two experiment signifies that the VBW of IM generator, must be greater than or equal to 800 MHz (i.e. $160 \text{ MHz} \times 5$).

2.5.2 Impact of R and C

The selection of R and C in the RC filter connected to the delta port also impacts the performance. Higher resistance value makes the predistortion signal weaker. The value of R

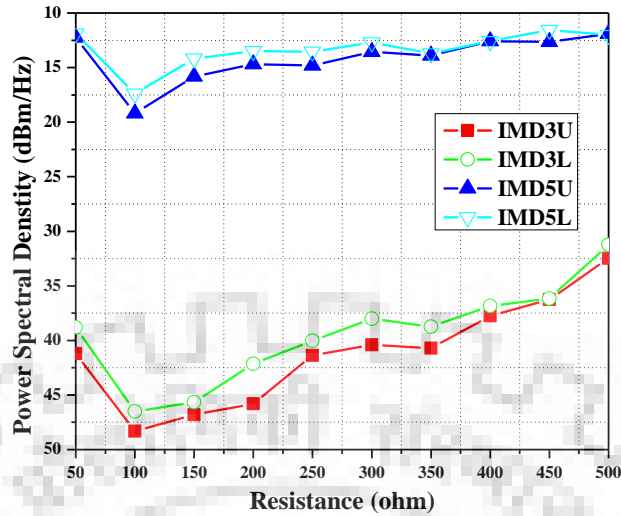


Figure 2.15: Intermodulation Distortion generation with fixed $C= 1\text{pF}$ and varying R .

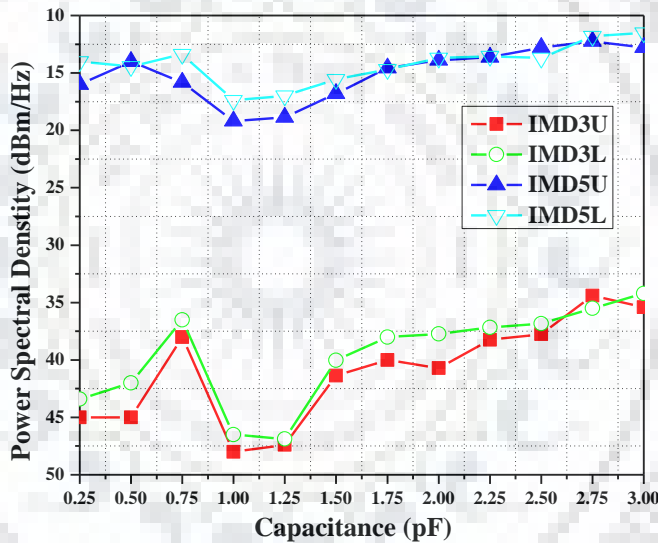


Figure 2.16: Intermodulation Distortion generation with fixed $R=100\Omega$ and varying C .

and C are chosen appropriately such that it cancels fundamental signal over wide frequency range. To find the values of R and C components, the design is simulated in ADS by varying R and C . Figure 2.15 and 2.16 shows the IMD_3 and IMD_5 generation depending on R and C respectively. In Figure 2.15, $C=1\text{pF}$ is fixed and output spectra is plotted by varying R . Similarly, in Figure 2.16, $R= 100 \Omega$ is fixed and output spectrum of IMD correction is plotted by varying C . After getting the appropriate values, we fixed RC filter at the delta port of RRC . From the figures, it is concluded that as the values of components diverge from its optimum values the cancellation provided by APD to IMD_3 and IMD_5 reduces.

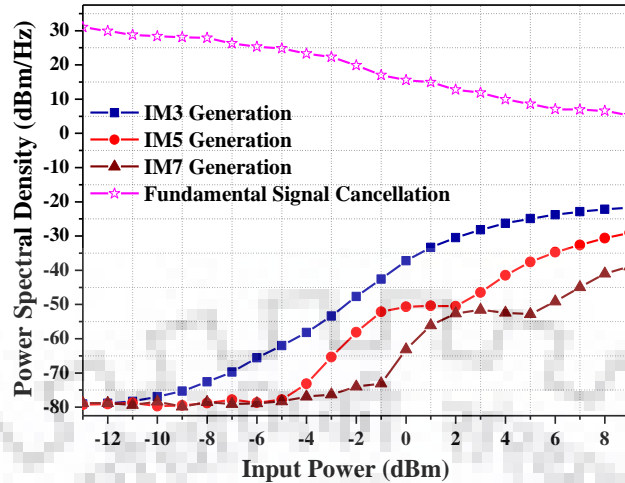


Figure 2.17: IM Generator modeling for two tone signal with 100 MHz frequency spacing, centered at 1.8 GHz.

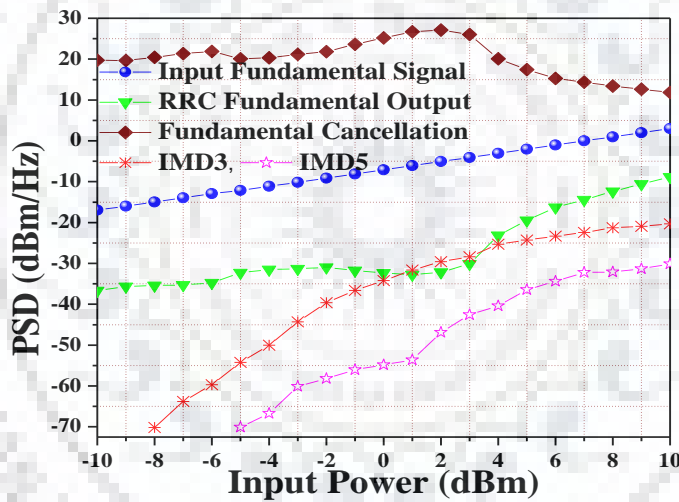


Figure 2.18: IM Generator modeling for two tone signal with 160 MHz frequency spacing, centered at 2 GHz.

2.5.3 Power Dependency of IM Generator

The modeling of IM Generator represents how efficiently it generates IMD products and cancels the fundamental signal. It can be done by applying the input signal to the IM generator at various power levels and observing its output power spectral density. Figure 2.17 and Figure 2.18 shows the output of IM Generator at various power levels for 100 MHz and 160 MHz two-tone signals, centered at 1.8 GHz and 2 GHz respectively.

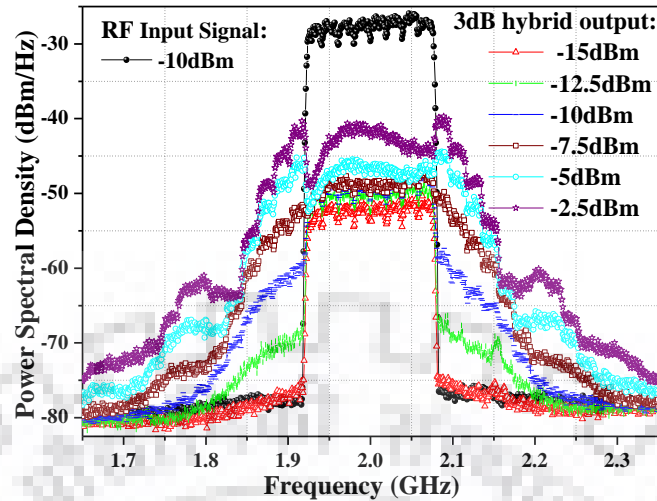


Figure 2.19: IM Generator modeling for 8CC 160MHz LTE signal, centered at 2 GHz.

At very low input power, it cancels the fundamental signal, however, it is not able to generate nonlinear distortion.

On the other hand, at very high input power levels, it generates stronger IMDs but does not achieve good fundamental signal cancellation. Therefore, appropriate input power is required at the input of IM generator to sufficiently cancel the fundamental signal and generate IM products. To target only IM3, the minimum input power which is required at the input of IM generator must be -8dBm. But at this input power, IM5 and IM7 are not generated by the IM generator, but it produces moderate IM3. Similarly for IM5 generation, the input power must be higher than -5dBm. In order to target higher order IMDs, the necessary power of the input signal must be greater than -1 dBm. Apart from producing stronger IM3 and IM5 at this input power, it also produces IM7 which is shown in Figure 2.17. From the Figure 2.17 and Figure 2.18, it is concluded that the generator performance is optimum between -3.5 dBm to 2 dBm input power. At this input signal power, it not only produces strong IMDs but also provides a good fundamental signal cancellation.

The behavior of IM generator excited by modulated signal is shown in Figure 2.19. It shows the output PSD excited by 160 MHz 8CC LTE signal at various power levels. Input signal power is adjusted depending upon the nonlinearity and required signal cancellation. Depending upon the IMD generated by PA, the power at the input of IM generator can be tuned. If the nonlinearity order of PA for 160 MHz 8CC LTE is up to third order only, the

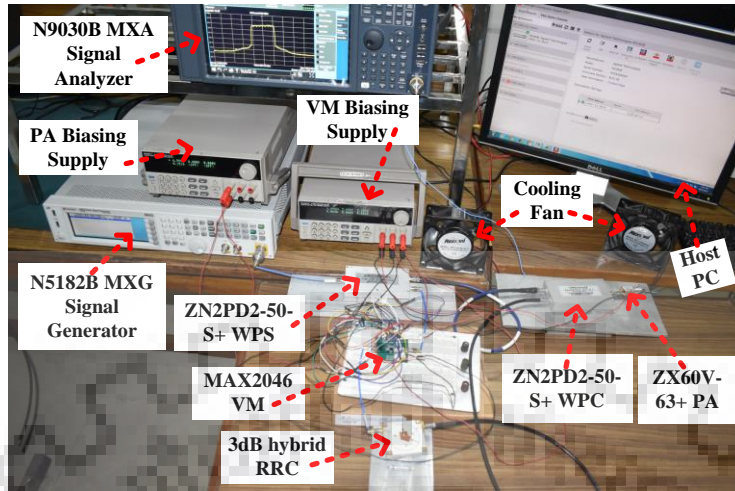


Figure 2.20: Test-bench for data extraction of the proposed RF-in RF-out APD.

power at the input of RRC can vary from -12.5 dBm to -10dBm. If the order of nonlinearity is high, the input power requirement of IM generator must be greater than -10 dBm.

2.6 Experimental Verification

2.6.1 Test-bench for data extraction

The test-bench for RF_{in} - RF_{out} APD is shown in Figure 2.20. The test signals are uploaded in the vector signal generator (MXG N9030B) using a host PC with the help of Matlab. The 2 way 0° ZN2PD2-50-S+ WPD from Mini-circuits is used at the output of the signal generator to split the output RF signal of MXG into two equal paths. The upper path is the linear path that only consists of an interconnect coaxial SMA Cable, however, lower path is phase adjusted IMD generator path that consists of VM and IM generator. The gain and phase of VM are voltage variable, it can be adjusted easily with the biasing network as shown in test-bench. The RC filter bank and anti-parallel diode circuit is combined by using the 3dB 180° hybrid coupler. The amplitude and phase of intermodes generated by the IM generator were controlled by the VM. The predistortion signal from the IMD generator path and the original fundamental signal from the linear path are combined using 2 way 0° ZN2PD2-50-S+ WPC from Mini-circuits, which is further given in the input of the PA. The RF-in RF-out APD performance is evaluated using 100 MHz two tone signal, 8CC 160 MHz contiguous and non-contiguous signal and 20 MHz LTE signal.

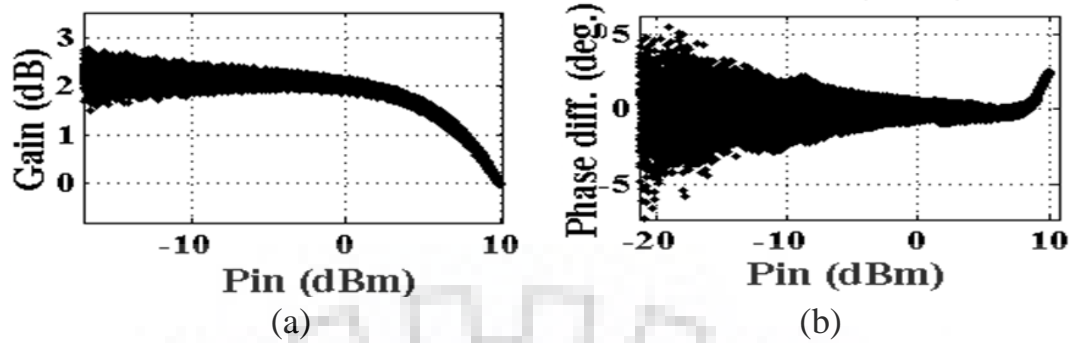


Figure 2.21 AM/AM and AM/PM characteristics of ZX60V-63+ Class AB PA.

2.6.2 Device under Test

The proposed RF-in RF-out APD is used to linearize ZX60V-63+ PA from Mini-circuits. The AM/AM and AM/PM characteristics of the ZX60V-63+ device-under-test (DUT) is shown in Figure 2.21. It is a wideband amplifier that works effectively from 500 MHz to 6 GHz. It offers high gain and high third order intercept point over a broad range of frequency. This amplifier supports a wide variety of applications requiring low distortion and moderate power output.

The high linearity of PA, high output power and high power efficiency are conflicting requirements. There are two key measurements in determining PA quality, efficiency, and linearity: the 3rd-order intercept (abbreviated TOI or IP3) point and the 1-dB compression (P1dB) point [10].

Linear amplifiers operate in class A or class AB. Class A operation is preferred if maximum linearity is desired, but its downside is poor efficiency, never more than 20% to 30% in practice. To achieve greater efficiency, class AB is used [10]-[14]. The disadvantage is that class AB biasing introduces signal distortion and produces harmonics and IM products. While proper filtering can eliminate some of these undesired side effects, it cannot reduce all of them. The ZX60V-63+ PA is a class AB amplifier, hence linearization is required to reduce IM products.

The 1 dB compression point is measure of PA linearity. The typical 1 dB compression point characteristics of ZX60V-63+ PA are shown in Figure 2.22. The 1-dB decrease may be

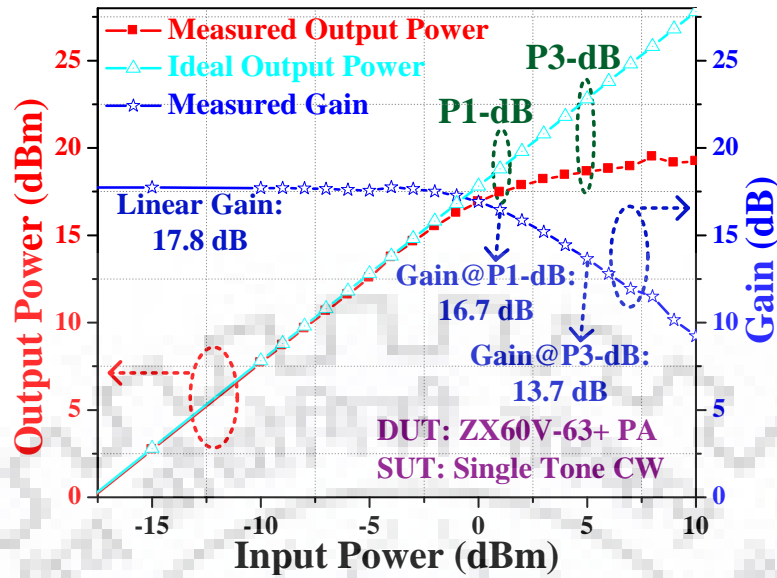


Figure 2.22: Linear and compression region of ZX60V-63+PA using Single tone CW signal at 2 GHz.

specified as the input level that produces it (1-dB input power) or the output power where the 1-dB drop occurs (1 dB-output power). Figure 2.22 depicts that the PA must operate in a near saturation region to satisfy the requirements on power efficiency. Similarly, P3dB is the point where the PA enters into the saturation mode. It is the point at which actual gain deviates from small signal gain by 3 dB.

The single tone continuous wave (CW) signal is applied at 2 GHz to determine the small signal gain, 1 dB and 3 dB compression point of ZX60V-63+ PA. Measurement shows that the input and output P1-dB of the DUT is 1 dBm and 17.45 dBm respectively. Similarly, the P3-dB compression point occurs at 5 dBm input power that provides an output power of 18.64 dBm as shown in Figure 2.22.

The IP3 of ZX60V-63+ PA is around 14 dB above the P1 dB point at 2 GHz. It is widely used metric in PAs, which gives information about the linearity of an amplifier. A higher IP3 indicates better linearity and lower distortion generation. It is the theoretical point at which the desired output signal and undesired IM3 signal are equal in levels considering an ideal linear gain for the PA. The DUT exhibits good IP3 performance relative to power consumption.

2.6.3 Signal under Test

2.6.3.1 Two-tone signal with 100 MHz frequency spacing

This experiment showcases the ability of the proposed RF-in RF-out APD to mitigate inter-band distortion. Two tones of equal power are situated at frequency 1.95 GHz and 2.05 GHz. Figure 2.23 shows the measured spectrum of PA output under two-tone signal with a frequency spacing of 100 MHz centered at frequency 2 GHz. When this signal is amplified via PA, the output contains out-of-band cross-modulation distortion. Table 2.1 presents the performance comparison of PA in terms of IM cancellation and output intercept point (OIP) without and with APD. The nonlinear products of the PA that are caused by the IM3 and IM5 are referred as 3rd-order OIP (OIP3) and 5th-order OIP (OIP5) respectively. The higher the output intercept point, the better is the linearity and lower is the IMD. As shown in Table 2.1 and Figure 2.23, proposed APD provides significant cancellation to higher order Intermodulation components and enhances the linearity of PA. It can be perceived that both IM3 as well as IM5 are reduced by employing the APD.

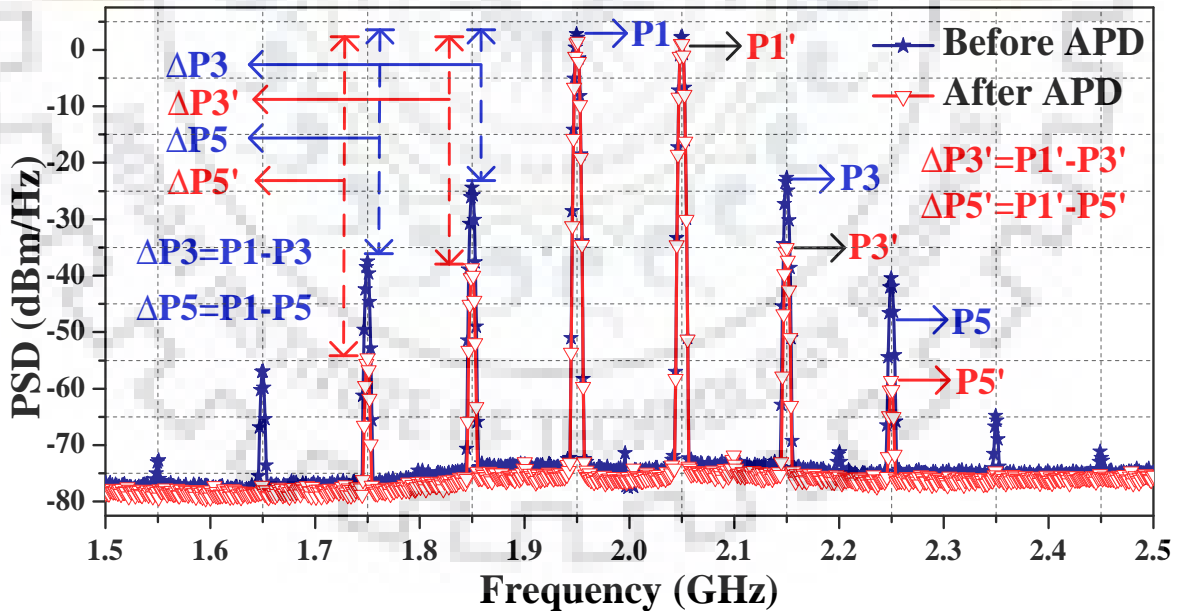


Figure 2.23: Measured Power Spectrum Density of PA with and without the proposed RF-in RF-out APD under two tone signal with a frequency spacing of 100 MHz.

TABLE 2.1

PERFORMANCE COMPARISON OF PA WITH/WITHOUT THE PROPOSED APD

IM & OIP	Before APD	After APD	Correction
IM3U	-22.18	-35.0	12.82
IM3L	-23.5	-37.6	14.1
IM5U	-40.1	-57.5	17.4
IM5L	-37.2	-55.3	18.1
IM7U	-65.1	-76.3	11.2
IM7L	-56.8	-77.3	20.5
IIP3	$P1 - G + \frac{\Delta P3}{2} = -5.41$	$P1' - G + \frac{\Delta P3'}{2} = -0.5$	4.91
OIP3	$P1 + \frac{\Delta P3}{2} = 15.59$	$P1' + \frac{\Delta P3'}{2} = 20.5$	4.91
IIP5	$P1 - G + \frac{\Delta P5}{2} = -7.225$	$P1' - G + \frac{\Delta P5'}{2} = -4.125$	3.105
OIP5	$P1 + \frac{\Delta P5}{2} = 13.775$	$P1' + \frac{\Delta P5'}{2} = 16.875$	3.105

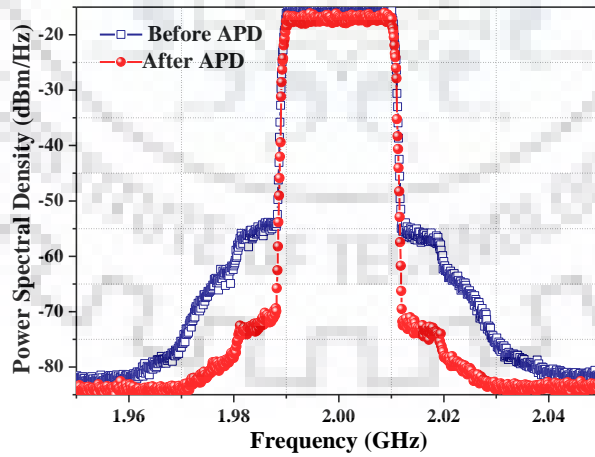


Figure 2.24: Measured Power Spectrum Density of PA with and without the proposed APD under 20 MHz LTE signal.

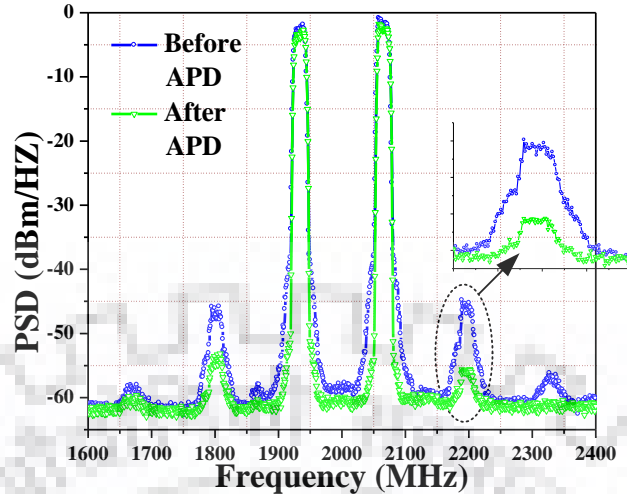


Figure 2.25: Measured Power Spectrum Density of PA with and without the proposed APD excited by non-contiguous 8CC 160 MHz LTE signal.

2.6.3.2 LTE 20 MHz signal

This experiment is conducted to demonstrate the impact of signal bandwidth on APD performance. As shown in Figure 2.24, for 20 MHz LTE signal, the proposed APD delivers an ACPR of -56.9dBc with a cancellation of 18.2 dB. The PAPR of LTE 20 MHz signal is 8.92 dB. As the bandwidth of the signal increases, it gives rise to PAPR of signal. High PAPR leads to low efficiency of the PA. All the measurements in this work is represented in terms of ACPR. It is the ratio of adjacent channel power (both lower and upper sidebands) with reference channel power. ACPR stands for Adjacent Channel Power Ratio and ACLR stands for Adjacent Channel Leakage Ratio. Though the name is different, both terms are used interchangeably to represent the same thing.

2.6.3.3 Non-Contiguous 8 CC LTE 160 MHz signal

Linearization of 160 MHz UWB signal is very demanding and challenging task. The proposed APD linearization scheme applies to non-contiguous 10000001 signal where 1 indicates carrier-on and 0 indicates carrier-off states with total instantaneous bandwidth of 160 MHz. The PAPR of non-contiguous 8CC LTE signal is 12.84 dB. Figure 2.25 shows the PSD of non-contiguous 8CC LTE signal with and without APD. When proposed APD is applied to linearize ZX60-V63+ PA using 160 MHz signal, an ACPR of -49.19 dBc is

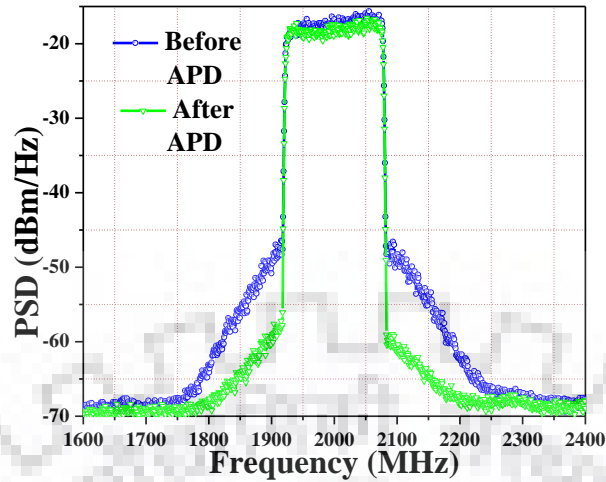


Figure 2.26: Measured Power Spectrum Density of PA with and without the proposed APD excited by contiguous 8CC 160 MHz LTE signal.

achieved with an improvement of over 12.22 dB at 1 dB OBO as compared to PA without linearization. It can also be appreciated from Figure 2.25, that APD also suppress out-of-band IMD components that reduces the co-channel interference. However, the APD achieves the ACPR improvement by compensating for in-band and out-of-band IMDs.

2.6.3.4 Contiguous 8 CC LTE 160 MHz signal

Figure 2.26 shows the PSD of contiguous 8CC LTE signal with and without APD. The PAPR of contiguous 8CC LTE signal is 14.17 dB. When proposed APD is applied to

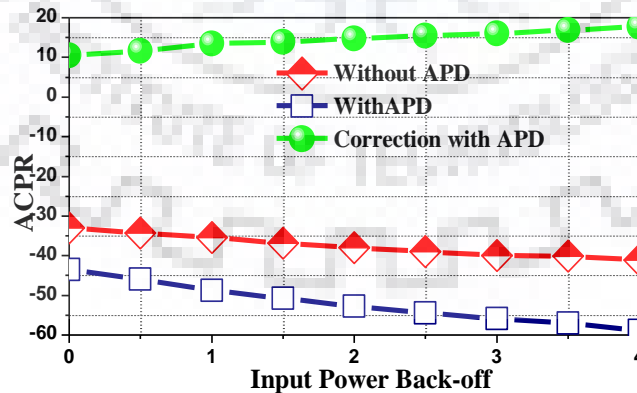


Figure 2.27: ACPR of PA output with and without proposed APD at different back-off power.

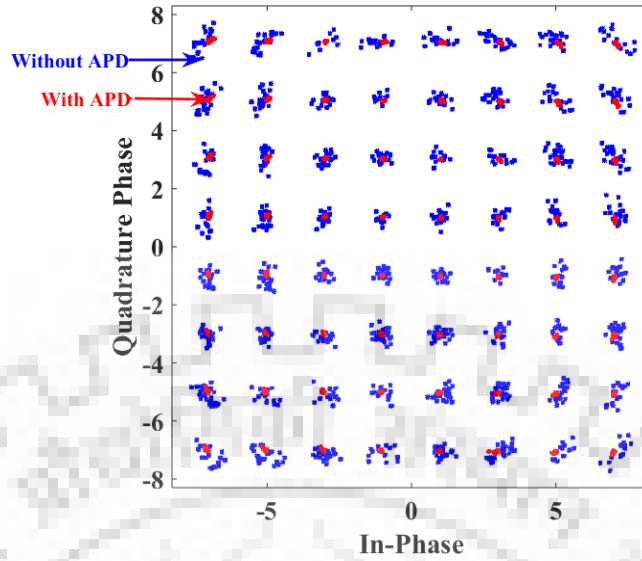


Figure 2.28: Measured constellation diagram with and without the proposed APD at 2 GHz under contiguous 8CC 160MHz LTE signal.

linearize ZX60-V63+ PA, an ACPR of -45.02 dBc is achieved with an improvement of over 11.12 dB at 1 dB back-off power as compared to PA without linearization. Figure 2.27 shows the measured ACPR improvement for the contiguous 8CC LTE 160 MHz signal with the proposed APD architecture at various input power back-offs. The input power is swept from 0 dBm to 4 dBm to observe the improvement in ACPR.

To showcase the in-band performance, EVM of contiguous 160 MHz LTE signal without and with proposed APD is also measured and its constellation plot using 64-QAM is shown in Figure 2.28. With proposed APD, EVM is reduced from 4.88% to 1.21 %, which satisfied 3GPP mask as illustrated in [80].

2.7 Comprehensive Comparison with State-of-the-art APD Linearization

The performance of the proposed RF-in RF-out APD architecture is summarized and compared with the state-of-the-art APD linearization techniques in Table 2.2. Table 2.3 discusses the strength and weakness of previously proposed APD architecture.

TABLE 2.2

PERFORMANCE COMPARISON OF THE STATE-OF-THE-ART APD LINEARIZER

Ref.	PD Type	Center freq.	Signal Type	Signal Bandwidth	Improvement
This Work	Proposed RF-in RF-out APD	2 GHz	Two tone LTE Intraband Interband	$\Delta f=100$ MHz 20 MHz 160 MHz 160 MHz	IM3 \approx 14 dB, IM5 \approx 18 dB ACPR: 18.2 dBc ACPR: 12 dBc@1dB OBO ACPR: 11 dBc@1dB OBO EVM: 4.88% to 1.21%
[66]	RF-PD	2.16 GHz	Two tone WCDMA	$\Delta f=5$ MHz 20 MHz	IM3: 30.63 dB, IM5: \approx 12dB ACLR: 6.19 dBc
[67]	Multi-branch APD	2.14 GHz	2 carrier WCDMA	$\Delta f=15$ MHz	ACLR: 25.3 dBc; 15 MHz offset
[68]	Transistor APD	2.14 GHz	WCDMA WCDMA	5 MHz 20 MHz	ACLR: 25 dBc ACLR: 20.3 dBc
[69]	Cascaded APD	2.14 GHz	Two tone WCDMA	$\Delta f=5$ MHz 20 MHz	IM3 \approx 36 dB, IM5 \approx 23 dB ACLR: 16.4 dBc
[81]	Transistor APD	2.4 GHz	Two tone WCDMA	$\Delta f=20$ MHz 5 MHz	IM3: 16 dB@6dB OBO ACLR: 9.5 dBc @3dB OBO
[82]	RF-PD	15 GHz	LTE	200 MHz	ACLR: 6.5dBc; EVM: 5.5%
[83]	APD	2.38 GHz	WCDMA	8.192MHz	ACLR: 9 dBc
[84]	Phase based PD	1.88 GHz	LTE 64QAM	10 MHz	ACLR: 4.2 dBc
[85]	APD	2.15 GHz	WCDMA	5 MHz	ACLR: 13 dBc
[86]	Third order PD	2.14 GHz	IS-95 WCDMA	≈ 1.5 MHz 20 MHz	ACLR: 14 dBc ACLR: 13.4 dBc
[87]	Third order PD	2.14 GHz	Two tone WCDMA	$\Delta f=5$ MHz 20 MHz	IM3: \approx 24 dB, IM5: \approx 12dB ACLR: 16.1 dBc
[88]	Closed	1.88 GHz	WCDMA	5 MHz	ACLR: 6 dBc at no offset;

	Loop PD				18dBc at 10 MHz offset
[89]	Envelope PD	2.14 GHz	Two tone WCDMA	$\Delta f=10$ MHz 20 MHz	IM3 \approx 21 dB, IM5 \approx 19 dB ACLR: 10.16 dBc
[90]	Harmonic Injection	2.1 GHz	384-kbps DQPSK	400KHz	ACLR: 20 dBc
[91]	Harmonic Injection	835 MHz	Two tone CDMA	$\Delta f=1$ MHz 1.23 MHz	IM3 \approx 20 dB, IM5 \approx 30 dB ACLR: 6 dBc
[91]	Active PD	1902 MHz	Two tone	$\Delta f=5$ MHz	IM3 \approx 17 dB
[93]	Work Function PD	1.96 GHz 1.93 GHz	Two tone CDMA	$\Delta f=10$ MHz 1.2 MHz	IM3 \approx 20 dB, IM5 \approx 14 dB ACLR: 18 dBc
[94]	Miniaturized PD	2.7 GHz	32-kbps QPSK	16 KHz	ACLR: 5 dBc

TABLE 2.3

SALIENT FEATURES OF VARIOUS APD PREDISTORTER LINEARIZER

Ref.	Strengths	Weakness
This Work	<p>Circuit topology is very simple as it only composed of IM generator and VM.</p> <p>Eliminate the delay line.</p> <p>It can suppress IM3, IM5 and IM7 simultaneously.</p> <p>Work effectively with UWB system.</p> <p>Hence a potential candidate for 5G.</p>	<p>Due to non-ideality of analog components used in the proposed architecture, linearization performance is not as good as DPD and HPD.</p> <p>In order to improve its linearizability, a new architecture is proposed in Chapter 5 which is a combination of digital and analog counterpart.</p>
[66]	<p>Compensates the memory effect of PA using the delayed IM3 path.</p> <p>It has the capability of auto cancelling the fundamental signal.</p>	<p>The separate IM3, IM5 and the delayed IM3 path makes the system more complex.</p> <p>Discrepancy of time delay due to</p>

		intermodes paths. ACLR correction is very limited
[67] [68]	Compensates the memory effects of PA. Linearizability of APD is quite impressive.	Nonlinear path composed of three separate paths that increases the complexity. Each path requires different delay lines and error generator circuit [79]. Each branch consists of VM [80].
[69]	Reduces memory effects of PA. It can suppress IM3 and IM5 simultaneously. Cascading of two APD circuits achieves better linearization.	Cascading of two APD increase cost and complexity. VM in IM3 and IM5 generation path captures 5X of the signal bandwidth.
[81]	Circuit topology is simple as it eliminates the use of VM, attenuators and delay lines.	Measured 1dB bandwidth of input and output coupler is only 80 MHz. The narrow bandwidth of coupler restricts its application in 5G. Two PA is used to generate predistorted signal that increases system cost. Very large back-off is required to get good ACLR improvement.
[82]	Employs very simple circuitry Capable to linearize the UWB signal	It suffers from limited ACPR correction capability
[83]	It can effectively cancel third and fifth order IMDs independently.	Five VM and two error generating PA are employed in the APD circuit that complicates the whole process.
[84]	It is fabricated in 0.32 μ m CMOS SOI technology.	Time delay adjustment for modulated signal is a tricky challenge. Linearization performance is not worthy.
[85]	The predistortion circuit is simple and consumes very less power.	ACLR improvement can be achieved at the cost of one additional driver

		amplifier, hence using one more amplifier makes the system more complex and costly.
[86]	<p>Three performance degradation factors, i.e. higher order terms, phase and amplitude mismatch are discussed quantitatively.</p> <p>Compensates the memory effects.</p> <p>Predistortion circuit is used to measure the relative phase of harmonics</p>	VM captures the five times bandwidth of the input signal. Hence, not a strong candidate for wideband systems.
[87]	It can suppress IM3 and IM5 simultaneously.	Phase controlled error generator expand the signal bandwidth by five times that is given in the input of VM.
[88]	<p>It exhibits low power consumption</p> <p>It is fabricated in 0.13μm complementary metal-oxide-semiconductor (CMOS) technology, that's why occupies a very small area</p>	<p>Predistortion circuit is highly complex as it requires transformers, loop filters, mixers etc.</p> <p>To address the stability issue separate magnitude and phase feedback path can be realized in order to compare the phase and magnitude of input and output signals.</p>
[89]	<p>Compensates the memory effects of PA.</p> <p>It can suppress IM3 and IM5 simultaneously.</p> <p>Separate adjustment of phase and magnitude of lower and upper IM products</p>	Use of a VGA, envelope delays, memory compensation circuit and the IM generator circuit makes the circuit very complex.
[90]	MESFET is used for the second order IM generation which further cancel	Circuit is highly complex as harmonic path composed of Variable phase shifter

	<p>IM3 of PA.</p> <p>There is no need of precise phase adjustment, that's why it is a very stable technique.</p>	<p>(VPS), high gain amplifier, pre amplifier, variable attenuator whereas baseband circuit composed of low pass filter (LPF), inverter and tunable PA.</p>
[91]	<p>The second harmonic and frequency difference between spectral components of the fundamental signal is applied along with the original input that provide an excellent reduction in IM.</p>	<p>Separate hardware is required to extract frequency difference between fundamental tones and for the injection of the second harmonic.</p> <p>Hardware circuitry includes VGA, VPS and LPF which increases the cost and complexity of the system.</p>
[92]	<p>The circuit is very simple and easy to implement.</p>	<p>Predistortion circuit requires two PA that increases the overall cost of the system.</p>
[93]	<p>It is not limited by loop delays.</p> <p>It can generate gain and phase corrected signal that can modulate RF signal</p>	<p>Predistortion output signal from work-function generator was distorted by a high pass filter.</p>
[94]	<p>Predistortion circuit is very simple as it composed of bias resistance, capacitor for DC block, Schottky diodes for nonlinearity generation</p>	<p>Linearization performance is not worthy.</p>
[95]	<p>Compensates IM3 via offset signals.</p>	<p>Due to circuit complexity, it is not considered a strong candidate for high frequency operation.</p> <p>It also reduces the output gain, which is the main disadvantage of this technique.</p>

2.8 Conclusion

In this chapter, RF-in RF-out APD has been proposed that compensates for the higher order IM products of PA. The operating principle of the linearizers was investigated and experimentally validated for UWB signals. To validate the proposed APD linearizer, a 100-MHz two-tone and a UWB 8CC 160 MHz linearization test are performed at 2 GHz. Experimental results of the proposed APD using two-tone excitation provide significant cancelation for higher order IM components and shift the intercept point to the upper region which further enhances the linearity of PA. Owing to its simple structure without any driver or error amplifier, this topology can be easily applied to implement linear PA for the potential 5G communication system.





Chapter 3

Implementation Challenges and Control Schemes

3.1 Introduction

Conventional APD finds its application in the 5G communication system, however the main skepticism is that it undergoes serious hardware non idealities that compromise the quality of signal. It is inadequate due to its inability to process UWB signal and imperfection in its associated circuitry. It is imperative to revise a new mechanism that cures the imperfection of Conventional APD and process UWB signal efficiently. To address the aforementioned limitation, Conventional APD is replaced by the proposed RF-in RF-out APD and UBB PD's.

APD is an attractive solution as the predistorted signal are not generated in the digital domain and need not go through DAC [83]. APD has three main necessities:

- (1) Precise control over the gain and phase of the IMDs generated in the nonlinear path that compensate the nonlinearity of PA.
- (2) The IMDs generated in the nonlinear path must be anti-phase and have an equal amplitude with respect to the IMD generated by the PA.
- (3) The diodes in the anti-parallel fashion must be matched, else it can generate second order IM products.

Two cases are discussed below, if the IMD generated in the nonlinear path does not match with the IMD of PA.

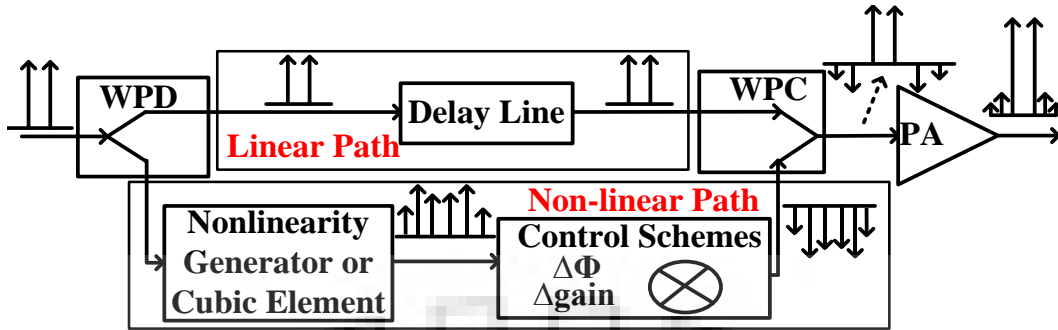


Figure 3.1: Conventional APD architecture.

(a) If the IMD generated in the nonlinear path of APD $>$ IMD generated by PA.

In this case, apart from cancelling the IMD of PA, predistorter adds its own distortion, hence reduces the linearizability of the system.

(b) If the IMD generated in the nonlinear path of APD $<$ IMD generated by PA.

In this case, the nonlinear path did not produce the required amount of nonlinearity. Hence, the APD is unable to cancel the IMD of PA. In turn, it again reduces the linearizability of the system.

Conventionally, VM has been used for gain and phase control in APD [83], however VM had some inherent limitations and therefore calibration techniques have been proposed with slight enhancements [96].

This work proposes and implements two independent control schemes (CS) for the proposed RF-in RF-out APD and UBB RF-PD for the 5G communication system. It also provides a comparative analysis between these two CS and the previous state-of-the-art linearization techniques.

3.1.1 Overview of the two Control Schemes

These two CS are more feasible than conventional APD [66]-[69], as Type-I CS uses the same hardware which was used in conventional APD to linearize wideband signal which is not possible with the conventional APD. In Type-II scheme, independent control over the

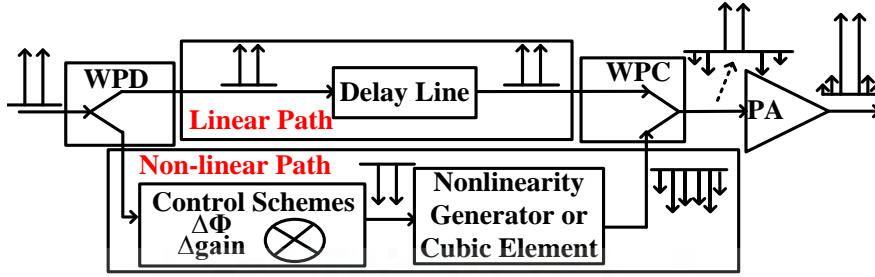


Figure 3.2: Proposed Type-I Control Scheme for the modified APD architecture.

gain and phase of the predistortion signal provides better linearizability as compared with conventional APD and Type-I CS. Similarly, it also extracts better benefits than HPD, which was proposed in [58], [59], [96] in a way that it replaces the data converters and FPGA with energy efficient passive components. But the linearizability of HPD is better than these two schemes, as it provides flexibility in terms of digitally compensation of delay, gain and phase control of the predistortion signal.

The Type-I APD has already been proposed in Chapter 2 in which VM was used as a CS to manipulate the gain and phase of the predistortion signal. Due to the certain limitation of Type-I CS which are elaborated further in Section 3.3, Type-II CS has been proposed. These two CS are compared in terms of control sensitivity, complexity and linearization capability.

3.2 Conventional APD and Type-I Control Scheme for modified APD

The conventional APD, shown in Figure 3.1, is limited by bandwidth of components utilized for a CS. When signal bandwidth approaches to hundreds of megahertz, distorted signal bandwidth approaches to 5 times of the signal bandwidth. In modified Type-I APD, there is a mutual exchange in the position of cubic element and CS which is shown in Figure 3.2 and already explained in Chapter 2 [58], [59]. This change is in favor to capture the wideband signal which is not possible with conventional APD [66]-[69]. For example, suppose 100 MHz signal is given at the input of conventional APD. It is divided into two paths using WPD, where one is directly given in the input of the WPC and, another is given

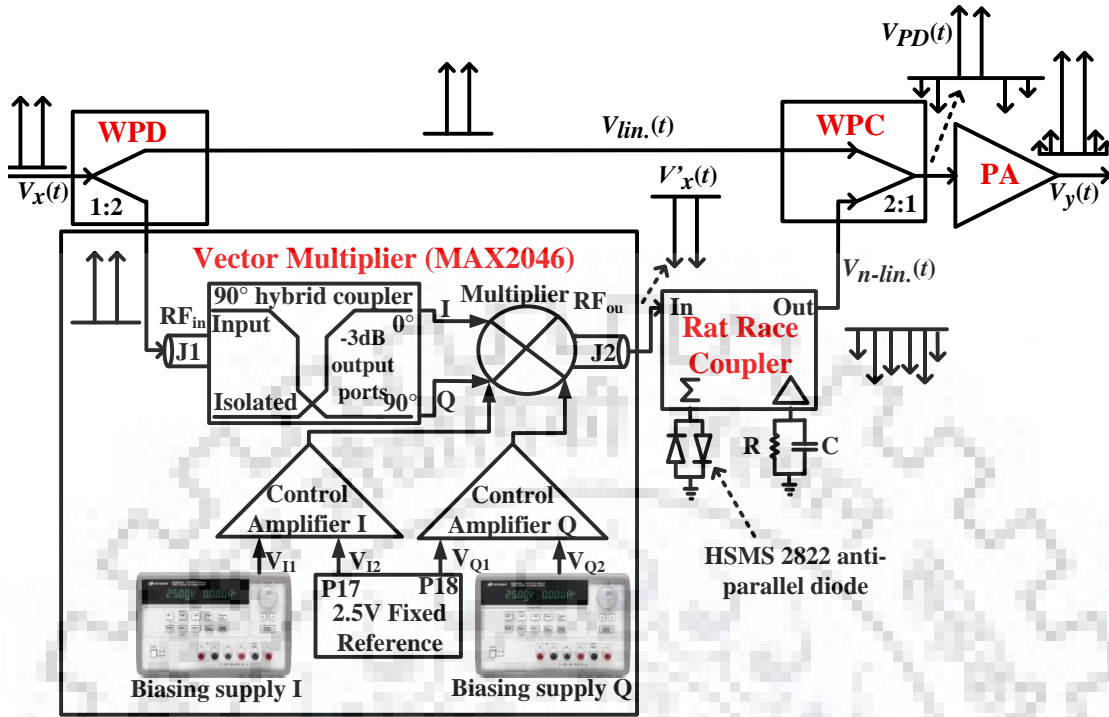


Figure 3.3: Proposed modified APD architecture, where Vector Multiplier is used as a Control Scheme.

to the input of cubic element [82]. In order to compensate IM5 components, the cubic IM generator expands the whole spectrum of signal by five times and produces an expanded output of 500 MHz. This expanded output is given in the input of the CS as shown in Figure 3.1. Optimizing the phase and gain of 500 MHz wideband signal is more cumbersome than that of 100 MHz signal as proposed in Type-I CS.

For successful operation of APD, careful monitoring of the gain and phase of the predistortion signal using particular CS is very crucial which is the main focus of the proposed implementation.

3.3 Type-I Control Scheme using Vector Multiplier

The Type-I CS for APD is shown in Figure 3.3 in which MAX2046 VM is used as a control element that monitor the gain and phase of the predistortion signal in the nonlinear path. The capturing bandwidth of MAX2046 VM is only 320 MHz, ranges from 1740 MHz

to 2060 MHz. When the same VM is deployed in conventional APD, it is not able to handle wideband signal. But with the slight modification in Type-I CS, it works competently for broadband applications. The utilization of VM is one of the most popular control schematic practiced in the literature so far. The RF inputs are internally phase shifted by 90° using coupler to produce in-phase/quadrature-phase (I/Q) signals. VM provides vector adjustment through the control amplifiers which are biased with individual biasing supplies as shown in Figure 3.3. These control amplifiers convert a voltage and current input to a predistortion voltage that controls the multipliers. By varying the biasing supply of control amplifier, gain and phase of the I/Q predistortion signal vary simultaneously.

3.4 Type-II Control Scheme using Digital Phase Shifter and Digital Attenuator

The proposed Type-II CS can be achieved by replacing the VM with a variable gain block and 8-bit DPS which is shown in Figure 3.4. Variable gain block consists of a 7-bit DSA and ZX60V-82+ linear amplifier (LA) from Mini-circuits. The LA provides a fixed gain of 13.5 dB at 1.9 GHz, which can be reduced significantly with the help of cascaded DSA. The gain and phase of the predistortion signal can be controlled digitally and independently with the help of the PC using their respective software and interface.

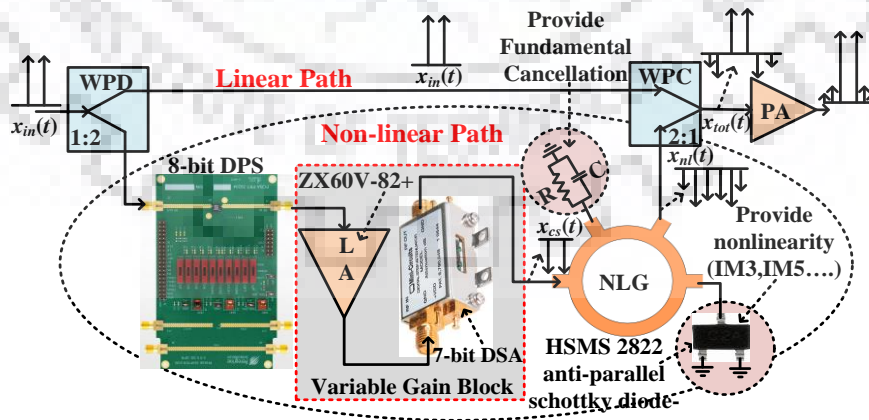


Figure 3.4: Proposed Type-II Control Scheme for the modified APD architecture.

It can also be viewed as an APD linearizer under the regulation of digital circuitry. Manual control of first scheme is replaced with digital control in second scheme, which in turn provide very precise tuning over the gain and phase of predistortion signal. It improves phase and amplitude parameters of the system in the entire range of the phase set points. Precise tuning over the independent parameters provide better sensitivity of control, nonlinearity compensation which in turn enhances the linearizability of the system.

3.4.1 Independent phase and gain control

The Type-II CS provides 358.6° phase shift and required amount of gain/attenuation to the predistortion signal in the nonlinear path. Depending upon the type of nonlinearity generated by PA, the power at the input of IM generator can be tuned. For example, to compensate higher order nonlinearity, IM generator must be excited with high power. If the order of PA nonlinearity is low, i.e. IMD3 only, IM generator require less power to generate IMD3 only. Depending upon the power requirement of IM generator in the nonlinear path, the gain/attenuation of variable gain block can be tuned. At any particular frequency point, the phase can be varied from 0° to 358.6° with the required amount of gain/attenuation, which is not possible with the Type-I CS. The description of DPS and DSA is given below:

3.4.1.1 Digital Step Attenuator

It is used in conjunction with LA to manipulate the gain/attenuation of the predistortion signal. The sensitivity of amplitude is an important parameter in APD as it defines the input power required to trigger IM generator. To compensate the PA nonlinearity, same amount of nonlinearity must be generated by the IM generator in the nonlinear path. For matching both the nonlinearity of PA and predistorter, the selection of power in the nonlinear path must be very accurate. The ZX76-31R75PP+ 7-bit DSA, provides attenuation of 31.75 dB in steps of 0.25 dB. It is controlled by 7-bit parallel interface and biased using a single supply voltage. It provides a very fine tuning of amplitude in the nonlinear branch and provides wideband operation up to 6 GHz.

3.4.1.2 Digital Phase Shifter

To counteract the nonlinear distortion of PA, the nonlinearity which is generated by IM generator must be of same amplitude and anti-phase with respect to the nonlinearity generated by PA. The variable gain block takes care of the amplitude and the requirement of anti-phase must be fulfilled by DPS. The PE44820 8-bit DPS from Peregrine, covers a wide phase range of 358.6° in 1.4° steps and provides very low RMS phase error of only 1° . It maintains excellent phase accuracy in the targeted band of 1.7 GHz-2.2 GHz.

3.4.2 Limitation of the Vector Multiplier

The VM is the backbone of APD and HPD for optimizing the gain and the phase of the input signal. However, the nonlinearity inherent in the VM distorts the input signal and results in efficiency reduction, limiting its use in 5G BS and electronic countermeasure application. VM suffers from misbalances and imperfections in the I/Q signal paths. Nonlinearities of the VM could further introduce more phase and amplitude errors depending on the set point value.

The test-bench for the characterization of VM is shown in Figure 3.5. The characterization some particular frequency points. Phase plot of the VM at different frequency under variable Q biasing supply (V_Q) is reported in Figure 3.6, where I biasing supply (V_I) for

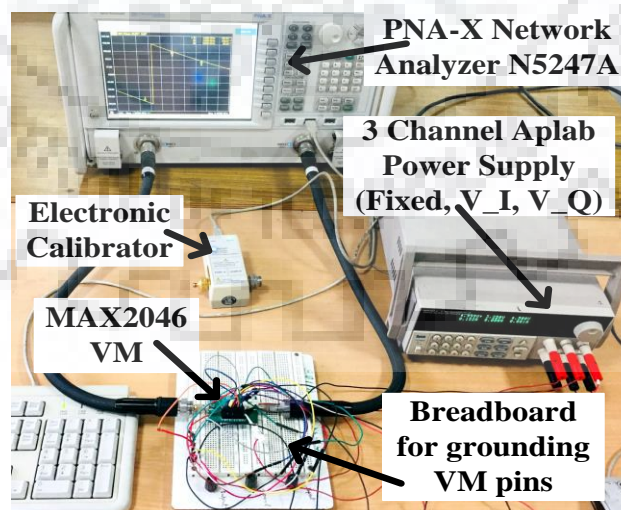


Figure 3.5: Test-bench for the characterization of MAX2046 Vector Multiplier

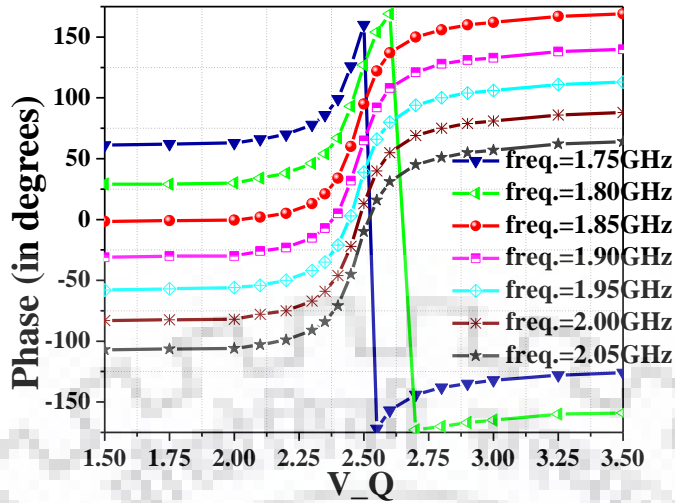


Figure 3.6: Phase plot of MAX2046 VM at different frequencies by varying V_Q supply, where V_I is kept constant.

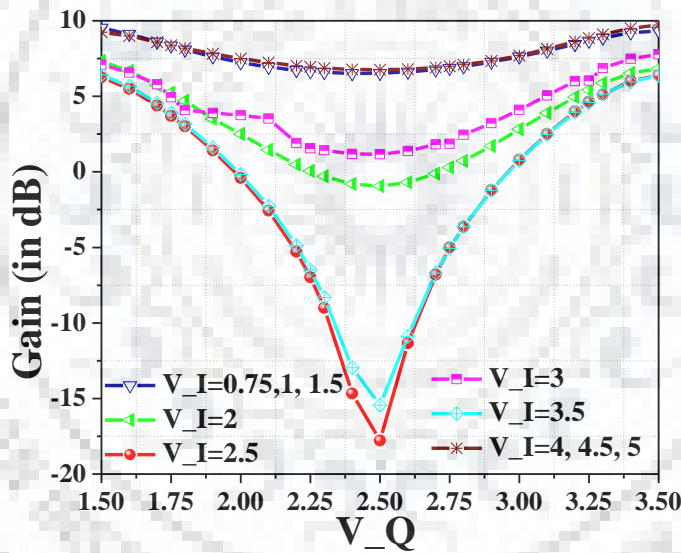


Figure 3.7: Gain plot of MAX2046 VM for the entire frequency band (1740 MHz - 2060 MHz) under variable I and Q biasing supply (V_I and V_Q).

in-phase component is kept constant. It signifies that the phase of the VM is a function of frequency and V_Q . The gain plot of the VM for the entire frequency band under variable I and Q biasing supply (V_I and V_Q) is reported in Figure 3.7. The gain plot of the VM signifies that the gain of VM is a function of V_I and V_Q . If V_I and V_Q is set to a fixed voltage value, the gain of the VM remains constant for the entire frequency band. The value

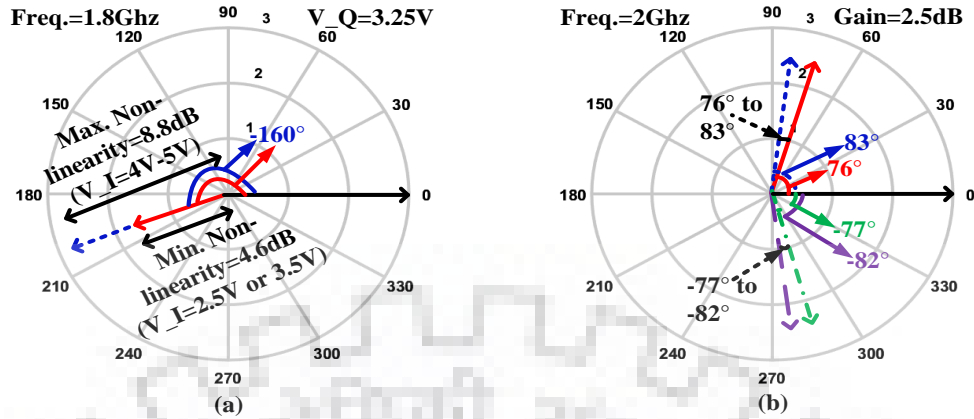


Figure 3.8: (a) Required phase in presence of non-linearity, and (b) Required gain with precise control over phase.

of gain and phase from 0V-1.5V and 3.5V-5.0V is same as 1.5V and 3.5V respectively. However, the discrepancy of the VM is elaborated below in the following cases:

3.4.2.1 Appropriate phase, but inappropriate gain

If the requirement of phase is fixed for a particular frequency point. Some constant value of V_Q is required to achieve this phase. This particular value of voltage maps the phase with some gain or attenuation. As evaluated from Figure 3.6 as V_Q is very low, i.e. 0V-1.5V or very high i.e. 3.5V-5.0V, the VM itself becomes a source of distortion and start adding nonlinearity to the original signal. The minimum gain it can add is 6.4 dB when V_I is fixed to 2.5V or 3.5V.

Suppose for PA nonlinearity compensation, if the phase requirement is -160° at 1.8 GHz. This phase can be attained by fixing V_Q at 3.25V, where value of V_I does not matter to obtain the required phase. But the value of V_I defines the value of the gain that is to be added to the required phase. Depending on the value of V_I, the gain that the VM will add ranges from 4.6 dB to 8.8 dB which is shown in Figure 3.8 (a). If V_I=2.5V or 3.5V it will add 4.6dB of gain and if V_I= 4V to 5V it will add 8.8 dB of gain. Addition of gain is the main cause of nonlinearity which affects the performance of the system. Similarly, if phase requirement is 111° at 1.95 GHz. It can be obtained by fixing V_Q to 3.4V. For obtaining this phase, a minimum of 6 dB gain will be added by VM which is not required.

TABLE 3.1

VARIOUS COMBINATIONS OF VOLTAGES AT 2 GHz FOR FIXED 2.5 DB GAIN

V_I	V_Q	Phase (in degree)
2V	2V	-82
	2.96V	80
2.5V	1.82V	-82
	3.12V	83
3V	2.14V	-77
	2.82V	76
3.5V	1.85V	-82
	3.12V	83

3.4.2.2 Appropriate gain, but inappropriate phase

If the gain required in the nonlinear branch is 2.5 dB at 2 GHz. There are eight combinations of VM biasing supplies (V_I & V_Q) shown in Table 4.1, that provide this required gain. These combinations of voltages, provide only a few values of phase angle at 2 GHz which is shown in Figure 3.8 (b) and Table 4.1. If the requirement of phase is different from these values, the VM will be unable to provide that phase angle. To fulfil the requirement of gain and phase, both at a particular frequency point using VM is very problematic.

3.4.2.3 Abrupt Change in Phase

One important point to be noticed is that varying the V_Q in steps of 0.05V cause an abrupt change in phase. Varying the V_Q from 2.40V to 2.45V at 1.75 GHz results in phase change from 99° to 126° as depicted from Figure 3.6. Similarly, at 2 GHz, when the voltage changes from 2.45V to 2.50V, it causes a phase change from -22° to 13° . Varying a very small step of 0.05V of V_Q , causes a huge jump in phase of approximately 27° to 35° . Similarly, for all other frequencies, the change of phase is very large in accordance with the small change in voltage step. This abrupt change increases the probability of phase error which can be avoided in Type-II CS.

3.4.2.4 Phase control range

The range of phase, which is obtained from VM by varying V_Q is quite less. For example at fixed frequency of 1.85 GHz, when the V_Q varies from 1.5V to 3.5V it causes a shift in the phase from -1° to 169° . Similarly, at 2 GHz the phase changes from -82° to 88° . In both the cases the overall phase shift is around 170° .

3.4.2.5 Laborious circuit connections

MAX 2046 was embedded with J3 lead head connector that consists of 20 pins. For single ended operation, R6 is mounted with 0Ω resistor. It provides 2.5V reference on-chip voltage. Three biasing supplies are required to ensure proper operation of the VM. One fixed supply that is capable of providing 5V and 160mA is connected at pin 20. Two variable biasing supply that can vary from 0V-5V are connected at V_I (pin 1) and V_Q (pin 5) to alter the gain and phase of the predistortion signal. A breadboard is required for grounding of all the current pins when VM operates in voltage mode.

In the proposed modified Type-II CS, a single fixed biasing supply is required for DSA. It is very easy to monitor the gain and phase of the predistortion signal in Type-II CS as compared to VM. In Type-II CS, a single host PC that contains Peregrine DPS software and Mini-circuits attenuator software is required to alter the gain and phase respectively. The phase of DPS can be easily triggered in serial mode using DPS evaluation software. Similarly, a software is required to manage the attenuation of DSA.

All the above problems are combated in the Type-II CS in which the phase can be tuned from 0° to 358.6° in the constant steps of 1.4° . Similarly, the attenuation can be tuned in very small step of 0.25 dB. The independent control over the gain and phase of the predistortion signal is the main focus of Type-II CS.

3.5 Quantitative and Qualitative comparison

In this section, quantitative and qualitative comparison between the proposed two versions and other implementation is carried out which are elaborated below:

TABLE 3.2

POWER REQUIREMENT AT 2 GHz TO GENERATE DIFFERENT IM PRODUCTS

Intermodes	Input power to Passive IM Generator (PIMG)	Input power at IM Generator
IM3	-3 dBm to -1 dBm	-8 dBm to -4 dBm
IM5	-1 dBm to 1 dBm	-4 dBm to -1 dBm
IM7	1 dBm to 4 dBm	-1 dBm to 2 dBm

3.5.1 Sensitivity of Control

It is defined as the relative measure of change in parameter variation. It gives us an indication how the output response of the system is behaving to the input response. Type-II CS has much better control over sensitivity as compared with Type-I which can be explained with the help of two cases.

Case I: assume input signal with bandwidth 'X MHz' and input power is ' λ dBm'.

Case II: signal bandwidth remains same, i.e. 'X MHz', but input power changes from ' λ dB' to ' $\lambda \pm \Delta\lambda$ dBm'.

Suppose, for Case I in conventional and Type-I APD, phase and gain of VM are tuned appropriately to find the sweet spot where best linearization was found. Now, the input power of the signal is increased by 20 dBm as per Case II. In Type-I CS, a change in power level of input needs attenuation of in the nonlinear path before IM generator such that it will excite properly and generate appropriate required IM products. As explained above, as the phase and gain of VM are dependent on each other. Hence, change in attenuation will automatically affect the phase of the predistortion signal. But in Type-II CS, both the parameters are independent of each other, hence, sensitivity of control is better than Type-I

CS. Type-II CS easily handles the Case II by providing the required attenuation using DSA in the non-linear path.

3.5.2 Nonlinearity order compensation

Depending upon the type of PA nonlinearity compensation, the power at the input of IM generator / PIMG can be tuned. Table 3.2 shows the requirement of power at the input of IM generator / PIMG to generate different IM products, centered at 2 GHz. If the linearity requirement is low, i.e. IM3 only, the power at the input of NLG must fall between -8 dBm to -4 dBm. If the target is to compensate higher order IMD till IM7, the requirement of power at the input of NLG rises to 0 dBm. As stated above, due to the limited control sensitivity of the Type-I CS, it is difficult to obtain the desired power in the nonlinear path along with the required phase as compared with the Type-II CS.

3.5.3 System complexity and power consumption

The proposed CS uses low cost and energy efficient passive components to claim the linearization of wideband signal. Hence the hardware complexity, cost and power overhead consumption is minimal in the proposed CS as compared with HPD [58], [141], [175] and DPD [42]-[49]. The feedback path of HPD proposed in [58], captures only the original signal bandwidth, unlike DPD where the bandwidth of the predistortion signal, is typically five times of the input signal which defines the speed of DAC [169]-[174]. Moreover, the speed of an ADC limits the capturing of wideband signal at the PA output, which typically has 5 times bandwidth of the input signal in DPD. Both HPD and DPD use power hungry data converters, FPGAs, transmitter and receiver chains. The proposed CS eliminates all these to make the BS greener and simultaneously reduce the capital and operational expenditure.

3.5.4 Linearizability

Due to the independent control parameters, Type-II CS is proven to extract better benefits of linearization as compared with Type-I CS. The HPD and DPD provide better linearization as compared with the proposed Type-I and Type-II CS due to digital

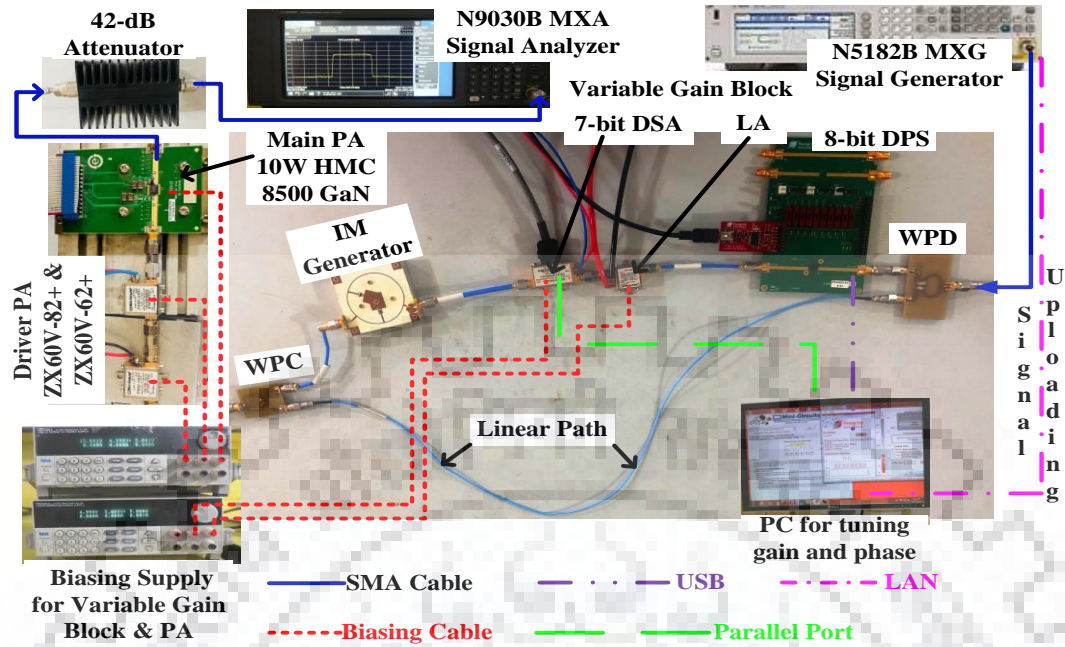


Figure 3.9: Test-bench of the proposed Type-II CS for data extraction.

flexibility of delay and other control parameters, but it comes at a price of higher cost, system complexity and power consumption.

3.6 Experimental verification

3.6.1 Test-bench for data extraction

To access the validity of the modified APD, a test-bench was constructed which is shown in Figure 3.9. The three CS for APD was studied in this chapter:

- (a) conventional APD using VM,
- (b) Type-I APD using VM,
- (c) Type-II APD using variable gain block and DPS.

The Five sets of experiments were devised to validate the system dexterity. In the first set of experiment, the 10W HMC8500 Broadband GaN PA is used as a DUT. The rest of the experiments are performed using a ZX60 14012L-S+ PA from Mini-Circuits.

- (a) In the first set of experiment, a 160 MHz 8CC LTE signal is used, where each CC consist of 20 MHz instantaneous bandwidth. The proposed Type-I and Type-II CS validate the effectiveness by linearizing a 10W HMC8500 PA, driven by 160 MHz signal. As stated earlier due to the bandwidth constraint of MAX2046 VM, a conventional APD is unable to linearize 100 MHz signal.
- (b) In the second set of experiment, a 5CC 100 MHz LTE signal is used, where each CC consist of 20 MHz instantaneous bandwidth. The proposed Type-I and Type-II CS for modified APD is used to linearize ZX60 14012L-S+ PA, driven by 100 MHz signal.
- (c) In the third set of experiment, a narrowband LTE signal of 10 MHz is used to compare the performance of conventional APD with the proposed Type-I and Type-II CS.
- (d) In the fourth set of experiment, an LTE signal of 5 MHz is used to compare the performance of conventional APD with the proposed Type-I CS. This experiment validates that the position of VM does not affect the linearization performance.
- (e) In the fifth set of experiment, two tone signal with frequency spacing of 150 MHz is used to compare the performance of the proposed Type-I and Type-II CS.

Using host PC, the signal is uploaded to the signal generator (MXG N5182B) via Matlab, which is further given to the input of WPD. One output of WPD is given directly to WPC and other output is given in the input of VM and DPS in Type-I and Type-II respectively. In Type-I CS, the control voltages of a VM in the non-linear path are exhaustively optimized to provide better performance for all the conditions required. VM adjusts the gain and phase of the predistortion signal with the help of control voltages in the Type-I CS, but in the Type-II CS, DPS and DSA uses the host PC to monitor the gain and phase. The amplitude and phase of the IM products generated by IM generator were controlled by the VM in Type-I CS. In the Type-II CS, phase of the generated IMD is controlled by DPS and gain is optimized by the variable gain block. Both gain and phase are optimized individually. Phase optimized output from IM generator combines with the fundamental

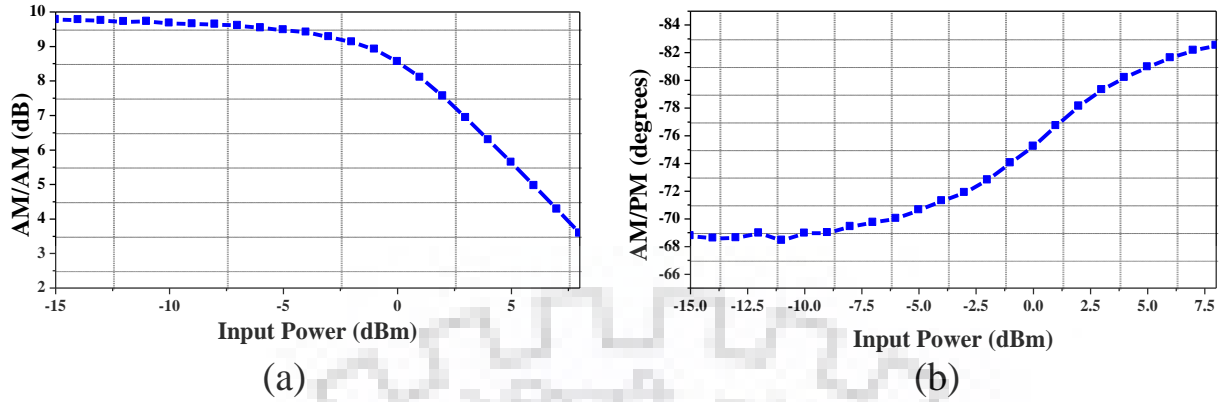


Figure 3.10. Measured AM/AM and AM/PM characteristics of ZX60 14012L-S+ PA.

signal using WPC, which is further given to the input of the PA. An N9030B MXA from Keysight is used to analyze the output of the PA. For all the measurement, the carrier frequency was set to 1.9 GHz. For demonstration, WPC, WPD and IM generator are fabricated in-house.

3.6.2 Device under Test

The proposed Type-I and Type-II CS is used to linearize 10W HMC8500 Broadband GaN PA from Analog devices and ZX60 14012L-S+ PA Mini-Circuits, driven by LTE and two

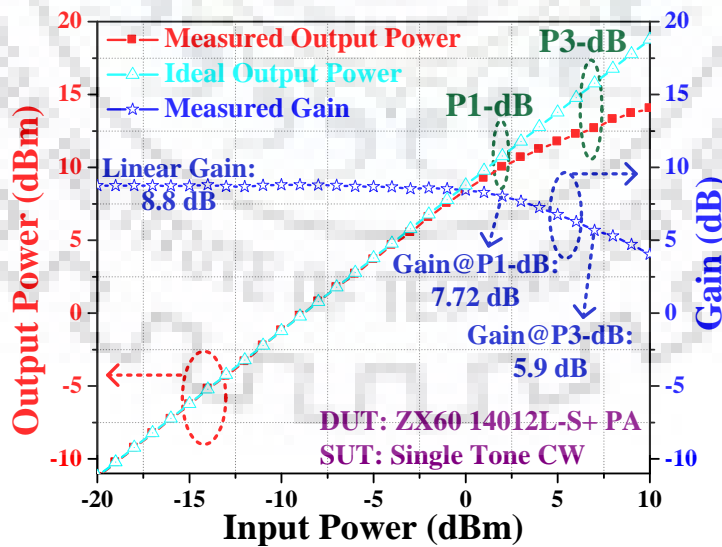


Figure 3.11. Linear and compression region of ZX60 14012L-S+ PA using Single tone CW signal, centered at 2 GHz.

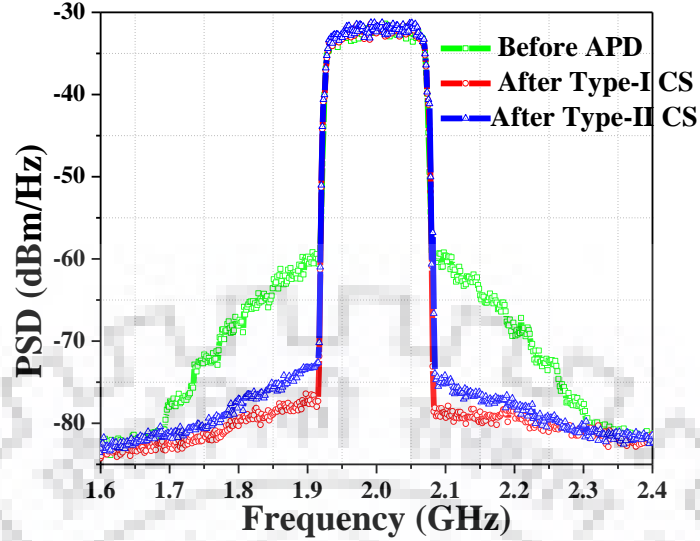


Figure 3.12: Measured Power Spectrum Density of HMC8500 GaN PA with and without the proposed APD excited by 8CC 160 MHz UBB LTE signal.

tone signal. The measured AM/AM and AM/PM characteristics of ZX60 14012L-S+ PA are shown in Figure 3.10. The typical 1 dB compression point characteristics of ZX60 14012L-S+ are shown in Figure 3.10. As depicted in Figure 3.11, for single tone CW signal, the input and output P1-dB of ZX60 14012L-S+ PA is 3 dBm and 10.67 dBm respectively. Similarly, the P3-dB compression point occurs at 7 dBm input power that provides an output power of 12.68 dBm. The ZX60 14012L-S+ PA supports wideband operation up to 14 GHz.

3.6.3 Signal under Test

3.6.3.1 LTE 5CC 100 MHz contiguous signal

It is not possible to linearize 100 MHz wideband signal using APD, hence a new technique has been devised that uses the same hardware and is capable of linearizing 100 MHz signal. Figure 3.12 shows the PSD for the contiguous 8CC 160 MHz LTE signal with and without the proposed linearization methods. A 10W HMC8500 PA is excited by 160 MHz LTE signal of PAPR 14.17 dB. Experimental results show that the PA along with the proposed Type-I CS delivers an ACPR of -41.09 dBc with an improvement of 14.11 dB. Furthermore, an incremental improvement of 3.96 dB in the ACPR was obtained when

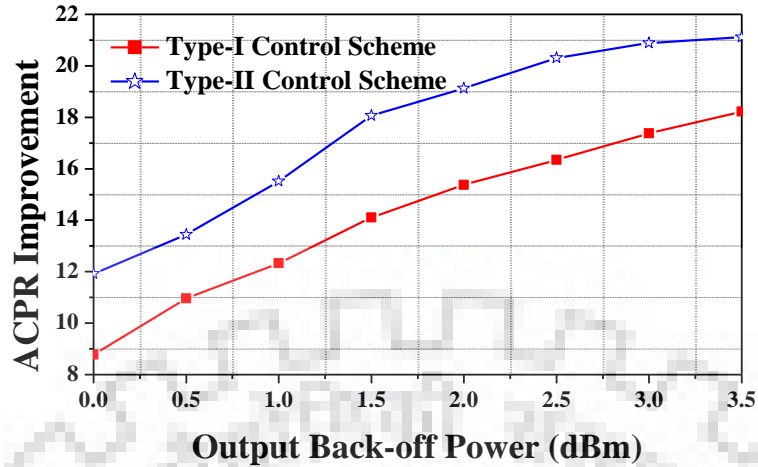


Figure 3.13: ACPR improvement of 10W HMC8500 GaN PA with the proposed CS at different output back-off powers.

using the DPS and DSA in place of VM. With independent control over phase and gain/attenuation intervention, the proposed Type-II CS, further provides a significant improvement in the linearization performance and delivers an ACPR of -45.05 dBc with an improvement of 18.07 dB.

The average output power of 10W HMC8500 PA before and after linearization is 18.58 dBm and 16.92 dBm respectively. It signifies that the ACPR improvement is obtained at

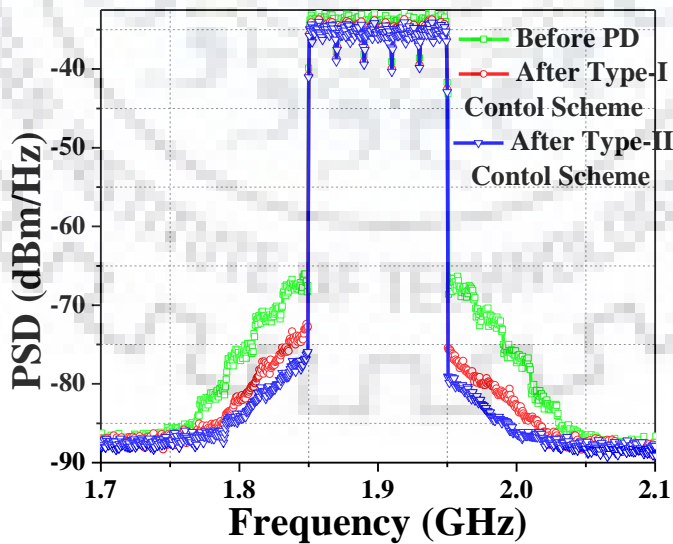


Figure 3.14: Measured Power Spectral Density of ZX60 14012L-S+ PA with and without the proposed Type-I and Type-II Control Scheme excited by 100 MHz LTE signal.

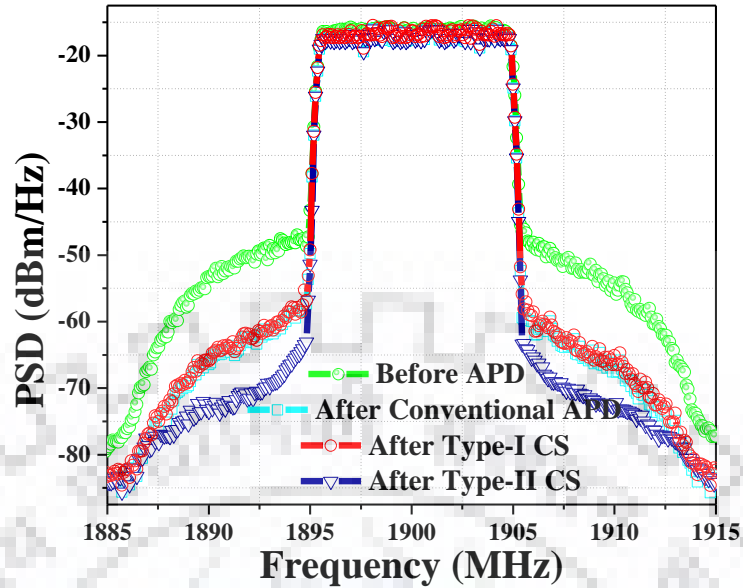


Figure 3.15: Measured Power Spectrum Density of PA with and without the conventional and proposed APD excited by 10 MHz LTE signal.

1.5 dB output back-off power (OBOP). Figure 3.13 shows the measured improvement in the ACPR using contiguous 8CC 160 MHz LTE signal with the proposed Type-I and Type-II CS at various OBOP. The OBOP refers to the power that is reduced from the P1 dB of PA, where PAPR of the input modulated signal is considered.

Figure 3.14 shows the PSD for the 5CC 100 MHz LTE signal with and without the proposed linearization methods. A ZX60 14012L-S+ PA is excited by 100 MHz wideband signal of PAPR 12.52 dB. Experimental results show that the PA along with the proposed Type-I CS delivers an ACPR of -40.39 dBc with an improvement of 7.03 dB. Furthermore an improvement of 3.72 dB in the ACPR was obtained when using the combination of variable gain block and DPS in place of VM. With independent control over phase and gain intervention, Type-II CS, further provides a significant improvement in the linearization performance and delivers an ACPR of -44.11 dBc with an improvement of 10.75 dB.

3.6.3.2 LTE 10 MHz and 5 MHz signal

These tests are conducted just to make sure that the position of VM does not affect the linearization of the system. It showcase that the performance of the conventional APD is almost similar to the Type-I CS.

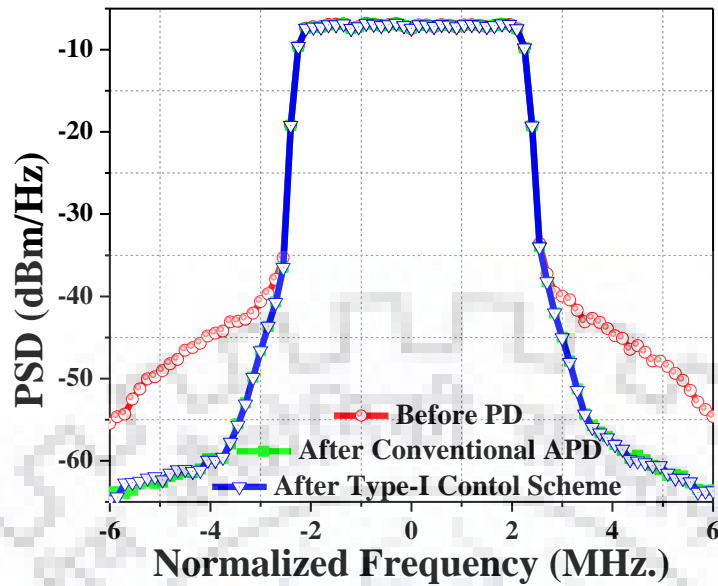


Figure 3.16: Measured Power Spectrum Density of PA with and without the CAPD and the proposed Type-I Control Scheme excited by the 5 MHz LTE signal, centered at 2 GHz.

A PA is excited by 10 MHz LTE signal of PAPR 10.09 dB. Figure 3.15 shows the PSD of PA with and without the proposed APD. For 10 MHz LTE signal, the conventional APD delivers an ACPR of -42.52 dBc with a cancellation of 13.71 dB. Similarly, the Type-I CS is able to deliver an ACPR of -41.97 dBc with an improvement of 13.16 dB. The linearization performance of the conventional and Type-I APD is almost similar. Furthermore, an improvement of 4.75 dB in the ACPR was obtained when using the proposed Type-II CS in place of the conventional APD. The Type-II CS delivers an ACPR of -47.27 dBc, with an improvement of 18.46 dB.

Figure 3.16 shows the PSD of PA with and without the proposed Type-I CS and conventional APD. A PA is excited by 5 MHz LTE signal of PAPR 8.77 dB, centered at 2 GHz. For 5 MHz narrow band signal, conventional APD also provides significant improvement in the ACPR, similar to Type-I CS.

3.6.3.3 Two tone signal with frequency spacing of 150 MHz

Figure 3.17 shows the measured spectrum of PA output with and without proposed Type-I and Type-II CS, excited by two tone signal with a frequency spacing of 150 MHz centered

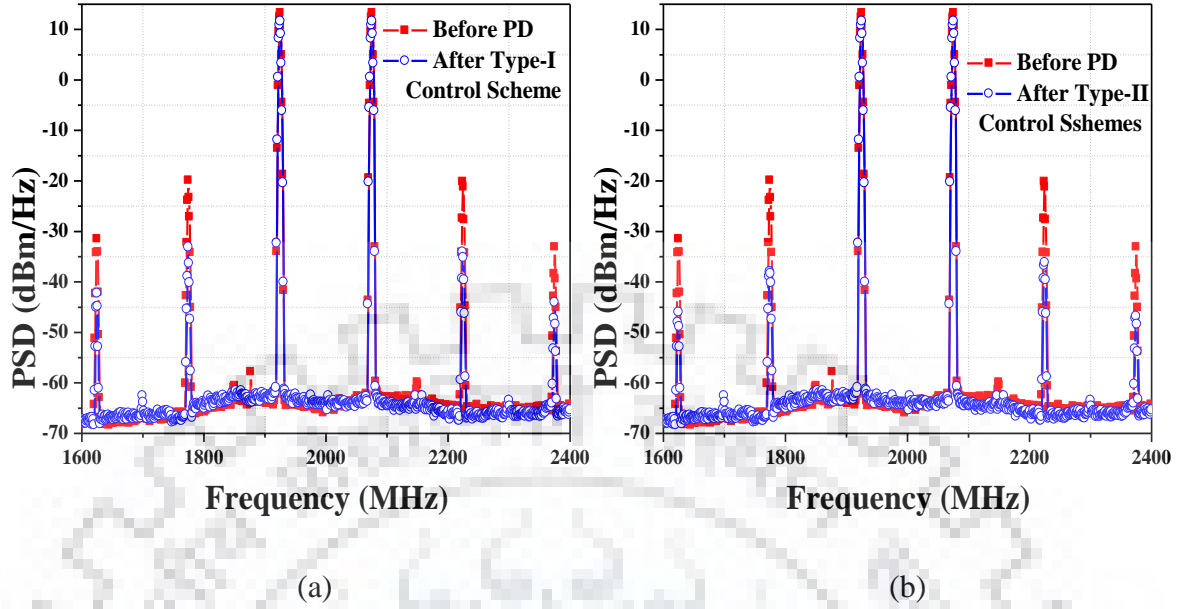


Figure 3.17: Measured Power Spectrum Density of PA excited by 150 MHz two tone signal, centered at 2 GHz (a) with and without the proposed Type-I Control Scheme, and (b) with and without the proposed Type-II Control Schemes

TABLE 3.3

IMD CORRECTION BEFORE AND AFTER TYPE-I AND TYPE-II CONTROL SCHEMES

IMDs	Before APD	IMD After Type-I CS	Correction (dB) Type-I	IMD After Type-II CS	Correction (dB) Type-II
IM3U	-20.86	-34.88	14.02	-37.71	16.85
IM3L	-19.89	-33.09	14.53	-37.98	18.09
IM5U	-33.49	-44.51	11.02	-46.80	13.31
IM5L	-31.5	-42.87	11.37	-45.52	14.02

at frequency 2 GHz. The ability of proposed CS is showcased by mitigating the higher order intermodulation products of the two tone signal, whose tones are situated at frequency f_1 and f_2 (1925MHz and 2075MHz) respectively. IM3 (IM3L and IM3U) distortions were generated around 1775MHz ($2f_1-f_2$) and 2225MHz ($2f_2-f_1$). Similarly IM5 (IM5L and IM5U) around 1625MHz ($3f_1-2f_2$), and 2375MHz ($3f_2-2f_1$).

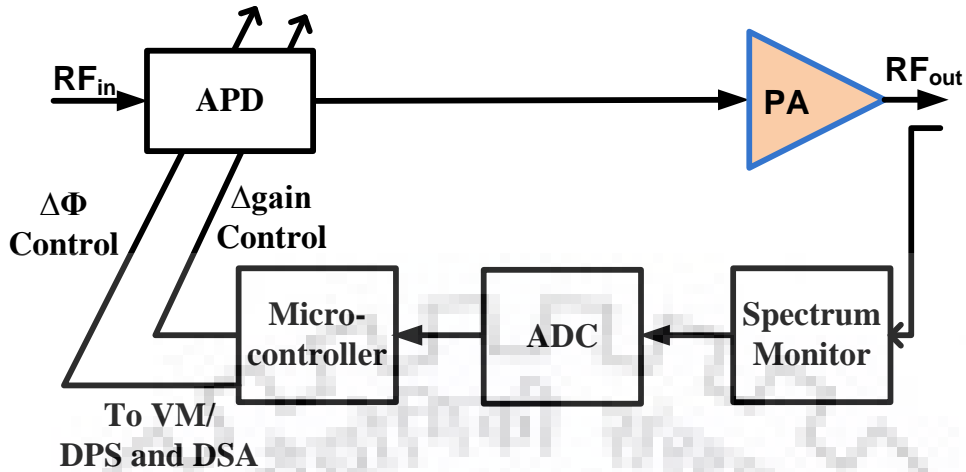


Figure 3.18: Automatic Calibrated adaptive Analog Predistorter architecture.

Table 3.3 shows the performance using two tone signal with and without the proposed Type-I and Type-II CS. It shows the effectiveness of proposed CS by providing a significant cancellation to higher order intermodes and enhances the linearity of PA.

The measurement result shows that using independent control over the gain and phase results in the better linearizability of the system. The Type-II CS provides better results than the Type-I CS in terms of IM cancellation.

3.6.4 Adaptive Spectrum Monitoring

As stated in the introduction of this chapter, the appropriate gain and phase control is the key to achieve good linearization. For both the CS, the control over the gain and phase has been done manually for proof-of-concept by controlling the gain and phase of the VM/DPS and DSA in the nonlinear path. It requires an adaptive scheme for controlling the gain and phase parameters of APD [97]-[102]. Moreover, in case of any change in process, voltage and temperature (PVT), an automatic compensation scheme based on automatic calibration must be employed in APD setup [103]-[105]. In this section, we will study how to perform the gain and phase calibration adaptively.

Figure 3.18 describes the block diagram of the proposed automatic calibrated APD. The proposed system contains two additional parts: The Spectrum Monitor and the Microcontroller.

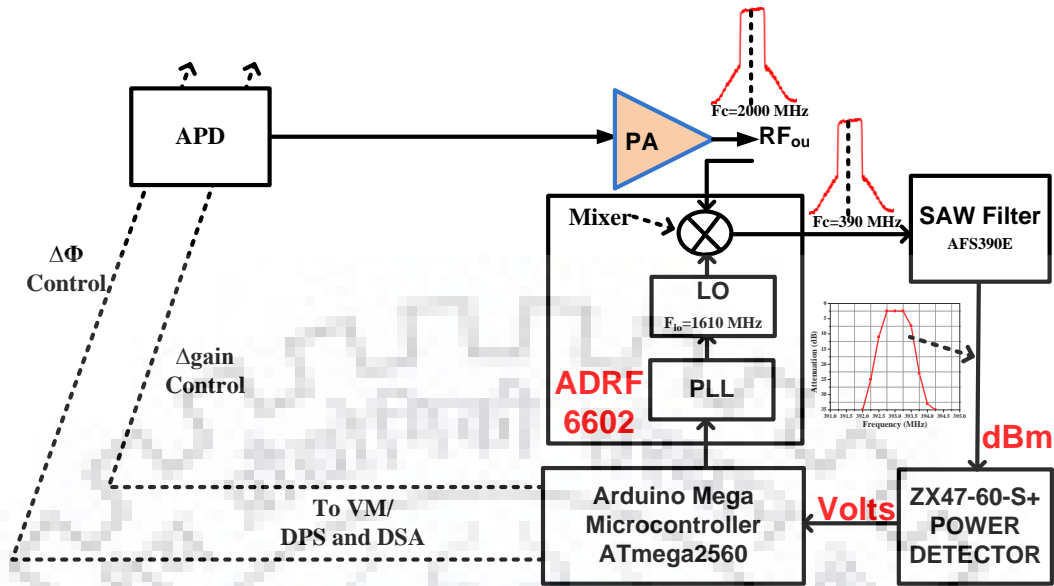


Figure 3.19: Block diagram of data acquisition for adaptive Analog Predistorter architecture.

The Spectrum Monitor detects output power spectrum density and sends that data to the microcontroller through an ADC interface [106]-[109]. The microcontroller can be used to monitor the CS of the predistorter that consists of variable attenuator and phase shifter whenever needed.

The Spectrum Monitor is composed of a phase locked loop (PLL), a mixer, a Surface Acoustic Wave (SAW) filter and a power detector made out of off the shelf components, which is shown in Figure 3.19 [110]. As depicted from Figure 3.19, PLL generates the stable LO signal and the RF output signals from the PA are sampled and are down-converted by the corresponding LO signal in the mixer. The spectrum of down converted IF signals are the same as those of RF signals as shown in Figure 3.19. The down converted IF signals become a continuous wave signal after passing through the SAW filters [64].

The internal frequency range of LO mixer is 1550 MHz to 2150 MHz. Hence, the LO frequency of the Mixer is swept in this range. If the PA output is centered at 2000 MHz, the frequency of the Mixer is fixed to 1610 MHz. The IF output of the down converter mixer is now appearing at 390 MHz that is made to pass through a AFS390E SAW filter, center frequency of 390 MHz and bandwidth typically 500 KHz. The transfer function of

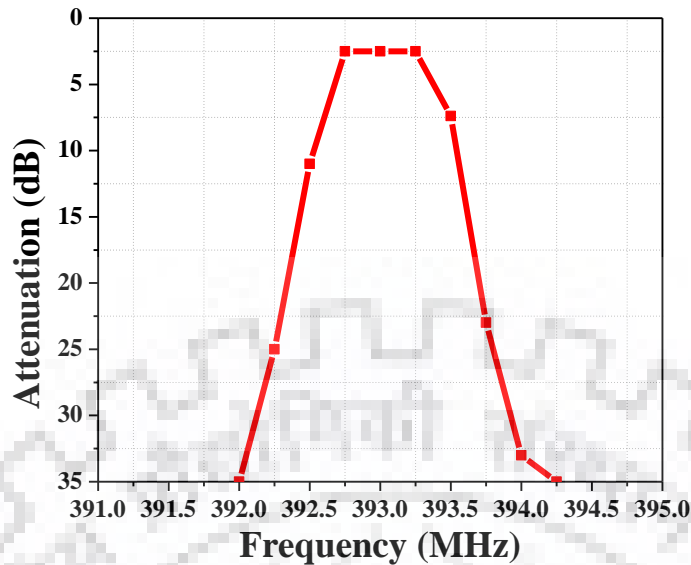


Figure 3.20: The transfer function of AFS390E SAW filter.

AFS390E SAW filter is shown in Figure 3.20. It signifies that outside pass band which is 392.75 MHz to 393.25 MHz, SAW filter offers very high attenuation. The high attenuation outside the pass band results in the extraction of CW signal from IF signal. The output of the filter is passed through a power detector, which gives output as a DC Voltage value proportional to the power of the input signal. In a power detector, the specific frequency component can be analyzed by sensing the CW signal.

The LO frequency in ADRF 6602 is swept gradually using PLL that causes the corresponding sweeping of the IF signal at the output of the mixer. This IF signal passes through the narrow windows of SAW filter. Gradually sweeping the IF signal with respect to a particular frequency band yields the corresponding magnitude value. Finally, the PSD of the PA output RF signal can be examined with the knowledge of the frequency in the ‘x-axis’ and the magnitude of the detected CW signal at the output of Power detector in the ‘y-axis’. The output of power detector can be measured using analog input pins in Arduino Mega.

The phase and gain of particular CS can be controlled using Arduino by sending digital control signals to the pins of VM/DPS and DSA. The different hardware components which can be used in the system assembly are listed as follows:

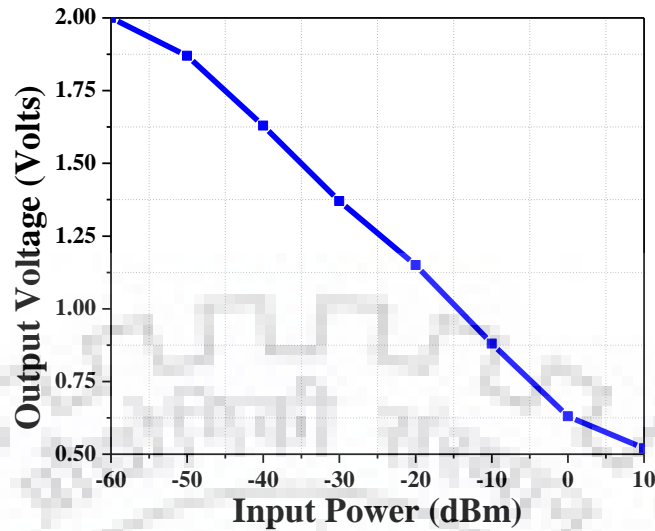


Figure 3.21: Amplitude v/s DC Output Voltage of Power Detector centered at 2 GHz.

ADRF 6602: The ADRF6602 is a high dynamic range active mixer with integrated PLL and voltage controlled oscillator. The PLL/synthesizer uses a fractional-N PLL to generate a f_{LO} input to the mixer. The reference input can be divided or multiplied and then applied to the PLL phase frequency detector. It was operated with different values of the RF input signal and LO frequencies. Specifications of the device are as follows:

- RF input frequency range: 1000 MHz to 3100 MHz
- Internal LO frequency range: 1550 MHz to 2150 MHz
- Input reference frequency range: 12 MHz to 160 MHz

Microcontroller: The ATmega2560, Arduino mega can be used as a microcontroller. Sampled values of the input signal can be taken as an analog input for obtaining the power levels at different LO frequency values. The microcontroller detects the continuous change in the spectrum components and uses the minimization algorithm to minimize spurious power.

Power Detector: ZX47-60-S+ from Mini-Circuits is used as a power detector that provides wideband operation ranging from 10 MHz to 8 GHz. The input power v/s DC Output Voltage of Detector for 2 GHz center frequency is shown in Figure 3.21.

3.7 Conclusion

Stemming from conventional APD as reference, a modified Type-I and Type-II CS for efficiently compensating the nonlinear distortion of PA in UBB stimulus has been pursued in this chapter. This chapter raises the issue of practical implementation of modified APD design in the analog domain and limitation of the state-of-art linearization technique. It relaxes the requirement of data converters, FPGA and still provide commendable linearization.

The proposed implementations yield the linearization of contiguous 160 MHz UBB LTE signal centered at 2 GHz, which is not possible with conventional APD. It is worth mentioning that Type-I CS, uses the same hardware which is used in conventional APD, to linearize 160 MHz UBB LTE signal. Due to its ability to operate in a UBB environment without gathering baseband information, the proposed CS is being considered as a strong candidate for multi carrier repeater system and 5G applications. It is a promising solution for 5G BS, since its cost and power overhead does not increase correspondingly with the increase of signal bandwidth. Furthermore, an improvement of 3.96 dB in the ACPR was obtained when using independent control parameters instead of VM to linearize PA excited by 160 MHz LTE signal.

Chapter 4

Ultra-Broadband RF Predistorter

4.1 Introduction

To pave the road for future 5G communication systems, LTE-A needs to improve its radio performance. Hence carrier aggregation (CA) is one of the proposed method in 5G to enhance the spectrum efficiency. It can be done by the concatenation of multiple component carrier (CC) that form an effective bandwidth. Based on the frequency band of operation, it can be characterized as intra- and inter-band which is shown in Figure 4.1. If multiple CC is operating in the same frequency band, it is referred as intra-band CA, whereas, simultaneous transmission of multiple CC in different frequency band results in inter-band or multi-band CA [111]-[115]. Intra-band is further classified as contiguous and non-contiguous, depending whether the CC are occupying the adjacent channels or not.

4.1.1 Inter-band and Intra-band Transmission

LTE- Advanced employs CA of CC in order to increase signal bandwidth and thereby increase the bitrate. Following two cases are considered:

Intra-band CA: Two CCs of 5 MHz each centered at frequency 1822.5 MHz (ω_1) and 1877.5MHz (ω_2) is simultaneously transmitted in the band-3 with a gap of 55 MHz as shown in Figure 4.2 (a).

When these CCs passes through the PA, it produces out-of-band distortion by generating IM products. Out-of-band IM3 products lie at frequency 1932.5 (IM3U) and 1767.5MHz (IM3L). Similarly, IM5 products lie at frequency 1987.5 MHz (IM5U) and 1712.5MHz (IM5L). These IM-products are very far away from fundamental signal frequency ω_1 and ω_2 . Hence it can be easily filtered out using a BPF.

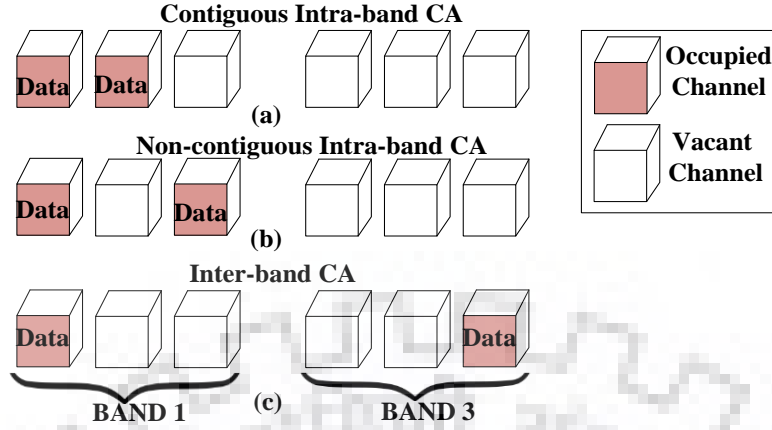


Figure 4.1: (a) Contiguous and (b) Non-contiguous intra-band CA communication scenario and, (c) the inter-band CA communication scenario.

Inter-band CA: Two CC are simultaneously transmitted in Band-2 and Band-3 shown in Figure 4.2 (b). Table 4.1 shows the location of CC and their IM products. IM3U and IM5U of Band-3 and IM3L' and IM5L' of Band-2 fall on the fundamental signal and causes cross modulation [116]. In this case, it is not possible to use the BPF because it can eliminate the fundamental signal. Therefore, every effort must be made to control inter-band cross modulation distortion to ensure maximum possible linearity by reducing out-of-band IM products. Hence predistortion is essentially required to reduce IMD.

TABLE 4.1
INTER-BAND COMPONENT CARRIER AND IM PRODUCTS

Inter-band Downlink Transmission	IM products	Center frequency of IM
Band-3	IM3U($2\omega_2 - \omega_1$)	1932.5 MHz *
$\omega_1 = 1822.5 \text{ MHz}$	IM3L($2\omega_1 - \omega_2$)	1767.5 MHz
$\omega_2 = 1877.5 \text{ MHz}$	IM5U($3\omega_2 - 2\omega_1$)	1987.5 MHz *
	IM5L($3\omega_1 - 2\omega_2$)	1712.5 MHz
Band-2	IM3U'($2\omega_2' - \omega_1'$)	2042.5 MHz
$\omega_1' = 1932.5 \text{ MHz}$	IM3L'($2\omega_1' - \omega_2'$)	1877.5 MHz *
$\omega_2' = 1987.5 \text{ MHz}$	IM5U'($3\omega_2' - 2\omega_1'$)	2097.5 MHz
	IM5L'($3\omega_1' - 2\omega_2'$)	1822.5 MHz *

* represents cross modulation terms.

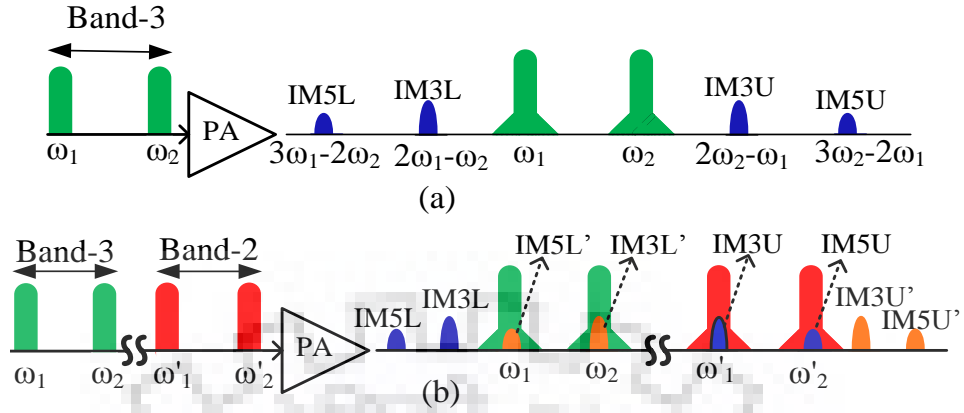


Figure 4.2: (a) Intra-band, and (b) Inter-band downlink transmission.

4.2 Carrier Aggregation and the Predistortion

CA was first introduced in Release 10, which allows operators to efficiently use its spectrum assets to boost user throughput. According to Release 10, the maximum allowed bandwidth per CC is 20 MHz. Through Release 12, CA of up to 5 CC and 100 MHz instantaneous bandwidth will be required in the forthcoming LTE-advanced systems [117] and it will further extend to 8 CC 160 MHz wideband signals. The framework of LTE allows the CA of the 32 CC in Release 13, which makes 640 MHz instantaneous signal bandwidth, part of which can be located in the unlicensed spectrum [118]-[121]. As per Release 14, for certain applications such as indoor hotspot, dense urban, urban macro, high speed, etc. around 4 GHz, the uplink and downlink supports bandwidth of up to 200 MHz [122]. For indoor wideband below 6 GHz, the CA bandwidth of up to 160 MHz are supported by 5G system [123].

Such a high bandwidth will remarkably increase the challenges for system design. Specifically, there will be limitations in the practical implementation of the DPD, which demands innovation in the predistortion linearizer. The state-of-the-art DPD models in current linearizer imposes serious bandwidth restrictions on ADC, DAC, and FPGA for UWB signal transmission [124]-[127]. Despite the breakthrough made in existing DPD, nontrivial hardware concern remains, and in some cases it will directly affect the design aspects. Heading among these is the exorbitant high cost and power overhead consumption of the power hungry data converters for processing hundreds of MHz signal bandwidth.

Moreover, DPD technique requires knowledge of digital baseband signal at the input [128]. This proves to be a limitation of the RF repeater system, where linearization needs to be applied to incoming RF signal before amplifying and transmitting it to the next station. Hence, a linearization technique that alleviates the need of power hungry data converters, FPGA for processing the UWB signal is desirable. A detailed investigation of hurdle in DPD, while transmitting an UWB signal, is carried out at the end of this chapter

The Conventional and the proposed RF-in RF-out APD discussed in Chapter 2, shown in Figure 2.1 and Figure 2.6 respectively, is attractive for PA in transmitters and repeaters for long distance communication. Such a system is desirable where baseband signal is not readily available and it also alleviates the need of FPGA and data converters. However, the inherent limitation in CAPD leads to the development of the proposed RF-in RF-out APD.

4.2.1 Multi-band CA and the Proposed UBB MRF-PD

The proposed RF-in RF-out APD provides a competent solution for the contiguous and non-contiguous intra-band signals. Moreover, it also works well for the multi-band CA communication within the specified bandwidth ranging from 1750 MHz to 2250 MHz [58], [59], and [70]. The proposed RF-in RF-out APD is frequency reconfigurable with an instantaneous bandwidth of 500 MHz. Inter-band CA utilizes two independent bands for the transmission of LTE signal. If we use single wideband PA that covers both the band, then predistortion requirements become very challenging.

Recently, broadband and multi-band PA designs have been proposed to support schemes such as CA and wideband communication in BS transmitters. Advancement in the PA technology makes it possible to use single wideband PA to support widely spaced signals in the frequency domain [129]-[136]. Being able to cover simultaneously two or more downlink frequency bands with single PA requires innovation in the predistortion architecture, which has the potential to linearize wideband/ multi-band PA.

The two cases are discussed below that showcase the need of the proposed multipath predistortion i.e. UBB MRF-PD for supporting multi-band communication instead of the proposed RF-in RF-out APD.

Case I: If the simultaneous downlink transmission is performed in Band-2 (1930MHz-1990MHz) and Band-3 (1805MHz-1880MHz), then instead of using individual PA for each band, the better solution is to use single wideband PA that covers both the bands. In this case the proposed RF-in RF-out APD can be seen as a promising technique for wideband PA without sacrificing linearization performance. It can effectively work for the concurrent transmission in Band-2 and Band-3 of 5G spectrum.

Case II: If inter-band communication is simultaneously carried out in Band-3 (1805 MHz - 1880 MHz) and Band-8 (925 MHz-960 MHz), either one can use the individual PA for processing each CC. However, it seems to be very impractical and costly process. The alternate way is to use single multiband PA or a single UWB PA that can easily process both the CC together. For efficiently processing both the CC together, a UBB predistortion is required that has the capability to linearize both the CC simultaneously. As explained above, the proposed RF-in RF-out APD works effectively from 1750 MHz to 2250 MHz, hence it is unable to provide the linearization for Band-8. Moreover, it is not a preferable choice for the multi-band PA.

To address the aforementioned limitations, two RF-in-RF-out UBB-predistortion designs are proposed in this chapter for the linearization of UWB signals. First predistorter is UBB RF-PD which works effectively for intra-band CA communication, while second predistorter is UBB MRF-PD that works well for inter-/multi-band CA communication. It is easier to integrate the proposed UBB MRF-PD with multiband PA due to its ability to operate in UWB environment ranging from 200 MHz to 2.5 GHz with an instantaneous bandwidth of 2.3 GHz.

Similar to the proposed RF-in RF-out APD, in UBB RF-PD and UBB MRF-PA, the non-linear function and corrections are applied in the analog domain without requiring access to the baseband. It also eliminates the need of ADC, DAC, FPGA, wideband transmitter and receiver chains, etc. In fact, being a complete RF-in RF-out system, UBB- predistortion are easier to integrate with 5G BS, RF PA, and repeater systems. It has the advantage of simple and cost-effective architecture since predistortion is performed by RF components in analog domain but provides a moderate linearity improvement.

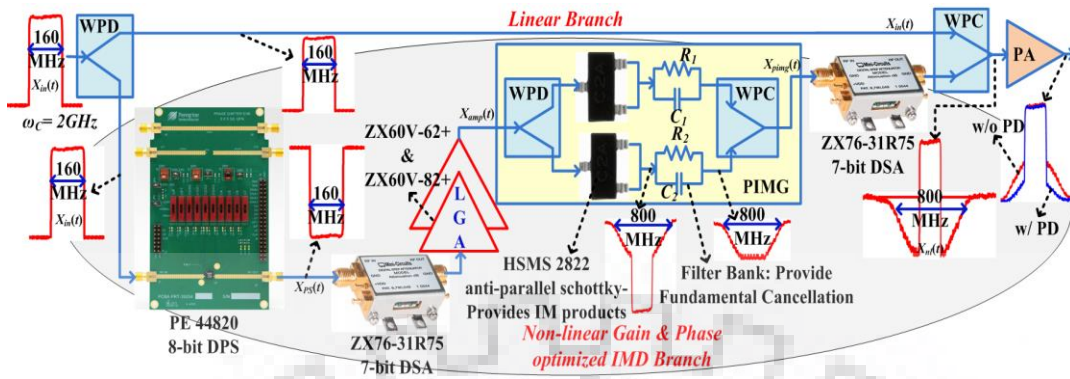


Figure 4.3: Proposed Ultra-Broadband RF-Predistorter for intra-band communication.

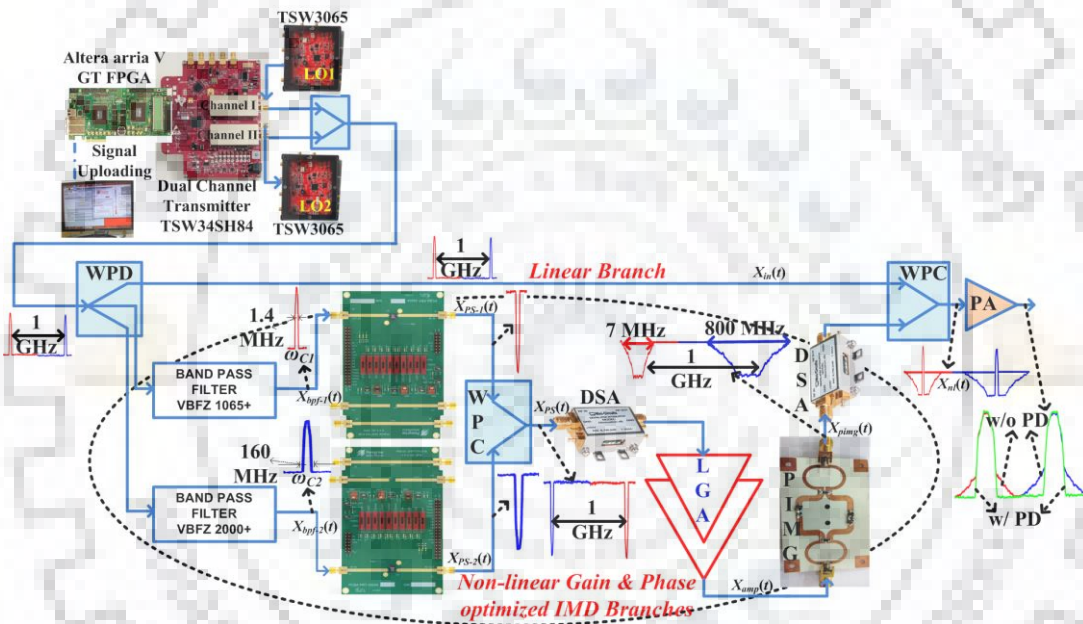


Figure 4.4: Proposed Ultra-Broadband Multipath RF-Predistorter for inter-/multi-band communication.

4.3 Proposed Ultra-Broadband RF-Predistortion and Ultra-Broadband Multipath RF-Predistortion

The proposed UBB RF-PD and UBB MRF-PD linearization schemes are shown in Figure 4.3 and Figure 4.4, when driven by intra- and inter-/multi-band CA signals respectively.

4.3.1 Reforms and Benefits

In order to convert conventional APD and the proposed RF-in RF-out APD into the proposed UBB predistortion, three modifications have been implemented, which are explained below along with their benefits:

Modification I: Mutual exchange in the position of IM generator and VM, the detailed investigation of which is already provided in Chapter 2. Instead of capturing $5\times$ of the signal bandwidth, VM captures only the original bandwidth of the input signal [59].

Modification II: Design of novel IM generator with UBB Passive Intermodulation Generator (PIMG). Wider the bandwidth it can support, more beneficial it is for multi-band communication scenarios. The multi-band signal whose bandwidth exceeds 500 MHz, is not supported by an IM generator [58], [59]. The proposed PIMG is frequency reconfigurable from 200 MHz to 2.5 GHz, with an instantaneous bandwidth of 2.3 GHz.

The first two modifications were made to capture the multi-band signal, which is not possible with the conventional and the proposed RF-in RF-out APD system. The asymmetric phases of IMDs are directly proportional to the bandwidth of the signal. As the signal width increases, the asymmetric phase between the upper and lower IMD products begin to rise [137]. It impairs the IMD cancellation performance of APD because Digital Phase Shifter (DPS)/VM is unable to provide the required phase throughout the signal bandwidth. Therefore, proposed UBB RF-PD cannot correct the signal, if the bandwidth exceeds 200 MHz. It is due to the practical limitation of DPS/VM.

Consequently, UBB MRF-PD is proposed to provide a linearization solution for inter-/multi-band communication which is shown in Figure 4.4. In UBB MRF-PD, two nonlinear paths have been optimized that process each CC individually. Instead of tuning the phase of both CC together using single DPS, MRF-PD uses individual DPS for individual CC. Hence, a DPS has to handle the bandwidth of individual CC, instead of the bandwidth of the entire multi-band signal.

Modification III: Replacement of VM with a combination of DPS and Digital Step

Attenuator (DSA). VM is the key component in APD and Hybrid PD, for tuning the phase and magnitude of the input signal. However, the nonlinearity inherent in the VM distorts the input signal and results in efficiency reduction, limiting its use for accurate and precise control. Both phase and magnitude of VM are voltage variable and also dependent on each other. If the requirement of phase is fixed for a particular frequency point, some constant value of voltage is required to achieve this phase. This particular value of voltage maps to the phase with some gain or attenuation, which affects gain when no change in gain is required. Similarly, if the gain/attenuation requirement is “x dB” at 2 GHz, this value of gain/attenuation corresponds to some fixed phase angle. It will be problematic if the phase requirement is different from the achieved phase. Hence, to fulfil the requirement of gain and phase simultaneously at a particular frequency, using VM, is very challenging.

Therefore, third modification has been done to replace the simultaneous variation of gain and phase with independent control, which in turn enhances the system efficiency. It is done by replacing the VM with a combination of the 7-bit DSA and 8-bit DPS. Manual control of VM is replaced with digital control. The gain and phase of the predistortion signal can be tuned independently and digitally using their respective interface and software. It can also be viewed as an analog linearizer under digital regulation. The detailed explanation of this modification is featured in Chapter 3.

4.3.2 Component Description

The components which are used in the proposed UBB predistortion schemes are elaborated below:

4.3.2.1 Wilkinson Power Divider

The input signal is split into two paths in UBB RF-PD where one goes directly to the WPC and other drives the nonlinear phase and gain optimized IMD path. The input signal at UBB RF-PD is given as:

$$X_{in}(t) = \text{Re} \left\{ A(t) \left[\left(e^{j\omega_1 t} + e^{j\omega_2 t} \right) e^{j\phi[A(t)]} \right] \right\} \quad (4.1)$$

$$X_{in}(t) = A(t) \left[\cos(\omega_1 t + \phi[A(t)]) + \cos(\omega_2 t + \phi[A(t)]) \right] \quad (4.2)$$

where $A(t)$ and $\phi[A(t)]$ is the amplitude and phase of the input signal. Assume the signal that lies at frequency ω_1 and ω_2 poses same phase angle. Hence a single DPS is required to tune the phase of the entire signal.

Similarly, in the UBB MRF-PD input signal is split into three paths using 1:3 WPD, where the lower two paths are the phase and gain optimized IMD paths and the upper path is the linear path that carries the fundamental signal via SMA coaxial cable at the input of 3:1 WPC. The input signal in UBB MRF-PD is given as:

$$X_{in}(t) = A(t) \left[\cos(\omega_1 t + \phi_1[A(t)]) + \cos(\omega_2 t + \phi_2[A(t)]) \right] \quad (4.3)$$

where $\phi_1[A(t)]$ and $\phi_2[A(t)]$ are the phase of lower and upper CC respectively in inter-/multi-band communication. As both the CCs are separated with huge frequency difference, hence, we assume that both pose different phase angles. In order to tune the phase of both the CC, two DPS are required in UBB MRF-PD. The output from WPD is given to the input of BPF.

4.3.2.2 Band Pass Filter

In the UBB MRF-PD two BPFs are used, one in each nonlinear IMD path that allow only one CC in each branch. The VBFZ-1065+ and VBFZ-2000+ BPFs from Mini-circuits meet rugged test lab system environment and require small space. These BPFs offer good rejection and low insertion loss.

It is not possible to tune the phase of entire several hundred MHz multi-band input signal using single DPS. Therefore, multipath technique has come into the picture for inter-/multi-band communication in which each CC has dedicated individual nonlinear IMD path. The output from BPF which is given to the input of DPS is shown below:

$$X_{bpf-1}(t) = A(t) \cos(\omega_1 t + \phi_1[A(t)]) \quad (4.4)$$

$$X_{bpf-2}(t) = A(t) \cos(\omega_2 t + \phi_2 [A(t)]) \quad (4.5)$$

4.3.2.3 Digital Phase Shifter

At any particular frequency point, the phase can be varied from 0° to 358.6° in the steps of 1.4° which is not possible with VM. It delivers small root mean square (RMS) phase error of only 1° . In UBB MRF-PD, BPF is followed by individual DPS that tune the phase of respective CC. The phase of the intermodulation products generated by the PIMG can be tailored by adjusting the phase of each CC with the help of individual DPS. The DPS output after phase optimization in UBB-MRF-PD is given as:

$$X_{PS-1}(t) = A(t) \cos(\omega_1 t + \phi_{PS-1} [A(t)]) \quad (4.6)$$

$$X_{PS-2}(t) = A(t) \cos(\omega_2 t + \phi_{PS-2} [A(t)]) \quad (4.7)$$

where $\phi_{PS-1}[A(t)]$ and $\phi_{PS-2}[A(t)]$ is the phase provided by the DPS to the lower and upper CC respectively. In UBB MRF-PD, the output from both the DPS is combined using WPC. The output of WPC is given as:

$$X_{PS}(t) = A(t) \left[\cos(\omega_1 t + \phi_{PS-1} [A(t)]) + \cos(\omega_2 t + \phi_{PS-2} [A(t)]) \right] \quad (4.8)$$

The signal at the output of DPS must be anti-phase with respect to the input signal, i.e. $\phi_{PS-1} = \pi + \phi_1[A(t)]$ and $\phi_{PS-2} = \pi + \phi_2[A(t)]$.

$$X_{PS}(t) = A(t) \left\{ \begin{array}{l} \left[-\cos(\omega_1 t) \cdot \cos(\phi_1 [A(t)]) - \sin(\omega_1 t) \cdot \sin(\phi_1 [A(t)]) \right] + \\ \left[-\cos(\omega_2 t) \cdot \cos(\phi_2 [A(t)]) - \sin(\omega_2 t) \cdot \sin(\phi_2 [A(t)]) \right] \end{array} \right\} \quad (4.9)$$

$$X_{PS}(t) = -A(t) \left[\cos(\omega_1 t + \phi_1 [A(t)]) + \cos(\omega_2 t + \phi_2 [A(t)]) \right] \quad (4.10)$$

-ve sign in the (4.10) represents a phase inversion at the output of DPS with respect to the input signal in the linear path. Similarly, in the UBB RF-PD, a single PE44820 DPS from

Peregrine is used, that can adjust the phase of the entire input signal in such a way that the intermodes products generated by the PIMG counteracts the IMD of the PA.

$$X_{PS}(t) = A(t) \left[\cos(\omega_1 t + \phi_{PS}[A(t)]) + \cos(\omega_2 t + \phi_{PS}[A(t)]) \right] \quad (4.11)$$

where $\phi_{PS}[A(t)]$ is the phase provided by the DPS to the input signal. The signal at the output of DPS must be anti-phase with respect to the signal in the linear path i.e. $\phi_{PS} = \phi + \pi$. Put the value of ϕ_{PS} in (4.11) yields:

$$X_{PS}(t) = A(t) \left\{ \begin{bmatrix} -\cos(\omega_1 t) \cdot \cos(\phi[A(t)]) \\ -\sin(\omega_1 t) \cdot \sin(\phi[A(t)]) \end{bmatrix} + \begin{bmatrix} -\cos(\omega_2 t) \cdot \cos(\phi[A(t)]) \\ -\sin(\omega_2 t) \cdot \sin(\phi[A(t)]) \end{bmatrix} \right\} \quad (4.12)$$

$$X_{PS}(t) = -A(t) \left[\cos(\omega_1 t + \phi[A(t)]) + \cos(\omega_2 t + \phi[A(t)]) \right] \quad (4.13)$$

(4.10) and (4.13) represents a phase reversal. For simplicity let

$$\cos(\omega_1 t + \phi[A(t)]) = \cos(\omega_1 t + \phi_1[A(t)]) = \cos(f_1) \quad (4.14)$$

$$\cos(\omega_2 t + \phi[A(t)]) = \cos(\omega_2 t + \phi_2[A(t)]) = \cos(f_2) \quad (4.15)$$

4.3.2.4 Digital Step Attenuator and Linear Gain Amplifier

The IMDs which are generated by RF PA must match with the nonlinearity generated by the predistortion. Mismatch between the order of IMDs between the PA and predistortion leads to inefficient performance. This combination guarantees that the amplitude of IMD generated by the PIMG must be same to that of the PA. Depending upon the amplitude and the type of IMD requirement, i.e. IM3, IM5 or IM7, the power at the input of PIMG can be tuned with the help of this combination. The phase optimized output from DPS is given in the input of the PIMG through a combination of DSA and linear gain amplifier (LGA). Similarly, in the UBB MRF-PD, the phase optimized signal which is combined from both the DPS using WPC, is given in the input of PIMG. For effective cancellation of PA IMD, the IM products which are generated by the PIMG must be anti-phase and have an equal

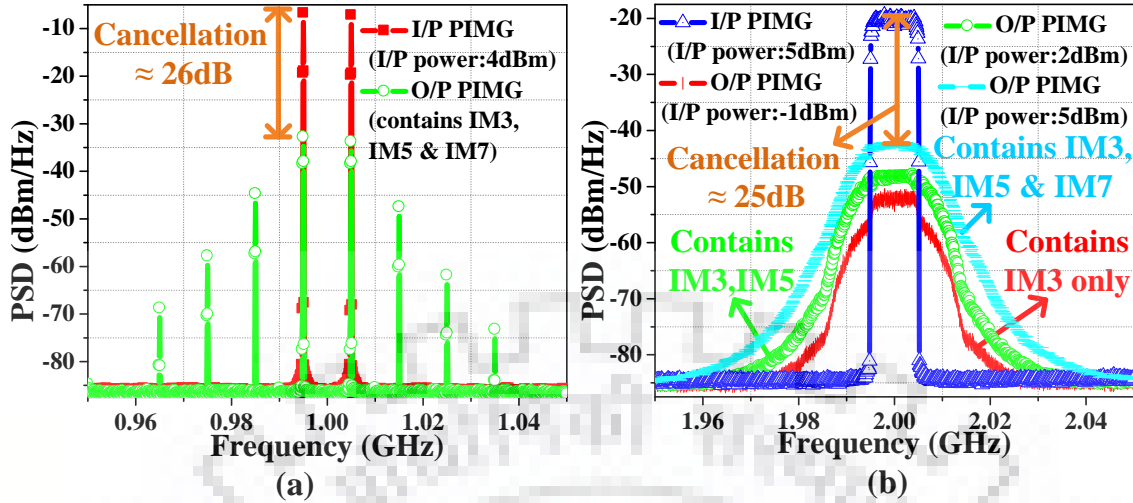


Figure 4.5: Analysis of PIMG excited by 10 MHz (a) two tone signal, centered at 1 GHz, (b) LTE signal, centered at 2 GHz.

amplitude compare to that of the PA. This combination, which is given to the input of PIMG makes sure that the power at the input should be fair enough to drive PIMG to generate the appropriate required IM product. The signal at the output of PIMG is given as:

$$X_{amp}(t) = -K(t) [\cos(f_1) + \cos(f_2)] \quad (4.16)$$

where $K(t) = A(t) \pm \Delta A(t)$, which signifies that the power of signal in the nonlinear IMD path can be tuned depending upon the requirement. LGA is using ZX60V-62+ and ZX60V-82+ amplifiers from Mini-circuits for providing fixed gain of 28 dB, which can be reduced significantly with the help of DSA. The requirement of gain and attenuation in different cases is explained in Section 4.4 and Table 4.2.

4.3.2.5 Passive Intermodulation Generator

The capability of the PIMG is judged by its ability to cancel the fundamental signal and to generate higher order IM products which is shown in Figure 4.5. Figure 4.5 shows the PSD of PIMG driven by 10 MHz two tone and LTE signal centered at 1 GHz and 2 GHz respectively. The detailed explanation of the PIMG is provided in Section 4.4. A pair of diodes connected in anti-parallel fashion, generate odd order and cancel even order IMD which is given as: (assuming PA is weakly nonlinear and taking only IM3 into account).

$$X_{pimg}(t) = k_1 X_{amp}(t) + k_3 X_{amp}^3(t) \quad (4.17)$$

From (4.16) and (4.17), we get:

$$X_{pimg}(t) = -K(t)k_1 \begin{bmatrix} \cos(f_1) + \\ \cos(f_2) \end{bmatrix} - \frac{9}{4} K(t)k_3^3 \begin{bmatrix} \cos(f_1) + \\ \cos(f_2) \end{bmatrix} - \frac{1}{4} K(t) k_3^3 \begin{bmatrix} \cos(3f_1) + \\ \cos(3f_2) \end{bmatrix} - \frac{3}{4} K(t)k_3^3 \begin{bmatrix} \cos(2f_2 - f_1) + \cos(2f_2 + f_1) + \\ \cos(2f_1 - f_2) + \cos(2f_1 + f_2) \end{bmatrix} \quad (4.18)$$

The RC filter bank employed on both the branches of PIMG has the capability to suppress the fundamental signal. First two terms are fundamental signal that can be easily suppressed using an RC filter bank. The third term is the third order harmonics are lying at frequency $3f_1$ and $3f_2$ that can also be easily filtered out using BPF. Last term includes IM3 products that lie at frequency $2f_1 + f_2$ and $2f_2 + f_1$, which can be easily filtered out because it lies far away from main signal. All these terms are discarded in (3.18). The output of PIMG is given as:

$$X_{pimg}(t) = -\frac{3}{4} K(t)k_3^3 [\cos(2f_2 - f_1) + \cos(2f_1 - f_2)] \quad (4.19)$$

4.3.2.6 Digital Step Attenuator

The ZX76-31R75 DSA from Mini-circuits provides attenuation of 31.75 dB in steps of 0.25 dB. It is biased using a single supply voltage and controlled by 7-bit parallel interface using host PC. It provides a very fine tuning of amplitude in the nonlinear IMD branch. Schmitt Triggers are used to buffer Control lines that allows a wide range of control levels. On top of DPS, this DSA provides further precise tuning of gain and phase, and significantly enhances the linearizability of both the proposed RF-predistortion schemes.

4.3.2.7 Wilkinson Power Combiner

At WPC, the signal from linear and nonlinear IMD path are combined with phase difference of 180° , so the fundamental signal and IM products have opposite phase. The signal output from linearizer that drives the PA is given as:

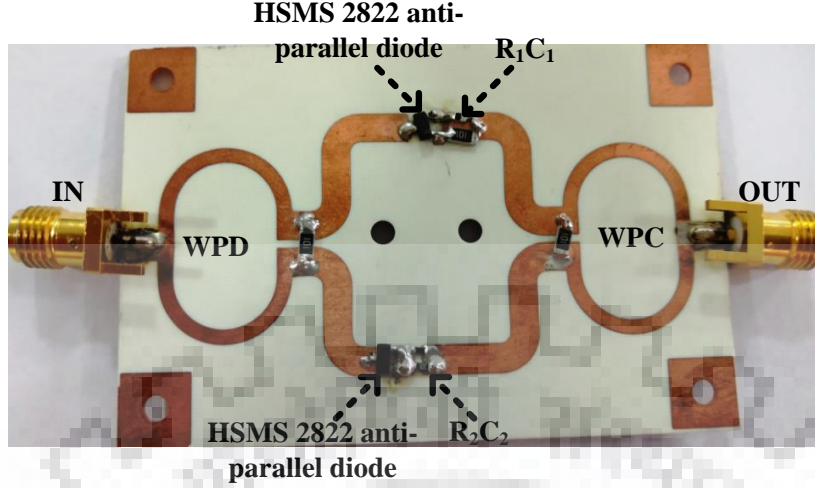


Figure 4.6: Fabricated PIMG mounted with RC filter banks and HSMS-2822 anti-parallel diode pair.

$$X_{nl}(t) = X_{in}(t) + X_{pimg}(t) \quad (4.20)$$

$$X_{nl}(t) = A(t) \left\{ \begin{bmatrix} \cos f_1 + \\ \cos f_2 \end{bmatrix} - \frac{3}{4} K(t) k_3^3 \begin{bmatrix} \cos(2f_2 - f_1) + \\ \cos(2f_1 - f_2) \end{bmatrix} \right\} \quad (4.21)$$

The IMD components in (4.21) that is generated by IMD path, cancel the IMD components of PA due to its opposite phase.

4.4 PIMG Modeling and Case Studies

The fabricated PIMG shown in Figure 4.6, was constructed using WPC, WPD, two RC filter banks and a pair of anti-parallel Schottky diodes i.e. HSMS 2822. The two output arms of WPC are fabricated with anti-parallel diode pair that can be considered the IMD source and a residual linear component exist due to the imperfect cubic characteristics. This residual signal along with the IMD is given in the input arm of WPD which is further processed through an RC component. These linear impedances gives rise to appropriate reflection coefficients for the cancellation of the residual linear component.

Diodes are nonlinearity generators and IMD source, while the RC resonant circuit suppresses the fundamental signal. Momentum simulation of Advance Design System

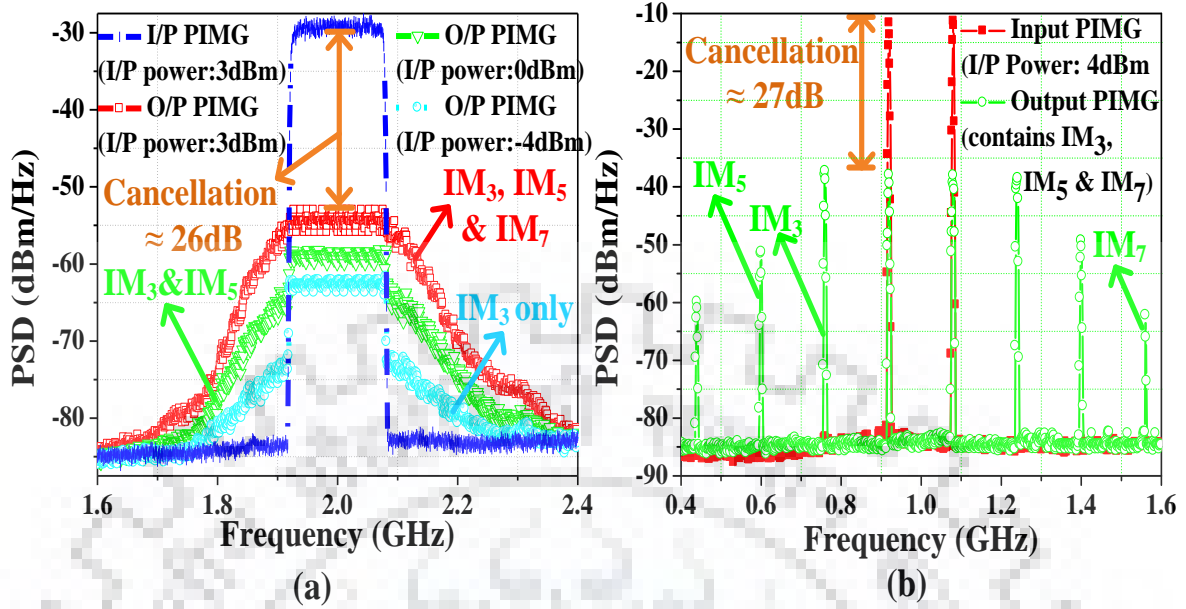


Figure 4.7: Measured Power Spectrum Density of the Passive intermodulation generator excited by 160 MHz (a) 8CC LTE signal, (b) two tone signal.

reveals the value of resonant circuit components, i.e. R_1C_1 and R_2C_2 that provide the best fundamental cancellation. PIMG was fabricated using Rogers 4350B substrate with the thickness of 20 mil and relative permittivity of 3.66.

Ideally, it was supposed that the PIMG can cancel the whole fundamental signal, but practically it provides 25-28 dB cancellation, which is shown in Figure 4.5 and Figure 4.7. The remaining signal at fundamental signal represents in-band IMD distortion appearing at the PIMG output. Figure 4.5 shows the response of PIMG when driven by narrowband signal. Similarly Figure 4.7 establishes the UWB capability of the proposed PIMG, where it demonstrates the behavior of PIMG when driven by UWB signal. Figure 4.7 (a) and Figure 4.7 (b) shows the measured PSD of the PIMG driven by 8CC 160 MHz LTE signal and two tone signal with frequency spacing of 160 MHz, centered at 2 GHz and 1 GHz respectively.

It is worth mentioning that Figure 4.7 (a) elaborates three cases. In the first case, there is only IM3 generation. In the second case, along with IM3, IM5 is also generated. Similarly, in the third case, IM generation up to seventh order is considered. Figure 4.7 (b) shows a case with a two-tone signal, with frequency spacing of 160 MHz, centered at 1 GHz. The

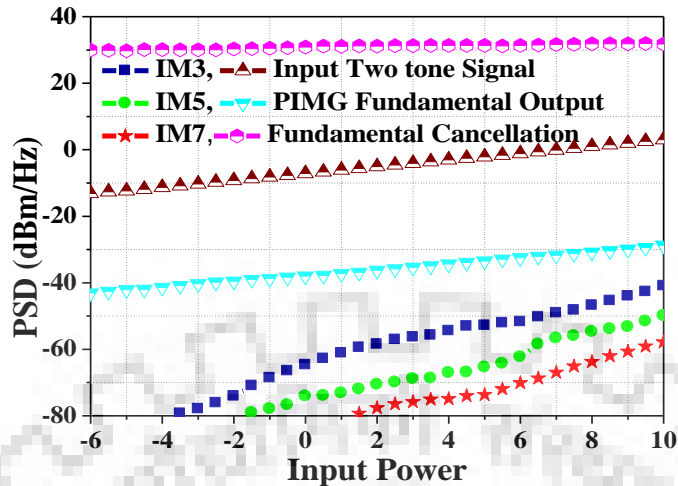


Figure 4.8: Modeling of PIMG using 10 MHz two tone signal at different input power, fixed frequency 2 GHz.

input power of signal is selected to provide maximum fundamental cancellation and to generate higher order IM product. With 4 dBm input power, it generates seventh order IMD and simultaneously cancels the fundamental signal up to 27 dB. Figure 4.8 provides the measured PIMG response with respect to the input power for two tone signal, centered at 2 GHz with frequency spacing of 10 MHz. Similarly, Figure 4.9 shows the measured response of the PIMG at a fixed input power of 0 dBm and the broadband capability of the PIMG is reported by varying the center frequency.

For input power (P_{in}), center frequency (F_c), fundamental signal cancellation (FSC) and IMD generation (IMG), we can perceive from Figure 4.8 that as P_{in} increases, IMG start rising, however signal cancellation performance FSC does not change significantly.

- To generate IM3 at 2 GHz, the input power of the PIMG must fall between -3.5 dBm to -0.5 dBm as shown in Figure 4.8.
- If the requirement is to generate IM3 and IM5 both at F_c of 2 GHz, the input power of the PIMG must fall between -0.5 dBm to 3.5 dBm.
- The PIMG input power must be more than 3.5 dBm to generate higher order IM products such as IM7.

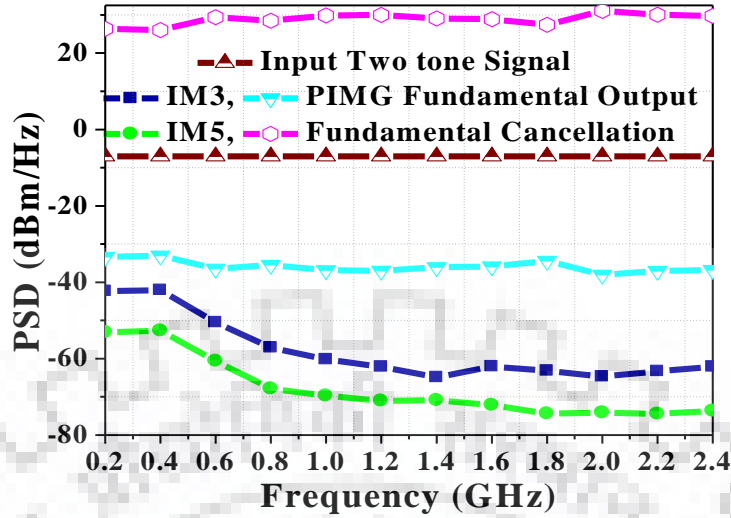


Figure 4.9: Modeling of PIMG using 10 MHz two tone signal at different frequency, fixed input power 0 dBm.

We can perceive from Figure 4.9 that as the F_c progresses the IMG reduces, however the performance is approximately constant beyond 800 MHz. To generate IM3 at a fixed F_c of 200 MHz, the power requirement reduces to -6 dBm to -2 dBm, which was -3.5 dBm to -0.5 dBm at a fixed F_c of 2 GHz. For a fixed center frequency, the fundamental signal cancellation (FSC) is constant.

4.4.1 Case Studies of the PIMG

Four case studies have been performed to verify the functionality of the PIMG. These case studies are elaborated in Table 4.2 and explained in Figure 4.10.

TABLE 4.2
VARIOUS OPERATING CONDITIONS OF THE PIMG

Case	I/P power (dBm)	Center Frequency	Target/ Application	Power required to trigger PIMG
I	-20	400 MHz	IM3	-5.5
II	-20	2000 MHz	IM3	-1
III	0	1200 MHz	IM3, IM5 & IM7	4.5
IV	10	2000 MHz	IM3 & IM5	2

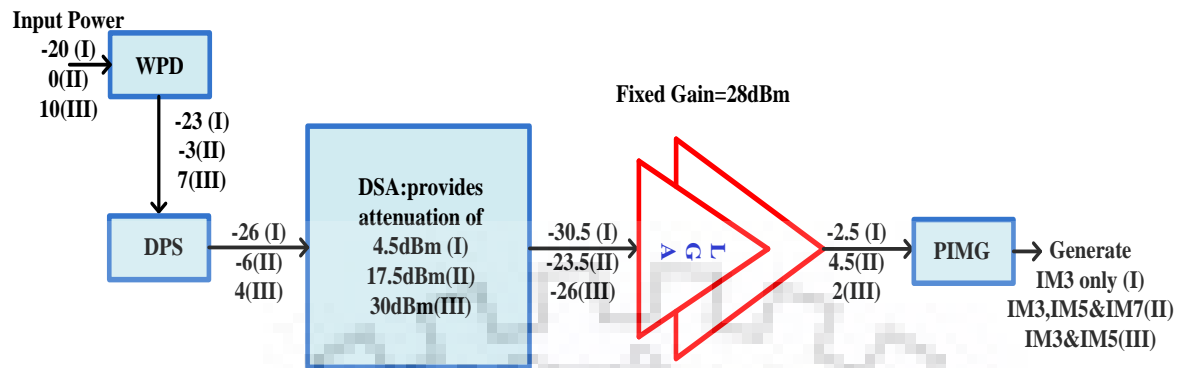


Figure 4.10: Power flow analysis of PIMG under various operating condition.

Assuming that the insertion loss of the WPD as well as DPS is 3 dB each, the gain optimization performed by the DSA for all the four cases is shown in Figure 4.10. The first two cases assume that the PA is weakly nonlinear and it will generate nonlinearity only up to third order. Moreover, the input power of the signal remains same but the center frequency of operation is different. It can be observed that where frequency of operation is low i.e. 400 MHz, the PIMG requires lesser power to generate IM3 as compared with second case where center frequency of operation approaches to 2 GHz.

The third case assumes the PA to be highly nonlinear. In this case the frequency of operation is 1.2 GHz and PIMG is required to generate higher order IM products till IM7. The minimum power requirement to generate IM7 must be at least 4.5 dBm. In the fourth case, PIMG needs to generate IM5 at the center frequency of 2 GHz and corresponding input power requirement is 2 dBm.

4.4.2 Video Bandwidth of the PIMG

VBW is a figure of merit for any predistortion architecture or PA, in which the efficient transmission of the signal is the primary concern. In order to find the VBW of PIMG, following three experiments are conducted at 2 GHz.

Exp. 1: PA is excited using two tone signal with frequency spacing of 10 MHz ($\Delta f = 10$ MHz), where input power is kept constant. The input power to PIMG is -2 dBm, such that it will generate IM3. To find the VBW of PIMG, the tone spacing is increased and the

symmetry between IM3H & IM3L is observed. For 160 MHz two tone signal, IM3H & IM3L are observed to be symmetrical.

Exp. 2: PIMG is again excited using the two tone signal with frequency spacing of 10 MHz ($\Delta f = 10$ MHz), where input power is now increases to 1 dBm, such that PIMG will generate fifth order IM products (IM5H & IM5L). When signal bandwidth is increased to 160 MHz, IM5H & IM5L are found to be symmetrical.

Exp. 3: The input power is now increases to 4 dBm, such that PA will generate seventh order IM products (IM7H & IM7L). Similarly, for 160 MHz two tone signal, IM7H & IM7L are symmetrical. It can also be visualized from Figure 4.7 (b), where it generates the IM products up to seventh order and maintain the symmetry between them.

From above three experiments, it is concluded that the VBW of PIMG is $\geq 160 \times 7 = 1120$ MHz.

4.5 Experimental Verification

4.5.1 Test-bench for data extraction

The test-bench of UBB RF-PD and UBB MRF-PD is shown in Figure 4.11 (a) and Figure 4.11 (b) respectively. In UBB MRF-PD, TSW34SH84 dual channel transmitter contains 1.5 giga-samples-per-second (GSPS) 16-bit DAC and two TRF3705 complex RF modulators, with output frequency ranging from 300 MHz to 4 GHz. The transmitter is connected to an Altera Arria V GT module which comprises of two 5AGTFD7K3 FPGA. A baseband I/Q signal is uploaded to the RAM of FPGA using Quatrus software and MATLAB. The I/Q data is sent to the transmitter using pre-programmed FPGA at a sampling frequency of 307.2 MHz. In DAC, it is further interpolated by a factor of 4 to a sampling frequency of 1228.8 MHz. The signal is up-converted using complex RF modulator TRF3705 and TSW3065 Local Oscillator (LO). After up-conversion, lower and upper CC are directed to the dual channel transmitter.

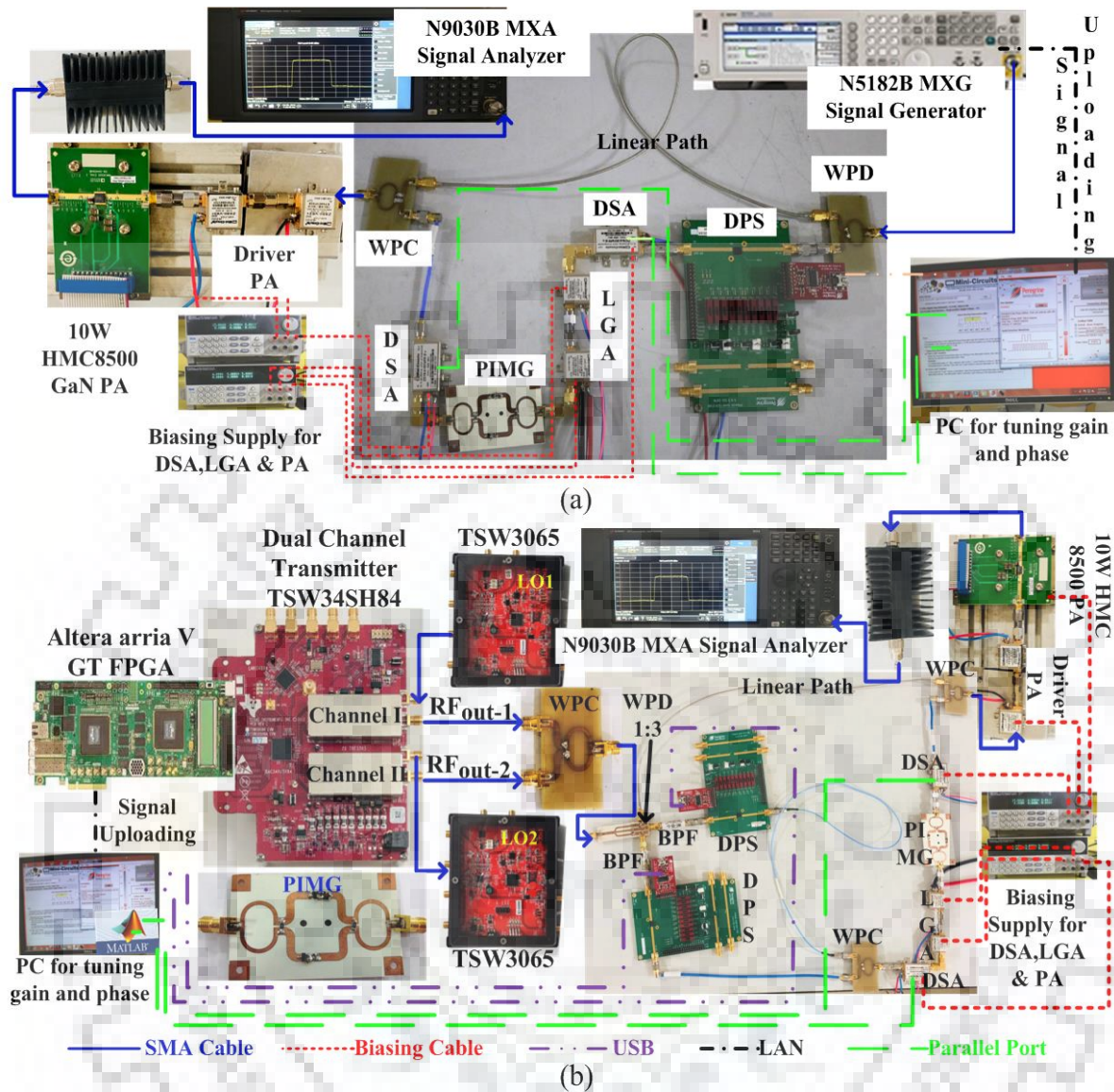


Figure 4.11: Test-bench for data extraction of (a) UBB RF-PD, (b) UBB MRF-PD.

Transmitter I and II contain lower and upper LTE CC of bandwidth 1.4 MHz and 160 MHz, which are centered at 1111 MHz and 2010MHz respectively. The output from both the transmitters are combined using WPC and directed to the input of 1:3 WPD, where one output of WPD is given directly to WPC and other two outputs are directed to two nonlinear IMD paths. These paths composed of different BPF that process the respective CC. VBFZ-1065+ BPF from Mini-circuits allows lower CC that lies at a frequency 1110 MHz, while, VBFZ-2000+ allows upper CC that lies at frequency 2010 MHz. The output

from both the BPF is given to the individual DPS. The phase optimized output from both the DPS are combined using 2:1 WPC and directed to the DSA.

In UBB RF-PD, the signal is uploaded to signal generator (MXG N5182B) via Matlab, which is further given at the input port of WPD. One output of WPD is given directly to WPC and other output is given in the input of DPS. To cancel the nonlinearity of PA, the new IMD products are introduced by a PIMG described in Section 4.3.2.5. The phase of IMDs generated by the PIMG was controlled by the DPS. The phase and the gain optimization of the predistortion signal is a responsibility of PE44820 8-bit DPS from Peregrine Semiconductor and ZX76-31R75-PP+7-bit DSA from Mini-circuits respectively. The optimized signal from IMD path combines with the fundamental signal using WPC, which is further given in the input of the PA.

An N9030B MXA from Keysight is used to analyze the output of the PA. For demonstration WPD, PIMG and WPC are fabricated in-house.

4.5.2 Device under Test

To validate the effectiveness of the proposed predistortion schemes, three DUT are tested, which are listed below:

- (a) 10W HMC8500 GaN Broadband PA from Analog Devices
- (b) ZFL-11 AD+ PA from Mini-circuits
- (c) ZX 60V-63+ PA from Mini-circuits.

The two measurements have been taken, first is using the single tone CW signal, while the second is using 8CC 160 MHz UBB LTE signal in order to examine 1-dB compression point (P1 dB), 3-dB compression point (P3 dB), and gain of PA. As the signal bandwidth increases, the PAPR of the signal also increases correspondingly that cause PA compression in the early stage.

As depicted in Figure 4.12 (a), for single tone CW signal, the input and output P1-dB of HMC8500 PA is 14 dBm and 26.1 dBm respectively. Similarly, for 160 MHz UBB LTE

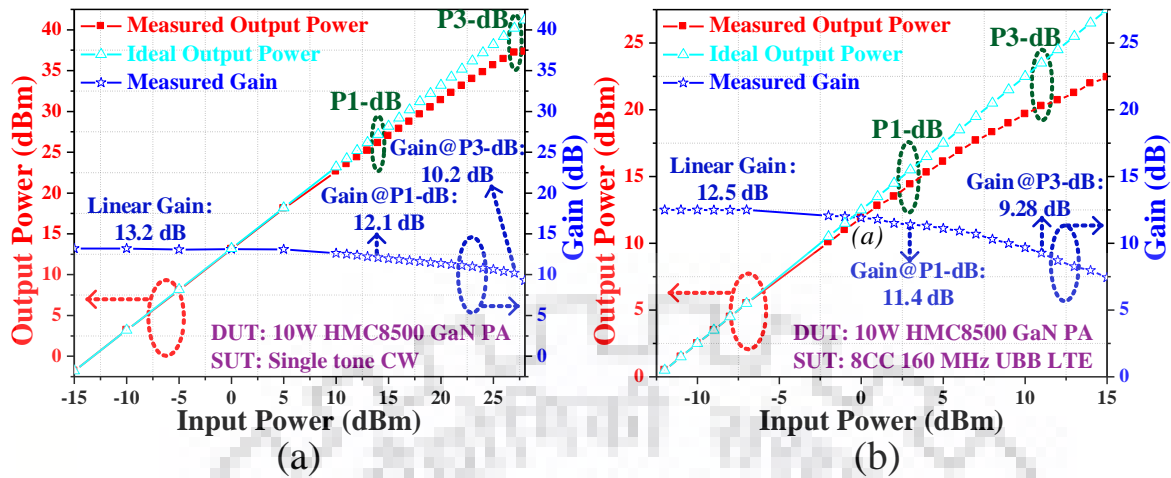


Figure 4.12: Measured linear and compression region of 10W HMC8500 Broadband GaN PA using (a) Single tone CW (b) 8CC 160 MHz LTE signal.

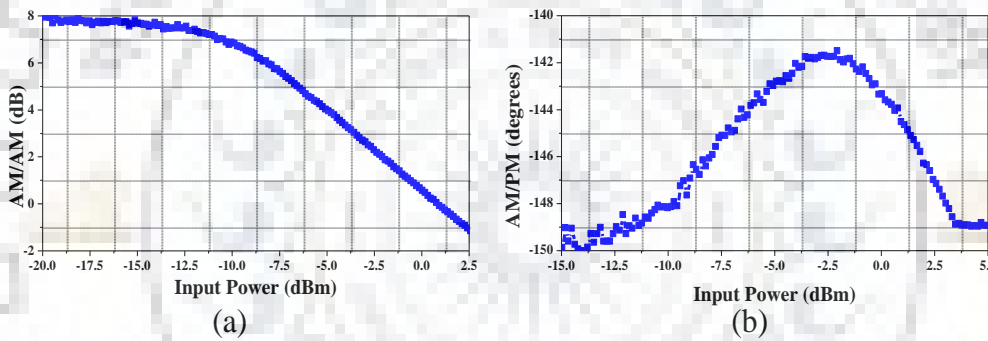


Figure 4.13: AM/AM and AM/PM characteristics of ZFL-11 AD+.

signal, whose PAPR is around 14.17 dB to a complementary cumulative distribution function of 0.01%, the input and output P1-dB of HMC8500 PA changes to 3 dBm and 14.4 dBm respectively which is shown in Figure 4.12 (b). As seen from Figure 4.12 (a), for single tone CW signal, the P3-dB compression point occurs at 27 dBm input power that provides an output power of 37.2 dBm, centered at 2 GHz. Similarly, for 160 MHz LTE signal, the P3-dB compression point occurs at 11 dBm input power that yield an output power of 20.28 dBm which is also highlighted in Figure 4.12 (b).

The HMC8500 supports wideband operation up to 2.8 GHz, similarly, ZFL-11 AD+ PA has a bandwidth from 2 MHz to 2 GHz. The measured AM/AM and AM/PM characteristics of ZFL-11 AD+ PA are shown in Figure 4.13. The measured input and output P1-dB of ZFL-

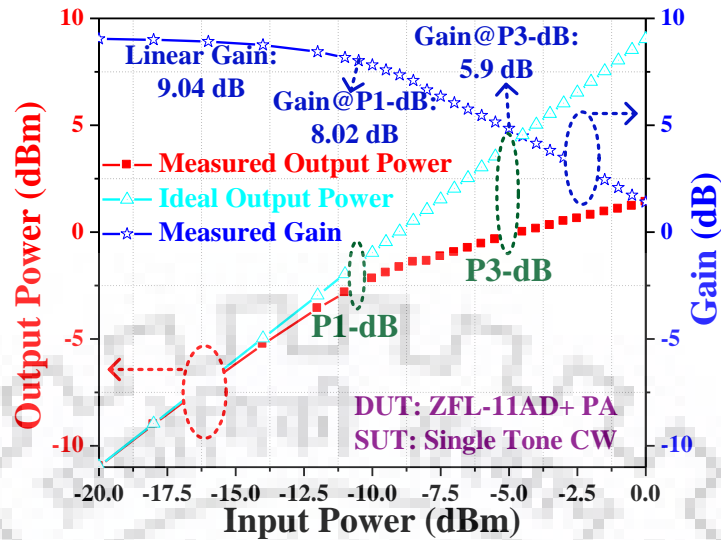


Figure 4.14: Measured linear and compression region of ZFL-11 AD+ Class AB PA using Single tone CW signal.

11 AD+ PA is -10.5 dBm and -2.48 dBm respectively, which is shown in Figure 4.14. Similarly, for single tone CW signal at 1.8 GHz, the measured P3-dB compression point occurs at -6 dBm input power that yield an output power of -0.75 dBm which is also highlighted in Figure 4.14. The 10 W HMC8500 GaN PA provides a linear gain of 13.2 dB at 2 GHz. The ZFL-11 AD+ PA provides a linear gain of around 9 dB at 1.8 GHz. The linear PA from Mini-circuits such as ZX60V-62+ and ZX60V-82+ are used as driver amplifier in conjunction with HMC 8500 PA.

4.5.3 Signal under Test

Signal bandwidth greater than or equal to 100 MHz is being considered as a key ingredient to deliver multi-Gbps data rates.

4.5.3.1 8CC 160 MHz Contiguous signal

Figure 4.15 shows the measured PSD of 10W HMC8500 GaN Broadband PA at an average output power of 21.83 dBm (about 2.4 dB back-off the output power from P1 dB) for a 160 MHz LTE signal, whose PAPR is 14.17 dB to a complementary cumulative distribution function of 0.01%. When PA is driven with 160 MHz LTE signal, centered at 1.8 GHz, the

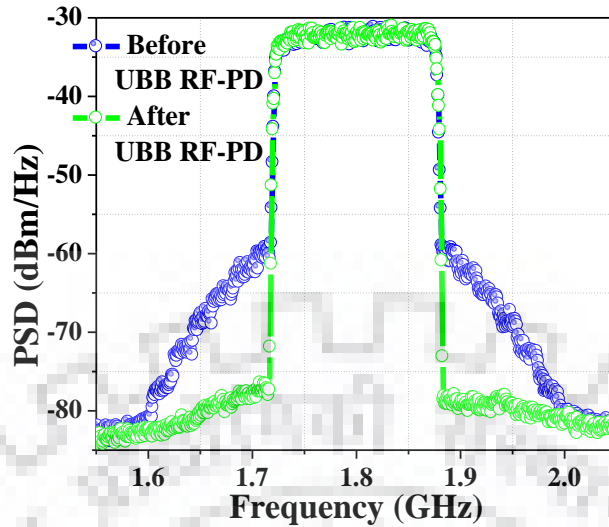


Figure 4.15: Measured Power Spectrum Density of 10W HMC8500 PA with and without the proposed UBB RF-PD excited by 8CC 160 MHz LTE signal, centered at 1.8 GHz.

proposed UBB RF-PD delivers an ACPR of -45.65 dBc, which is an improvement of around 16.87 dB, compared to the PA without linearization. Figure 4.16 shows the PSD of ZFL-11AD+ PA with/without the proposed UBB RF-PD for a 160 MHz LTE signal at the frequency of 2 GHz. The proposed UBB RF-PD delivers an ACPR of -44.58 dBc with an improvement of around 11.7 dB at 1 dB output back-off power as compared to the PA without linearization.

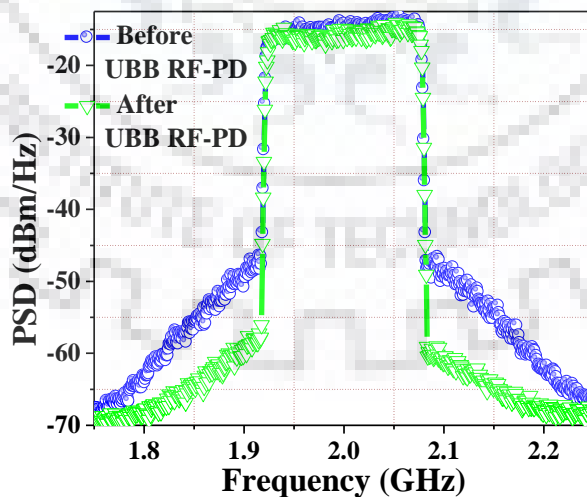


Figure 4.16: Measured Power Spectrum Density of ZFL-11 AD+ PA with and without the proposed UBB RF-PD excited by 8CC 160 MHz LTE signal, centered at 2 GHz.

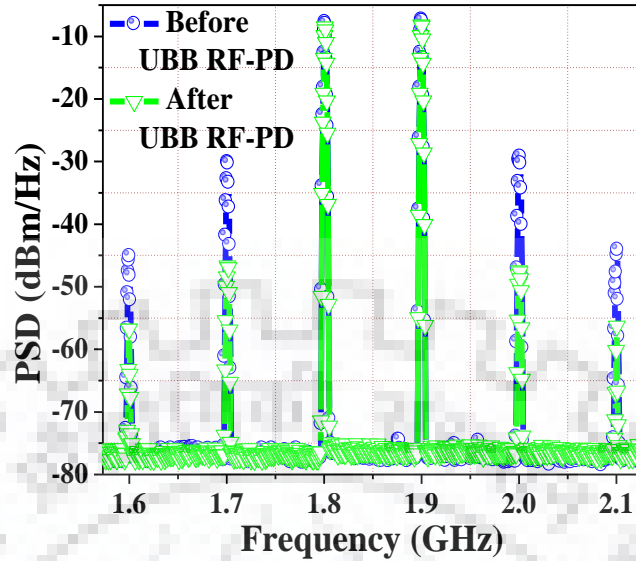


Figure 4.17: Measured Power Spectrum Density of ZFL-11 AD+ PA with and without the proposed UBB RF-PD excited by 100 MHz two tone signal at 1.85 GHz.

4.5.3.2 Two tone signal with 100 MHz frequency spacing

Figure 4.17 shows the measured PSD of the two tone signal with and without the proposed UBB RF-PD at 1.85 GHz and operating at an average output power of 1.5 dBm. The IM improvement factor when the proposed RF- predistortion is equipped with a ZFL-11 AD+ PA for the different output power is shown in Figure 4.18. The proposed UBB RF-PD maintains a tradeoff between the efficiency and the linearity of PA, hereby, providing the linearization when PA operates at 1 dB compression point. Previously proposed APD architecture claims the suppression of IM3 components, but the higher order IMDs are not affected. This problem is eliminated in the proposed RF-predistortion, where IM3 and IM5

TABLE 4.3

IMD CORRECTION BEFORE AND AFTER UBB RF-PD LINEARIZATION

IMDs	Before RF-PD	After RF-PD	Correction
IM3U	-30.26	-48.67	18.41
IM3L	-29.91	-46.83	16.92
IM5U	-44.05	-56.11	12.06
IM5L	-45.17	-56.66	11.49

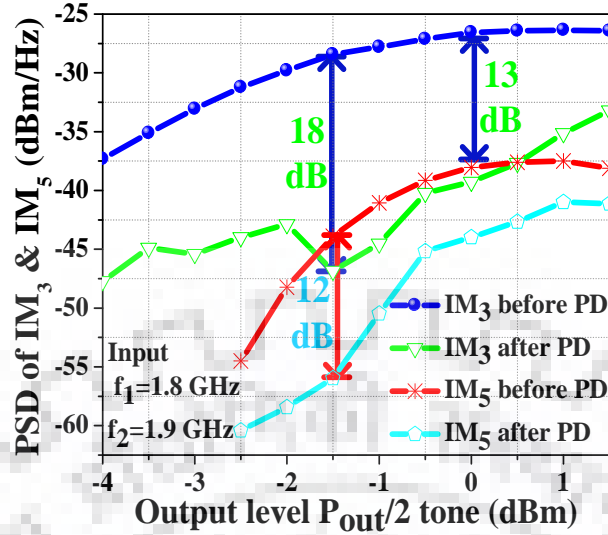


Figure 4.18: Intermodulation characteristics of ZFL-11 AD+ PA with and without the proposed UBB RF-PD at different output power.

are suppressed simultaneously. Table 4.3 shows the IM performance of the PA with and without the proposed UBB RF-PD which is excited by two-tone signal with the frequency spacing of 100 MHz, centered at 1.85 GHz.

4.5.3.3 Inter-/Multi-band LTE signal

The bandwidth of lower and upper CC is 1.4 MHz and 160 MHz respectively. They are separated with the frequency spacing of 900 MHz. Figure 4.19 (a) and Figure 4.19 (b) shows the measured PSD of 10W HMC8500 GaN Broadband PA at an average output power of 21.6 dBm for 1.4 MHz lower CC and 160 MHz upper CC, whose PAPR are around 7.22 dB and 14.17 dB respectively. For the lower CC, which is situated at 1111 MHz, the proposed MRF-PD delivers an ACPR of -50.74 dBc, which is an improvement of around 19.81 dB as compared to PA without linearization. Similarly, for the upper CC which is situated at 2010 MHz, the proposed UBB MRF-PD delivers an ACPR of -46.93 dBc, which is an improvement of around 13.80 dB at 2.2 dB back-off the output power from P1 dB.

The PSD of ZX60V-63+ PA with and without proposed UBB MRF-PD is shown in Figure 4.20. The bandwidth of lower and upper CC is 10 MHz and 20 MHz respectively. They are

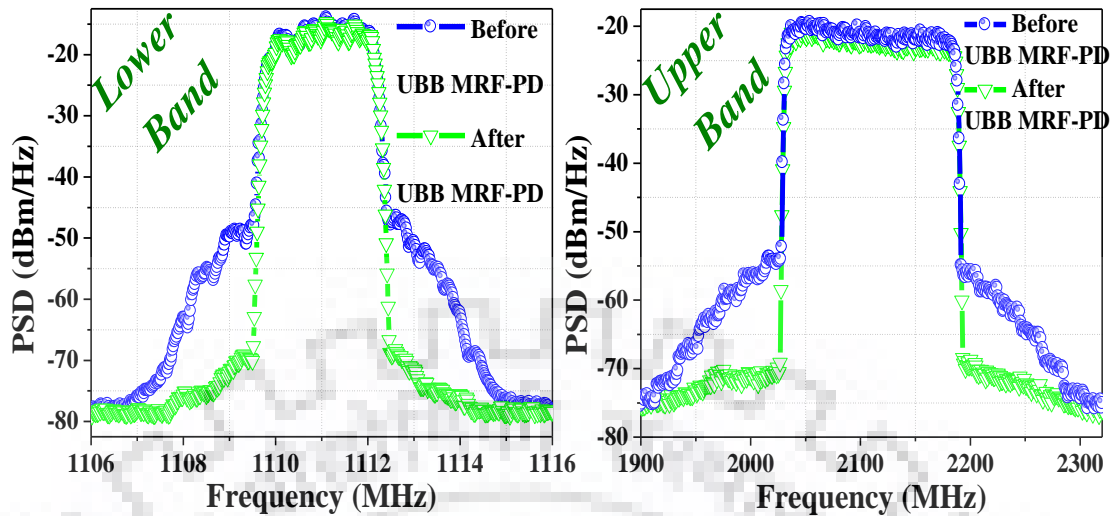


Figure 4.19: Measured Power Spectrum Density of HMC8500 PA with and without the proposed UBB MRF-PD at the (a) lower band consists of 1.4 MHz LTE signal, centered at 1111 MHz, and (b) upper band consists of 160 MHz LTE signal, centered at 2100 MHz.

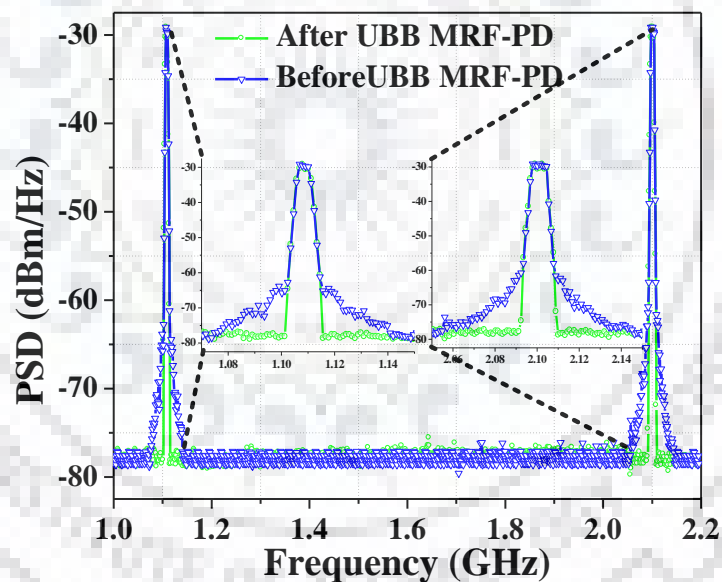


Figure 4.20: Measured Power Spectrum Density of ZX60V-63+ PA with and without the proposed UBB MRF-PD excited by 2CC 1GHz LTE inter-band signal.

separated with the frequency spacing of ≈ 1 GHz. The proposed UBB MRF-PD delivers an ACPR of about -48 dBc for both the CC, which are situated at 1111 MHz and 2100 MHz. For upper and lower CC, it provides an ACPR improvement of 16.6 dB and 18.7 dB respectively at 1 dB OBO.

4.6 Comprehensive Comparison with the State-of-the-art UBB-Predistortion Linearization

The performance of the proposed UBB RF-PD and UBB MRF-PD architectures are summarized and compared with the state-of-the-art UBB linearization techniques in Table 4.4. Similarly, Table 4.5 discusses the strength and weakness of previously proposed UBB architecture.

TABLE 4.4

PERFORMANCE COMPARISON OF THE STATE-OF-THE-ART HPD LINEARIZER

Ref.	PD Type	PD Bandwidth	Center freq.	Signal Type	Signal Bandwidth	Improvement
This work	UBB RF-PD	200 MHz-2.5 GHz	1.8 GHz	LTE 8CC contiguous	160 MHz	ACPR:17 dBc @2.4dB OBO
			2.0 GHz	LTE 8CC contiguous	160 MHz	ACPR:12dBc @1dB OBO
			1.85 GHz	2-tone	100 MHz	IM3=18.5 dB IM5=12 dB
This work	UBB MRF-PD	200 MHz-2.5 GHz	1560 MHz	LTE 2CC (160MHz@2010 MHz 1.4 MHz@1111 MHz)	$\Delta f=900$ MHz	ACPR:13.8 dBc@2.2dB OBO ACPR:19.81 dBc
			1605 MHz	LTE 2CC (20 MHz@2100 MHz 10 MHz @1111 MHz)	$\Delta f \approx 1$ GHz	ACPR:18.7 dBc@1dB OBO ACPR:16.6 dBc
[138]	Freq. Sele	2-600 MHz	Entire	2-tone	$\Delta f=1$ MHz	IM3:4.9 dB

	-ctive APD		PD BW			
[139]	Equipath PD	2.1-2.2 GHz	2.142 GHz	2-tone WCDMA	$\Delta f=5$ MHz 5 MHz	IM3: 20 dB ACPR: 16dBc
[140]	Transmiss- ion line PD	1.5-2.4 GHz	Entire PD BW	2-tone	$\Delta f=2$ MHz	IM3: 17 dB to 25 dB
[141]	Analog Broadband	3.1-4.8 GHz	3.962 GHz	2-tone	$\Delta f=4.125$ MHz	IM3: 9.5 dB; EVM: 1 dB SFDR: 11 dB
[142]	Broadband PD	7-18 GHz	Entire PD BW	2-tone	$\Delta f= 4$ MHz	SFDR: 10 dB P1 dB=0.4 to 2.2 dB
[143]	APD for RoF	DC-6 GHz	2 GHz 2-5 GHz	2- tone 16QAM	$\Delta f=2$ MHz 20 MHz	IM3=18dB, IM5=7dB EVM: 3.9 dB
[144]	UBB PD	10 MHz- 40 GHz	8 GHz 2.4 GHz	2-tone OFDM	$\Delta f=2$ MHz 20 MHz	IM3: 18.7 dB EVM: 5.1 dB
[145]	X-band PD	8.38-8.58 GHz	X-Band	2-tone	$\Delta f=10$ MHz	IM3: 11.8dB @3 dB OBO
[146]	Diode based PD	11.45-11.7 GHz	Ku- Band	2-tone	--	IM3: 16dB@7 dB OBO
[147]	Multiband PD	C- to K- Band	C-Band X-Band	2-tone	--	IM3: 21dB@6 dB OBO IM3: 19dB@6 dB OBO
[148]	APD	60 MHz	1.96 GHz	CDMA	4 MHz	ACPR: 6dBc
[149]	Resonator PD	65 MHz	1.8 GHz	NADC	12.5 KHz	ACPR: 11dBc P1 dB=21 to 22.8 dB

TABLE 4.5

SALIENT FEATURES OF VARIOUS HPD PREDISTORTER LINEARIZER

Ref.	Strengths	Weakness
This Work	<p>Able to linearize the UWB signal, Hence a potential candidate for 5G system.</p> <p>Simple, cost effective circuit.</p> <p>No need of baseband information.</p>	<p>Predistortion is performed by analog components, hence linearization performance is not as good as DPD.</p>
[138]	<p>Predistortion circuit is very compact and simple as it only requires a capacitor and a Schottky diode</p>	<p>Linearization performance is not worthy.</p> <p>Improvement is only limited to IM3.</p>
[139]	<p>Better insertion gain and lower power consumption at the linearizer</p>	<p>Performance is only limited to IM3.</p> <p>Hardware requirement is too massive, it requires four branch line couplers, three attenuators, two amplifiers, two couplers, two phase shifters and a pre-amplifier.</p>
[140]	<p>Complex circuit, but provide good linearization.</p>	<p>Performance is only limited to IM3.</p> <p>Delay adjustment for modulated signal is tricky challenge.</p> <p>Hardware requirement is too massive as it requires, WPC, two voltage variable attenuator, WPD, two driver amp, coupler and broadband phase shifter.</p>
[141]	<p>A very simple and cost effective APD circuit that neither uses VM nor uses drive amplifier, it's only use two anti-parallel diodes to linearize modulator.</p>	<p>Improvement is only limited to IM3, unable to cancel higher order IM products.</p>
[142]	<p>It uses a capacitor and two zero bias GaAs diodes to generate predistorted</p>	<p>Predistortion circuit is limited by IM5, as it is unable to cancel IM3 and IM5</p>

	<p>signal.</p> <p>It provides low cost broadband linearization solution.</p> <p>Due to the high resistance of the diodes, no broadband matching network is required.</p>	simultaneously
[143]	<p>Using two Schottky diodes it can suppress IM3 and IM5 simultaneously.</p> <p>It is broadband predistortion circuit up to 6 GHz, yet it is very simple, low cost and consume less power</p>	--
[144]	<p>A Schottky diode based ultra-broadband predistortion circuit is very simple and compact.</p>	<p>Unable to compensate IM3 and IM5 simultaneously.</p> <p>The power at IM3 frequency is a 5th order limited which means, when IM5 was eliminated, IM3 becomes dominated.</p>
[145]	<p>Provides UBB operation.</p>	<p>IMD improvement is very small at no OBO.</p> <p>For achieving good linearity improvement in the TWT, large OBO are required</p>
[146]	<p>Separate control of AM/AM and AM/PM.</p> <p>It is cost effective and quite easy to manufacture.</p>	<p>Control Bandwidth is only 60 MHz, hence, not a strong candidate for 5G.</p> <p>Linearization performance is not worthy.</p>
[147]	<p>A very simple yet cost effective predistorter as it only employs a series tunable resonator.</p> <p>It works well for narrowband PA and handheld system.</p>	<p>Does not provide a solution to wideband system, hence not a potential candidate for 5G.</p>

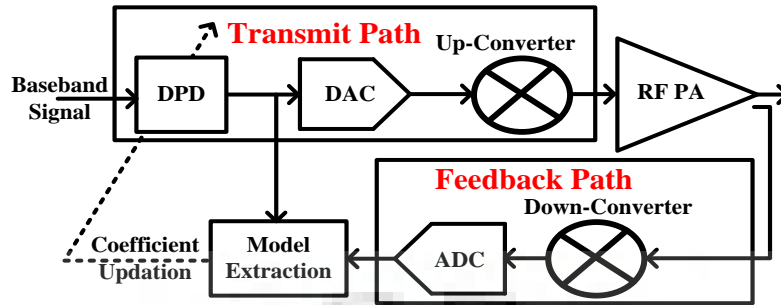


Figure 4.21: Conventional DPD architecture.

4.7 Conventional Digital Predistortion and its limitation imposed on 5G

4.7.1 Conventional Digital Predistortion

The conventional DPD has been a prominent linearization technique that was used in abundance to provide better efficiency in the BS transmitters. In the last decade, DPD had been a popular choice due to its reconfigurable nature and better linearization results due to accurate inverse model in the digital domain. It compensates the nonlinearity of RF PA by feeding predistorted signal to the PA. The predistorted signal is generated from the complex input baseband signal after passing it from the inverse nonlinear characteristics of PA implemented in the digital domain. Thus, the conventional DPD consists of two paths, one being the transmit path and the other is a feedback path as shown in Figure 4.21. The feedback path is used to collect the PA output sample, which in turn is used for modeling the nonlinearity of PA along with the input baseband signal [150], [151]. Transmitter path restricts the digital to analog conversion of predistorted signal corresponding to wideband input baseband signals.

4.7.2 System NMSE versus Signal Bandwidth

The system performance of 50 MHz wideband measurement setup in terms of normalized mean square error (NMSE) between transmitted and received signal is reported in Figure 4.22 (a). This setup consists of a dual channel transmitter (TSW 34SH84) from Texas

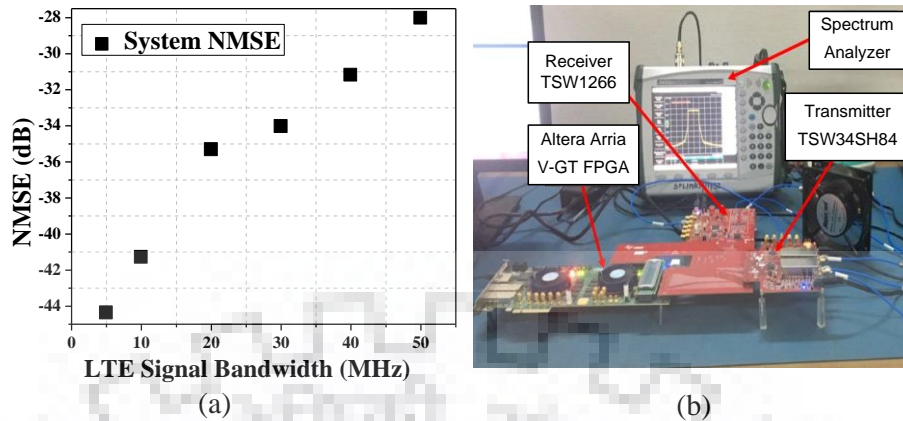


Figure 4.22 (a) DPD System performance deterioration observed in experimental setup in terms of NMSE for increasing LTE signal bandwidth, (b) Measurement setup for Data extraction.

Instrument, Broadband receiver (TSW1266), Arria V GT FPGA, LO (TSW3065) which is shown in Figure 4.22 (b). The transmitter is connected to the FPGA and programmed using Quartus software. Using pre-programmed FPGA, data is sent to transmitter at a sampling rate of 307.2 MHz. Data is further interpolated to a sampling frequency of 1228.8 MHz in DAC. The signal is up-converted using complex RF modulator TRF3705. The signal is down-converted and received using TSW1266 at a sampling frequency of 614.4 MHz. The transmitter and receiver LO is synchronized using TSW3065. To observe the system performance, dual channel transmitter and receiver are directly connected using SMA coaxial cable without using PA. The performance is evaluated using an LTE signal. In each turn we increase the bandwidth of LTE signal and record the NMSE of the system. This test-bench supports 500 MHz bandwidth, however, still NMSE performance deteriorates with the increase in bandwidth as depicted from Figure 4.22 (a).

4.7.3 Linearization Bandwidth constraint of the Conventional DPD

Application like virtual reality and video based multimedia is only possible when multiple CC are aggregated in the base-station. It creates a challenging job for the implementation of DPD. A rule of thumb for the application of DPD is that it requires five times bandwidth to

that of the input signal bandwidth for capturing the expanded spectrum to ensure that up to 5th order IM products of PA are digitized. Earlier for 3G/4G communication systems, DPD is a potent linearization approach because maximum signal bandwidth is not more than 20 MHz. For 20 MHz input signal, expanded spectrum is about 100 MHz. It necessitates ADC that will run at 200 mega-samples-per-second (MSPS), which is readily available.

If the existing DPD is employed for 5G system, where signal bandwidth can approach up to 160 MHz in the sub 6 GHz band, which means at least 800 MHz linearization bandwidth is required. Such a high bandwidth will remarkably increase the difficulty in system design. DPD feedback path requires RF filters of bandwidth 800 MHz. This expanded bandwidth is then propagated through the feedback path to the entire transmitter chain. It unnecessarily burdens the entire system with high power consumption and increased clock speed requirement [152]-[155]. It also adds complexities for wideband linear up-mixer, multi-pole high frequency reconstruction filters. The frequency response of the filter which is used for up-conversion in DPD application has to be wide enough to accommodate the full spectrum of the expanded signal. Unfortunately, if DAC and up-converters generates any sort of noise within the passband of the filter, it will be amplified by the PA.

To capture 800 MHz-expanded signal, it also requires ADC with a very high sampling rate (more than 1600-MSPS). The numbers of calculation per second that the DPD need to accomplish fall in the teraflop range. It can be achieved with the high-speed processor that operates at a higher clock-rate, however this will incur higher overhead power consumption [150]-[155]. This power overhead will be in the same order of magnitude as the power transmitted in the BS [156]. For a commercial transmitter, high-speed ADC and DAC is one of the most expensive and power hungry component. Hence it becomes impractical to deploy ADC with that much high sampling rate. DPD of broadband PA, when applied to wideband signal under these constraints is cumbersome due to its system bandwidth.

4.7.4 Restriction on Data Converters

The bandwidth of predistorted signal, containing higher order IMD components, is typically five-times of the input baseband signal which defines the speed of DAC. Moreover, the speed of an ADC in the feedback path limits the capturing of wideband

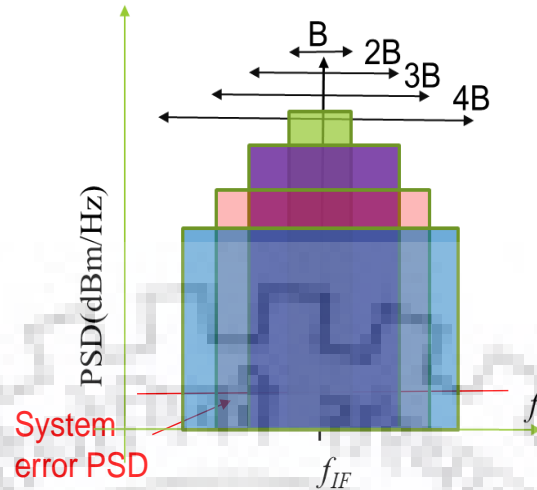


Figure 4.23: Impact of ADC saturation for Broadband signal.

of wideband signals at the output of a PA which typically has bandwidth 5 times of the input baseband signal due to the presence of IMD components generated by PA [150]-[156].

In addition, the dynamic range of DAC and ADC, both are affected due to IF filter bandwidth and saturation of DAC and ADC as we increase the bandwidth of the signal, which again limits the nonlinearity correction applied by DPD [157], [158]. Figure 4.23 shows the concept behind the decrease in the dynamic range (ACPR), with the increase in the signal bandwidth. The decrease in the dynamic range is represented by system error PSD in Figure 4.23. The power required to saturate the ADC is concentrated for single carrier leading to maximum dynamic range, which provides a theoretical dynamic range of $ADC = 6.02n + 1.76$ dB, where n is the number of bits. As bandwidth increases, the same power is distributed in different frequencies leading to reduction in signal dynamic range. The signal is closer to noise for each frequency in a wideband signal.

Although due to the limited number of bits and aliasing phenomena, ADC is inherently nonlinear component [159]. Figure 4.23 signifies that as the requirement of transmission bandwidth arises, the limited dynamic range of the ADC becomes a key obstacle for the effective linearization. Consequently, it has become impractical and unaffordable to deploy ADC with satisfactory dynamic range under the constraint of high cost and power overhead

consumption. The dynamic range and the sampling speed requirement of the ADC has been the focus of recent research. This provides the motivation for DPD schemes utilizing slower ADC to reduce power overhead consumption.

The three major problems are inherent in DAC that restrain their high frequency performance are nonlinearity spurs, image replica generation and frequency dependent amplitude distortion. At close to Nyquist zone, the inherent nonlinear effects in the DAC are well pronounced, which results in harmonic emission and IMD generation at the DAC output. To cope with this problem, delta-sigma modulators have been proposed for DAC in [160], [161]. However, its performance degrades due to large generation of out-of-band noise. Moreover, it poses a stringent requirement for filtering, hence limiting the instantaneous bandwidth of operation below 100 MHz.

4.7.4.1 Sampling speed Reduction

A band-limited DPD model proposed in [162] eliminate the system bandwidth constraint of the conventional DPD with undersampling ratio of 1.6. The efficient reduction in the sampling speed was achieved in [163]-[165], however, it consists of quadrature modulator and a pair of ADCs to capture the complex feedback. It increases the system complexity, add hardware cost and might suffer from an IQ mismatch in feedback receiver, which further lead to performance degradation. The ADC sampling rate was reduced aggressively and effectively in [165], in which 40 MHz LTE signal was linearized effectively with 20 MHz ADC sampling speed. The method in [166] uses spectral extrapolation of band-limited feedback channel for the linearization of 160 MHz UWB signal with an undersampling ratio of 2.4. However, it also requires band-limiting filters before the ADC sampling and uses computational intensive signal processing algorithm. [167] - [169] focus on reducing the feedback signal bandwidth to reduce the ADC sampling rate requirement. One more approach is proposed in [170], in which sampling speed of ADC was reduced at the cost of extra RF cancellation chain. An undersampling method in which ADC sampling rate was reduced aggressively and efficiently is proposed in [171] and [172]. It avoids the IQ imbalance and efficiently linearize the 100 MHz and 800 MHz UWB signal at the sampling speed of 25-MSPS and 500-MSPS respectively.

4.8 Proposed UBB RF-PD/UBB MRF-PD vs. Conventional DPD/2D-DPD

Above methods achieved a reduction in the sampling speed of the ADC, but with the significant increase in the computational complexity. Despite the low sampling speed, the analog bandwidth of ADC must be sufficient enough to capture the feedback signal in the receiver path. However, this is the easy constraint compared with the sampling speed requirement. The proposed scheme does not stress ADC and DAC sampling rates and bandwidth requirements, as the predistorter function is in analog (RF) domain and application is also in analog (RF) domain. The linear functions such as linear gain and phase adjustment have been adapted using analog methods, which may be especially useful for 5G communication systems.

Moreover, DPD also requires the knowledge of digital baseband signal at the input and computational speed of digital circuits limits the operational bandwidth. It also proves to be a limitation of the RF repeater system because linearization is applied to the incoming RF signal before amplifying and transmitting it to the next station.

In the proposed RF-in RF-out APD, power is consumed by only VM where three biasing supplies are required to adjust its control voltages. Other components are passive in nature. Overall maximum power consumption is 805mW. Similarly, in UBB RF-PD schemes power is consumed only by DPS, DSA and LGA. However, power consumption is in very small order. The proposed UBB RF-PD and UBB MRF-PD represent low cost and energy efficient alternative to DPD and 2D-DPD respectively.

The inter-/multi-band CA scheme requires the simultaneous transmission of signals in different frequency bands, has renewed the interest of multiband PA linearization using concurrent 2D-DPD [173]-[181]. A frequency selective algorithm for the linearization of multicarrier PA is proposed in [182], where large-signal network analyzer is used to characterize the nonlinear behavior of a PA. It employs two medium speed ADC and DAC in each feedback path. A conventional 2D-DPD architecture is proposed in [183]-[185] that

consists of two feedback paths, where each path consist of RF filter, down-conversion mixer and ADC for separately capturing the lower and the upper band.

For inter-band CA communication, the 2D-DPD doubles the cost and consume more power as compared with single feedback path DPD. It is also stated in [186] that the conventional 2D-DPD suffers from time delay misalignment and numerical instability resulting in the degradation of the DPD performance. The DPD model proposed in [186] is robust against time-delay misalignment. To overcome the above problem, a single feedback loop DPD for the concurrent dual band is proposed in [187]. However, it employs a high sampling speed ADC in the feedback path. To reduce the sampling speed of ADC, a technique called down-conversion carrier colocation (DC³) is proposed in [188]. It employs two external mixers at the PA output to assure the position of both the bands. In [189], a single feedback loop is shared among multiple band during different time slots. But it requires an appropriate model for the predistortion signal generation based on the band-limiting filter that increases the signal processing complexity.

To the best of the author's knowledge, dual band linearization using energy efficient passive components is not reported in the literature so far. The proposed UBB MRF-PD linearizer caters to the high signal bandwidth requirement of 5G and does not require access to the baseband information. If considered cost as one of design parameters in 5G cellular, then the proposed RF-in RF-out APD, UBB RF-PD and UBB MRF-PD linearizers are qualified to make a big debut in the near future. An all-in price of single high speed data converter includes everything of the proposed RF-predistortion linearizers.

4.9 Conclusion

The proposed RF- predistortion linearizer will be a powerful incentive to adopt a 5G BS, the multi-antenna PA design and the multi-carrier repeater system. It caters to the strong demand for the linearizer that has a simple circuit configuration, minimal power consumption and provides adequate linearity for an UWB signal without gathering baseband information.

Experimental results validate the dexterity of the proposed UBB RF-PD scheme by providing a linearization with 160 MHz 8CC LTE signal and 100 MHz two tone signal. For 160 MHz intra-band contiguous signal, the proposed UBB RF-PD delivers an ACPR of -45.65 dBc, with an improvement of 16.87 dB, and for intra-band non-contiguous two tone signal, IM3 and IM5 are significantly reduced by 18 dB and 12 dB, respectively. Similarly, the effectiveness of the proposed UBB MRF-PD scheme is advertised by linearizing the inter-band 2CC LTE signal, where CCs are separated by 900 MHz. The proposed UBB MRF-PD delivers an ACPR of -50.74 dBc and -46.93 dBc, which is an improvement of around -19.81 dB and -13.80 dB for 1.4 MHz lower and 160 MHz upper LTE CC respectively. To the best of the authors' knowledge, this achieved linearization for the UWB signal using passive components is the highest reported in the literature so far.





Chapter 5

Hybrid RF-Digital Predistortion

5.1 Introduction

To overcome the challenges of the proposed RF-in RF-out APD and UBB RF-PD, the HRF-DPD has been proposed. As stated in the previous chapters, precise control over the gain and phase of the predistortion signal is the key to achieve better linearization. The requirement of data converters and reconstruction filters are relaxed in the proposed RF-in RF-out APD and UBB RF-PD architecture, whereas the proposed HRF-DPD eliminates the need of analog components by compensating the delay digitally. Moreover, the proposed method reduces the hardware requirement of the conventional APD by alleviating the need of VM, hybrid 90° branch line coupler and bulky delay lines.

In the conventional APD shown in Figure 2.1, an accurate delay adjustment is required between the two paths to appropriately combine the fundamental and IMD components at the output of APD. This problem had been solved in the literature by calculating the time delay in the lower path using a vector network analyzer (VNA). After finding exact time delay in the IMD generator path, one can compensate it by connecting a delay line or by connecting a proper length of cable in the upper path i.e. linear path. Practically, being an analog component, the accuracy of this delay compensation is also limited.

The proposed HRF-DPD is a digitally assisted analog predistortion architecture for the linearization of PA output that takes the advantage of low complexity, yet flexible digital control. Instead of using RF delay lines for delay compensation, it is easier to compensate the delay digitally. Also gain and phase of a signal can be controlled digitally instead of using VM in Type-I CS and DPS/DSA in Type-II CS. The proposed architecture also eliminates the need of the 90° hybrid RF coupler which is used in the APD setup in order to provide in-phase and quadrature-phase signals to the VM. Therefore, by utilizing the

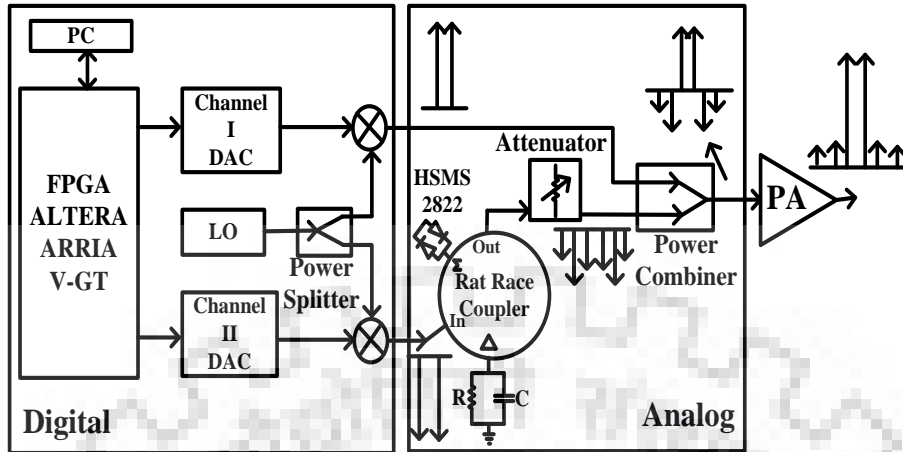


Figure 5.1 The proposed Hybrid RF-Digital Predistortion Architecture.

proposed HRF-DPD architecture with RF PA, due to better control of parameters, better linearization is achieved as compared to the proposed RF-in RF-out APD and UBB RF-PD Linearizer.

Being a completely RF-in RF-out system, APD is anticipated to be easier to integrate with 5G BS, RF PA, and repeater systems. The proposed RF-in RF-out APD has the ability to capture the UWB signal, which is not possible with the conventional APD. Conventional APD and the proposed RF-in RF-out APD and UBB RF-PD had the advantage of simple and cost-effective architecture since predistortion is performed by RF components in the analog domain, but are known to provide moderate linearity improvement. In order to get better linearity improvement, we further propose an HPD i.e. HRF-DPD which is a hybridization of APD. It caters to the high signal bandwidth requirement of 5G, which provides flexibility as well as accuracy. Moreover, it eliminates the constraint on system bandwidth of conventional DPD.

5.2 Proposed Hybrid RF-Digital Predistortion

The proposed HRF-DPD shown in Figure 5.1 is an intermediate solution between the APD and baseband DPD, which provides higher accuracy than APD and better bandwidth than DPD. The proposed HRF-DPD is attractive for PA in transmitters and repeaters for long

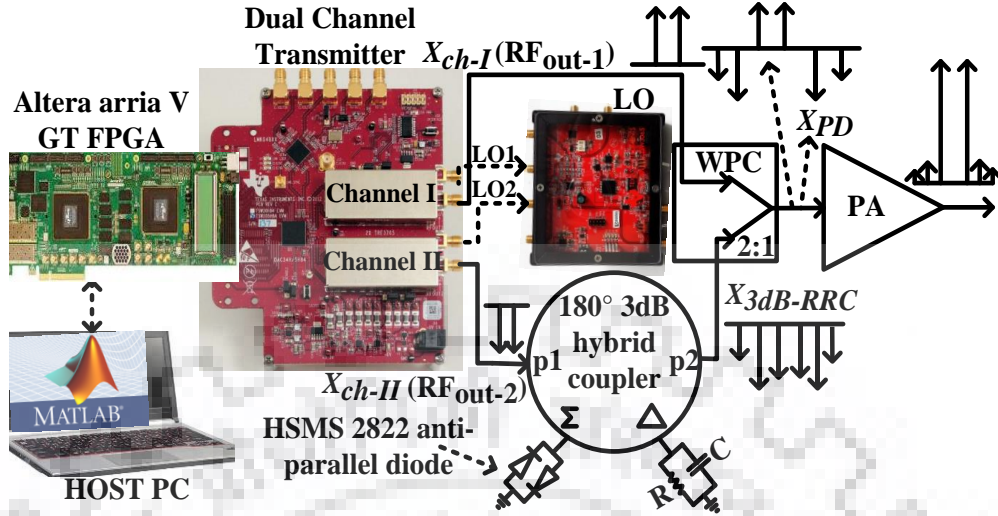


Figure 5.2 Hardware realization of the proposed Hybrid RF-Digital Predistortion Architecture.

distance communication. Such an RF-in RF-out system is desirable where baseband signal is not readily available. The performance of such system depends on accurate characterization and implementation in analog and digital domain of the system. It is to be noted that the proposed HRF-DPD is different from the HPD presented in [190] and [191], where nonlinear inverse function is synthesized in the digital domain and applied in the analog domain by linear operations. HPD in [156], [157], and [190] still requires high speed DAC, ADC while characterizing the PA for inverse modeling in the digital domain.

This chapter proposes a wideband HRF-DPD, where, the concept of APD is adopted. However, linearity correction is quite high as compared to APD, while it can be applied to wideband signals unlike DPD. Figure 5.1 shows the architecture of the proposed HRF-DPD. It can be observed that the VM, hybrid coupler and delay lines are eliminated, which are essential part of the APD schemes. The proposed scheme generates the input baseband signal and its inverse using two synchronized modulated sources. This is implemented using two-channel transmitter (TSW30SH84) from Texas instruments. The baseband part of the modulated sources are implemented in Arria V (GT series) FPGA platform as shown in Figure 5.2. A base-band I/Q data are fed to random access memory (RAM) of the FPGA allocated to each channel using MATLAB and Quartus software. This baseband data is then converted to analog signals using 16-bit DACs sharing the same clocks. These signals are

further modulated and up converted to RF signals using quadrature modulators in each path.

Since, the two channels are synchronized with the same baseband clock of FPGA, an accurate magnitude and phase between the two channels can be set at the baseband level. This provides required magnitude and phase control between the two paths accurately as compared to APD. If the upper path described as channel 1 in Figure 5.2, has an input signal $V_i(t)$, the signal in lower path depicted as channel 2 is represented by $\text{Re} [V_i(t)e^{-j\phi}]$. The phase difference of 180° is required to generate inverted signal whereas ϕ is required to compensate for any additional errors due to analog components in the lower path. The input to PA can be given as:

$$V_{tot.}(t) = V_i(t) + E_n(V_i(t) \cos \phi) \quad (5.1)$$

where $E_n(\cdot)$ is the nonlinear function implemented by IMD generator in the lower path. Using the value of $\phi=180^\circ+\theta$, (5.1) can be rewritten as:

$$V_{tot.}(t) = V_i(t) + E_n(-V_i(t) \cos(\theta)) \quad (5.2)$$

The above equation (5.2) has two terms, first representing the fundamental input signal and the second representing an error signal (E_n) from the output of a nonlinear component generated from the input signal with an appropriate phase shift and main signal removed.

In case of 2-tone signals, such nonlinear components will be IMD terms with appropriate phase shift. The selection of the appropriate value of ϕ to facilitate 180° phase difference with respect to the input signal provides cancellation of the nonlinearity at the output of the PA.

5.3 Two Tone Analysis

The analysis is based on two-tone signals of equal power, which can then be extended for the two LTE carrier aggregated signals. The two-tone signal at the input of channel-I of dual channel transmitter is given as:

$$x(t) = \text{Re}\left(Ae^{j\omega_1 t} + Ae^{j\omega_2 t}\right)e^{j\phi} \quad (5.3)$$

$$x(t) = A\left[\cos(\omega_1 t + \phi) + \cos(\omega_2 t + \phi)\right] \quad (5.4)$$

where ω_1 and ω_2 are the carrier frequencies of the two tones. The HRF-DPD setup composed of the two channels, where ϕ denotes the phase variation in the channel I due to the delay in the lower branch. Channel I is the upper channel which is considered as the linear channel, whereas Channel II is the lower channel which is considered as the nonlinear channel. The output from channel I is given directly at the input of WPC, whereas the output from Channel II is given in the input of IM generator. The signal at lower branch is 180° out of phase with respect to the signal at upper branch

$$x_{inv.}(t) = A\left[\cos(\omega_1 t + [\phi + \pi]) + \cos(\omega_2 t + [\phi + \pi])\right] \quad (5.5)$$

$$x_{inv.}(t) = A\left(\cos \omega_1 t \cos(\phi + \pi) - \sin \omega_1 t \sin(\phi + \pi)\right) + A\left(\cos \omega_2 t \cos(\phi + \pi) - \sin \omega_2 t \sin(\phi + \pi)\right) \quad (5.6)$$

$$x_{inv.}(t) = -A\left[\cos \omega_1 t + \cos \omega_2 t\right] \quad (5.7)$$

The output of lower branch, i.e. $x_{inv.}(t)$ is applied at the input of IM generator. The detailed explanation of IM generator is already provided in Chapter 2. The sigma port of RRC is mounted with anti-parallel HSMS2822 Schottky diodes as depicted from Figure 5.1 and Figure 5.2. The anti-parallel diodes produce the odd order nonlinearities. The output of anti-parallel diode in RRC for the third order nonlinearity is given as:

$$V_{HSMS}(t) = a_1 x_{inv.}(t) + a_3 x_{inv.}^3(t) \quad (5.8)$$

Substituting (5.7) in to (5.8), we get

$$V_{HSMS}(t) = -Aa_1[\cos \omega_1 t + \cos \omega_2 t] - A^3a_3[\cos^3 \omega_1 t + \cos^3 \omega_2 t] - 3A^3a_3[\cos^2 \omega_1 t \cos \omega_2 t + \cos \omega_1 t \cos^2 \omega_2 t] \quad (5.9)$$

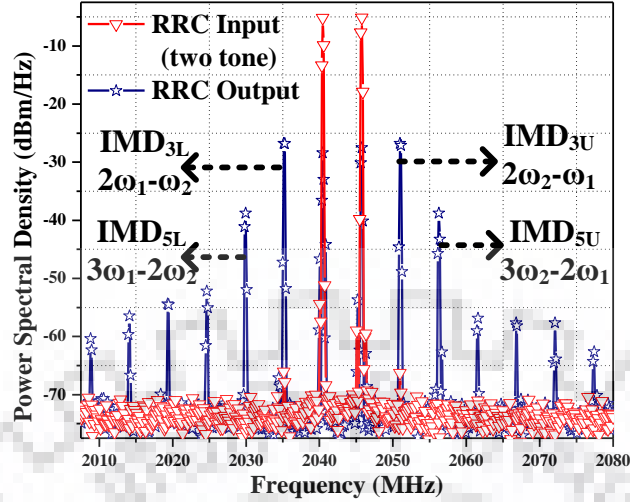


Figure 5.3: Two tone test of IM Generator.

Delta port of IM generator is mounted with a resistor and capacitor, which cancels the main tones at frequencies ω_1 and ω_2 . RRC is used to combine the anti-parallel diode circuit and RC circuit. The output of RRC is given as:

$$V_{RRC}(t) = \frac{a_3 A^3}{4} (\cos 3\omega_1 t + \cos 3\omega_2 t) - \frac{3a_3 A^3}{4} [\cos(2\omega_1 t + \omega_2 t) + \cos(2\omega_1 t - \omega_2 t) + \cos(2\omega_2 t + \omega_1 t) + \cos(2\omega_2 t - \omega_1 t)] \quad (5.10)$$

Figure 5.3 shows the IM generator output for the tone input with two tones at 2.041 GHz and 2.046 GHz respectively. First term in (5.10) represents the third order harmonics at $3\omega_1$ and $3\omega_2$ that can be easily filtered out. Next four terms are 3rd order IMD's. Filters can be used to remove the 3rd order IMD components that lie at frequency $2\omega_1 + \omega_2$ and $2\omega_2 + \omega_1$. After discarding all these terms, the output of IM generator is given as:

$$V_{RRC}(t) = -\frac{3a_3 A^3}{4} (\cos(2\omega_1 t - \omega_2 t) + \cos(2\omega_2 t - \omega_1 t)) \quad (5.11)$$

However, the 3rd-order IMD terms ($2\omega_1 - \omega_2$ and $2\omega_2 - \omega_1$) will be very close to the fundamental frequencies and therefore cannot be easily filtered out. For wider bandwidth input signal, these third-order IMD is of greater concern [83]. In order to remove the 3rd order IMD components that lie at frequency $2\omega_1 - \omega_2$ and $2\omega_2 - \omega_1$, the output of IM

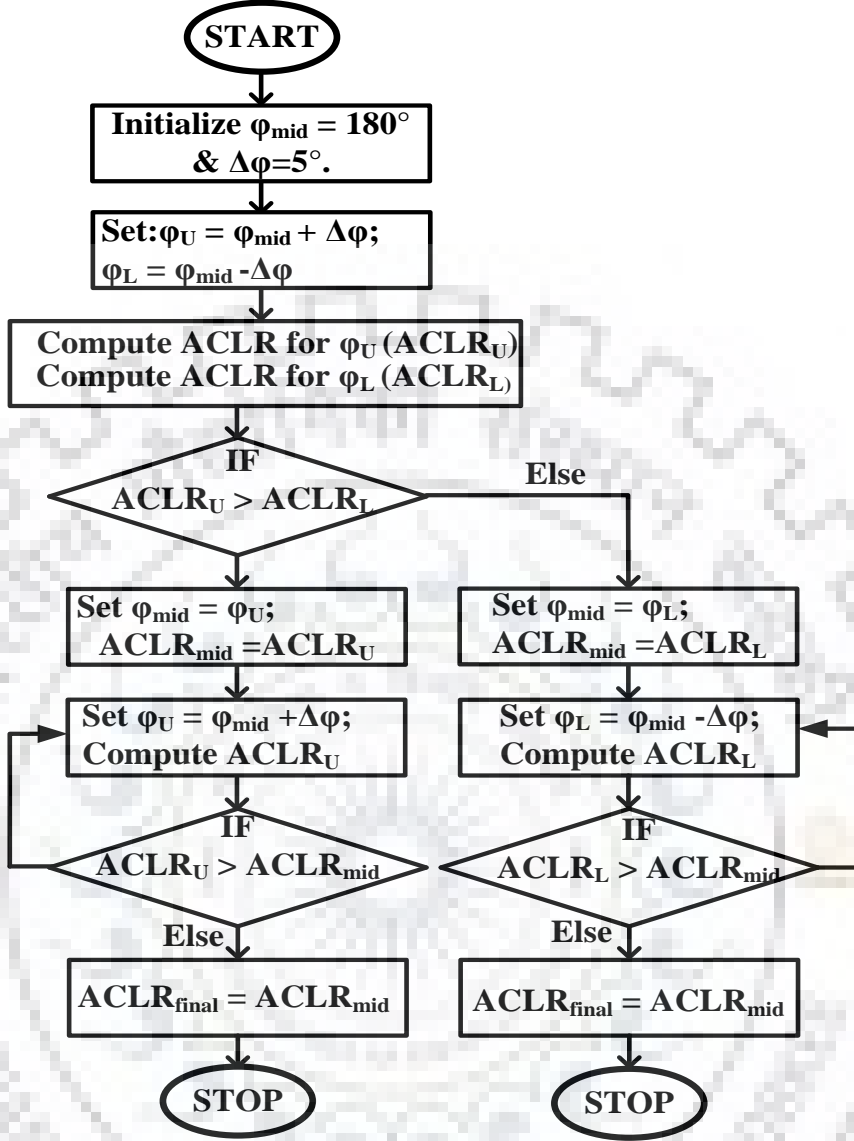


Figure 5.4: Flowchart for automatic phase delay compensation.

generator is combined with the original signal at out-of-phase and provided to the PA. The phase of the signal can also be varied digitally for the best IMD cancellation. The overall reduction in IMD is achieved by optimizing predistorter linearizer parameters R , C and φ of HRF-DPD setup. It takes the advantage of low complexity of analog circuit and input signal. Ignoring the harmonics and filterable third order IMDs, combined output is given as input to RF-PA, which is given as:

$$y_{PD}(t) = x(t) + V_{RRC}(t) \quad (5.12)$$

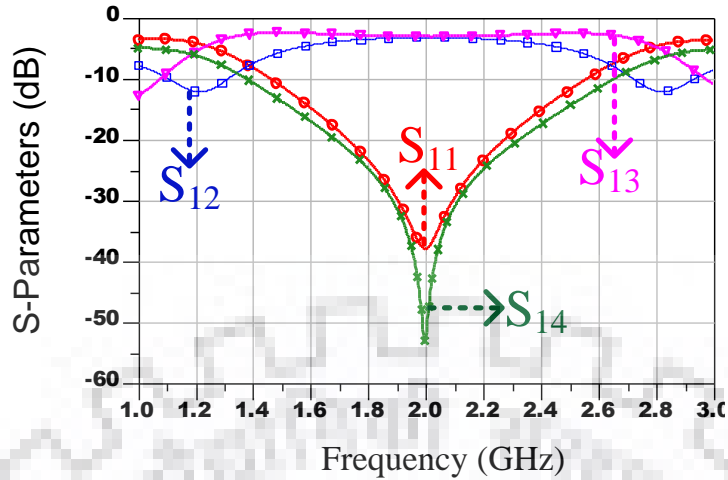


Figure 5.5: Simulated S parameters of RRC.

$$y_{PD}(t) = A[\cos(\omega_1 t + \varphi) + \cos(\omega_2 t + \varphi)] - \delta_0[\cos(2\omega_1 t - \omega_2 t) + \cos(2\omega_2 t - \omega_1 t)] \quad (5.13)$$

Here, the coefficient δ_0 affects the original signal and third order IMD, φ is used to compensate the phase delay that occurs in the lower branch. Phase delay that arises in lower branch is compensated digitally by introducing a phase difference in the digital domain. The steps followed in the algorithm to find φ are shown in Figure 5.4. Once ACPR performance stops improving further, phase can be further fine-tuned by reducing $\Delta\varphi$ to 0.5° .

5.4 Experimental Verification

5.4.1 Intermodulation generator

Nonlinear component: An anti-parallel diode pair, i.e. HSMS 2822 surface mount RF Schottky barrier diode with series configuration is used as a nonlinear component. It requires a low turn on voltage as low as 0.34V at 1mA.

IMD generator and main signal suppressor circuit: RRC is a well-known four port passive circuit used for analog predistortion, which has been designed and fabricated for IMD generation and main signal cancellation. Figure 5.5 shows the simulated S-parameters

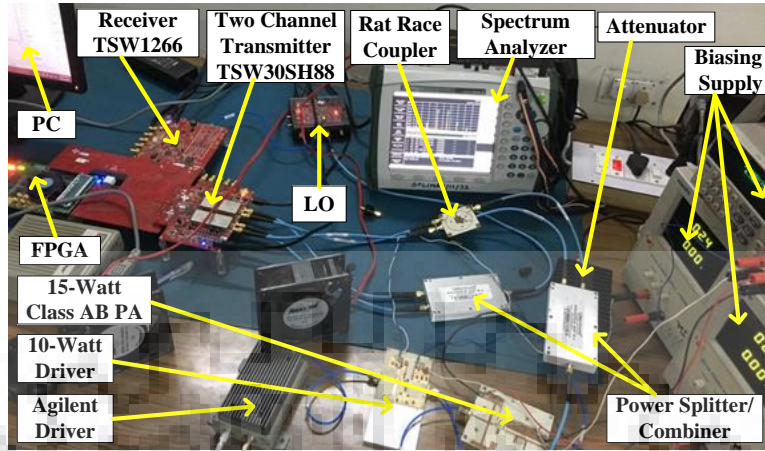


Figure 5.6: Test bench for data extraction of HRF-DPD.

of the RRC. It can be observed that the coupled ports (S13 and S12) maintain their performance of -3 dB and the delta-port (isolated port) and return loss (S14 and S11) <-10 dB over a limited bandwidth (approx. 500 MHz) around 2 GHz.

5.4.2 Test-bench for data extraction

The performance of HRF-DPD linearizer is showcased by the proof-of-concept using setup shown in Figure 5.6. It consist of a broadband receiver (TSW1266), dual channel transmitter (TSW34SH84), LO (TSW3065), phase adjusted IMD generator, i.e. RRC, , 2 way 0° power combiners/ splitters (ZN2PD2-50-S+), fixed attenuator at the PA output, 15-W Class AB PA and ZX60-V63+ PA from Mini circuits. The AM/AM and AM/PM characteristics of 15W Class AB PA is shown in Figure 5.7.

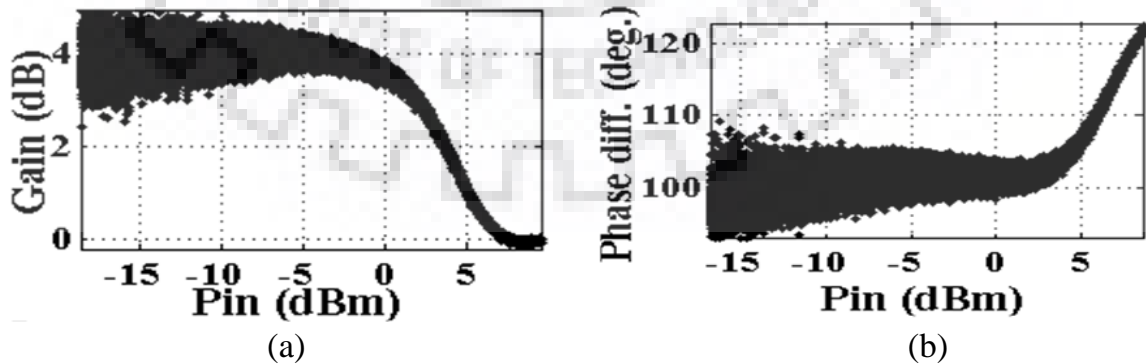


Figure 5.7: AM/AM and AM/PM characteristics of 15W Class AB PA.

The transmitter contains an RF modulator of frequency range 300 MHz to 4 GHz. Both channels are of 16-bit DAC, which are synchronized with 10 MHz clock, programmed using Quartus software from Altera. The on-board HSMC connector input allows direct connection to the HSMC compatible Altera FPGA.

A baseband I/Q signal is uploaded to the RAM of FPGA using Quartus and Matlab software. TSW34SH84 includes LMK 04808B low noise clock generator that provides sampling clock to 16 bit-DAC. DAC has two pairs of In-phase/Quadrature-phase outputs that are directly provided to two TRF3705 IQ modulator. It forms two transmit chains that provide IF-to-RF conversion. The signal is up-converted using a complex RF modulator TRF3705 and passed through the PA.

Synchronization between the two channels has been done and an accurate adjustment in the phase between two channels can be achieved at baseband level. The phase shift between the two channels can be adjusted using Matlab. Channel I contain LTE signal and Channel II contains digitally phase-shifted (180° phase change due to path delay) LTE signal, which is provided to the input of RRC. Both the signals are baseband synchronized. Transmitter and receiver can support the bandwidth of 500 MHz around its carrier frequency. The data are sent to a transmitter using pre-programmed FPGA at a sampling rate of 307.2 MHz. The data is interpolated with an interpolation factor of 4 and up-convert it to a sampling frequency of 1228.8 MHz. The performance of the proposed linearizer is evaluated for a 15-W Class-AB PA, which is driven by a 10-W driver PA.

- (a) 100 MHz CA-LTE signal centered at frequencies 1985 MHz and 2080MHz with a PAPR of around 13.26 dB and
- (b) 50 MHz carrier aggregated (CA)-LTE signal with frequencies 2010 MHz and 2055 MHz with a PAPR of around 13.18 dB.

For 100 MHz and 50 MHz LTE signal, the bandwidth of each carrier is 5 MHz and they are separated by the spacing of 90 MHz and 40 MHz respectively.

The HRF-DPD performance is evaluated and compared with the proposed RF-in RF-out APD for ZX60-V63+ PA using contiguous and non-contiguous 8CC 160 MHz signal.

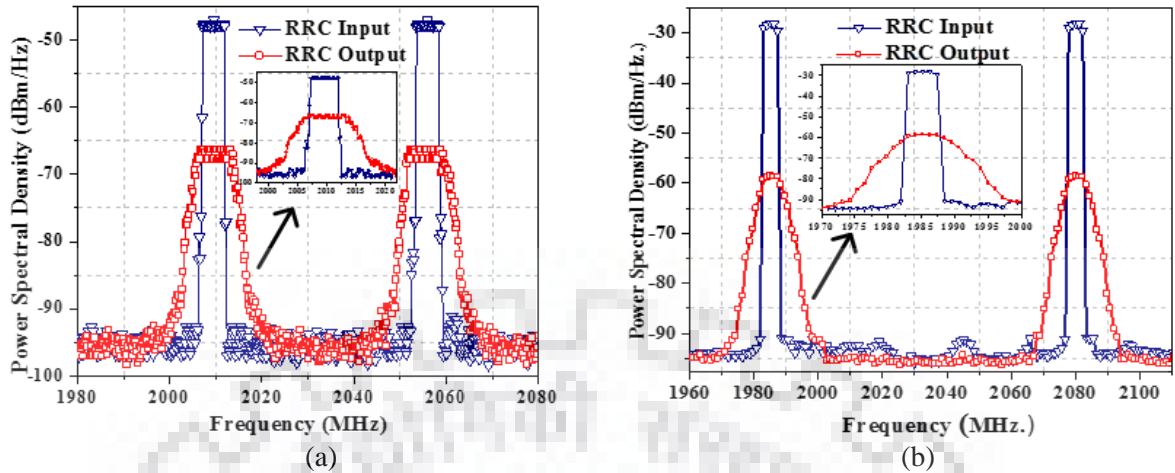


Figure 5.8: Cancellation of fundamental signal and generation of in-band IMD for (a) LTE 50 MHz, (b) LTE 100 MHz signal.

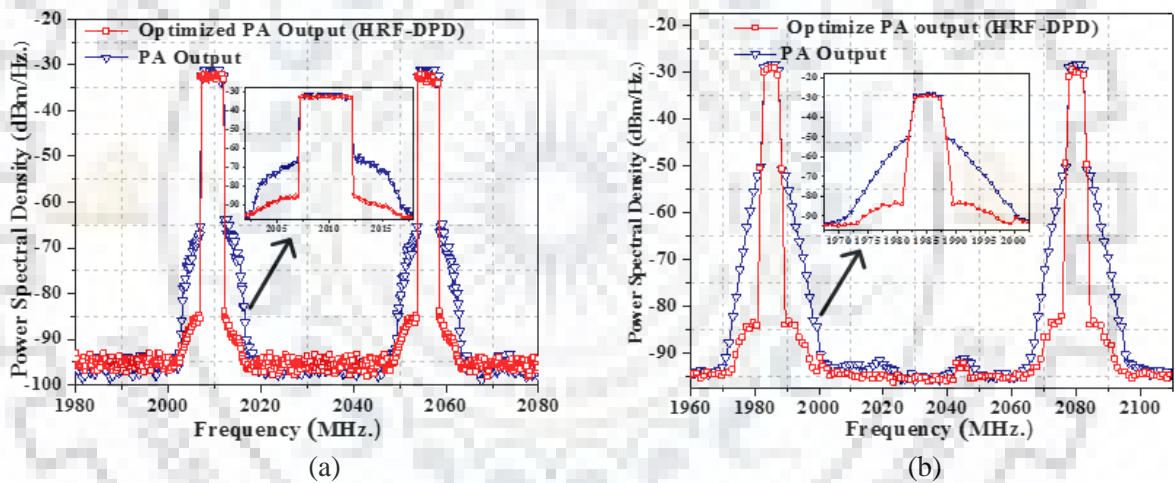


Figure 5.9: Cancellation of in-band IMD for (a) LTE 50 MHz, (b) LTE 100 MHz signal.

5.4.3 Signal under Test

5.4.3.1 LTE 50 MHz and 100 MHz signals

Experimental results show that the proposed approach provides good linearization performance for wideband signals. The output of a phase adjusted IMD generator (i.e. RRC) for the two carriers LTE 50 MHz and 100 MHz signals are shown in Figure 5.8 (a) and Figure 5.8 (b). The RRC effectively cancels the fundamental signal and produces only

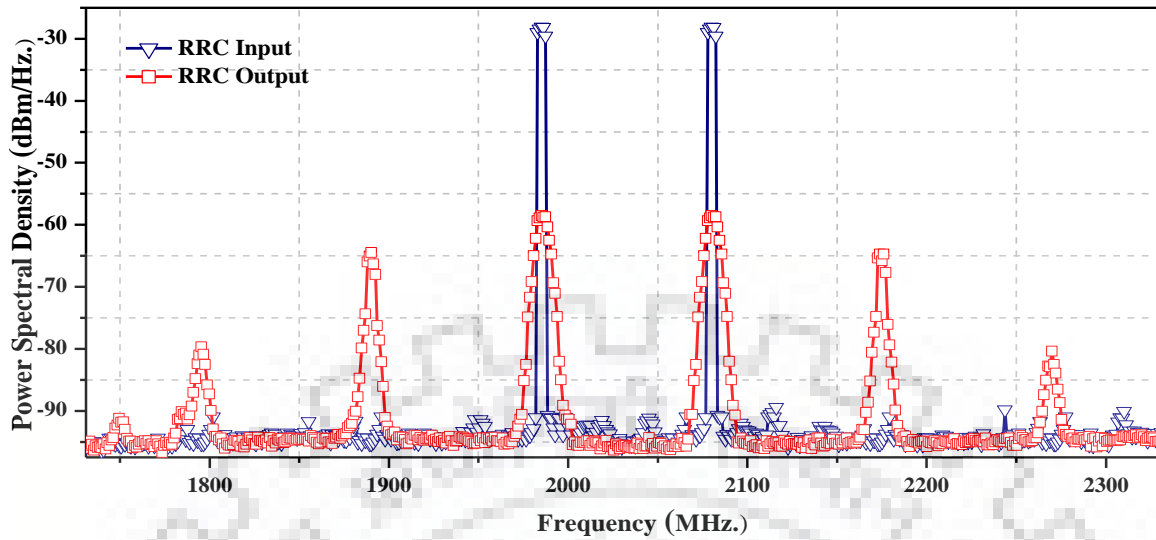


Figure 5.10: Output of phase adjusted IM generator (RRC) showing the out-of band IM3 and IM5 generation of the two carrier LTE 100 MHz signal.

the IMD terms. The frequency spectrum at the output of the PA is plotted in Figure 5.9 (a) and Figure 5.9 (b) for the cases with and without HRF-DPD set up. More than 20 dB ACPR improvement has been reported for both the signal conditions. For achieving this performance, DAC in the transmitter has to process only signal bandwidth for the proposed method. However, DPD operation would require 250 MHz and 500 MHz bandwidths respectively. Moreover, from Figure 3.22 (a), it can be observed that DPD for this measurement setup is not possible due to very poor system NMSE at such high bandwidth.

Table 5.1 shows the results for IMD terms near transmission band, however, it is to be noted that the APD contains diodes, which can support quite wideband application. Figure 5.10 shows all the IMD terms generated by RRC circuit. For the two carriers modulated

TABLE 5.1

NEAR BAND ACLR PERFORMANCE WITH AND WITHOUT THE HRF-DPD LINEARIZER

Signals under test	ACLR before HRF-DPD	ACLR after HRF-DPD	Correction
LTE 50MHz	-33.2 dBc	-53.2 dBc	20 dB
LTE 100MHz	-23.4 dBc	-54 dBc	30.6 dB

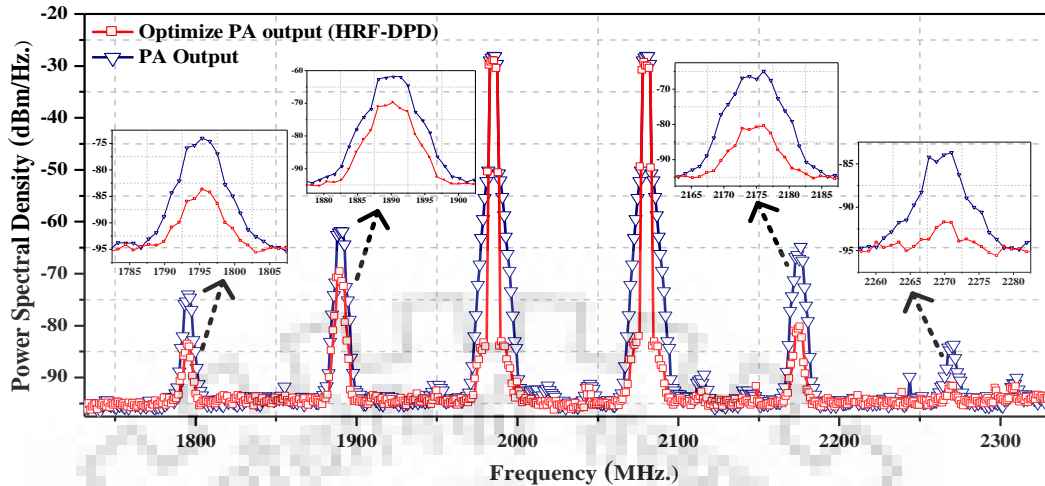


Figure 5.11: Measured Power Spectrum Density of HRF-DPD showing cancellation of out-of-band IM3 and IM5 of LTE 100 MHz signal

TABLE 5.2

AWAY FROM THE BAND ACLR PERFORMANCE WITH AND WITHOUT THE PROPOSED HRF-DPD LINEARIZER FOR LTE 100 MHz SIGNAL

IMD	ACLR before HRF-DPD	ACLR after HRF-DPD	Correction
IMD3 LOWER	-33.7 dBc	-43.2 dBc	9.5 dB
IMD3 UPPER	-39.9 dBc	-55.4 dBc	15.5 dB
IMD5 LOWER	-47.7 dBc	-57.3 dBc	9.6 dB
IMD5 UPPER	-57.5 dBc	-65.5 dBc	8 dB

signal with 100 MHz bandwidth whose carrier frequencies are located at 1985 MHz and 2080 MHz. IM3 distortions were generated by RRC around 1890 MHz (IM3L) and 2175 MHz (IM3U) and IM5 distortions were generated around 1795 MHz (IM5L) and 2270 MHz (IM5U). These IMD's of RRC circuits also reduces the out-of-band IMDs generated by RF PA. The linearization results for bandwidth of 500 MHz is shown in Figure 5.11.

The results are summarized in the Table 5.2. It can be concluded that even without the use of filters, ACLR of more than 45 dB is maintained in all IMD terms.

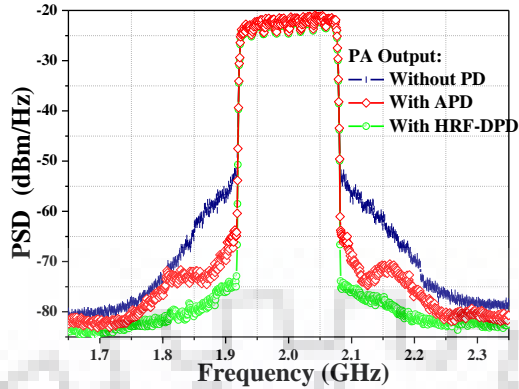


Figure 5.12: Measured Power Spectrum Density of PA with and without the proposed RF-linearization in RF-out APD and HRF-DPD excited by contiguous 8CC 160 MHz LTE signal.

5.4.3.2 Contiguous and Non-Contiguous 8CC 160 MHz LTE signal

Linearization of 160 MHz UWB signal is a challenging task. Figure 5.12 and Figure 5.13 shows the measured PSD for the contiguous and non-contiguous 8CC 160 MHz LTE signal with and without proposed linearization methods. When proposed RF-in RF-out APD is applied to linearize ZX60-V63+ PA using contiguous 160 MHz LTE signal, an ACPR of -43.9 dBc is achieved. There is an improvement of over 10.9 dB as compared to PA without linearization. This performance is improved further by applying digitally supported HRF-DPD model. As shown in Figure 5.12, with HDC-APD, an ACPR of -53.5 dBc, which is an improvement of over 20.5 dB as, compared to PA without linearization.

Similarly, when proposed linearization scheme is applied to non-contiguous 10001001 where 1 indicates on-state and 0 indicates off-state with total instantaneous bandwidth of 160 MHz LTE signal. When proposed RF-in RF-out APD is applied to linearize ZX60-V63+ PA using non-contiguous 160 MHz LTE signal, an ACPR of -45.1 dBc is achieved with an improvement of 9.2 dB. Its performance is further enhanced using HRF-DPD. As shown in Figure 5.13, with HDC-APD, an ACPR of -56.1 dBc is achieved, which is an improvement of over 20.2 dB. It can be appreciated from Figure 5.13 that the proposed linearization not only provide in-band ACPR correction near the band, but it is also able to correct out-of-band IMD.

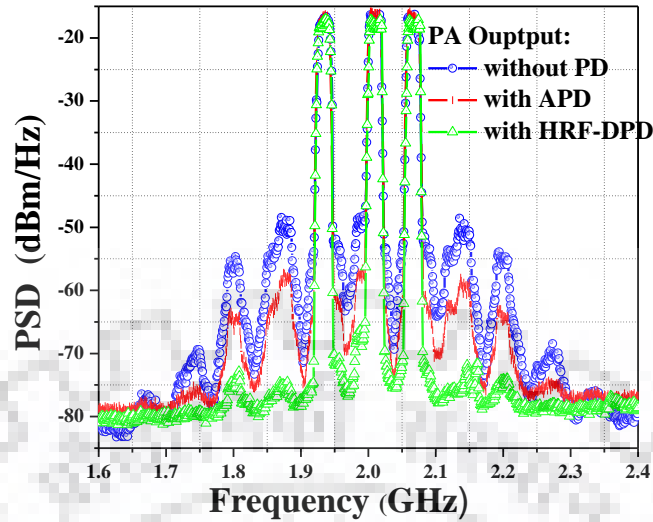


Figure 5.13: Measured Power Spectrum Density of PA with and without the proposed RF-in RF-out APD and HRF-DPD excited by non-contiguous 8CC 160MHz LTE signal.

5.5 Comprehensive Comparison with the State-of-the-art Hybrid Predistortion Linearization

The previously proposed HPD is an intermediate solution between APD and baseband DPD, where, the non-linear predistortion model is implemented in the digital domain [141], [142]. The performance of such system depends on accurate characterization and implementation in analog and digital domain of the system. It provides higher accuracy than the APD and better bandwidth than the DPD.

Table 5.3 elaborates the components required for various predistortion linearization techniques and Table 5.4 summarize various linearizer techniques and their salient features in comparison with the features of the proposed techniques. It describes the bandwidth and other specifications of the components used in various linearizer techniques. Similarly, Table 5.5 discusses the pros and cons of previously proposed HRF-DPD architecture [66]-[71]. From the above tables, it can be concluded that proposed APD and HRF-DPD captures the UWB signal, which is not possible with the conventional APD. In the proposed HRF-DPD architecture, baseband information of the input signal is not required. It also

TABLE 5.3
 COMPONENT REQUIREMENT IN VARIOUS PREDISTORTER LINEARIZER;
 R: REQUIRED, NR: NOT REQUIRED

COMPONENT REQUIRED	APD	DPD	HPD	PROPOSED HRF-DPD	PROPOSED RF-IN RF-OUT APD
DAC	NR	R	R	R	NR
ADC	NR	R	R	R	NR
VM	R	NR	R	NR	R
DELAY LINE	R	NR	R	NR	NR
FPGA	NR	R	R	R	NR
EDET	NR	NR	R	NR	NR
BRANCH LINE COUPLER	R	NR	NR	NR	NR
FILTERS	NR	R	R	NR	NR
IMD GENERATOR	R	NR	NR	R	R
DIGITAL RECEIVER	NR	R	R	NR	NR

alleviates the signal bandwidth limitation because there is no need to capture five times of the input signal bandwidth. The data converters and FPGA only processes the original bandwidth of the signal. The advanced DSP platform can perform linear operation, i.e. digital compensation of delay and analog circuits perform a nonlinear operation by generating IMD. It provides wideband, yet effective predistortion solution which makes best of ‘analog’ and ‘digital’ techniques.

TABLE 5.4

BANDWIDTH AND OTHER SPECIFICATIONS OF VARIOUS PREDISTORTER LINEARIZER

Specifications	APD	DPD	HPD	PROPOSED HRF-DPD	PROPOSED RF-IN RF- OUT APD
Nonlinearity inducing element	Analog-typically diodes	Digital models	Digital models	Analog antiparallel diode	Analog antiparallel diode
Bandwidth of ADC	Not applicable	5 × of the input signal	5 × of the input signal	1 × of the input signal	Not applicable
Bandwidth of DAC	Not applicable	5 × of the input signal	5 × of the input signal	1 × of the input signal	Not applicable
Bandwidth of VM	5 × of the input signal	NA	5 × of the input signal	Not applicable	1 × of the input signal
Delay Compensation	Bulky Delay lines	Offline Delay compensation	Offline Delay compensation	Online Delay compensation	SMA coaxial Cable
Compensation bandwidth	Wide	Narrow	Wide	Ultra-wide	Ultra-wide
ACPR correction	Moderate 10-15 dB	High 20-30 dB	Moderate 10-18 dB	High 20-30 dB	Moderate 10-20 dB
Sampling rate	NA	5 × of the input signal	5 × of the input signal	1 × of the input signal	NA

TABLE 5.5

VARIOUS HYBRID PREDISTORTION LINEARIZER

Hybrid PD Type	Salient Features	Signal Used	Correc-tion
Proposed HRF-DPD	<p>Nonlinear element: Analog using a diode, Application: analog domain, adaptation digital domain.</p> <p>No need of baseband information of input signal.</p> <p>Input signal bandwidth limitation relaxed as there is no need to process five times of the signal bandwidth.</p>	<p>LTE 50 MHz</p> <p>LTE 100 MHz</p> <p>LTE 160 MHz</p>	<p>20-dB</p> <p>30.4-dB</p> <p>20.5</p>
Hybrid RF Envelope Predistortion [55]	<p>Nonlinear element: Digital LUT, Application: analog domain.</p> <p>No need of baseband information of input signal.</p> <p>Input signal bandwidth limitation due to EDET sampling rate.</p> <p>Input signal bandwidth limitation due to ADC sampling rate in the feedback loop (5X Signal bandwidth).</p>	<p>Eight tone signal with 25 MHz bandwidth</p>	<p>12-dB (ACLR)</p>
Analog RF-Predistortion [156]	<p>Nonlinear element: Digital LUT, Application: analog domain, adaptation analog domain.</p> <p>Does not relax the bandwidth constraint.</p> <p>Doesn't require access to baseband information.</p> <p>Addressed hardware imperfection in the RF-DPD of [191].</p> <p>DC offsets, wideband IQ imbalance and relative magnitude and phase difference of hybrid branch line coupler is compensated by two constants and eight FIR filters.</p>	<p>LTE 40 MHz with PAPR of 8.3dB</p>	<p>16-dB (ACLR)</p>

Hybrid RF/DPD [190]	<p>Nonlinear element: Digital LUT, Application: analog domain, adaptation analog domain.</p> <p>Data converters and FPGA capture 5X of the input signal bandwidth.</p> <p>Addressed IQ imbalance due to hardware imperfection in the RF-DPD of [177].</p> <p>IQ imbalance compensated using adaptive look-up-table (LUT) based calibration system.</p> <p>Modified LUT effectively compensate IQ imperfection without tuning control voltages of RF VM.</p>	Three carrier WCDMA signal	10.5-dB (ACLR)
Adaptive digital/ RF- Predistortion [191]	<p>Nonlinear element: Digital LUT, Application: analog domain, adaptation analog domain.</p> <p>No need of baseband information of input signal.</p> <p>Input signal bandwidth limitation due to EDET sampling rate.</p> <p>Input signal bandwidth limitation due to ADC sampling rate in the feedback loop (5 x Signal bandwidth). An adjustment in the phase and envelope magnitude is adapted in VM.</p>	Three carrier WCDMA signal with PAPR of - 11.5dB	10-dB (ACLR)
HPD [192]	<p>Deploying DPD puts burden on the system design.</p> <p>Data converters capture 5X of the signal bandwidth that increases power overhead consumption.</p>	LTE 120 MHz	19.4- ACPR 11.3-EVM
HPD [193]	<p>Requires large back-off of 6dB for simultaneously compensating IM3 and IM5</p> <p>Requires a combination of harmonic injection and cubic-predistortion circuit</p>	2-tone and WCDMA	20-IM3 20-IM5 13- ACPR

5.6 Challenges in the Implementation

The proposed predistortion techniques offer several advantages over the existing predistortion architectures which are discussed in the previous chapters. There are certain challenges which are observed during the implementation of the proposed predistortion architectures.

Transmitter Efficiency: In the proposed architectures, the fundamental signal cancellation and intermodulation generation are performed simultaneously using a low cost and energy efficient intermodulation generator. The operation and architecture of IM generator and PIMG is very simple and compact, as it is composed of RRC, WPC and WPD, which are further equipped with Schottky diodes and a pair of resistor and capacitor.

As for the concern of transmitter efficiency, the proposed predistortion architecture is two path structure in which linear path is equipped with only SMA Cable that carries the original fundamental signal and a nonlinear path composed of digitally controlled elements such as a DPS/VM and DSA. It exhibits some insertion loss which can be combatted using LGA in the nonlinear branch. These amplifiers also assure that the power at the input of the PIMG and IM generator must be appropriate enough to generate required intermodes products. The power at the input of the main PA with/without predistortion is not always same, it is reduced after predistortion in a small order. For 10W HMC8500 and ZFL-11 AD+ PA, the output power after predistortion is only reduced by 0.97 dB and 0.83 dB respectively.

The proposed architecture reduces the transmitter efficiency in a small order that can be negotiated when performance parameter come into the picture.

Power Balance: The proposed predistortion architecture is a two path structure, in which power balance between the linear and nonlinear path is one of the primary requirement. The tuning of the RF components in the nonlinear path must be very accurate. The linear signal power is very much desired and there is every intention of maintaining the power, however some power is lost at power splitting, controlled elements etc. and linearizer works at a small back-off.

Depending upon the IMD generated by the PA, the power at the input of PIMG/ IM generator can be tuned. If PA nonlinearity is up to third order, the power requirement in the nonlinear path is low. Similarly, if the PA nonlinearity is up to seventh order, the power requirement in the nonlinear path is high.

Linearizability: When we focus on designing even broader predistorter, limitation of control elements becomes even more prominent, which does not perform uniformly over the complete frequency range. As the bandwidth of the signal increases, the asymmetry between the intermodulation products also rises. The behavior of the controlled elements such as DPS, VM become worse due to the asymmetry between lower and upper intermodulation components that deteriorates the performance of the proposed predistortion architectures. Moreover analog components are not as accurate as digital ones.

Control Scheme Selection: Instead of using single component for gain and phase monitoring in the Type-I CS, the Type-II CS uses separate components that definitely increases the cost and complexity of the system. But independent monitoring of gain and phase, both using DPS and DSA, provide enhancements in the linearization performance. In terms of performance, DPS and DSA are advantageous over a VM. But in terms of cost and complexity, VM is advantageous over DPS and DSA.

Control Elements selection: It must be noted that the control elements such as LGA, DSA, and VM which are used in the nonlinear path of the proposed UBB RF-PD, RF-in RF-out APD always remain linear. Suppose if the input power of the signal is very high. The selection of DSA in the nonlinear path must assure that it has ability to provide sufficient attenuation to the input signal such that the power that reaches at the input of LGA does not cause saturation of it. In the second case, suppose if the input power of the signal is very low. The selection of LGA in the nonlinear path must assure that it has ability to provide sufficient gain to the input signal such that it will excite the PIMG/ IM generator.

5.7 Scope of the proposed technique

The proposed linearization method can be especially useful while working with the UWB PA. IMD of wideband PA can be filtered out by selecting band-pass filters around band-of-transmission. However, whenever we need to change the frequency of operation of UWB PA, we require new band-pass filters. This leads to the requirement of tunable filters or stand-by filter banks. When we want to implement UWB PA at chip level for handheld devices, such bulky filter banks create hindrances for the purpose of portability. With proposed technique, already available DSP can take care of linear operations and RRC can be implemented in smaller size along with the PA for portable, wideband yet effective predistortion solution.

5.8 Conclusion

In this chapter, a novel HRF-DPD linearizer was proposed and analyzed. Measurement results showed that the proposed method can significantly improve the RF PA linearity when tested with wide bandwidth 100 MHz LTE, two carrier signal allowing it to achieve an ACLR of -54 dBc. Away-from-the-band IMD terms are also maintained at ACLR of -45 dBc. In addition to improving the in-band and out-of-band performance, it also eliminates the system bandwidth constraint, which is a major drawback of conventional DPD. The proposed method also supports the filter-less linearization of UWB PA for reconfigurable frequencies.

Chapter 6

Conclusions

6.1 Concluding Remarks

In a modern wireless transmitter, the demand of linear and highly efficient operation of an RF PA has been increased drastically in the recent years. DPD has been a potent linearization method to mitigate the nonlinearity of PA, but shows its restrictions when the spectrum efficiency of modulated RF signals gets higher. As an alternative HPD and APD are the promising solutions because of its lower power consumption, cost effectiveness, fewer complexities and compact size. In this work, two analog predistortion systems and a hybrid predistortion architecture are proposed.

The research presented in this thesis has been directed toward exploring ways to implement the PA linearization in the form of analog and hybrid predistortion linearization circuits or systems, while providing the highest levels of performance required by the future 5G cellular systems. The achievement of this work can be summarized as follows:

Identification of RF components: Currently, no hardware implementation exists in the analog domain which claim the linearization of UWB signal. The RF components for use in the proposed linearization systems such as DPS, DSA, LGA, VM, couplers and combiners are identified and analyzed to predict their behavior in the linearization systems.

Specification Requirements: Through excessive simulation in the ADS from Keysight, the required specification of each linearization module are shown in this work. Based on the specification required, the IM generator in the proposed RF-in RF-out APD and PIMG in the proposed UBB RF PD are designed. These circuits are fabricated and experimentally verified, which proves that these are suitable for wideband application in the RF domain.

Outperforming Existing APD: First of all, the previously proposed APD architectures such as CAPD, cascaded APD, Fifth order APD and multi-branch APD have been analyzed by discussing their limitation. The proposed RF-in RF-out APD was shown to outperform the existing APD approaches, establishing itself as an attractive choice for wideband domain. As a result, the linearization of wideband RF systems is more feasible going forward.

Multi-band APD: In this area, a UBB MRF-PD for compensating multi-band IMD without requiring dedicating feedback loops has been developed. It has strong performance in correcting IMD in multi-band systems ranging from 200 MHz to 2.5 GHz, without the additional cost associated with the feedback loop. Similar to the proposed RF-in RF-out APD, it also alleviates the need of data converters, FPGA and provide commendable linearization using passive RF components.

Simultaneous Suppression of higher order Intermodulation: In this work, the focus has been placed on designing the predistortion linearization system that can simultaneously suppress IM3, IM5, and IM7 simultaneously. Experiments were conducted in various different environments using two tone and modulated LTE signal that validates the dexterity of the proposed predistortion linearization architectures.

Digital Calibration: A HRF-DPD utilizing the digital calibration technique is proposed. The digital calibration technique, already available DSP can take care of linear operations that manage the gain and phase of the signal in a precise manner. For reconfigurable frequencies, the proposed HRF-DPD supports filter less linearization of UWB PA. These digital calibration capabilities are used to compensate for higher order PA nonlinearities. Moreover, it also eliminates the system bandwidth constraint of the conventional DPD.

Low Cost and Low Power: In a nutshell, the proposed solution significantly improves the system accuracy and provides a lower overhead power consumption and lower cost solution that is practically viable for future 5G applications. The objective of this work is to produce the low cost and low power consuming predistortion linearization architecture.

Moreover, the Pros and Cons of the proposed architectures are discussed in Table 6.1.

TABLE 6.1

PROS AND CONS OF THE PROPOSED PREDISTORTER LINEARIZER

Architecture	Pros	Cons
RF-in RF-out APD	<ul style="list-style-type: none"> -Able to linearize wideband signal up to 200 MHz. -Simple, cost effective circuit: Does not require DSA, DPS, and a VGA/drive amplifier. -Eliminates the use of wideband linear up-mixer, data converters and FPGA. -No need of baseband information. -It's easier to integrate with the 5G base station and repeater systems. 	<ul style="list-style-type: none"> -Moderate linearization capability due to the non-ideality of analog components. -For adjusting the magnitude and phase it requires three biasing supply for VM. -Unable to provide linearization for multi-band signal whose bandwidth is higher than 200 MHz.
UBB RF-PD & UBB MRF-PD	<ul style="list-style-type: none"> -Provide linearization to multiband signal up to 1 GHz -No need of baseband information. -It's easier to integrate with the 5G base station, multi-carrier antenna design and repeater systems. - Eliminates the use of data converters and FPGA. -cost effective circuit -In terms of performance, DPS and DSA are advantageous over a VM 	<ul style="list-style-type: none"> -Moderate linearization capability -Requires Linear gain amplifier in the nonlinear IMD path. -the number of required digitally controlled blocks such as LGA, DPS, and DSA increase the complexity. -The use of separate components for gain and phase monitoring increases the cost and complexity of the system. -In terms of cost and complexity, VM is advantageous over DPS and DSA.
HRF- DPD	<ul style="list-style-type: none"> -No need of digital receiver to capture the whole spectrum of the output signal, which is 5 times to that of the input signal. 	<ul style="list-style-type: none"> -Predistortion is performed by analog components, but under the control of DSP platforms. -Digital circuitry includes extra DAC

<ul style="list-style-type: none"> -Sampling rate requirement is quite low as compared to DPD. -Less power consumption as DAC and ADC are running at low speed. -Provide excellent linearization because the phase and gain adjustment is digital. -No need of baseband information. -Input signal bandwidth is not limited by the EDET sampling rate. 	<p>and ADC, which increase overall cost and complexity of signal as compared to RF-in RF-out APD.</p>
---	---

6.2 Suggestions for Future Work

The research conducted as part of this work opens some thought-provoking avenues of further investigation going forward. Among such opportunities are increase in frequency range and bandwidth, improved designs of low power circuits, and finally monolithic integration of this architecture.

To further enhance the efficiency of the PA, the proposed HRF-DPD linearization architecture can be integrated with the PAPR reduction techniques. Combining the predistortion techniques with PAPR reduction methods will ensure higher energy efficiency while maintaining signal quality.

The fabricated IM generator and PIMG have since been improved for bandwidth, fundamental signal cancelation, generation of IM products, and power consumption. Their measured performance can be verified as future exercise. In addition, the optimization of the diode at the device level should be investigated.

One of the future studies about the predistortion linearization architectures will focus on the simultaneous suppression of higher order intermodes while at the same time compensating the memory effects of PA.

The fractional bandwidth of the RF components such as PIMG, RRC, combiner, couplers

etc. is usually proportional to the center frequency of operation. The fractional bandwidth of an RF component is a measure of how wideband the component is. The fractional bandwidth is often quoted as a percentage. The higher the percentage, the wider the bandwidth. At higher frequency, the fractional bandwidth of an RF components increase. Therefore, another enhancement would be the implementation of the proposed RF-in RF-out APD and UBB RF-PD at higher frequency band such as K, Ku-band, where the frequency shifts due to fabrication challenges may present new directions.





Bibliography

1. Cisco Systems Inc., “Cisco Visual Networking Index: Global Mobile Data Traffic Forecast Update 2014-2019 White Paper,” Tech. Rep., 2015.
2. United Nations, “Concise Report on the World Population Situation in 2014,” Tech. Rep., 2014.
3. Ericsson Mobility Report, Jun. 2018.
4. M. LaPedus, “Waiting for 5G technology,” Manufacturing and Process technol., Jun 23rd 2016, retrieved Sep. 2nd 2016.
5. N. Kelly, W. Cao, and A. Zhu, “Preparing linearity and efficiency for 5G: Digital predistortion for dual-band doherty power amplifiers with mixed-mode carrier aggregation,” IEEE Micro. Mag., vol. 18, no.1, pp. 76-84, Feb. 2017.
6. A. Katz, J. Wood, and D. Chokola, “The evolution of PA linearization: From classic feedforward and feedback through analog and digital predistortion,” IEEE Micro. Mag., vol. 17, no.2, pp. 32-40, Feb. 2016.
7. J.G. Andrews, S. Buzzi, W. Choi, S.V. Hanly, A. Lozano, A.C.K. Soong, and J.C. Zhang, “What will 5G be,” IEEE J. Sel. Areas Commun., vol. 32, no. 6, pp. 1065-1082, Jun. 2014.
8. The Climate Group, “Smart 2020: Enabling the Low Carbon Economy in the Information Age,” Report for Global e-Sustainability Initiative, GeSI, 2008, pp. 1 - 86.
9. “EARTH - energy aware radio and network technologies deliverable d2.3: Energy efficiency analysis of the reference systems, areas of improvements and target breakdown,” 2012. Available: <https://bscw.ict-earth.eu/pub/bscw.cgi/>

10. S. Cripps, "RF power amplifiers for wireless communications," 2nd ed. Boston: Artech House, 2006.
11. U. Goyal, S. K. Tomar, M. Mishra and S. Vinayak, "Design and development of S band 10W and 20W power amplifier," 2015 IEEE Applied Electromagnetics Conf. (AEMC), Guwahati, India, 2015, pp. 1–2.
12. A. Jain, A. K. Gupta, D. K. Sharma, P. R. Hannurkar, and S. K. Pathak, "Design and analysis of a high-power radial multi-way combiner," *Int. J. of Microw. Wireless Technol.*, vol. 6, no. 1, pp. 83-91, Feb 2014.
13. L. Albasha, C. Clifton, Y. Jingu, A. Lawrenson, H. Motoyama, S. Bensmida, K. A. Morris, and K. Kohama, "An ultra-wideband digitally programmable power amplifier with efficiency enhancement for cellular and emerging wireless communication standards," *IEEE Trans. Circuits Syst. I: Regular papers*, vol. 63, no. 10, pp. 1579-1591, Sept. 2016.
14. A. Jain, P. R. Hannurkar, S. K. Pathak, and D. K. Sharma, "System efficiency analysis for high power solid state radio frequency transmitter," *Review of Scientific Instruments*, vol. 024707, no. 85, pp. 1-8, April 2014..
15. A. Jindal, U. Goyal, S. K. Tomar, M. Mishra, and S. Vinayak, "Design of a 2.8 W S-band power amplifier using load pull measurement," 2015 IEEE Applied Electromagnetics Conf. (AEMC), Guwahati, India, 2015, pp. 1–2.
16. M. Mishra, S. Kumar, S. K. Tomar, S. Vinayak, and B. K. Sehgal, "Effect of traps on small signal equivalent circuit in AlGaIn/GaN HEMTs," 2014 IEEE 2nd International Conf. on Emerging Electronics (ICEE), Bangalore, 2014, pp. 1–4.
17. H. Jang, P. Roblin and Z. Xie, "Model-Based Nonlinear Embedding for Power-Amplifier Design," *IEEE Trans. Microw. Theory Techn.*, vol. 62, no. 9, pp. 1986–2002, Sep. 2014.

18. H. Jang, P. Roblin, C. Quindroit, Y. Lin, and R. D. Pond, "Asymmetric Doherty Power Amplifier Designed Using Model-Based Nonlinear Embedding," *IEEE Trans. Microw. Theory Techn.*, vol. 62, no. 12, pp. 3436–3451, Dec. 2014.
19. N. Potheary, "Feedforward Linear Power Amplifiers," Artech House Inc, 1999.
20. I. Mayordomo, J. Legarda, J. Presa, and D. Valderas, "High-resolution ACLR measurement architecture for adaptive feed forward amplifiers," *IEEE Tran. Instrum. Meas.*, vol. 58, no. 2, pp. 429-433, Feb. 2009.
21. Y. Yang, Y. Y. Woo, and B. Kim, "Optimization for Error-Canceling Loop of the Feedforward Amplifier Using a New System-Level Mathematical Model," *IEEE Trans. Microwave Theory Tech.*, Vol. 51, No. 2, February, 2003.
22. J. Kim, C. Park, J. Moon, and B. Kim, "Analysis of adaptive digital feedback linearization techniques," *IEEE Trans. Circuits Syst. I: Regular papers*, vol. 57, no. 2, pp. 345-354, Feb. 2010.
23. S. Yamanouchi, Y. Aoki, K. Kunihiro, T. Hirayama, T. Miyazaki, and H. Hida, "Analysis and design of dynamic predistorter for WCDMA handset power amplifiers," *IEEE Trans. Microw. Theory Techn.*, vol. 55, no. 3, pp. 493-503, Mar. 2007.
24. T. B. Bako and T. Daboczi, "Reconstruction of nonlinearly distorted signals with regularized inverse characteristics," *IEEE Tran. Instrum. Meas.*, vol. 51, no. 5, pp. 1019-1022, Oct. 2002.
25. I. L. Mato, M. Pereira, J. J. Rodriguez-Andina, J. Faria, E. Soto, and R. Prez, "Distortion mitigation in RF power amplifiers through FPGA based amplitude and phase predistortion," *IEEE Trans. Ind. Electron.*, vol. 55, no. 11, pp. 4085–4093, Nov. 2008.
26. Y. Hu and S. Boumaiza, "Power-scalable wideband linearization of power amplifiers," *IEEE Trans. Microw. Theory Techn.*, vol. 64, no. 5, pp. 1456-1464, May 2016.

27. A. Prata, J.C. Santos, A.S.R. Oliveira, and N.B. Carvalho, "Agile all-digital DPD feedback loop," *IEEE Trans. Microw. Theory Techn.*, vol. 65, no. 7, pp. 2476-2484, Jul. 2017.
28. M. Rawat, K. Rawat, and F.M Ghannouchi, "Generalized rational function for reduced complexity behavioural modelling and digital predistortion of broadband wireless transmitter," *IEEE Tran. Instrum. Meas.*, vol. 63, no. 2, pp. 485-498, Feb. 2014.
29. H. Wang, G. Li, C. Zhou, W. Tao, F. Liu, and A. Zhu, "1-bit observation for direct-learning-based digital predistortion of RF power amplifiers," *IEEE Trans. Microw. Theory Techn.*, vol. 65, no. 7, pp. 2465-2475, Jul. 2017.
30. C. Shannon, "Communication in the Presence of Noise," *Proceedings of the IRE*, vol. 37, no. 1, pp. 10-21, Jan. 1949.
31. A. Goel, P. Gupta, and M. Agrawal, "SER analysis of PTS based techniques for PAPR reduction in OFDM systems", *Digital Signal Processing*, vol. 23, no. 1, pp. 302-313, 2013.
32. M. Agrawal and S. Prasad, "A modified likelihood function approach to DOA estimation in the presence of unknown spatially correlated Gaussian noise using a uniform linear array," *IEEE Trans. Signal Process.*, vol. 48, no. 10, pp. 2743-2749, Oct. 2000.
33. P. Colantonio, F. Giannini, and E. Limiti, *High Efficiency RF and Microwave Solid State Power Amplifiers*, New York, NY, USA: Wiley, 2009.
34. F. M. Ghannouchi and O. Hammi, "Behavioral modeling and predistortion," *IEEE Microw. Mag.*, vol. 10, no. 7, pp. 52-64, Dec. 2009.
35. K. Rawat and F. M. Ghannouchi, "Design methodology for dual-band Doherty power amplifier with performance enhancement using dual-band offset lines," *IEEE Trans. Ind. Electron.*, vol. 59, no. 12, pp. 4831-4842, Dec. 2012.

36. A. Jain, P.R. Hannurkar, S. K. Pathak, O.K. Sharma, and A.K. Gupta, "Investigation of Class J continuous mode for high power solid state RF amplifier," *IET Microw. Antennas Propag.*, vol. 7, no. 8, pp. 686 - 692, Jun 2013.
37. J. Wood, *Behavioral Modeling and Linearization of RF Power Amplifiers*, Norwood, MA: Artech House, 2014.
38. D. Lopez-Bueno, T. Wang, P. L. Gilabert, and G. Montoro, "Amping up, saving power: Digital predistortion linearization strategies for power amplifier under wideband 4G/5G burst like waveform operation," *IEEE Micro. Mag.*, vol. 17, no.1, pp. 79-87, Jan. 2016.
39. S. Kusunoki, K. Yamamoto, T. Hatsugai, H. Nagaoka, K. Tagami, N. Tominaga, K. Osawa, K. Tanabe, S. Sakurai, and T. Lida "Power amplifier module with digital adaptive predistortion for cellular phones," *IEEE Trans. Microw. Theory Techn.*, vol. 50, no. 12, pp. 2979-2986, Dec. 2012.
40. M. Rawat, K. Rawat, and F.M. Ghannouchi, "Three layered biased memory polynomial for dynamic modelling with predistortion of transmitter with memory," *IEEE Trans. Circuits Syst. I: Regular papers*, vol. 60, no.3, pp. 768-777, Mar. 2013.
41. M. Younes, A. Kwan, M. Akbarpour, M. Helaoui and F. M. Ghannouchi, "Two dimensional piecewise behavioral model for highly nonlinear dual-band transmitters," *IEEE Trans. Ind. Electron.*, vol. 64, no. 11, pp. 8666-8674, Nov. 2017.
42. P. Jaraut, M. Rawat, and F. M. Ghannouchi, "Composite neural network digital predistortion model for joint mitigation of crosstalk, I/Q imbalance, nonlinearity in MIMO transmitters," *IEEE Trans. Microw. Theory Techn.*, vol. 66, no. 11, pp. 5011–5020, Nov. 2018.
43. M. Younes, O. Hammi, A. Kwan, and F. M. Ghannouchi, "An accurate complexity-reduced PLUME model for behavioral modeling and digital predistortion of RF

- power amplifiers,” *IEEE Trans. Ind. Electron.*, vol. 58, no. 4, pp. 1397–1405, Apr. 2011.
44. P. Jaraut, M. Rawat, and F. M. Ghannouchi, “2-D curtailed harmonic memory polynomial for reduced complexity in concurrent dual-band modeling and digital predistortion with the second band at harmonic frequency,” *IET Commun.*, vol. 12, no. 12, pp. 1438–1447, Jul. 2018.
 45. Y. J. Liu, W. Chen, and B. H. Zhou, “A robust augmented complexity reduced generalized memory polynomial for wideband RF power amplifiers,” *IEEE Trans. Ind. Electron.*, vol. 61, no. 5, pp. 2389–2401, May 2014.
 46. A. E. Abdelrahman, O. Hammi, A. K. Kwan, A. Zerguine, and F. M. Ghannouchi, “A novel weighted memory polynomial for behavioral modeling and digital predistortion of nonlinear wireless transmitters,” *IEEE Trans. Ind. Electron.*, vol. 63, no. 3, pp. 1745–1753, Mar. 2016.
 47. D. R. Morgan, Z. Ma, J. Kim, M. G. Zierdt, and J. Pastalan, “A generalized memory polynomial model for digital predistortion of RF power amplifiers,” *IEEE Trans. Signal Process.*, vol. 54, no. 10, pp. 3852–3860, Oct. 2006.
 48. P. Jaraut, M. Rawat, and P. Roblin, “Curtailed Digital Predistortion Model for Crosstalk in MIMO Transmitters,” *IEEE MTT-S Int. Microw. Symp. Dig.*, Philadelphia, PA, USA, Jun. 2018, pp. 927–930.
 49. I. Ding, G.T. Zhou, D.R. Morgan, Z. Ma, J.S. Kenney, J. Kim and C.R. Giardina, “A robust digital baseband predistorter constructed using memory polynomial,” *IEEE Trans. Commun.*, vol. 53, no.9, pp. 1468-1479, Sep. 2006.
 50. H. Deng, D. Zhang, D. Lv, D. Zhoy, and Y. Zhang, “Analog predistortion linearizer with independently tunable gain and phase conversions for Ka-band TWTA,” *IEEE Trans. Electron Devices*, vol. 66, no. 3, pp. 1533-1539, Mar. 2019.

51. K. Yamauchi, K. Mori, M. Nakayama, Y. Itoh, Y. Mitsui, and O. Ishida, "A novel series diode linearizer for mobile radio power amplifiers," in Proc. MTT-S 1996 Int. Microwave Symp., 1996, pp. 831–834.
52. J. Sun, B. Li, and M. Y. W. Chia, "Linearized and highly efficient CDMA power amplifier," *Electron. Lett.*, vol. 35, no. 10, pp. 786–787, May 1999.
53. J. L. Mato, M. Pereira, J. J. Rodriguez-Andina, J. Faria, E. Soto, and R. Prez, "Reduction of intermodulation effects in power amplifiers through segmented predistortion," *IEEE Int. Symp. Ind. Electron.*, Vigo, Spain, Jun. 2007.
54. Y. Yang, Y. Y. Woo, and B. Kim, "New predistortion linearizer using low-frequency even-order intermodulation components," *IEEE Trans. Microw. Theory Techn.*, vol. 50, no. 2, pp. 446-452, Feb. 2002.
55. W. Woo, M.D. Miller, and J.S. Kenney, "A hybrid digital/ RF envelope predistortion linearization system for power amplifier," *IEEE Trans. Microw. Theory Techn.*, vol. 53, no. 1, pp. 229-235, Dec. 2005.
56. J. Xia, A. Islam, H. Huang and S. Boumzaia, "Envelope memory polynomial reformulation for hardware optimization of analog RF predistortion," *IEEE Microw. Compon. Lett.*, vol. 25, no. 6, pp. 415-417, Jun. 2015.
57. H. Huang, A. Islam, J. Xia and S. Boumaiza, "Linear filter assisted envelope memory polynomial for analog/ radio frequency predistortion of power amplifiers," *IEEE MTT-S International Microwave Symposium*, pp. 1-3, 2015.
58. K. Gumber and M. Rawat, "A modified hybrid RF predistorter linearizer for ultra-wideband 5G systems," *IEEE J. Emerg. Sel. Topics Circuits Syst.*, vol. 7, no. 4, pp. 547-557, Dec 2017.
59. K. Gumber and M. Rawat, "Low cost RFin-RFout predistorter linearizer for high power amplifiers and ultra-wideband signals," *IEEE Trans. Instrum. Meas.*, vol. 67, no. 9, pp. 2069-2081, Sep. 2018.

60. J. Wood, "System-level design consideration for digital pre-distortion of wireless base station transmitter," *IEEE Trans. Microw. Theory Techn.*, vol. 65, no. 5, pp. 1880-1890, May 2017.
61. M. R. Bhatnagar and M. K. Arti, "Performance analysis of hybrid satellite terrestrial FSO cooperative system," *IEEE Photon. Technol. Lett.*, vol. 25, no. 22, pp. 2197-2200, Nov. 2013.
62. M. R. Bhatnagar and Arti M.K., "Performance analysis of AF based hybrid satellite-terrestrial cooperative network over generalized fading channels," *IEEE Commun. Lett.*, vol. 17, no. 10, pp. 1912-1915, Oct. 2013.
63. M. K. Arti and M. R. Bhatnagar, "Beamforming and Combining In Hybrid Satellite-Terrestrial Cooperative Systems," *IEEE Commun. Lett.*, vol. 18, no. 3, Mar. 2014, pp. 483-486.
64. S-Y. Lee, Y-S. Lee, S-H. Hong, H-S. Choi, and Y-H. Jeong, "An adaptive predistortion RF power amplifier with a spectrum monitor for multicarrier WCDMA applications," *IEEE Trans. Microw. Theory Techn.*, vol. 53, no. 2, pp. 786-793, Feb. 2005.
65. X. L. Sun, S. W. Cheung, and T.I. Yuk, "A 5th-order analog predistorter for NADC system," *IEEE Int. Conf. Commun.*, Nov. 2010, Singapore.
66. K-H Lim, G. Ahn, H-C park, M-S Kim, J-H Van, H. Cho, J-H Jeong, C-S Park, and Y. Yang, "A 60-W multicarrier WCDMA power amplifier using an RF predistorter," *IEEE Trans. Circuits Syst. II: Express Briefs*, vol. 56, no. 4, pp. 265-269, Apr. 2009.
67. Y. Lee, M. Lee, and Y. Jeong, "A wideband analog predistortion power amplifier with multi-branch nonlinear path for memory effect compensation," *IEEE Microw. Compon. Lett.*, vol. 19, no. 7, pp. 476-478, Jul. 2009.

68. Y-S. Lee, M-W. Lee, S-H Kam, and Y-H. Jeong, "A transistor based analog predistorter with unequal delays for memory compensation," *IEEE Microw. Compon. Lett.*, vol. 19, no. 11, pp. 743-745, Nov. 2009.
69. Y-S. Lee, M-W. Lee, S-H Kam, and Y-H. Jeong, "A high linearity wideband power amplifier with cascaded third order analog predistorters," *IEEE Microw. Compon. Lett.*, vol. 20, no. 2, pp. 112-114, Feb. 2010.
70. Y. Kim, I. Chang, and Y. Jeong, "An Analog Predistortion Linearizer Design," *Microwave J.*, vol. 48, no. 2, pp. 118-126, Feb. 2005.
71. T. Nojima and T. Konno, "Cuber Predistortion Linearizer for Relay Equipment in 800 MHz Band Land Mobile Telephone System," *IEEE Trans. Veh. Technol.*, Vol. 34, No. 4, Nov.1985
72. M. Faulkner, "Amplifier linearization using RF feedback and feedforward techniques," *IEEE Trans. Veh. Technol.*, vol. 47, no. 1, pp. 209-215, Feb. 1998.
73. M. G. Overmann and J. F. Long, "Feedforward Distortion Minimization Circuit," US Patent No. 5,077,532, 1991.
74. K. Gumber, P. Jaraut, M. Rawat, and K. Rawat, "Digitally assisted analog predistortion technique for power amplifier," *IEEE 88th Microw. Meas. Conf. (ARFTG)*, Dec. 2016.
75. Y. Xu, J. Xia, and S. Boumaiza, "A 0.6–2.8GHz CMOS RF vector multiplier with low RMS magnitude and phase errors and high P1dB," in *IEEE MTT-S Int. Microw. Symp. Dig.*, Honolulu, HI, USA, Oct. 2017.
76. A. Asoodeh and M. Atarodi, "A Full 360° vector-sum phase shifter with very low RMS phase error over a wide bandwidth," *IEEE Trans. Microw. Theory Techn.*, vol. 60, no. 6, pp. 1626-1634, Jun. 2012.
77. Maxim Integrated "High gain vector Multipliers: MAX2045/MAX2046/MAX2047".

78. S. Chandravanshi and M. J. Akhtar. "Design of efficient rectifier using IDC and harmonic rejection filter in GSM/CDMA band for RF energy harvesting" *Microw. Opt. Technol. Lett.*, vol. 59, pp. 681- 686, March 2017.
79. T. Gupta, M. J. Akhtar, and A. Biswas, "Dual-mode dual-band compact balanced bandpass filter using square patch resonator," in *Proc. Asia– Pacific Microw. Conf. (APMC)*, New Delhi, India, Dec. 2016.
80. 04.2013-1MA221_1E: "LTE system specification and their impact on RF and baseband circuits, Application Note Rohde & Schwarz," 2013.
81. Q. Cai, W. Che, K. Ma, and M. Zhang, "A simplified transistor based analog predistorter for a GaN power amplifier," *IEEE Trans. Circuits Syst. II: Express Briefs*, vol. 65, no. 3, pp. 326-330, Mar. 2018.
82. N. Rostomyan, J.A Jayamon, and P.M. Asbeck, "15 GHz Doherty power amplifier with RF predistortion linearizer in CMOS SOI," *IEEE Trans. Microw. Theory Techn.*, vol. 66, no. 3, pp. 1339-1348, Mar. 2018.
83. J. Yi, Y. Yang, M. Park, W. Kang, and B. Kim, "Analog predistortion linearizer for high power RF amplifiers," *IEEE Trans. Microw. Theory Tech.*, vol. 48, no. 12, pp. 2709-2713, Dec. 2000.
84. U. Kim and Y. Kwon, "A high efficiency SOI CMOS stacked-FET power amplifier using phase based linearization," *IEEE Microw. Compon. Lett.*, vol. 24, no. 12, pp. 875-877, Dec. 2014.
85. K. H. Kim, G. B. Kim, S. W. Hwang, S. H. Lee, and D. Ahn, "A wide dynamic range analog predistortion-type linearizer using self-cancellation scheme," *IEEE Microw. Compon. Lett.*, vol. 15, no. 10, pp. 661-663, Oct. 2005.
86. J. Cha, J. Yi, J. Kim, and B. Kim, "Optimum design of predistortion RF power amplifier for multicarrier WCDMA application," *IEEE Trans. Microw. Theory Techn.*, vol. 52, no. 2, pp. 655-663, Feb. 2004.

87. Y. Lee, S. Lee, K. Jeon, and Y. Jeong, "Highly linear predistortion power amplifiers with phase controlled error generator," *IEEE Microw. Compon. Lett.*, vol. 16, no. 12, pp. 690-692, Dec. 2006.
88. S. Kousai, K. Onizuka, T. Yamaguchi, Y. Kuriyama, and M. Nagaoka, "A 28.3mW PA closed loop for linearity and efficiency improvement integrated in a +27.1dBm WCDMA CMOS power amplifier," *IEEE J. Solid-State Circuits*, vol. 47, no. 12, pp. 2964-2973, Dec. 2012.
89. S-C Jung, H-C Park, M-S. Kim, J-H Van, H. Hwangbo, C-S Park, S-K Park, and Y. Yang, "A new envelope predistorter with envelope delay taps for memory effect compensation," *IEEE Trans. Microw. Theory Techn.*, vol. 55, no. 1, pp. 52-59, Jan. 2007.
90. C-W Fan and K-K M. Cheng, "Theoretical and experimental study of amplifier linearization based on harmonic and baseband signal injection technique," *IEEE Trans. Microw. Theory Techn.*, vol. 50, no. 7, pp. 1801-1806, Jul. 2002.
91. C. S. Aitchison, M. Mbabele, M. R. Moazzam, D. Budimir, and F. Ali, "Improvement of third-order intermodulation product of RF and microwave amplifiers by injection," *IEEE Trans. Microw. Theory Techn.*, vol. 49, no. 6, pp. 1148-1154, Jun. 2001.
92. K. Madani, "Reducing the intermodulation in multi-carrier microwave power amplifiers," *Proc. Symp. High Perform. Electron Devices Microw. and Optoelectron. Appl.*, 1999, pp. 153-157.
93. C. G. Rey, "Adaptive Polar Work-Function Predistortion," *IEEE Trans. Microwave Theory Tech.*, vol. 47, no. 6, pp. 722-726, June 1999.
94. K. Yamauchi, K. Mori, M. Nakayama, Y. Mitsui, and T. Takagi, "A microwave miniaturized linearizer using a parallel diode with a bias feed resistance," *IEEE Trans. Microw. Theory Tech.*, vol. 45, no. 12, pp. 2431-2435, Dec. 1997.

95. X. Wang, Z. Zhang, L. Liu, and T. Ren, "Amplifier high linearization method based on offset cancellation technique," IEEE Int. Symp. Ind. Electron. Seoul, Korea, Jul. 2009.
96. K. Rawat, M. Rawat, and F.M. Ghannouchi, "Compensating I-Q imperfections in hybrid RF/ digital predistortion with adapted look up table implemented in FPGA," IEEE Trans. Circuits Syst. II: Express Briefs, vol. 57, no. 5, pp. 389-393, May 2010.
97. Y. Y. Woo, Y. Yang, J. Yi, J. Nam, J. Cha, and B. Kim, "An adaptive feedforward amplifier for WCDMA base stations using imperfect signal cancellation," Microwave J., vol. 46, no. 4, pp. 22-44, Apr. 2003.
98. S. P. Stapleton, "Amplifier linearization using adaptive digital predistortion," Applied Microwave and Wireless, vol. 13, pp. 72-77, Feb. 2001.
99. Y. Y. Woo, Y. Yang, J. Yi, J. Nam, J.H. Cha, and B. Kim, "Feedforward amplifier for WCDMA base stations with a new adaptive control method," in IEEE MTT-S Int Microwave Symp. Dig., vol. 2, Jun. 2002, pp. 769-772.
100. J.K. Carvers, "Adaptive behavior of a feedforward amplifier linearizer," IEEE Trans. Veh. Tech., vol. 44, pp. 31-39, Feb. 1995.
101. G. Zhao, F.M. Ghannouchi, F. Beaugard, and A.B. Kouki, "Digital implementations of adaptive feedforward amplifier linearization techniques," IEEE MTT-S Int. Microwave Symp. Dig., pp. 543-546, June 1996.
102. J. W. Huh, I. S. Chang, and C. D. Kim, "Spectrum monitored adaptive feedforward linearization," Microwave J., vol. 44, no. 9, pp. 160-167, Sep. 2001.
103. S. C. Bera, R. V. Singh, V. K. Garg, and S. B. Sharma, "Optimum bias load-line compensates temperature variation of junction diode's RF resistance," IEEE Trans. Microw. Theory Tech., vol. 55, no. 2, pp. 215-221, Feb. 2007.

104. S. C. Bera, R. V. Singh, and V. K. Garg, "Driver circuits for temperature invariant performance of junction diodes," *IET Circuits, Devices Syst.*, vol. 3, no. 4, pp. 143–152, Aug. 2009.
105. S. C. Bera, V. Kumar, S. Singh, and D. K. Das, "Temperature behavior and compensation of diode-based pre-distortion linearizer," *IEEE Microw. Wireless Compon. Lett.*, vol. 23, no. 4, pp. 211–213, Apr. 2013.
106. R. N. Braithwaite, "Memory correction for a WCDMA amplifier using digital-controlled adaptive analog predistortion," *2010 IEEE Radio and Wireless Symposium*, New Orleans, LA, Jan. 10-14, 2010, pp. 144-147.
107. Y. Seto, S. Mizuta, K. Oosaki, and Y. Akaiwa, "An adaptive predistortion method for linear power amplifiers," in *Proc. of IEEE Vehicular Technology Conference*, Tokyo, Japan, May 2000, pp. 1889–1893.
108. R. N. Braithwaite, "Low cost, low delay UMTS power amplifier using digital-controlled adaptive analog predistortion", in *Proc. 36th European Microwave Conf.*, Manchester, UK, Sep. 10-15, 2006, pp. 1641-1644.
109. R. N. Braithwaite, S. Carichner, and M. J. Hunton, "Data acquisition for digital-controlled adaptive analog predistortion of a power amplifier", in *Proc. IEEE Radio and Wireless Symp.*, Long Beach, CA, USA, Jan. 9-11, 2007, pp. 411-414.
110. S. Y. Lee, Y. S. Lee, and Y. H. Jeong, "Fully-automated adaptive analog predistortion power amplifier in WCDMA applications," in *35th IEEE Eur. Microw. Conf.*, Paris, France, Oct. 2005.
111. S.A Bassam, W. Chen, M. Helaoui, and F.M. Ghannouchi, "Transmitter architecture for CA: Carrier aggregation in LTE advanced systems," *IEEE Micro. Mag.*, vol. 14, no. 5, pp. 78-86, Jul.-Aug. 2013.
112. A. Osseiran et al., "Scenarios for 5G mobile and wireless communications: The vision of the METIS project," *IEEE Commun. Mag.*, vol. 52, no. 5, pp. 26–35, May 2014.

113. K. I. Pedersen, F. Frederiksen, C. Rosa, H. Nguyen, L. G. U. Garcia, and Y. Wang, "Carrier aggregation for LTE-advanced: Functionality and performance aspects," *IEEE Commun. Mag.*, vol. 49, no. 6, pp. 89–95, Jun. 2011.
114. Z. Shen, A. Papasakellariou, J. Montojo, D. Gerstenberger, and F. Xu, "Overview of 3GPP LTE-advanced carrier aggregation for 4G wireless communications," *IEEE Commun. Mag.*, vol. 50, no. 2, pp. 122–130, Feb. 2012.
115. G. Yuan, X. Zhang, W. Wang, and Y. Yang, "Carrier aggregation for LTE-advanced mobile communication systems," *IEEE Commun. Mag.*, vol. 48, no. 2, pp. 88–93, Feb. 2010.
116. S. Amin, W. V. Moer, P. Handel, and D. Ronnow, "Characterization of concurrent dual-band power amplifiers using a dual two-tone excitation signal," *IEEE Tran. Instrum. Meas.*, vol. 64, no. 10, pp. 2781-2791, Oct. 2015.
117. S. Yan, X. Yang, X. Li, and F. Li, "On dual-band amplifications using dual two-tones: clarifications and discussion," *IEEE Tran. Instrum. Meas.*, vol. 66, no. 10, pp. 2792-2794, Oct. 2017.
118. S. Parkvall, A. Furuskar, and E. Dahlman, "Next generation LTE, LTE-Advanced or LTE Rel-10 is the next step in radio access technology," *Ericsson review* 2010.
119. Ericsson, "LTE Release 13, White Paper," Tech. Rep., 2015.
120. Executive Summary, Inside 3GPP Release 13, 5G Americas "Understanding the standards for LTE advanced enhancements,".
121. 5G Americas Wireless Technology Evolution towards 5G: 3GPP Release 13 to Release 15 and beyond, Feb. 2017.
122. Samsung Electronics. (2015). 5G Vision White Paper [Online]. Available: [http://www.samsung.com/global/business-images/insights/2015/Samsung-5G Vision-0.pdf](http://www.samsung.com/global/business-images/insights/2015/Samsung-5G-Vision-0.pdf)

123. ETSI Technical Report Study on Scenarios and Requirements for next generation access technologies, 3GPP TR 38.913 version 14.3.0 Release 14, Oct. 2017.
124. Qualcomm Designing 5G NR a commercial reality, a unified, more capable 5G interface, Apr. 2018.
125. J. Kim and K. Konstantinou, "Digital predistortion of wideband signals based on power amplifier model with memory," *Electron. Lett.*, vol. 37, no. 23, pp. 1417–1418, Nov. 2001.
126. F. Mkadem, M. C. Fares, S. Boumaiza, and J. Wood, "Complexity reduced Volterra series model for power amplifier digital predistortion," *Analog Integr. Circuits Signal Process.*, vol. 79, no. 2, pp. 331–343, May 2014.
127. K. Gumber and M. Rawat, "Digital predistorter design using linear splines and its fixed point implementation," in *Proc. Asia– Pacific Microw. Conf. (APMC)*, New Delhi, India, Dec. 2016.
128. Y. Beltagy, A. Chung, P. Mitran, and S. Boumaiza, "On the calibration of the feedback receiver using reduced sampling rate and its application to digital predistortion of 5G power amplifiers," in *IEEE MTT-S Int. Microw. Symp. Dig.*, Jun. 2017, pp. 1549–1552.
129. R. N. Braithwaite, "Closed-loop digital predistortion (DPD) using an observation path with limited bandwidth," *IEEE Trans. Microw. Theory Techn.*, vol. 63, no. 2, pp. 726–736, Feb. 2015.
130. B. Kim, J. Kim, I. Kim, and J. Cha, "The Doherty power amplifier," *IEEE Microw. Mag.*, vol. 7, no. 5, pp. 42–50, Oct. 2006.
131. K. Rawat, M. S. Hashmi, and F. M. Ghannouchi, "Double the band and optimize," *IEEE Microw. Mag.*, vol. 13, no. 2, pp. 69–82, Mar./Apr. 2012.

132. W. Chen, S. Zhang, Y. Liu, Y. Liu, and F. M. Ghannouchi, "A concurrent dual-band uneven Doherty power amplifier with frequency-dependent input power division," *IEEE Trans. Circuits Syst. I, Reg. Papers*, vol. 61, no. 2, pp. 552–561, Feb. 2014.
133. P. Saad, P. Colantonio, L. Piazzon, F. Giannini, K. Andersson, and C. Fager, "Design of a concurrent dual-band 1.8–2.4-GHz GaN-HEMT Doherty power amplifier," *IEEE Trans. Microw. Theory Techn.*, vol. 60, no. 6, pp. 1840–1849, Jun. 2012.
134. X. A. Nghiem, J. Guan, T. Hone, and R. Negra, "Design of concurrent multiband Doherty power amplifiers for wireless applications," *IEEE Trans. Microw. Theory Techn.*, vol. 61, no. 12, pp. 4559–4568, Dec. 2013.
135. R. Kalyan, K. Rawat, and S. K. Koul, "Design strategy of concurrent multi-band Doherty power amplifier," *IET Microw. Antenna Propag.*, vol. 9, no. 12, pp. 1313–1322, Sep. 2015.
136. A. Barthwal, K. Rawat, and S. Koul, "Bandwidth enhancement of three-stage Doherty power amplifier using symmetric devices," *IEEE Trans. Microw. Theory Techn.*, vol. 63, no. 8, pp. 2399–2410, Aug. 2015.
137. C-S. Leung and K-K.M. Cheng, "A new approach to amplifier linearization by the generalized baseband signal injection method," *IEEE Microw. Compon. Lett.*, vol. 12, no. 9, pp. 336–338, Sep. 2002.
138. M. Seo, K. Kim, M. Kim, H. Kim, J. Jeon, M-K Park, H. Lim, and Y. Yang, "Ultra broadband linear power amplifier using a frequency selective analog predistorter," *IEEE trans. Circuits Syst. II: Express Briefs*, vol. 58, no. 5, pp.264-268, May 2011.
139. S. Tanaka, N. Taguchi, T. Kimura, and Y. Atsumi, "A predistortion-type equi-path linearizer for radio-on-fiber system," *IEEE Trans. Microw. Theory Techn.*, vol. 54, no. 2, pp. 938–944, Feb. 2006.

140. H. park, H. Yoo, S. Kahng, and H. Kim, "Broadband tunable third-order IMD cancellation using left-handed transmission-line-based phase shifter," *IEEE Microw. Compon. Lett.*, vol. 25, no. 7, pp. 478-480, Jul. 2015.
141. Y. Shen, B. Hraimel, X. Zhang, G.E.R. Cowan, K. Wu, and T. Liu, "A novel analog broadband RF predistortion circuit to linearize electro-absorption modulators in multiband OFDM radio-over-fiber systems," *IEEE Trans. Microw. Theory Tech.*, vol. 58, no. 11, pp. 3327-3335, Nov. 2010.
142. R. Zhu, X. Zhang, B. Hraimel, D. Shen, and T. Liu, "Broadband predistortion circuit using zero bias diodes for radio over fiber systems," *IEEE photon. Technol. Lett.*, vol. 25, no. 21, pp. 2101-2104, Nov. 2013.
143. X. Zhang, S. Saha, R. Zhu, T. Liu, and D. Shen, "Analog predistortion circuit for radio over fiber transmission," *IEEE photon. Technol. Lett.*, vol. 28, no. 22, pp. 2541-2544, Nov. 2016.
144. R. Zhu, X. Zhang, and D. Shen, "Ultra broadband predistortion circuit for radio-over fiber transmission systems," *J. Lightw. Technol.*, vol. 34, no. 22, pp. 5137-5145, Nov. 2016.
145. X. Hu, G. Wang, Z-C. Wang, and J-R. Luo, "Predistortion linearization of an X-band TWTA for communications applications," *IEEE Trans. Electron Devices*, vol. 58, no. 6, pp. 1768-1774, Jun. 2011.
146. S.C. Bera, R.V. Singh, and V.K. Grag, "Diode-based predistortion linearizer for power amplifier," *Electron. Lett.*, vol. 44, no. 2, pp. 125-126, Jan. 2008.
147. A. Katz, R. Gray, and R. Dorval, "Wideband/multiband linearization of TWTA using predistortion," *IEEE Trans. Electron Devices*, vol. 56, no. 5, pp. 959-964, May 2009.
148. C. W. Park, F. Beaugerard, G. Carangelo, and F. M. Ghannouchi, "An independently controllable AM/AM and AM/PM predistortion linearizer for cdma2000 multicarrier applications," in *IEEE Radio Wireless Conf.*, Aug. 2001, pp. 53-56.

149. N. Gupta, A. Tombak, and A. Mortazawi, "A predistortion linearizer using a tunable resonator," *IEEE Microw. Wireless Compon. Lett.*, vol. 14, pp. 431-433, Sep. 2004.
150. M. Rawat, K. Rawat, and F. M. Ghannouchi, "Adaptive digital predistortion of wireless power amplifiers/transmitters using dynamic real-valued focused time-delay line neural networks," *IEEE Trans. Microw. Theory Techn.*, vol. 58, no. 1, pp. 95-104, Jan. 2010
151. N. Narahariseti, P. Roblin, C. Quindroit, M. Rawat, and S. Gheitanchi, "Quasi-Exact Inverse PA Model for Digital Predistorter Linearization," in 2013 82nd ARFTG Microwave measurement conference, 2013.
152. M. Rawat, P. Roblin, C. Quindroit, K. Salam, and C. Xie, "Digitally supported feed-forward harmonic cancellation for filter-less ultra-wideband transmitters," in *IEEE Int. Microw. RF Conf.*, Bangalore, India, Dec. 2014, pp. 1-4
153. P. Roblin, M. Rawat, and V. Ratnasamy, "RF Frontend Flexibility, Self-calibration, and Self-linearization," *IEEE Microw. Mag.*, vol. 19, no. 2, pp. 49-61, Mar./ Apr. 2018
154. M. Rawat, C. Quindroit, P. Roblin, N. Narharishetti, R. Pond, K. Salam and C. Xie, "Characterization and modeling scheme for harmonics at power amplifier output", 83rd ARFTG Microwave Measurement Symposium, Tampa, Florida, June 2014.
155. M. Rawat and F. M. Ghannouchi, "A mutual distortion and impairment compensator for wideband direct-conversion transmitters using neural networks," *IEEE Trans. Broadcast.*, vol. 58, no. 2, pp. 168-177, Jun. 2012.
156. J. Xia, E. Ng, and S. Boumaiza, "Wide band compensation of RF vector multiplier for RF predistortion system," *IEEE Trans. Circuits Syst. II: Express Briefs*, vol. 63, no. 11, pp.1084-1088, Nov. 2016.
157. O. Hammi, F.M. Ghannouchi, and B. Vassilakis, "A compact envelope memory polynomial for RF transmitters modeling with application to baseband and RF digital predistortion," *IEEE Microw. Compon. Lett.*, vol. 18, no. 5, pp. 359-361, Dec. 2008.

158. W.J. Kim, K.J. Cho, S.P. Stapleton and J.H. Kim, "Baseband derived RF digital predistortion," *IEEE Electron. Lett.*, vol. 42, no.8, pp. 468-470, Apr. 2006.
159. A. Prata, D. C. Ribeiro, P. M. Cruz, A. S. R. Oliveira, and N. B. Carvalho, "Improving DPD performance by compensating feedback loop impairments in RF ADCs," *IEEE MTT-S Int. Microw. Symp. Dig.*, May 2015.
160. M. Helaoui, S. Hatami, R. Negra and F. M. Ghannouchi, "A Novel Architecture of Delta-Sigma Modulator Enabling All-Digital Multiband Multistandard RF Transmitters Design," *IEEE Trans. Circuits Syst. II: Express Briefs*, vol. 55, no. 11, pp. 1129-1133, Nov. 2008
161. M. M. Ebrahimi, M. Helaoui, F. M. Ghannouchi, "Delta-sigma based transmitters: Advantages and disadvantages," *IEEE Microw. Mag.*, vol. 14, no. 1, pp. 68-78, Feb. 2013.
162. C. Yu, L. Guan, E. Zhu, and A. Zhu, "Band-limited volterra series based digital predistortion for wideband RF power amplifiers," *IEEE Trans. Microw. Theory Techn.*, vol. 60, no. 12, pp. 4198-4208, Dec. 2012.
163. L. Ding, F. Mujica, and Z. Yang, "Digital predistortion using direct learning with reduced bandwidth feedback," *IEEE MTT-S Int. Microw. Symp. Dig.*, Jun. 2013.
164. H. Huang, P. Mitran, and S. Boumaiza, "Digital predistortion function synthesis using undersampled feedback signal," *IEEE Microw. Wireless Compon. Lett.*, vol. 26, no. 10, pp. 855-857, Oct. 2016.
165. Z. Wang, W. Chen, G. Su, F. M. Ghannouchi, Z. Feng, and Y. Liu, "Low feedback sampling rate digital predistortion for wideband wireless transmitters," *IEEE Trans. Microw. Theory Techn.*, vol. 64, no. 11, pp. 3528-3539, Nov. 2016.
166. Y. Ma, Y. Yamao, Y. Akaiwa, and K. Ishibashi, "Wideband digital predistortion using spectral extrapolation of band-limited feedback signal," *IEEE Trans. Circuits Syst. I, Reg. Papers*, vol. 61, no. 7, pp. 2088-2096, Jul. 2014.

167. Y. Liu, J.J. Yan, H-T Dabag, and P.M. Asbeck, "Novel Technique for wideband digital predistortion of power amplifier with an under-sampling ADC," *IEEE Trans. Microw. Theory Techn.*, vol. 62, no.11, pp. 2604-2616, Nov. 2014.
168. Y. Liu, W. Pan, S. Shao, and Y. Tang, "A general digital predistortion architecture using constrained feedback bandwidth for wideband power amplifier," *IEEE Trans. Microw. Theory Techn.*, vol. 63, no. 5, pp. 1544-1555, May 2015.
169. Q. Zhang, J. Zhou, W. Chen, and S. Zhang "A band-divided memory polynomial for wideband digital predistortion with limited bandwidth feedback," *IEEE Trans. Circuits Syst. II: Express Briefs*, vol. 62, no. 10, pp. 922-926, Oct. 2015.
170. Y. Liu, C. Huang, X. Quan, P. Roblin, W. Pan, and Y. Tang, "Novel linearization architecture with limited ADC dynamic range for green power amplifier," *IEEE J. Sel. Areas Commun.* vol. 34, no. 12, pp. 3902-3914, Dec. 2016.
171. N. Guan, N.Wu, and H. Wang, "Digital predistortion of wideband power amplifier with single undersampling ADC," *IEEE Microw. Wireless Compon. Lett.*, vol. 27, no. 11, pp. 1016–1018, Nov. 2017.
172. A. Chung , M. B. Rejeb , Y. Beltagy, A. M. Darwish, H. A. Hung, and S. Boumaiza, "IQ imbalance compensation and digital predistortion for millimeter-wave transmitters using reduced sampling rate observations," *IEEE Trans. Microw. Theory Techn.*, vol. 66, no. 7, pp. 3433-3442, Jul. 2018
173. M. Rawat et al., "Concurrent dual-band modeling and digital predistortion in the presence of unfilterable harmonic signal interference," *IEEE Trans. Microw. Theory Techn.*, vol. 63, no. 2, pp. 625–637, Feb. 2015.
174. N. Naraharisetti, P. Roblin, C. Quindroit and S. Gheitanchi, "Efficient least square 2-D cubic splines for concurrent dual band systems," *IEEE Trans. Microw. Theory Techn.*, vol. 63, no. 7, pp. 2199-2210, Jul. 2015.
175. Y. Lin, H. Jang, C. Quindroit, N. Naraharisetti, and P. Roblin, "New supply modulation optimization methodology for concurrent dual band envelope tracking

- power amplifier,” in Proc. 2014 IEEE 15th Annu. Wireless and Microwave Technology Conf. (WAMICON’2014), June 2014, pp. 1–4.
176. P. Roblin, N. Narahariseti, C. Quindroit, S. Gheitanchi, V. Mauer, and M. Fitton, “2D multisine mapping for robust 2 band PA modeling and 2D predistorter extraction,” in 81st ARFTG Microw. Meas. Conf., Jun. 2013, pp. 1–3.
 177. N. Narahariseti, C. Quindroit, P. Roblin, S. Gheitanchi, V. Mauer, and M. Fitton, “2D cubic spline implementation for concurrent dual-band system,” in IEEE MTT-S Int. Microw. Symp. Dig., Jun. 2013, pp. 1–4.
 178. M. Rawat, K. Rawat, M. Younes, and F. M. Ghannouchi, “Joint mitigation of nonlinearity and modulator imperfections in dual-band concurrent transmitter using neural networks,” *Electron. Lett.*, vol. 49, no. 4, pp. 253–255, Feb. 2013.
 179. M. Rawat, N. Narharishetti, C. Quindroit, P. Roblin, R. Pond, K. Salam, and C. Xie, “Dual-band transmitter behavioral modeling with physically motivated 2-D rational functions,” in 82nd ARFTG Microw. Meas. Symp., Columbus, OH, USA, Nov. 2013, pp. 1–4.
 180. C. Quindroit, N. Narahariseti, P. Roblin, S. Gheitanchi, V. Mauer, and M. Fitton “FPGA implementation of orthogonal 2D digital predistortion system for concurrent dual-band power amplifiers based on time-division multiplexing,” *IEEE Trans. Microw. Theory Tech.*, vol. 61, no. 12, pp. 4591-4599, Dec. 2013.
 181. P. Roblin, C. Quindroit, N. Narahariseti, Shahin Gheitanchi, Mike Fitton, “Concurrent linearization: The state of the art for modeling and linearization of multiband power amplifiers,” *IEEE Microw. Mag.*, vol. 14, no. 7, pp 75-91, Nov. 2013
 182. P. Roblin, S. K. Myoung, D. Chaillot, Y. G. Kim, A. Fathimulla, J. Strahler, and S. Bibyk, “Frequency-selective predistortion linearization of RF power amplifiers,” *IEEE Trans. Microw. Theory Tech.*, vol. 56, no. 1, pp. 65–76, Jan. 2008.

183. S. A. Bassam, M. Helaoui, and F. M. Ghannouchi, "2-D digital predistortion (2-D-DPD) architecture for concurrent dual-band transmitters," *IEEE Trans. Microw. Theory Techn.*, vol. 59, no. 10, pp. 2547–2554, Oct. 2011.
184. Y. J. Liu, W. Chen, J. Zhou, B. H. Zhou, and F. M. Ghannouchi, "Digital predistortion for concurrent dual-band transmitters using 2-D modified memory polynomials," *IEEE Trans. Microw. Theory Techn.*, vol. 61, no. 1, pp. 281–290, Jan. 2013.
185. H. Qian, S. Yao, H. Huang, X. Yang, and W. Feng, "Low complexity coefficient estimation for concurrent dual-band digital predistortion," *IEEE Trans. Microw. Theory Techn.*, vol. 63, no. 10, pp. 3153–3163, Oct. 2015.
186. F. Mkaem, A. Islam, and S. Boumaiza, "Multi-band complexity reduced generalized-memory-polynomial power-amplifier digital predistortion," *IEEE Trans. Microw. Theory Techn.*, vol. 64, no. 6, pp. 1763–1774, Jun. 2016.
187. S. A. Bassam, A. Kwan, W. Chen, M. Helaoui, and F. M. Ghannouchi, "Subsampling feedback loop applicable to concurrent dual-band linearization architecture," *IEEE Trans. Microw. Theory Techn.*, vol. 60, no. 6, pp. 1990–1999, Jun. 2012.
188. Y. Liu, J. J. Yan, and P. M. Asbeck, "Concurrent dual-band digital predistortion with a single feedback loop," *IEEE Trans. Microw. Theory Techn.*, vol. 63, no. 5, pp. 1556–1568, May 2015.
189. C. Yu, J. Xia, X.-W. Zhu, and A. Zhu, "Single-model single-feedback digital predistortion for concurrent multi-band wireless transmitters," *IEEE Trans. Microw. Theory Techn.*, vol. 63, no. 7, pp. 2211–2224, Jul. 2015.
190. K. Rawat, O. Hammi, and F.M. Ghannouchi, "Investigating effects of quadrature imperfection of vector multiplier in implementing RF/ Digital predistortion," *IEEE 10th Annual Wireless and Microwave Technology Conference, WAMICON*, pp. 1-4, 2009.

191. S. Boumaiza, J. Li, M.J. Saidane and F.M. Ghannouchi, "Adaptive Digital/RF predistortion using a nonuniform LUT indexing function with built in dependence on the amplifier nonlinearity," *IEEE Trans. Microw. Theory Techn.*, vol. 52, no. 12, pp. 2670-2677, Dec. 2004.
192. X. Xie, M. Hui, T. Liu, X. Zhang, "Hybrid linearization of broadband radio-over fiber transmission," *IEEE photon. Technol. Lett.*, vol. 30, no. 8, pp. 2541-2544, Apr. 2018
193. H. Matsubara, K. Ishihara, N. Miyadai, T. Nojima, "Hybrid predistortion to compensate third-and fifth-order intermodulation of a 2GHz power amplifier using cuber predistortion and second harmonics injection," *IET Microw. Antennas Propag.*, vol. 2, no. 8, pp. 813-822, Dec. 2008.





